AD-A090 528 NEW YORK UNIV N Y DEPT OF PHYSICS F/G 7/4
THEORETICAL STUDIES RELATING TO THE INTERACTION OF RADIATION WI--ETC(U)
OCT 80 N00014-77-C-0553
UNCLASSIFIED NL

1 OF 2
AD A090528

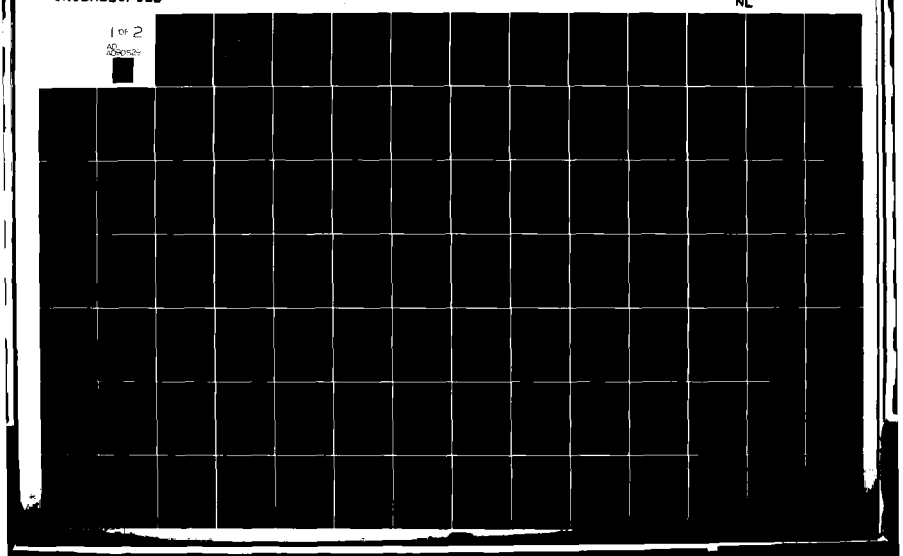

AD A090528

SECURITY CLASSIFICATION OF THIS PAGE (When Data Entered)

REPORT DOCUMENTATION PAGE

READ INSTRUCTIONS BEFORE COMPLETING FORM

1. REPORT NUMBER: AR 3	2. GOVT ACCESSION NO.: AD-A090528 / 3. RECIPIENT'S CATALOG NUMBER
4. TITLE (and Subtitle): Theoretical Studies Relating to the Interaction of Radiation with Matter: Atomic Collision Processes Occurring in the Presence of Radiation Fields	5. TYPE OF REPORT & PERIOD COVERED: 8/1/79 - 7/31/80
	6. PERFORMING ORG. REPORT NUMBER
7. AUTHOR(s): P.R. Berman	8. CONTRACT OR GRANT NUMBER(s): N00014-77-C-0553
9. PERFORMING ORGANIZATION NAME AND ADDRESS: Prof. P.R. Berman, Physics Dept. - New York University, 4 Washington Pl., New York, N.Y. 10003	10. PROGRAM ELEMENT, PROJECT, TASK AREA & WORK UNIT NUMBERS
11. CONTROLLING OFFICE NAME AND ADDRESS: Office of Naval Research - Code 613C: MAK, 800 N. Quincy St., Arlington, Virginia 22217	12. REPORT DATE: October 1, 1980 / 13. NUMBER OF PAGES: 150
14. MONITORING AGENCY NAME & ADDRESS (if different from Controlling Office): Office of Naval Research Resident Representative New York, 715 Broadway - 5th Floor, New York, N.Y. 10003	15. SECURITY CLASS. (of this report): Unclassified / 15a. DECLASSIFICATION/DOWNGRADING SCHEDULE

LEVEL II

AD A074 183

16. DISTRIBUTION STATEMENT (of this Report)

Approved for public release; distribution unlimited

17. DISTRIBUTION STATEMENT (of the abstract entered in Block 20, if different from Report)

DTIC ELECTE OCT 15 1980 S C

18. SUPPLEMENTARY NOTES

THIS DOCUMENT IS BEST QUALITY PRACTICABLE. THE COPY FURNISHED TO DDC CONTAINED A SIGNIFICANT NUMBER OF PAGES WHICH DO NOT REPRODUCE LEGIBLY.

19. KEY WORDS (Continue on reverse side if necessary and identify by block number)

Laser Spectroscopy, Optical Collisions, Radiative Collisions, Velocity-Changing Collisions, Two-Level System.

20. ABSTRACT (Continue on reverse side if necessary and identify by block number)

Work is reported in the areas of:-
(1) Collisionally-Aided Radiative Excitation;
(2) Model Potential Calculations in Atom-Field-Radiation Systems;
(3) Coherence Effects in Radiative Collisions;
(4) Two-Level Atom & Radiation Pulse;
(5) Resonance Fluorescence in Three-Level Systems;
(6) Modulation Spectroscopy; and
(7) Effects of Collisions on Atomic Coherences.

DD FORM 1 JAN 73 1473 EDITION OF 1 NOV 68 IS OBSOLETE S/N 0102-LF-014-6601

80 10 8 035

SECURITY CLASSIFICATION OF THIS PAGE (When Data Entered)

DISCLAIMER NOTICE

THIS DOCUMENT IS BEST QUALITY PRACTICABLE. THE COPY FURNISHED TO DTIC CONTAINED A SIGNIFICANT NUMBER OF PAGES WHICH DO NOT REPRODUCE LEGIBLY.

(9) Annual Report, ~~(ARPA)~~ no. 3, 1 Aug 79 - 31 Jul ..

Title: (6) Theoretical Studies Relating to the Interaction of Radiation with Matter: Atomic Collision Processes Occurring in the Presence of Radiation Fields

Supported by the U.S. Office of Naval Research

Contract No.: (15) N0014-77-C-0553 (12) 15 p.

Report Period: August 1, 1979 - July 31, 1980

Date of Report: October 1, 1980

406850

JCB

Research has been carried out in the areas of (1) Collisionally-Aided Radiative Excitation, (2) Model Potential Calculations of Atom-Field-Collisional Interactions, (3) Coherence Effects in Radiative Collisions, (4) Two-level Atom and Radiation Pulse, (5) Resonance Fluorescence in Three-level Systems, (6) Modulation Spectroscopy, and (7) Effects of Collisions on Atomic Coherences.

1. Collisionally-Aided Radiative Excitation (S. Yeh, P. Berman)

A detailed analysis of Collisionally Aided Radiative Excitation (CARE) in three-level systems in the weak field limit has been completed.[1*] Two off-resonant laser pulses are applied to a three-level atom which simultaneously undergoes a collision with a perturber. The energy levels of the active atom are perturbed in such a way that during a collision, the atom may be instantaneously brought into single-photon resonance with either of the fields or into two-photon resonance with both fields (see figure)

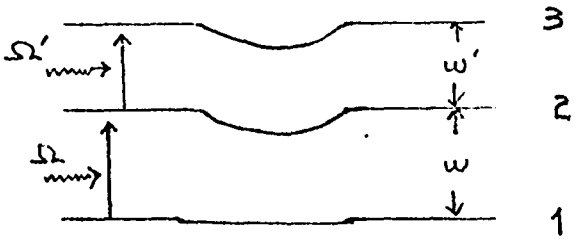

Energy levels during a collision

*Asterisks on references indicate reprints or preprints appended to this report.

We have determined the level three population as a function of both field detunings. Of particular interest is the asymptotic behavior for large detunings which is intermediate between that predicted for single and two-photon CARE. In addition, we have explained in more detail the intereference effect[2*] that arises from contributions to the final state population from both the "step-wise" and "two-photon" excitation channels.

2. Model Potential Calculations of Atom-Field-Collisional Interactions (E. Robinson)

Many calculations of CARE or Radiatively Assisted Inelastic Collisiona (RAIC) tend to involve lengthy, costly computational work (a RAIC is a process in which one or more laser photons provide the needed energy to permit a collisional interaction that would be otherwise energetically forbidden). Moreover, qualitative conclusions are not easily derived from the numerical results. It is, therefore, useful to have analytically soluable model potential calculations in which the collisional interaction or radiation pulse envelope is approximated by a smooth function.

Two such model potential calculations for RAIC have already been carried out in the weak-field (perturbation theory) limit.[3*,4*] Both models approximate the collisional coupling by a hyperbolic secant function; the collisional level-shifting is approximated by a delta function in one model and a hyperbolic secant squared in the other. Results were found to be in general agreement with numerical calculations. Both solutions have been extended to allow for arbitrary field strengths. The solutions can be expressed in series form, although the series are not among those tabulated in standard mathematical texts. Analysis of the results is currently in progress.

The Rozen-Zener problem (two-level atom subjected to a hyperbolic secant radiation pulse) has been extended to three level systems in which the field couples one of the states to the other two, but those two states are not coupled. A preliminary report on this work was presented at the EGAS conference in September, 1980, at Pisa, Italy.

3. Coherence Effects in Radiative Collisions (P. Berman)

This work is discussed in detail in two preprints which are appended to this report.[5*,6*] A traditional RAIC reaction is of the form

$$A_i + A'_{i'} + \hbar\Omega \rightarrow A_f + A'_{f'}$$

where two atoms (A and A') collide in the presence of a field to undergo reaction taking them from some initial state $A_iA'_{i'}$ to a final state $A_fA'_{f'}$. In all previous theories the initial and final states were taken to be non-degenerate and the transition rate as a function of Ω was calculated. The transition rate profile provides some information on the interatomic potential.

We have extended the theory to include degeneracy in the initial and final states. Such a study leads to qualitatively new predictions in the RAIC profiles. The quantity which is calculation is the polarization of fluorescence or quantum beats originating from the final state manifold of one of the atoms. The polarization of fluorescence or quantum beats directly reflects the final state coherence properties of the atom being detected. The final state coherence, in turn, can serve as a signature of the collisional interaction taking part in RAIC. The final state coherence is produced by the combined action of the laser field (which tends to produce coherence) and the collision (which tends to destroy it). A physical model in which the collision is viewed as unpolarized "fields" has been developed.

The advantage over conventional RAIC detection can be enormous. In conventional RAIC the collisional interaction is inferred from the profile wings, where signal is weak. In contrast, polarization measurements at line center can often (but not always) provide the same collisional information. Thus, such measurements can provide a valuable means for analyzing RAIC. To date, the theory has been limited to the weak field (perturbation theory) limit and is valid

only in the impact core of the RAIC profile. An experiment to test the predictions may be carried out at Laboratoire Aime Cotton, Orsay, France.

4. Two-level Atom & Radiation Pulse. (P. Berman)

One of the most fundamental problems in the interaction of radiation with matter is to calculate the excitation of a two-level atom produced by a nearly resonant (detuning Δ) radiation pulse. Ironically, the only <u>smooth</u> pulse envelope for which an analytic solution has been found is the hyperbolic secant. In collaboration with Dr. A. Bambini (Institute for Quantum Electronics, Florence, Italy), analytic solutions to this problem have been found for an entire class of positive envelope functions. This class of functions includes the hyperbolic secant as a special case. Except for the hyperbolic secant, however, all pulse shapes are not symmetric. A paper on this work is currently in preparation. Of particular interest is the fact that the excitation probability does not vanish for any field strengths not equal to zero, in contrast to the results for symmetric pulses. One can also see which pulse shapes provide maximum excitation for a given pulse area.

Work has continued in the asymptotic dependence of excitation probability. Progress has been made on evaluating the time consuming integrals appearing in adiabatic theories of this effect.[7] It also appears that the asymptotic dependence is intimately linked to the pole structure of the envelope functions, but attempts to find rigorous mathematical proofs of our results have not been successful.

5. Resonance Fluorescence in Three-Level Systems. (S. Yeh)

A calculation of the resonance fluorescence of a three-level system has been carried out. An incident field couples the ground state to either of two nearly degenerate excited

states, which, themselves, are not coupled by the fields. Using a dressed atom picture, one can predict that the fluorescence spectrum consists of seven components. If the field is tuned midway between the excited states and if the coupling constant is the same for both excided states, the spectrum collapses to five components. A paper on this subject is in preparation.

6. Modulation Spectroscopy. (P. Berman)

Although contained implicitly in the laser theory of Lamb,[8] the use of modulation spectroscopy to probe collisional effects is just beginning to surface. In this technique one modulates an applied field frequency in a saturated absorption experiment at some frequency δ. To second order in the field, there will be a component of the atomic state <u>populations</u> which oscillates at a frequency 2δ. This population component can be thought to have an effective lifetime of $(2\delta)^{-1}$ when $\delta >>$ (natural lifetime). If collisions are occurring within the system, one can increase delta so that, at most, one collision occurs during the effective lifetime of the levels under investigation. In this way, one can isolate the role of a single velocity-changing collision, which, in turn, reflects the properties of the collision kernel giving rise to the scattering.

Although experiments of this type are under way,[9-11] no results have yet been published. A collaborative attempt to analyze a saturated absorption experiment in Ne, yielded qualitatively consistent results, but experimentally reproducible data was not obtained.

7. Effect of Collisions on Atomic Coherences. (P. Berman)

In collaboration with J. LeGouët, (Laboratoire Aimé Cotton, Orsay, France), a study of the basic equations that

appear in quantum-mechanical transport equations[12] was initiated. We are seeking some physical insight into the way in which collisions alter any coherences that may have been created in a nearly degenerate manifold of levels. As a specific example, we consider the effects of collisions on Zeeman coherences (coherences created between magnetic sublevels of a level of a given J - i.e. alignment, orientation).

The major conceptual problem is that the collision trajectories are different for the different magnetic substates. Since the collision can couple the various magnetic substates, at any time during a collision, the possibility of determining all density matrix elements following the collision seems intractable. We have been able to show, however, that a type of semi-classical picture is valid under very general conditions. In this picture, the collision can be broken down into two overlapping zones. In the region of large internuclear separations, the difference in substate trajectories can be ignored. The region of small internuclear separations can be treated by an adiabatic method. This work represents the first progress in the evaluation of certain terms in the quantum-mechanical transport equation. Implications with regard to laser spectroscopy will be explored. A paper on this subject is in preparation.

8. Previous Work

Reprints representing either earlier work[13*-16*] or review articles[17*,18*] that appeared during this report period are appended to this report.

References

1. S. Yeh and P.R. Berman, to appear in Phys. Rev. A.
2. S. Yeh and P.R. Berman, Phys. Rev. Letters 43, 848 (1979).
3. E.J. Robinson, J. Phys. B12, 1451 (1979).
4. E.J. Robinson, J. Phys. B13, 2359 (1980).
5. P.R. Berman, to appear in Phys. Rev. A.
6. P.R. Berman, to appear in Phys. Rev. A.
7. J.C. Light, J. Chem. Phys. 66, 5241 (1977).
8. W.E. Lamb, Jr., Phys. Rev. 134, A1429 (1964).
9. D. Bloch, R.K. Raj, J.J. Snyder, and M. Ducloy, Proceeding of IEEE 11th International Quantum Electronics Conference, p. 624 (1980).
10. F. Laloë, private communication.
11. C.G. Aminoff, private communication.
12. P.R. Berman, Phys. Rev. A5, 927 (1972); A6, 2157 (1972).
13. J.L. LeGouet and P.R. Berman, Phys. Rev. A20, 1105 (1979).
14. P.F. Liao, J.E. Bjorkholm and P.R. Berman, Phys. Rev. A20, 1489 (1979); A21, 1927 (1980).
15. P.R. Berman, P.F. Liao and J.E. Bjorkholm, Phys. Rev. A20, 2389 (1980); also in Laser Spectroscopy IV (H. Walther and K. Rothe, Eds., Apringer-Verlag, Berlin, 1979) p. 622.
16. E.J. Robinson, J. Phys. B13, 2243 (1980).
17. P.R. Berman, to appear in Annales de Physique.
18. R. Vetter and P.R. Berman, to appear in Comments on Atomic and Molecular Physics.

Photon echoes in standing-wave fields: Time separation of spatial harmonics

J.-L. Le Gouët
Laboratoire Aimé Cotton, Centre Nationale de la Recherche Scientifique II, Bâtiment 505, 91405-Orsay, France

P. R. Berman
Physics Department, New York University, 4 Washington Place, New York, New York 10003
(Received 12 February 1979)

A calculation is presented to describe the response of an atomic system subjected to two strong standing-wave field pulses separated in time. One finds a sequence of output pulses following input pulses which is reminiscent of classical photon echoes. A physical picture of the processes involved in echo formation is presented, and connection is made with the classical picture of photon echoes. The application of these techniques to collision studies is emphasized. It is shown that studies of echoes produced by standing-wave fields can prove advantageous for exploring the effects of small-angle scattering on both level populations and atomic coherences.

I. INTRODUCTION

There has been recent interest in using time resolved methods in laser spectroscopy. These include time-resolved saturation spectroscopy,[1] free-induction decay,[2] photon echo,[3,4] quantum beats,[5] coherent Raman beats,[6] superradiance,[7] and excitation in separated fields.[8-13] In most of these experiments one observes the transient response of atoms to the application or removal of laser fields. In addition to providing a means for carrying out high-precision spectroscopy, these methods are useful, to varying degrees, for studying relaxation processes.

In this paper we consider the response of an atomic system to excitation by separated fields, sometimes referred to as optical Ramsey fringes. To observe optical Ramsey fringes, one applies a laser-generated *standing wave* to atoms during a short time τ, at two instants separated by a delay T. Experimentally, this process has been studied using gas cells[10-13] as well as atomic beams[8,9] for both two-photon[10,12] and one-photon[8,9,11,13] excitation. In the case of two-photon transitions, which are free from the Doppler effect, the evolution of the atoms after the second pulse is probed by the fluorescence decay from the upper level. For one-photon transitions, the field-induced coherence among the atomic dipoles is rapidly destroyed for different velocity subclasses of atoms owing to the Doppler effect, *except* at a time T after the second pulse. At this instant a coherent radiation is emitted by the gas, which is reminiscent of the classical photon echo. In either case the signals exhibit a detuning-dependent structure of width $1/T$, which does not exist in the usual photon echo. The ultimate resolution of separated-field spectroscopy [with width $(T)^{-1}$] may be much better than that in saturation spectroscopy (limited by transit-time broadening).

In the last papers of the group of Novosibirsk,[11,13] a new feature was noted, which is the occurence of coherent radiations, not only at time T; but also at $2T, 3T$ after the second pulse. The aim of this paper is to qualitatively and quantitatively discuss the origin of the successive coherent radiation in separated fields (CRSF). The buildup of echoes at successive times is directly connected with the cancellation of the Doppler phase of various spatial harmonics of both the atomic coherences and level populations. We show that the spatial component of order n between the two pulses, is the source of an echo at time nT after the second pulse. The characteristics of the phenomenon in the frequency domain are investigated and the difference with the usual photon echo is elucidated. Moreover a calculation of the CRSF intensity is carried out using a simple model.

In Sec. II the CRSF intensity is calculated, assuming that the field seen by the atoms is provided by the external fields only (i.e., polarization fields are neglected). The details of this calculation are given in Appendix A. Discussions of the origin of the various echoes and the detuning dependence of the fields is given in Secs. III and IV, respectively. Finally, the possibilities of using CRSF for collisional studies is explored in Sec. V.

II. CRSF INTENSITY

Consider a gas cell (Fig. 1) illuminated by two successive standing wave laser pulses. The pulses are applied at times t_0 and t_1 having durations τ_0 and τ_1, respectively. The laser field of

Supp... ...arch
under C...

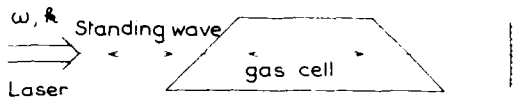

FIG. 1. Two standing-wave pulses of duration τ_0 and τ_1 separated by time T are incident on an atomic system.

frequency ω, is taken to be of the form

$$\vec{E}(z,t) = \hat{i}E(z,t) = \hat{i}E_0 \cos\omega t \sin kz[\theta(t_0) + \theta(t_1)],$$

where

$$\theta(t_i) = \begin{cases} 1 & 0 < (t - t_i) < \tau_i, \\ 0 & \text{otherwise}, \end{cases}$$

and $\hat{i}$ is a unit vector in the direction of polarization.

In the rotating-wave approximation, the equations of motion for density-matrix elements $\rho(z, v_z, t)$ (only motion in the direction of the field-propagation vector need be considered) are

$$\begin{aligned}
\frac{\partial \rho_{11}}{\partial t} + v_z \frac{\partial \rho_{11}}{\partial z} &= i\chi(\rho_{21}e^{-i\omega t} - \rho_{12}e^{i\omega t}) \\
&\quad \times \sin kz[\theta(t_0) + \theta(t_1)] - \gamma_{11}\rho_{11}, \\
\frac{\partial \rho_{22}}{\partial t} + v_z \frac{\partial \rho_{22}}{\partial z} &= i\chi(\rho_{12}e^{i\omega t} - \rho_{21}e^{-i\omega t}) \\
&\quad \times \sin kz[\theta(t_0) + \theta(t_1)] - \gamma_{22}\rho_{22}, \\
\frac{\partial \rho_{12}}{\partial t} + v_z \frac{\partial \rho_{12}}{\partial z} &= i\chi(\rho_{22} - \rho_{11})e^{-i\omega t} \\
&\quad \times \sin kz[\theta(t_0) + \theta(t_1)] - \gamma_{12}\rho_{12} - i\omega_0\rho_{12},
\end{aligned} \tag{1}$$

where ω_0 is the 1-2 transition frequency, $\chi = \mu E_0/2\hbar$, μ is the dipole moment associated with the transition 1-2, and γ_{ij} is the natural decay rate of ρ_{ij}.

It is assumed that the applied pulses are well separated ($t_1 - t_0 \gg \tau_k$), and that the detuning $\Delta = \omega - \omega_0$ and the decay rates γ_{ij} satisfy $|\Delta|\tau_k \ll 1$, $\gamma_{ij}\tau_k \ll 1$, respectively, as is common experimentally. Moreover, to ensure that the Doppler dephasing *between* pulses is complete, one assumes that $kuT \gg 1$, where u is the width of the thermal-velocity distribution. Finally, the effect of the polarization fields on the atoms is neglected, which is valid provided that the echo fields are much less intense than the external ones. In these limits Eqs. (1) are solved in Appendix A.

All spatial harmonics are contained in the atomic polarization $P = \mu(\rho_{12} + \rho_{21})$ which is of the form

$$P(v_z, z, t) = P_c(v_z, z, t)\cos\omega t + P_s(v_z, z, t)\sin\omega t, \tag{2}$$

where P_c and P_s are slowly varying functions of time, compared with $\cos\omega t$. However, it follows from this form of the polarization and Maxwell's equations that only the component of $P(v_z, z, t)$ proportional to $\sin kz$ gives rise to a significant electric field (i.e., the absence of polarization frequencies $3\omega, 5\omega, \ldots$ implies that polarization components varying as $\sin 3kz, \sin 5kz, \ldots$ are negligible). It then follows[1] from Maxwell's equations that the echo field amplitude exiting the sample is given by

$$\mathcal{E}(t) = \int 2\pi kl[\bar{P}_c(v_z, t)^2 + \bar{P}_s(v_z, t)^2]^{1/2} dv_z, \tag{3}$$

where

$$\bar{P}_{c\atop s}(v_z, t) = \frac{2\pi}{k}\int_0^{\pi/k} P_{c\atop s}(v_z, z', t)\sin kz' dz' \tag{4}$$

and l is the length of the sample. The echo amplitude is calculated in Appendix A (using the simplifying, but not critical, assumption that $\gamma_{11} = \gamma_{22} = \gamma$) as

$$\begin{aligned}
\mathcal{E}(t) &= 4\pi kl \int dv_z N_0(v_z) \\
&\quad \times (Ae^{-\gamma_{12}T}\cos\Delta T + Be^{-\gamma T}),
\end{aligned} \tag{5}$$

where

$$N_0(v_z) = \rho_{22}(v_z, t_0) - \rho_{11}(v_z, t_0) \tag{6}$$

is the population difference density inside the cell before the first pulse, and

$$\begin{aligned}
A = \sum_{\text{odd}} \\
B = \sum_{\text{even}}
\end{aligned}
\Bigg\{ (-)^n J_{n+1}\left[\frac{4\chi}{kv_z}\sin\left(\frac{kv_z\tau_1}{2}\right)\right] \times J_n\left[\frac{4\chi}{kv_z}\sin\left(\frac{kv_z\tau_0}{2}\right)\right] \times \exp[-\gamma_{12}(t - t_1)] \times \cos[kv_z(nT - (t - t_1))] \Bigg\}. \tag{7}$$

The physical content of this equation will be discussed in Secs. III and IV. We may note here some general features of the solution. The echo

amplitude is a maximum for $t - t_1 = nT$ (n is an integer). For other times, the velocity integration leads to a negligible echo amplitude. The maximum amplitude of the nth echo is given by

$$\mathcal{E}_{\max}(t_1 + nT) = (-)^n 4\pi k l \int dv_z\, N_0(v_z) J_{n+1}\left[\frac{4\chi}{kv_z}\sin\left(\frac{kv_z\tau_1}{2}\right)\right] \times J_n\left[\frac{4\chi}{kv_z}\sin\left(\frac{kv_z\tau_0}{2}\right)\right] e^{-\gamma_{12}nT} \begin{cases} e^{-\gamma_{12}T}\cos\Delta T, & n \text{ odd}, \\ e^{-\gamma T}, & n \text{ even}. \end{cases} \tag{8}$$

For odd n the maximum amplitude oscillates as a function of detuning Δ, with the fringes having a width $\sim 1/T$. For even n, the signals do not exhibit this detuning dependence. From Eqs. (5) and (7), one can see that the duration of a given echo in time is $(k\Delta v_z)^{-1}$, where Δv_z is the range of significant v_z entering the integration in Eq. (5); the range Δv_z is a function of χ, ku, τ_0, τ_1. The general qualitative features of the results are illustrated schematically in Fig. 2.

One can determine the most suitable values of parameters τ_0, τ_1, χ in order to maximize the intensity of a given echo. As a first attempt at this choice of parameters, consider the simple situation where all the velocity classes are equally excited by the pulses, i.e., $ku\tau \ll 1$. In this limit the arguments of the Bessel functions reduce to $2\chi\tau_0$ and $2\chi\tau_1$, respectively. Taking a Maxwellian distribution for N_0,

$$N_0(v_z) = (N_0/u\sqrt{\pi})\exp(-v_z^2/u^2), \tag{9}$$

one obtains the echo:

$$\mathcal{E}(t) = 4\pi k l N_0 \exp\{-\tfrac{1}{4}k^2u^2[nT - (t - t_1)]^2 \times [A'e^{-\gamma_{12}T}\cos(\Delta T) + B'e^{-\gamma T}], \tag{10}$$

where

$$A' = \sum_{n\ \text{odd}} \left\{ (-)^n J_{n+1}(2\chi\tau_1) J_n(2\chi\tau_0) \times \exp[-\gamma_{12}(t - t_1)] \right.$$
$$B' = \sum_{n\ \text{even}} \left\{ \right. \tag{11}$$

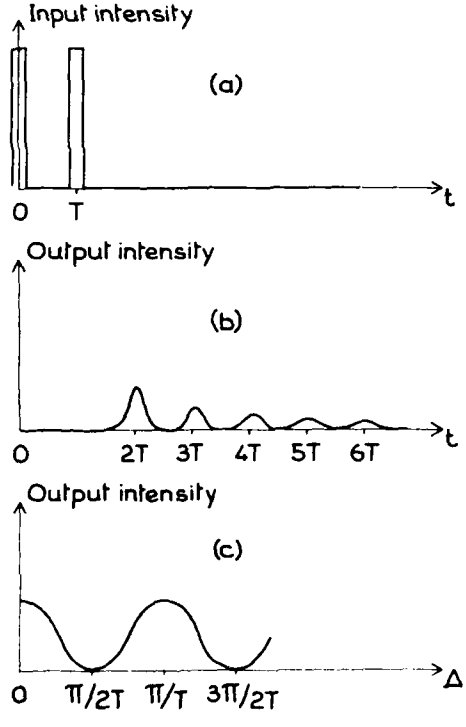

FIG. 2. Schematic representation of the results: (a) input pulses, (b) |output| as a function of time, (c) output as a function of detuning for fixed t located at one of the echoes occuring at $t = t_1 + nT$ with n odd.

The duration of each of these echoes (at half-maximum) is $3.4/ku$, and to maximize $\mathcal{E}(t)$, τ_0 and τ_1 must be chosen so that the Bessel functions of the observed echo have their first maximum for $2\chi\tau_0$ and $2\chi\tau_1$ (Ref. 14):

$$\chi\tau_0 = 0.9 \text{ and } \tau_1 = 1.72\tau_0 \text{ for } n = 1,$$
$$\chi\tau_0 = 1.55 \text{ and } \tau_1 = 1.35\tau_0 \text{ for } n = 2.$$

In the limit $ku\tau \ll 1$ under consideration, this optimization procedure requires field strengths $\chi \gg ku$.

The ratio R_n of the optimized intensity of the first echo to that of the others is shown as follows:

n	1	2	3	4	5
R_n	1	1.82	2.7	3.57	5

If $ku\tau > 1$, Eq. (5) must be evaluated by a numerical integration. Figures 3 and 4 show $\mathcal{E}_{\max}$ for the two first echoes, as a function of $ku\tau_1$ for several values of χ. In this calculation the ratio between τ_0 and τ_1 is fixed at the optimum value which has been determined previously for the limiting case

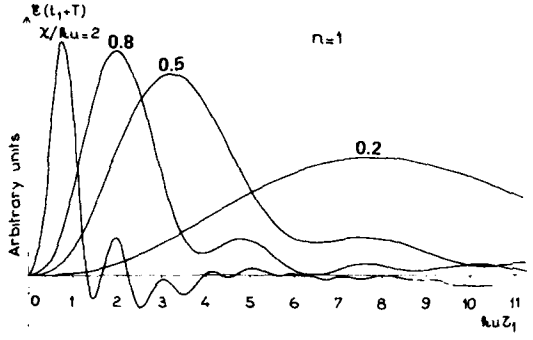

FIG. 3. Maximum value of the first echo amplitude as a function of $ku\tau_1$ for various ratios χ/ku. The value of τ_0 was taken equal to $0.58\tau_1$.

$ku\tau \ll 1$. It turns out that the intensity maxima shown by Figs. 3 and 4 are approximately located at the same values of $\chi\tau_0$ and $\chi\tau_1$, as in the $ku\tau_i \ll 1$ case. The echo amplitude maximum is decreased by a factor of 2 (first echo) or a factor of 2.8 (second echo) when the Rabi frequency is changed from $2ku$ to $0.2ku$.

Figures 5 and 6 represent the time evolution of the echoes around the instant t_1+nT. For each value of χ, τ_0, and τ_1 are chosen to give the maximum intensity. The duration of the echoes (at half-maximum) is increased from about $3.5/ku$ to $8/ku$ (first echo) and $3.5/ku$ to $12/ku$ (second echo) when χ varies from $2ku$ to $0.2ku$. The physical implications of the above results are discussed in Secs. III and IV.

III. PHYSICS OF ECHO FORMATION

To investigate the physical origin of the echoes, we first consider the limiting case $ku\tau \ll 1$ (all velocity subclasses excited by the pulses). For

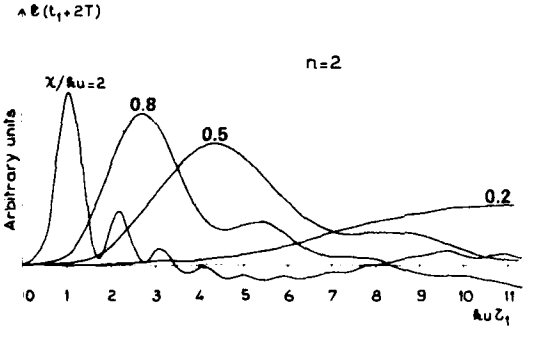

FIG. 4. Maximum value of the second echo amplitude as a function of $ku\tau_1$ for various ratios χ/ku. The value of τ_0 was taken equal to $0.74\tau_1$.

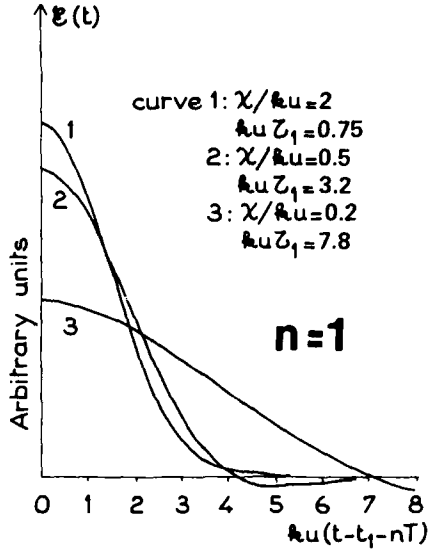

FIG. 5. First echo amplitude ($n=1$) as a function of time for various field strengths χ/ku. The values of $ku\tau_1$ used to maximize the amplitude are indicated.

an initial given phase kz of the applied field at (z, t_0), the phase of the m-order spatial harmonic of the induced polarization is mkz (m odd). From time t_0 to t with the field off, the atoms keep the same phase mkz. Owing to their motion, the atoms at (z, t) are the ones which were at $(z_0 = z - v_z(t-t_0), t_0)$. Consequently, the spatial phase

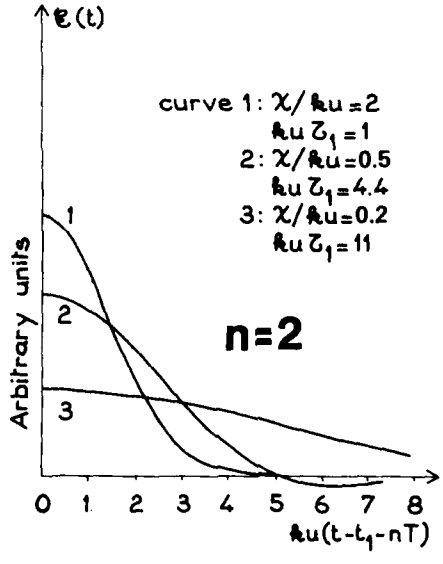

FIG. 6. Second echo amplitude ($n=2$) as a function of time for various field strengths χ/ku.

of atoms with velocity v_z at z is

$$\phi_m(v_z, z, t) = mkz_0 = mkz - mkv_z(t - t_0).$$

In a standing wave field, populations as well as off-diagonal density matrix elements acquire phases. Thus the phase of an arbitrary density matrix element harmonic at $t = t_1$ is $nkz - nkv_z(t_1 - t_0)$, where n can be even (population) *or* odd (polarization). The second pulse causes each nth harmonic, present at time t, to drive the mth harmonic of the polarization. The phase of the mth harmonic after the pulse is obtained by adding $(m-n)kz$ to the phase of the nth harmonic before the pulse. This leads to

$$\phi_m(v_z, z, t_1) = mkz - nkv_z(t_1 - t_0).$$

This total phase differs from the value of ϕ_m before the pulse by a phase jump $(m-n)kv_z(t_1 - t_0)$. Note that the phase of the mth harmonic after the pulse actually reflects the time development of the nth harmonic, and not that of the mth harmonic, between t_0 and t_1. In the same way that the phase at time t after the first pulse was obtained, one can calculate the spatial phase at time $t > t_1$, as

$$\phi_m(v_z, z, t) = mkz - kv_z(n(t - t_1) + nT),$$

where $T = t_1 - t_0$. All the velocity classes of the polarization combine their contributions to produce coherent radiation of the gas after the second pulse. The spatial average gives rise to negligible contributions from the various harmonics (provided the dimension of the sample is much larger than the radiation wave length) except for the components having spatial phase $\pm kz$. Thus, the signal originates from components such that $m = \pm 1$, with a phase

$$\phi_{\pm 1}(v_z, z, t) = \pm kz - kv_z(nT \pm (t - t_1)).$$

In the integration over v_z, the atomic polarization is small, owing to the Doppler phase $kv_z(nT \pm (t - t_1))$, except at times $t = t_1 + |n|T$ when this Doppler phase is zero. Thus an echo occurs at time $|n|T$ after the second pulse and reflects the buildup of either polarization (n odd) or population (n even) harmonics in the $t_0 - t_1$ region. Figure 7 represents this result for the case $n = +8$, $m = -1$, $z = 0$. The result is analogous to that in classical photon echoes—independent of velocity, all dipoles are in phase at a specific time where an echo is observed. Since the nth harmonic is either a population or a polarization component depending on whether n is even or odd, coherent radiation in separated fields is an extension of photon echo in traveling-wave fields, where only the lowest polarization components may be excited. The usual interpretation of photon echo in gases considers the effect of the second pulse as

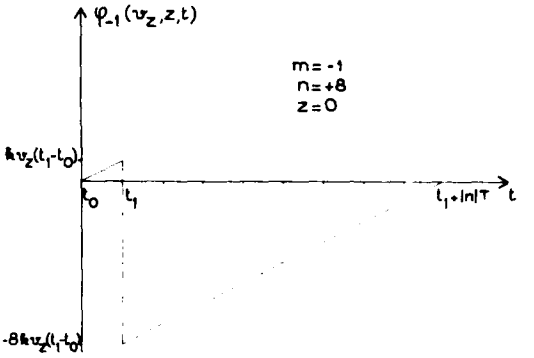

FIG. 7. Evolution of the spatial phase of the (−1) harmonic as a function of time, showing only the contribution from the 8th harmonic following the second pulse. This contribution leads to an echo at $t = t_1 + 8T$. Contributions from other harmonics (not shown) lead to echoes at $t = t_1 + |n|T$.

a reversal of the Doppler phase[4]: $-kv(t_1 - t_0) \rightarrow kv(t_1 - t_0)$. This result is a limiting case of the more general result in CRSF where the second pulse induces a change of $(1-n)kv(t_1 - t_0)$ in the Doppler phase (for classical) photon echo $n = -1$). Thus the presence of the various echoes may be explained by the simple "phase-jump" picture.

The time duration of CRSF may also be explained using a simple picture. The atomic dipoles lose their relative phase coherence in a time equal to the inverse of the frequency bandwidth excited by the laser fields. If $ku\tau_i \lesssim 1$, all velocity subclasses are equally excited by the field, giving an excitation bandwidth of ku and consequently, an echo duration of $\sim(ku)^{-1}$. For larger values of $ku\tau_i$ such that $ku\tau_i \gtrsim 1$, the excitation bandwidth approaches τ_i^{-1}, leading to an echo duration $\sim(\tau_0 + \tau_1)$. This effect is clearly seen in Figs. 5 and 6 as the echo duration increases with $ku\tau_i$.

Excitation bandwidth is also an important factor in explaining the decrease in echo amplitude with decreasing field strength shown in Figs. 3 and 4. For large field strengths leading to optimization pulse widths such that $ku\tau_i \ll 1$, all velocity subclasses are equally excited and the parameters χ, τ_0, τ_1 can be chosen to maximize each echo intensity independently of velocity [see Eq. (8) in which the Bessel-function arguments are velocity independent for $ku\tau_i \ll 1$]. As the field strength decreases, the optimal pulse widths are such that $ku\tau_i \gtrsim 1$. The condition $ku\tau_i > 1$ corresponds to atoms moving through at least one wavelength of the standing wave field pattern during the pulses. Each atom starting at (z_0, t_0) then experiences an average field (see Appendix B)

$$\langle \chi(z_0, t' - t_0) \rangle_{t_0, t_0+\tau} = (2\chi / k v_z \tau) \sin(k z_0 + \tfrac{1}{2} k v_z \tau) \sin(\tfrac{1}{2} k v_z \tau) .$$

which is velocity dependent if $ku\tau \gtrsim 1$. Thus a set of parameters which is optimal for one velocity subclass is not optimal for another [see Eq. (8) in which the Bessel function arguments depend on v_z if $ku\tau \gtrsim 1$]. One is effectively using fewer atoms to provide the echo signal (atoms having $kv_z\tau_i < 1$ are most efficient) as $ku\tau$ increases, leading to a decrease in echo amplitude.

IV. DETUNING DEPENDENCE

Following the first pulse, the induced atomic polarization oscillates freely at frequency ω_0 while the level populations exhibit no oscillatory behavior [see Eqs. (1) for ρ_{12} and ρ_{ii}, respectively]. When the second pulse acts on the system (assuming that both pulses arise from the same cw laser) the atomic dipoles have acquired a temporal phase difference ΔT with the field. For CRSF echoes driven by polarization harmonics (odd n), the echo amplitudes are maximal if this phase difference is an integral multiple of 2π and they oscillate as a function of Δ with period T giving rise to "fringes" of width $1/T$. For CRSF echoes driven by population harmonics (even n), the phase difference plays no role and no fringes appear.

The structure is typical of Ramsey fringes in which one creates a polarization phase difference by sampling a field at two separate times. This effect is also present in traveling-wave photon echoes, but in a less useful way. For traveling-wave fields, the detuning always enters as $\Delta - \vec{k}\cdot\vec{v}$ so that, in order to achieve the Doppler-phase cancellation necessary for echo formation, the detuning dependence as well as the Doppler phase, vanishes at $t = 2T$. The traveling-wave echo exhibits[4] a detuning dependence of $\cos\Delta(t - 2T)$ which, for $t \simeq 2T \pm$ (time duration of the echo), gives a fringe pattern of width ~1/(echo duration) $\gg T^{-1}$. Thus CRSF is much better suited for high-precision spectroscopy than traveling-wave photon echoes.

The fringe pattern in CRSF extends for a range of detuning $|\Delta|\tau \lesssim 1$, after which it disappears. This result is in contrast to typical Ramsey fringe patterns where only the central fringe may be seen (the other fringes are lost owing to phase destruction arising from different values of T for different velocity groups).

V. COLLISIONS

CRSF offers some interesting possibilities for collisional studies. Echo formation is intimately related to the spatial phases acquired by atoms as a result of their motion following application of the field. An echo corresponds to the rephasing of the signal at some particular instant $t = t_1 + nT$ when the atoms of velocity v_z are at distance nv_zT from their position at the time of the second pulse (see Fig. 7). Collisions during the time of flight, which prevent the atoms of a given v_z from being at the right position at the right time, result in a decrease of the echo intensity. This phenomenon of "collisional Doppler dephasing" was already observed in photon-echo experiments.[4] In that case the signal reflects only the evolution of the first spatial harmonic of the atomic coherence. In CRSF, the spatial harmonics of the population difference, as well as coherences, contribute to the echo formation. Thus the CRSF method extends the possibility of observing a "collisional Doppler dephasing effect" to the population difference. Moreover, the spatial structure may be probed systematically since every spatial harmonic produces a CRSF echo. However, the relative contribution of an harmonic decreases with increasing n since the detected atoms have a phase associated with the nth harmonic during the time between the two pulses only and this delay is smaller and smaller in comparison with the total time of flight $(n+1)T$ as n increases. Therefore most of the interest of the method seems to be concentrated in the first few echoes.

It is true that the observed microscopic collisional process—namely, the velocity-changing process—is the same one that can be investigated in steady-state saturation spectroscopy (SSSS).[15] However in SSSS the contribution of the coherence and of the level population are mixed in the same signal. This may present difficulties of interpretation when coherence and level populations are both sensitive to the velocity changing effect. In contrast in CRSF the occurence of distinct echoes enables one to separate the coherence and the level population signals.

In order to illustrate the physics involved in collisional Doppler dephasing, we adopt a simple model with the following features: (i) binary foreign-gas collisions in the impact approximation, (ii) equal natural decay and inelastic collisional rates for levels 1 and 2 (Ref. 16), (iii) inelastic collisions that can be accounted for by one rate constant Γ_1 for all density matrix elements, and (iv) short-pulse times $ku\tau \ll 1$ such that all velocity subclasses are equally excited.[17] With these assumptions we need consider only elastic collisions and do so using three collision models.[18]

(a) In the first model, collisions are assumed to produce only instantaneous phase changes on atomic coherences. This model is valid generally for

electronic and vibrational transitions.[18] For echoes driven by coherences, the effect of collisions is to replace γ_{12} by a collision broadened Γ_{12} and Δ by a collisionally shifted Δ' giving a maximum echo amplitude

$$\mathcal{E}_{\max}(t_1+nT) = (-)^n 4\pi kl \int dv_z\, N_0(v_z) \times J_{n+1}(2\chi\tau_0) J_n(2\chi\tau_1) \times e^{-\Gamma_1(1+n)T} e^{-\Gamma_{12}(1+n)T} \cos\Delta' T . \quad (12)$$

For echoes driven by populations, the Doppler phase factor $\exp\int_0^T inkv_z\,dt$ developed between t_0 and t_1 by the nth harmonic (n even), must be averaged over velocity-changing collisions. Following Ref. 4, one can obtain

$$\mathcal{E}_{\max}(t_1+nT) = (-)^n 4\pi kl \int dv_z\, N_0(v_z) J_{n+1}(2\chi\tau_0) \times \tfrac{1}{2}\sum_i J_n(2\chi\tau_1) e^{-\Gamma_1(1+n)T} e^{-\gamma T} e^{-\Gamma_{12}nT} \times \begin{cases} \exp[-\alpha\Gamma_i(nk\Delta u)^2T^3], & nk\Delta uT \ll 1, \\ \exp(-\Gamma_i T), & nk\Delta uT \gg 1, \end{cases} \quad (13)$$

where Γ_i is the state i elastic collision rate, Δu is the rms change in velocity per collision and α is a constant of order unity which depends on the specific collision kernel describing the collisions.[19] Thus, one can probe elastic velocity-changing collisions with this method by studying the maximum echo amplitude of even harmonics as a function of pulse separation T. Note the possibility of a different functional dependence on T for even and odd harmonics.

(b) In the second collision model, valid generally for rotational and some vibrational transitions, collisions are assumed to be velocity changing in their effect on coherences.[18] In this model, the elastic scattering amplitudes are identical for levels 1 and 2; a state independent collision interaction can lead only to velocity changes (no instantaneous phase changes) associated with level coherences. Collisions affect populations and coherences in the same manner in this model, resulting in a maximum echo amplitude depending on an average of

$$\exp\left(in\int_0^T kv_z\,dt - i\int_T^{(n+1)T} kv_z\,dt\right)$$

over collisions, and given by[4,19]

$$\mathcal{E}_{\max}(t_1+nT) = (-)^n 4\pi kl \int dv_z N_0(v_z) J_{n+1}(2\chi\tau_0) J_n(2\chi\tau_1) e^{-\Gamma_1(1+n)T} e^{-\gamma_{12}nT} \left(\frac{1-(-)^n}{2}\cos\Delta T e^{-\gamma_{12}T} + \frac{1+(-)^n}{2} e^{-\gamma T}\right) \times \begin{cases} \exp[-\alpha\Gamma(nk\Delta u)^2T^3(1+n)], & nk\Delta uT \ll 1, \\ \exp[-\Gamma(1+n)T], & nk\Delta uT \gg 1, \end{cases} \quad (14)$$

where n is even or odd.

(c) A modified collision model, valid for collision interactions that are nearly state independent allows for both a velocity change and small phase shift to occur in level coherences as a result of a collision. This model, which may be valid for some vibrational transitions, can be described by replacing γ_{12} and Δ appearing in Eq. (14) by collisionally modified values Γ_{12} and Δ'. It should be noted that even small collisional shifts may be important in high precision spectroscopy.

An examination of Eqs. (13) and (14) reveals the special functional dependence on T in the factor which comes from velocity changes in small angle scattering. Thus CRSF could be very useful to extract this latter effect from the background of other collisional contributions (inelastic collisions, phase-interrrupting collisions, strong collisions). Photon echo in traveling waves has already proved useful for that purpose[4] but, as it has been said previously, coherences only may be probed using classical photon echoes, while CRSF allows a study of collisional effects on level populations as well. The same possibility of studying small velocity changes is also present in time resolved saturation spectroscopy[1,4] but the signal is then an intricate mixture of contributions from both coherences and level populations. An alternative method for studying the effects of velocity-changing collisions on level populations using stimulated photon echoes has recently been reported.[20]

ACKNOWLEDGMENTS

One of us (J.L.L.G.) is grateful to New York University for welcoming him for a stay during which this work was prepared. Support was received from the U. S. Office of Naval Research and the New York University Challenge Fund.

APPENDIX A: SOLUTION OF THE EQUATIONS OF MOTION

The first step is to solve the nonstationary equations of motion in the presence of a permanent standing-wave field. We seek a solution to describe the evolution of the system within a short time τ after the field has been switched on assuming the following conditions

$$|\Delta|\tau \ll 1, \quad \gamma_{ij}\tau \ll 1.$$

Starting with Eqs. (1), and using the new variables

$$\tilde{\rho}_{12} = \rho_{12}e^{i\omega t}, \quad D = \tilde{\rho}_{12} - \tilde{\rho}_{21},$$
$$S = \tilde{\rho}_{12} + \tilde{\rho}_{21}, \quad N = \rho_{22} - \rho_{11}, \tag{A1}$$

we obtain the set of equations:

$$\dot{N} + v_z \frac{\partial}{\partial z} N = 2i\chi D \sin kz, \tag{A2a}$$

$$\dot{D} + v_z \frac{\partial}{\partial z} D = 2i\chi N \sin kz, \tag{A2b}$$

$$\dot{S} + v_z \frac{\partial}{\partial z} S = 0. \tag{A2c}$$

The spatial derivative is eliminated by substitution using Fourier-series developments for the variables N, D, S:

$$\dot{N}_n + inkv_z N_n = \chi(D_{n-1} - D_{n+1}), \tag{A3a}$$
$$\dot{D}_n + inkv_z D_n = \chi(N_{n-1} - N_{n+1}), \tag{A3b}$$
$$\dot{S}_n + inkv_z S_n = 0, \tag{A3c}$$

where the Fourier components are defined by

$$A = \sum_{n=-\infty}^{\infty} A_n e^{inkz}, \quad A = D, S, N, \tag{A4}$$

at $t = t_0$, $D_0 = 0$, and $N_0 \neq 0$. It then follows from Eqs. (A3), that N_n is nonzero for even n only and D_n is nonzero for odd n only. Consequently, Eqs. (A3a) and (A3b) may be written in the form

$$\dot{y}_n + inkv y_n = \chi(y_{n-1} - y_{n+1}), \tag{A5}$$

where $y_n = N_n$ for even n and $y_n = D_n$ for odd n. The y_n may be regarded as the components of a vector Y which can be expanded on a basis of eigenvectors of Eq. (A5). The components x_n of an eigenvector X associated with the eigenvalue λ satisfy

$$\dot{x}_n = \lambda x_n$$

and we obtain the system of linear equations

$$(\lambda + inkv)x_n = \chi(x_{n-1} - x_{n+1}). \tag{A6}$$

Equation (A6) may be solved by a method analogous to that used by Feldman and Feld.[21] One sets

$$x_n = (-i)^n C_\nu(\zeta), \tag{A7}$$

with $\nu = n - i\lambda/kv_z$ and $\zeta = 2\chi/kv_z$, which transforms Eq. (A6) into

$$C_{\nu+1} + C_{\nu-1} = (2\nu/\zeta)C_\nu. \tag{A8}$$

The general solution of this system is

$$C_\nu(\zeta) = AJ_\nu(\zeta) + BJ_{-\nu}(\zeta), \tag{A9}$$

where the J_ν's are Bessel functions. In terms of the initial variables we obtain

$$x_n = (-i)^n\left[A(\lambda, \chi, kv_z, t)J_{n-i\lambda/kv_z}\left(\frac{2\chi}{kv_z}\right) + B(\lambda, \chi, kv_z, t)J_{-n+i\lambda/kv_z}\left(\frac{2\chi}{kv_z}\right)\right].$$

Since there is no damping in the initial equations, we retain only the purely imaginary eigenvalues in (A6). An even more-restrictive condition on the eigenvalues is placed by requiring $x_n \to 0$ as $n \to \infty$ for convergence of series (A4). Since $J_\nu(z)$ diverges when $n \to -\infty$ and ν is not an integer, we keep λ such that $i\lambda/kv_z$ is an integer. Thus the general solution for $y_n(t)$ given as a linear combination of the $x_n(t)$ is

$$y_n(t) = (-i)^n \sum_{p=-\infty}^{+\infty} a_p(\chi, kv_z) \times J_{n+p}\left(\frac{2\chi}{kv_z}\right)e^{ipkv_z(t-t_0)}. \tag{A10}$$

In order to express $y_n(t)$ in terms of initial conditions, Eq. (A10) is inverted at $t = t_0$, using the closure relation of Bessel functions[22]

$$\sum_{m=-\infty}^{+\infty} J_m(r)J_{m'}(r) = \delta_{m,m'}, \tag{A11}$$

to obtain

$$a_p(\chi, kv_z) = \sum_m J_{m+p}\left(\frac{2\chi}{kv_z}\right)y_m(t_0)i^m. \tag{A12}$$

Substituting Eq. (A12) into (A10) and using the summation formula for Bessel functions[22]

$$e^{im(\tau/2-\phi/2)}J_m\left(2\tau\sin\frac{\phi}{2}\right) = \sum_{s=-\infty}^{+\infty} J_s(\tau)J_{s+m}(\tau)e^{is\phi}, \tag{A13}$$

we finally obtain

$$y_n(t) = \sum_m y_m(t_0)e^{-i(n+m)(kv_z/2)(t-t_0)} \times J_{n-m}\left(\frac{4\chi}{kv_z}\sin\frac{kv_z(t-t_0)}{2}\right). \tag{A14}$$

This solution is equivalent to that obtained in Appendix B by directly integrating Eqs. (A2). One notes that the nth harmonic is driven by all mth harmonics present at t_0.

This result enables us to calculate the polarization of the gas sample after a sequence of two square pulses. At t_0, the only nonzero spatial component is $N_0 = y_0$. The external field is on until $t_0 + \tau_0$. At this time the atomic spatial components are

$$y_n(t_0+\tau_0) = N_0(t_0) e^{-inkv_z\tau_0/2} J_n\left(\frac{4\chi}{kv_z}\sin\frac{kv_z\tau_0}{2}\right),$$

$$S_n = 0.$$

Following the pulse, the atoms evolve freely, and obey the equations:

$$\begin{aligned} &\dot N_n + inkv_z N_n + \gamma N_n = 0, \\ &\dot D_n + inkv_z D_n + \gamma_{12} D_n = i(\omega-\omega_0) S_n, \\ &\dot S_n + inkv_z S_n + \gamma_{12} S_n = i(\omega-\omega_0) D_n, \end{aligned} \tag{A15}$$

where, for sake of simplicity, we have assumed that $\gamma_{11} = \gamma_{22} = \gamma$. At time t_1, the solutions are

$$\begin{aligned} N_n(t_1) &= N_n(t_0+\tau_0)\exp[-\gamma(t_1-t_0) - inkv_z(t_1-t_0)], \\ D_n(t_1) &= D_n(t_0+\tau_0)\cos(\omega-\omega_0)(t_1-t_0) \\ &\quad\times\exp[-inkv_z(t_1-t_0-\tau_0) - \gamma_{12}(t_1-t_0)], \\ S_n(t_1) &= iD_n(t_0+\tau_0)\sin(\omega-\omega_0)(t_1-t_0) \\ &\quad\times\exp[-inkv_z(t_1-t_0-\tau_0) - \gamma_{12}(t_1-t_0)]. \end{aligned} \tag{A16}$$

The field is switched on from t_1 to $t_1+\tau_1$, and $y_n(t_1+\tau_1)$ can be determined from Eq. (A14) using initial conditions (A16). Following this pulse the system evolves freely until time t according to Eqs. (A15).

At time t, one must calculate

$$\bar P(v_z, t) = 2\frac{k}{\pi}\int_0^{\pi/k} P(v_z, z', t) \times \sin kz'\,dz', \tag{A17}$$

where

$$\begin{aligned} P(v_z, z, t) &= \mu(\rho_{12}+\rho_{21}) \\ &= \mu(S\cos\omega t - iD\sin\omega t). \end{aligned} \tag{A18}$$

Substituting (A18) into (A17) and using the Fourier expansions of D and S, one finds

$$\bar P(v_z, t) = \bar P_c(v_z, t)\cos\omega t + \bar P_s(v_z, t)\sin\omega t, \tag{A19}$$

where

$$\bar P_c(v_z, t) = i\mu(S_1 - S_{-1})$$

and

$$\bar P_s(v_z, t) = \mu(D_1 - D_{-1}).$$

The quantities $S_{\pm1}, D_{\pm1}$ calculated by the procedure above are

$$\begin{aligned} D_{\pm1} &= N_0\cos[\Delta(t-t_1)](A_\pm\cos\Delta T e^{-\gamma_{12}T} + B_\pm e^{-\gamma T}), \\ S_{\pm1} &= iN_0\sin[\Delta(t-t_1)](A_\pm\cos\Delta T e^{-\gamma_{12}T} + B_\pm e^{-\gamma T}), \end{aligned} \tag{A20}$$

where[23]

$$\left.\begin{aligned} A_\pm &= \sum_{\text{odd } n} \\ B_\pm &= \sum_{\text{even } n} \end{aligned}\right\} (-)^{\frac{n\pm1}{2}} J_{\frac{n\pm1}{2}}\left(\frac{4\chi}{kv_z}\sin\frac{kv_z\tau_1}{2}\right) J_n\left(\frac{4\chi}{kv_z}\sin\frac{kv_z\tau_0}{2}\right) \times\exp\left[-ikv_z\left(nT\pm(t-t_1) - \frac{n}{2}(\tau_0-\tau_1)\pm\frac{\tau_1}{2}\right) - \gamma_{12}(t-t_1)\right]. \tag{A21}$$

Using the symmetry properties of the Bessel functions one finds the echo amplitude

$$\mathcal{E}(t) = 2\pi kl\int dv_z[\bar P_c(v_z,t)^2 + \bar P_s(v_z,t)^2]^{1/2} = 4\pi kl\int dv_z N_0(v_z)[A\cos(\Delta T)e^{-\gamma_{12}T} + Be^{-\gamma T}], \tag{A22}$$

where

$$\left.\begin{aligned} A &= \sum_{\text{odd } n} \\ B &= \sum_{\text{even } n} \end{aligned}\right\} (-)^n J_{\frac{n\pm1}{2}}\left(\frac{4\chi}{kv_z}\sin\frac{kv_z\tau_1}{2}\right) J_n\left(\frac{4\chi}{kv_z}\sin\frac{kv_z\tau_0}{2}\right) \times\cos\left\{kv_z\left[n\left(T-\frac{\tau_0-\tau_1}{2}\right) - \left(t-t_1+\frac{\tau_1}{2}\right)\right]\right\}\exp-\gamma_{12}(t-t_1). \tag{A23}$$

APPENDIX B

In Appendix A we solved the equations in a manner that exhibits the successive echoes which are associated with the Fourier components of the solution. The equations may also be solved directly to exhibit the motion of a group of atoms starting at (v_z, z_0, t_0). Adding Eqs. (A2a) and (A2b) term to term, we obtain

$$\dot{y} + v_z \frac{\partial y}{\partial z} = 2i\chi y \sin kz , \tag{B1}$$

where

$$y = N + D . \tag{B2}$$

Changing variables (z, t) to $(x = z - v_z t, t)$ one gets

$$\frac{\partial y}{\partial t} = 2i\chi y \sin k(x + v_z t) . \tag{B3}$$

The integration leads to

$$y(x, t) = y(x, t_0) \times \exp\left(2i\chi \int_{t_0}^{t} \sin k(x + v_z t')\, dt'\right), \tag{B4}$$

where

$$x = z - v_z t = z_0 - v_z t_0 .$$

With a boundary value condition at (z_0, t_0), one obtains

$$y(z_0 + v(t - t_0), t) = y(z_0, t_0) \exp\left(2i\chi \int_{t_0}^{t} \sin k(z_0 + v_z(t' - t_0))\, dt'\right).$$

As an atom experiences the field $\chi(z_0, t' - t_0) = \chi \sin k(z_0 + v_z(t' - t_0))$ at time t', the integral in (B5) can be understood as an average over the field amplitude along the atomic path during the pulse.

Thus we get

$$(t - t_0)\langle \chi(z_0, t' - t_0)\rangle_{t_0 \to t} = \chi \int_{t_0}^{t} \sin k(z_0 + v_z(t' - t_0))\, dt'$$

and

$$N(z_0 + v(t - t_0), t_0) = N(z_0, t_0) \cos[2(t - t_0)\langle \chi(z_0, t' - t_0)\rangle] - D(z_0, t_0) \sin[2(t - t_0)\langle \chi(z_0, t' - t_0)\rangle] ,$$

$$D(z_0 + v(t - t_0), t_0) = D(z_0, t_0) \cos[2(t - t_0)\langle \chi(z_0, t' - t_0)\rangle] + N(z_0, t_0) \sin[2(t - t_0)\langle \chi(z_0, t' - t_0)\rangle] .$$

[1] T. W. Hänsch, I. S. Shahin, and A. L. Shawlow, Phys. Rev. Lett. 27, 707 (1971); Ph. Cahuzac and X. Drago, Opt. Commun. 24, 63 (1978).

[2] R. G. Brewer and R. L. Shoemaker, Phys. Rev. A 6, 2001 (1972).

[3] J. P. Gordon, C. H. Wang, C. K. N. Patel, R. E. Slusher, and W. J. Tomlinson, Phys. Rev. 179, 294 (1969).

[4] P. R. Berman, J. M. Levy and R. G. Brewer, Phys. Rev. A 11, 1668 (1975).

[5] S. Haroche, J. A. Paisner, and A. L. Shawlow, Phys. Rev. Lett. 30, 948 (1973).

[6] J. R. R. Leite, R. L. Sheffield, M. Ducloy, R. D. Sharma, and M. S. Feld, Phys. Rev. A 14, 1151 (1976).

[7] J. C. Mac Gillivray and M. S. Feld, Phys. Rev. A 14, 1169 (1976).

[8] Ye. V. Baklanov, V. P. Chebotayev, and B. Ya. Dubetsky, Appl. Phys. 11, 201 (1976).

[9] J. C. Bergquist, S. A. Lee, and J. L. Hall, Phys. Rev. Lett. 38, 159 (1977).

[10] V. P. Chebotayev, A. V. Shishayev, B. Ya. Yarshin, and L. S. Vasilenko, Appl. Phys. 15, 43 (1978).

[11] S. N. Bagayev, V. P. Chebotayev, and A. S. Dychkov, Appl. Phys. 15, 209 (1978); V. P. Chebotayev, *ibid.* 15, 219 (1978).

[12] M. M. Salour and C. Cohen-Tannoudji, Phys. Rev. Lett. 38, 757 (1977).

[13] V. P. Chebotayev, N. M. Dyuba, M. I. Skvorstov, and L. S. Vasilenko, Appl. Phys. 15, 319 (1978).

[14] The values for $n = 1$ are close to those required to maximize the classical photon echo: $2\chi\tau_0 = \frac{1}{2}\pi$, $2\chi\tau_1 = \pi$.

[15] S. N. Bagaev, E. V. Baklanov, and V. I. Chebotayev, Zh. Eksp. Teor. Fiz. Pis'ma Red. 16, 15 (1972); 16, 344 (1972) [JETP Lett. 16, 9 (1972); 16, 243 (1972)]; P. W. Smith and T. W. Hänsch, Phys. Rev. Lett. 26, 740 (1971); C. Bréchignac, R. Vetter, and P. R. Berman, J. Phys. B 10, 3443 (1977); Phys. Rev. A 17, 1609 (1978); J. L. Le Gouët, J. Phys. B 11, 3001 (1978).

[16] Unequal decay rates are treated by A. Schenzle and R. G. Brewer [Phys. Rev. A 14, 1756 (1976)].

[17] Longer pulses lead to a modification of the maximum echo amplitude through Eq. (9) and to the possibility that collisions can remove atoms from the limited velocity classes excited by a long pulse. The collisional effect can be compensated for by an appropriate increase in Γ_1.

[18] P. R. Berman, Appl. Phys. (Germany) 6, 283 (1975).

[19] For weak velocity-changing collisions $\alpha = \frac{1}{8}$. [Note: Δu in Ref. 4 $= \sqrt{2}\,(\Delta u)$ of this work.] For weak collisions, an expression for the entire range of $nk\Delta uT$ [see Ref. 4; and A. Flusberg, Opt. Commun. (to be published)] may be obtained. Expressions of the form

$$\exp\left(i n \int_{\tau_1}^{\tau_2} k v_z dt\right)$$

lead to an echo contribution going as

$$\exp\left[-\int_0^{\tau_2-\tau_1}\left(\Gamma-\int W(v'\to v)\exp[ink(v-v')t]\,dv'\right)dt\right],$$

where $W(v'\to v)$ is the collision kernel. This equation provides the limits shown in Eqs. (13) and (14).

[20]T. Mossberg, A. Flusberg, R. Kachru, and S. R. Hartmann, Bull. Am. Phys. Soc. 24, 25 (1979).

[21]B. J. Feldmann and M. S. Feld, Phys. Rev. A 1, 1375 (1970).

[22]I. S. Gradshteyn and I. M. Ryzhik, *Table of Integrals Series and Products* (Academic, New York, 1965).

[23]It follows from Eqs. (A19)–(A21) that for short excitation pulses ($ku\tau \ll 1$), the echo frequency is ω_0. This result differs from that for optical Ramsey fringes in which the emission always occurs at frequency ω (Refs. 11 and 13).

Theory of Collisionally Aided Radiative Excitation in Three-Level Systems: A New Interference Effect

S. Yeh and P. R. Berman
Department of Physics, New York University, New York, New York 10003
(Received 23 May 1979)

Collisionally aided radiative excitation in a three-level atomic system is investigated with use of a stationary-phase method for the case of large atom-field detunings and weak incident fields. It is found that collision-induced coherent phase-interference effects can give rise to oscillatory structure in the total absorption cross section as a function of relative speed (energy). An example is given for a specific interatomic potential, indicating that experimental observation of such an effect is feasible.

The theory of saturation spectroscopy has led to an understanding of the physical processes that occur when two nearly resonant radiation fields are incident on a three-level atomic system. Collisional effects have been incorporated,[1] but such calculations have generally been limited to the impact region (|field detunings| ≪ inverse collision time). Although calculations *not* restricted to the impact approximation have been carried out for two-level systems,[2] there is, to our knowledge, only one calculations of collisionally aided radiative excitation (CARE, often referred to as "optical collision") in the nonimpact limit for three-level systems.[3] This calculation was done using an effective two-level method and had serious restrictive conditions on the detunings.

In this Letter we report on a new type of quantum interference effect that occurs in three-level atomic systems subject to both collisions and off resonant (|field detunings| ≫ inverse collision time) radiation fields. This effect results from an interference between contributions to the transition amplitudes from the various collision-induced crossings of the dressed atomic states[4] (see Fig. 1). When the crossings are well separated, the effect manifests itself as an oscillation in the total cross section as a function of active-atom–perturber relative speed (energy). An analogous oscillatory feature was discussed by Rosenthal and Foley for charge-exchange inelastic collisions[5,6] in a He-He$^+$ system which is characterized by atom-ion interatomic-potential curves similar to those in Fig. 1. However, there is an important difference between the two. In charge-exchange inelastic collisions, the collision-induced crossings (or lack thereof) are completely determined by the atom-ion interatomic potentials. In CARE, on the other hand, the crossings are *additionally* dependent on the field detunings since they affect the dressed-atom level spacings.[7] Consequently, the nature and positions of the crossings may be altered in CARE (by varying the detunings) but not in charge-exchange inelastic collisions. This feature of CARE allows us to gain information on the diatomic systems which would be otherwise difficult to obtain.[8]

The system consists of a three-level active atom (levels labeled 1, 2, and 3) undergoing transitions from state 1 to state 3, simultaneously subjected to the collision of a structureless perturber and to two external fields of amplitudes E and E', frequencies ω and ω'. Fields E and E' drive only 1-2 (frequency ω_{21}) and 2-3 (frequency ω_{32}) transitions, respectively, their interaction being characterized by the detunings $\Delta = \omega - \omega_{21}$, $\Delta' = \omega' - \omega_{32}$, and the coupling strengths $\chi = \mu E/2\hbar$ and $\chi' = \mu' E'/2\hbar$, where μ and μ' are the 1-2 and 2-3 dipole matrix elements. The collision is as-

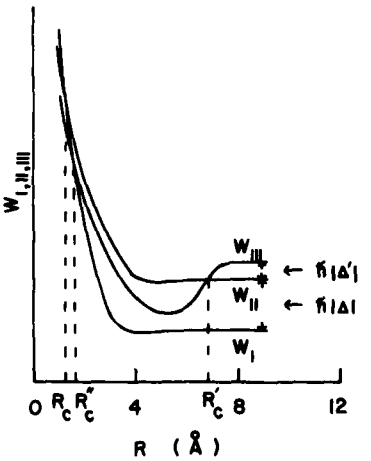

FIG. 1. Collisionally modified dressed-state energies W_I, W_{II}, and W_{III} of a three-level active atom and applied fields as a function of internuclear separation R, in the weak-field limit. The energies $\hbar|\Delta|$ and $\hbar|\Delta'|$ set the energy scale; $\Delta = -8\times10^{13}$ sec^{-1} and $\Delta' = -3\times10^{13}$ sec^{-1}.

Supported by [illegible] Office of Naval Research under Contract No. N00014-77-C-0553.

sumed to only shift the energies of the atomic levels without coupling them.

Figure 1 shows the system in a dressed-atom diabatic representation for some particular interatomic potentials and atom-field detunings; the atom-field dressed states are labeled I, II, and III. The existence of crossings and their relative positions depend on the interatomic potential as well as the detunings.[9] Various crossing situations may occur, leading to different features in the absorption cross section. We chose to focus our attention on the case when the detunings are large ($|\Delta|, |\Delta'| \gg$ inverse collision time), when the field strengths are weak ($\chi \ll |\Delta|$, $\chi' \ll |\Delta'|$), and when there are three well-separated crossings, since an interesting interference phenomenon emerges under these conditions.

To better understand this interference effect, we use a time-dependent classical-trajectory description of the collision event. For large detunings, states II and III can be excited directly from initial state I only at the crossing positions labeled by R_c and R_c'', respectively, in Fig. 1. In the time domain, the R_c and R_c'' crossings occur at corresponding times $\pm\tau_c$ and $\pm\tau_c''$ provided that the impact parameter is such that the distance of closest approach in the collision is less than the smaller of R_c and R_c''. Between their creation at times $\pm\tau_c$, $\pm\tau_c''$, and the crossing at time τ_c' (corresponding to internuclear distance R_c'), the amplitudes of states II and III evolve adiabatically with phases given by $\exp[-i\int_{\pm\tau_c}^{\tau_c'} W_{II}(R(t))dt]$ and $\exp[-i\int_{\pm\tau_c}^{\tau_c'} W_{III}(R(t))dt]$, where W_{II} and W_{III} are the collisionally modified energies shown in Fig. 1. At τ_c' transitions between states II and III are possible, and for times greater than τ_c' the amplitude of state III again evolves adiabatically.

Thus, there are four paths for excitation to state III, two from direct excitation I → III at $\pm\tau_c''$, the other two from stepwise excitation I → II → III at $(\pm\tau_c, \tau_c')$, with each contributing to the probability amplitude. The cross term in the state-III excitation probability contains six oscillatory terms varying as $\sin(\Delta\varphi_i)$, $i = 1, \ldots, 6$. Only one of these phases, $\Delta\varphi_1 \sim \int_{\tau_c}^{\tau_c'} W_{II}(R(t))dt - \int_{\tau_c}^{\tau_c'} W_{III}(R(t))dt$, is a slowly varying function of the impact parameter b for the system under consideration. On integrating over b to obtain the excitation cross section, this term is the only one to survive. Since $\Delta\varphi_1$ is essentially proportional to the time separation $\Delta\tau \simeq (R_c' - R_c)/v$ (v is the relative atomic speed) between the inner and outer crossings, the total cross section oscillates as a function of $1/v$. These ideas are made more quantitative by the calculation given below.

The calculation is most conveniently carried out in the "bare"-state picture. In the rotating-wave approximation and weak-field limit, the time-dependent Schrödinger equation is solved by perturbation theory to yield the following expression for the state-3 amplitude $a_3(\infty)$, using as initial conditions $a_1(-\infty) = 1$, $a_2(-\infty) = a_3(-\infty) = 0$,

$$a_3(\infty) = -\chi\chi' \int_{-\infty}^{\infty} \exp\{-i[\Delta' t - \int_0^t V'(\tau)d\tau]\} \int_{-\infty}^{t} \exp\{-i[\Delta t_1 - \int_0^{t_1} V(\tau)d\tau]\} dt_1\, dt, \tag{1}$$

where V and V' are defined by $V(t) = V_2(t) - V_1(t)$ and $V'(t) = V_3(t) - V_2(t)$, with $V_i(t)$ ($i = 1, 2, 3$) the collision-induced shift in energy of level i [$V_{1,2,3}(R) = W_{I,II,III}(R) + C_{1,2,3}$, where C_i's are constants]. Because of the condition that |field detunings| ≫ inverse collision time, we have neglected any Doppler phase shifts or level decays in Eq. (1).

Assuming that transitions occur only near the crossings, we use a stationary-phase method to evaluate Eq. (1). For $R_c < R_c'' < R_c'$, the result is

$$|a_3(\infty)|^2 = A_S + A_D + A' \tag{2}$$

with

$$A_S = (\chi\chi' 2\pi)^2 (1 + s\sin 2\varphi)/2\alpha\alpha', \tag{3}$$

$$A_D = (\chi\chi' \pi)^2 (f^2 + g^2)[1 + s''\sin 2(\varphi'' - s\theta)]/\alpha\alpha'', \tag{4}$$

$$A' = -s\frac{(\chi\chi'\pi)^2}{\alpha}\left(\frac{2(f^2+g^2)}{\alpha'\alpha''}\right)^{1/2} \{\sin[\varphi + \varphi' - \varphi'' + (s + s' - s'')\pi/4 + s\theta] + \sin[\varphi + \varphi' + \varphi'' + (s + s' + s'')\pi/4 - s\theta]$$
$$+ \sin[\varphi' + \varphi'' - \varphi + (s' + s'' - s)\pi/4 - s\theta]$$
$$+ \sin[\varphi' - \varphi'' - \varphi + (s' - s'' - s)\pi/4 + s\theta]\}, \tag{5}$$

where α, α', and α'' are one-half of the absolute values of the time derivatives of $V(t)$, $V'(t)$, and $V''(t) = V(t) + V'(t)$, respectively, evaluated at τ_c, τ_c', and τ_c'', respectively, with the signs of these derivatives given by s, s', and s'', respectively, f and g are the auxiliary functions of Fresnel integrals[10] with argument given by $|(2\alpha/\pi)^{1/2}(\tau_c'' - \tau_c)|$, and $\theta = \tan^{-1}(g/f)$.

The phases φ, φ', and φ'' can be written in a time-independent form; $\varphi = (1/v)\int_b^{R_c} \{[V(R) - \Delta]/(R^2 - b^2)^{1/2}\} RdR$, where b is the impact parameter. Expressions for φ' and φ'' are of the same form with R_c, $V(R)$, and Δ replaced by R_c', $V'(R)$, Δ' and by R_c'', $V''(R)$, and Δ'', respectively. The only phase appearing in Eqs. (2)–(5) which is a slowly varying function of b is the one associated with the first term in A' since $\varphi + \varphi' - \varphi''$ leads to integrals with limits independent of b (θ is slowly varying in b). On integrating Eqs. (2)–(5) over b to get the total cross section, the sine function in this term survives and oscillates as a function of $1/v$.

Equations (2)–(5) are poor approximations near the impact parameter at which incoming and outgoing crossings coalesce, i.e., $b \approx R_c$. To obtain an accurate cross section, one must integrate the time-dependent Schrödinger equation numerically near such impact parameters. However, a first approximation is achieved by assuming that all the sine terms in Eqs. (3)–(5) average to zero on integrating over b *except* the one varying as $\sin[\varphi + \varphi' - \varphi'' + (s + s' - s'')\pi/4 + s\theta]$. In this term the phase is evaluated at $b = 0$ and the cross section is than approximated as $\sigma \simeq 2\pi \int_0^{R_c} |a_3(\infty)|^2 b\, db$, yielding

$$\sigma \simeq \frac{(\chi\chi'\pi)^2 R_c}{v^2 |(dV/dR)_{R_c}|} \left\{ \frac{4R_c'}{|(dV'/dR)_{R_c'}|} \ln \frac{R_c' + R_c}{R_c' - R_c} + \frac{2R_c''(f^2+g^2)}{|(dV''/dR)_{R_c''}|} \ln \frac{R_c'' + R_c}{R_c'' - R_c} - 2s\left[\frac{2R_c' R_c''(f^2+g^2)}{|(dV'/dR)_{R_c'}(dV''/dR)_{R_c''}|}\right]^{1/2} \ln \frac{R_c' + R_c'' + 2R_c}{R_c' + R_c'' - 2R_c} \sin(A/v + \varphi_0) \right\}, \quad (6)$$

where A is the area enclosed by the three crossing points and $\varphi_0 = (s + s' - s'')\pi/4 + s\theta$ is a constant phase. A comparison of this cross section with the corresponding one obtained from computer solutions indicates that Eq. (6) is accurate to within 15%.

The calculation of cross section using Eq. (6) is remarkably simple. For given potential curves and detunings, one can graphically obtain the slopes at the crossing point and the area A enclosed by the crossing points. Substitution of these values into Eq. (6) yields σ. The CARE cross section for the interatomic potential shown in Fig. 1 as a function of $1/v$ is shown in Fig. 2. The range of speed varies from 10^5 cm sec^{-1} to 4×10^5 cm sec^{-1}. By varying the detunings, one can change A as well as the slopes at crossing points, and hence the frequency and amplitude of the oscillation in the total cross section. Although the example above is for a specific potential, we emphasize that the oscillatory feature occurs regardless of the form of the potential as long as three conditions are satisfied: first, there must be three crossings as in Fig. 1; second, the area enclosed by the crossings must be large enough to produce a phase change of the order π when the speed is varied in a convenient range; and third, the stepwise and the direct excitation contributions must be comparable. The first condition allows for a phase factor that is nearly b independent, and the second and the third conditions determine the frequency and amplitude of the oscillatory term.

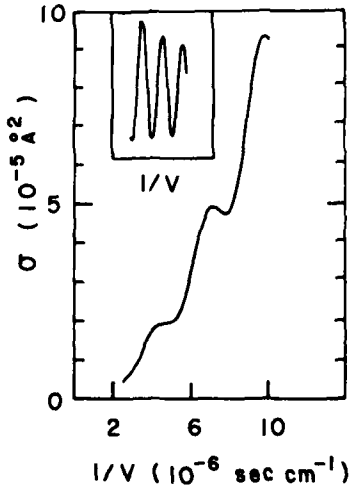

FIG. 2. Total excitation cross section as a function of inverse relative speed v for a potential shown in Fig. 1 with $\chi = \chi' = 10^{11}$ sec^{-1}, $\Delta = -8\times10^{13}$ sec^{-1}, and $\Delta' = -3\times10^{13}$ sec^{-1}. The curve rises as v^{-2}. As the speed varies from 10^5 cm sec^{-1} to 4×10^5 cm sec^{-1}, equally spaced peaks are clearly seen. In the inset, the product of the total cross section and v^2 is shown as a function of $1/v$.

For the potential and detunings shown in Fig. 1, the excitation cross sections are of the order of $10^{-34} II'$ cm^2, with I and I' the power density given in W/cm^2. Thus the effect should be observable with moderate laser power. The experiment must be performed with use of crossed atomic beams or a beam interacting with a gas sample. The beam-gas sample method works only if the active-atom–perturber relative velocity is approximately equal to the beam velocity.

This work was supported by the U. S. Office of Naval Research through Contract No. N00014-77-C-0553. Conversations with Professor E. J. Robinson are acknowledged.

---

[1]P. R. Berman, in *Advances in Atomic and Molecular Physics*, edited by D. R. Bates and B. Bederson, (Academic, New York, Vol. 13, 1977, pp. 57–112 and references therein.

[2]An extensive list of papers, books, and reviews regarding radiative collision and optical collision for all limits including impact and nonimpact regions can be found in a recent review. See S. I. Yakovlenko, Sov. J. Quantum Electron. 8, 151 (1978).

[3]M. H. Nayfeh, unpublished.

[4]Dressed states are the eigenstates of the active-atom–external-field system. See C. Cohen-Tannoudji, *Cargèse Lecture in Physics* (Gordon and Breach, New York, 1968), Vol. 2, p. 347.

[5]H. Rosenthal and H. M. Foley, Phys. Rev. Lett. 23, 1480 (1969); H. Rosenthal, Phys. Rev. A 4, 1030 (1971).

[6]S. H. Dworetsky and R. Novick, Phys. Rev. Lett. 23, 1484 (1969).

[7]The dressed states and their spacings depend also on the field strengths. In this Letter, the discussion is confined to the weak-field limit.

[8]Similar ideas have been suggested in J. I. Gersten and M. H. Mittleman, J. Phys. B 9, 383 (1976).

[9]For large field intensities, crossings will disappear. See, for example, S. Yeh and P. R. Berman, Phys. Rev. A 19, 1106 (1979).

[10]Equations (7.3.9) and 7.3.10) in M. Abramowitz and I. A. Stegun, *Handbook of Mathematical Functions* (Dover, New York, 1972), p. 301.

Collisional Effects in the Saturation Spectroscopy of Three-Level Systems: Theory and Experiment

P.R. Berman[1]

Physics Department, New York University, New York, NY 10003, USA

and

P.F. Liao and J.E. Bjorkholm

Bell Telephone Laboratories, Holmdel, NY 07733, USA

We report on a theoretical and experimental study of the influence of collisions on the saturation spectroscopy line shapes associated with three-level gas vapor systems. The study is carried out with the goal of gaining new information concerning (a) the collisional processes that occur in atomic vapors, (b) the nature of the interatomic potential between a ground state and an excited-state atom and (c) the possibility of collision-induced enhancement of the absorption of radiation by an atomic system. In each of these areas, new results are obtained.

Theory Using a model in which collisions are assumed to be phase-interrupting in their effect on level coherences and velocity-changing in their effect on population densities, we calculate the absorption profiles associated with three-level atoms that are subjected to two incident radiation fields while undergoing collisions with structureless perturber atoms. One of the fields (pump) is of arbitrary strength and acts on a given transition while the other field (probe) is weak and acts on a transition sharing a common level with the first. In the absence of collisions, the probe absorption profile can exhibit many well-known features [1], including narrow Doppler-free resonances and strong-pump field induced ac Stark splittings. Collisions distort these profiles and can actually lead to enhanced probe absorption in cases of either large pump detunings or strong pump fields. Moreover the collisional modifications of the profiles may be used to extract information on both total and differential scattering cross sections. Theoretical profiles illustrating these features have been derived.

Experiment The theory is applied to explain the $3S_{1/2}\rightarrow 3P_{1/2}\rightarrow 4D_{3/2}$ excitation spectra that we have obtained for Na atoms undergoing collisions with foreign gas perturbers. A pump laser is detuned either 4.0 GHz or 1.6 GHz below the $3S_{1/2}\rightarrow 3P_{1/2}$ transition frequency and a probe laser beam, counter-propagating with the first, completes transitions to the $4D_{3/2}$ state. The population of the $4D_{3/2}$ state is monitored (via fluorescence) as a function of probe frequency for pump detunings of -4.0 GHz and -1.6 GHz, using various pressures of He, Ne, and Kr perturbers. With a pump detuning of -4.0 GHz, which is greater than the Doppler width ≈1.6 GHz, we are able to systematically study collisional redistribution [2] (resulting from

[1] Supported by the U.S. Office of Naval Research.

Supported by the U.S. Office of Naval Research under Contract No. N00014-77-C-0553.

collisionally-induced excitation of the $3P_{1/2}$ state) and to obtain a fit to theory containing essentially no free parameters. For a detuning of -1.6 GHz, the pump laser excites a given longitudinal velocity class of atoms. Velocity-changing collisions cause this velocity group to relax back towards equilibrium, and the probe absorption monitors the progress of this relaxation. Attempts to fit the data were made using both the Keilson-Storer and classical hard sphere collision kernels to describe the velocity-changing collisions. The theory includes the effects of $3P_{1/2} \rightarrow 3P_{3/2}$ state-changing collisions, which significantly modify the excitation line shapes.

References

1 See, for example, I.M. Beterov and V.P. Chebotaev, Prog. Quantum Elec. 3, 1 (1974) and references therein.

2 D.L. Huber, Phys. Rev. 178, 93 (1969); A. Omont, E.W. Smith and J. Cooper, Astrophys. J. 175, 185 (1972).

PHYSICAL REVIEW A VOLUME 20, NUMBER 4 OCTOBER 1979

Study of collisional redistribution using two-photon absorption with a nearly-resonant intermediate state

P. F. Liao and J. E. Bjorkholm
Bell Telephone Laboratories, Holmdel, New Jersey 07733

P. R. Berman
Physics Department, New York University, New York, New York 10003

(Received 11 April 1979)

The authors report studies of collision-induced features of the $3S_{1/2} \rightarrow 3P_{1/2} \rightarrow 4D_{3/2}$ two-photon absorption in atomic-sodium vapor undergoing collisions with several rare-gas perturbers. The results yield the collisional redistribution function which describes the nonresonant excitation of the $3P_{1/2}$ intermediate state. Good agreement with theory is obtained only if effects of $3P_{1/2} \leftrightarrow 3P_{3/2}$ state-changing collisions are included in the calculations. Results are used to obtain a value for a pressure-broadening coefficient in the Na–Kr system.

The spectrum of light scattered by an atomic vapor illuminated by nearly resonant radiation has attracted considerable interest.[1-6] Experiments have been reported in which narrow-band laser radiation is scattered by an atomic or molecular vapor.[3-6] For a two-level system, low laser intensities, and radiation tuned outside the Doppler width of the transition, the scattered-light spectrum is found to contain two components. One component is centered at the incident laser frequency and is due to Rayleigh scattering. The second component is found to be centered at the frequency of the atomic resonance line and has a pressure-dependent intensity which vanishes in the absence of collisions. The appearance of this component at the frequency of the resonance transition is known as collisional redistribution. In this paper we report measurements of the collisional-redistribution function which are made in absorption rather than in emission. Two-photon absorption spectra are obtained with two cw dye lasers operating at different frequencies. The absorption is measured as the frequency of one laser is scanned. The resulting line shape contains two components which are similar in nature to the two components found in emission experiments. One component is a collision-induced signal corresponding to the collisional redistribution; it results from the collisionally aided excitation of the nonresonant intermediate state followed by the subsequent absorption of a photon which causes a transition to the final state. The second component is due to direct two-photon transitions from the ground state to the excited state and is analogous to the Rayleigh scattering observed in emission. The redistribution process which we observe is important to problems of radiative energy transport.[7] It must also be included to correctly analyze line-shape experiments which probe velocity-changing collisions.[8,9]

The theory of spectral redistribution of scattered light in the impact approximation is well developed.[1,2,10] In this approximation the detuning of the incident light from the resonance must be much less than $2\pi/\tau_c$, where τ_c is the duration of a collision. Recent experiments have investigated various aspects of collisional redistribution. The first experimental evidence appears to have been obtained by Rousseau *et al.*,[5] although they were not able to completely resolve the various components. More recently the resonance scattering from sodium in high-pressure helium was found to exhibit complete collisional redistribution.[6] Carlsten *et al.*[3,4] have made investigations in the regime where the laser detuning is large and the impact approximation is not valid. In our work we use two-photon spectroscopy to examine in detail the redistribution function in the impact regime for sodium atoms undergoing collisions with rare-gas perturbers. To our knowledge this work represents the only study which measures both the shape and amplitude of the collisional redistribution; furthermore, it demonstrates the importance of state-changing collisions on the redistribution. The theory of the effect of collisions on two-photon line shapes has been discussed (see Ref. 10, and references therein) and our results are found to be in good agreement with these theories if the theory is extended to include the effects of fine-structure state-changing collisions. An experiment which demonstrated the different time dependences of the two components we have observed in two-photon absorption has been reported by Grischkowsky.[11]

Our experimental apparatus[12] consists of two cw single-mode frequency-stabilized dye lasers (Coherent 599) whose unfocused output beams were passed in opposing directions through a 1-

Supported by [illegible] of Naval Research under Contract No. [illegible]-77-C-0503.

cm-long cell at 200 °C containing sodium vapor. Both laser beams were linearly polarized in the same direction and had intensities of about 1 W/cm^2. The sodium-vapor density was maintained at approximately 10^{11} cm^{-3}. The pressure of rare gas introduced into the cell was measured with a capacitance manometer. One dye laser was held at a fixed frequency Ω nearly resonant with, but outside the Doppler width of, the $3S_{1/2} - 3P_{1/2}$ transition (~5896 Å) while the other frequency Ω' (~5682 Å) was scanned to complete transitions to the $4D_{3/2}$ state. Transitions to $4D_{5/2}$ are extremely weak and can be neglected in comparison to those to $4D_{3/2}$ since the nearly resonant $3P_{1/2}$ intermediate state enhances only transitions to $4D_{3/2}$. The population of the $4D_{3/2}$ state is monitored by observing the ~330-nm fluorescence which occurs when the $4D_{3/2}$ state decays via the $4P$ state back to the ground state.

Figure 1 illustrates spectra obtained in our experiment for various pressures of neon gas. Similar data was obtained with helium and krypton. The fixed-frequency laser is set 4.0 GHz below the $3S_{1/2}$ $(F=2) - 3P_{1/2}$ transition frequency. Three distinct lines are readily identified. The two narrow lines correspond to direct two-photon transitions from the two hyperfine states of the ground state to the $4D_{3/2}$ final state. These lines are nearly Doppler free because the excitation is made with oppositely propagating waves with nearly

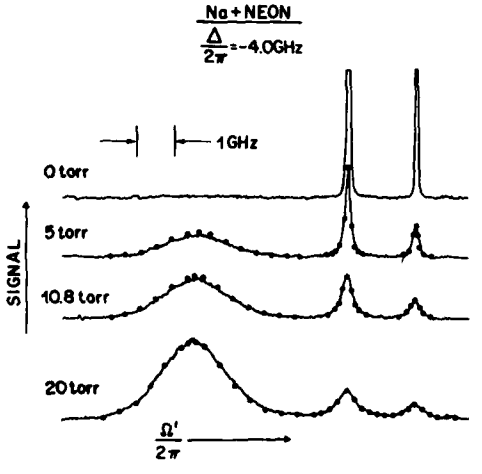

FIG. 1. Two-photon excitation spectra of the sodium $3S_{1/2}$-$4D_{3/2}$ transition at various pressures of neon perturber gas. The detuning of the fixed frequency laser from intermediate-state resonance is $\Delta/2\pi = -4.0$ GHz. The broad resonance is centered near the $3P_{1/2} - 4D_{3/2}$ transition frequency. All spectra taken with the same detection sensitivity. Solid line, experimental curve; points, theory.

the same frequency.[12] The broad line is the collision-induced signal. As shown in Fig. 1, it vanishes in the absence of buffer gas; this collisional-redistribution signal increases as the buffer-gas pressure increases.

The source of the redistribution signal is collisionally induced population of the $3P_{1/2}$ state. Collisions can supply the energy to compensate for the mismatch between $\hbar\Omega$ and the energy of the resonant transition. The excitation of the intermediate state is essentially velocity independent and hence the redistribution component is broad with a width which is dominated by the Doppler width of the $3P_{1/2}$-$4D_{3/2}$ transition. For a more detailed discussion of the origin of the redistribution component, see, for example, Ref. 10 or 13.

Collision-induced transfer of population between various sublevels within the $3P_{1/2}$ state does not affect our signals because with linearly polarized light the total excitation transition rate from each sublevel to the $4D_{3/2}$ level is the same. The field at Ω can create coherence between the $F=2$, $M_F = \pm 1$ and $F=1$, $M_F = \pm 1$ levels of the $3P_{1/2}$ state but these coherences contribute negligibly to our signal. Thus it is only the total population of the $3P_{1/2}$ state that enters in calculating the redistribution signal.

For a three-level system the line shapes and relative amplitudes of the redistribution and two-photon resonances can be approximated by the following expressions.[10] The narrow two-photon resonance is proportional to

$$\rho_{33} \approx C \frac{k}{|k'-k|}\left(\frac{ku}{\Delta}\right)^2 Z_i\left(\frac{i\tilde{\eta}_{13}}{|k'-k|u}\right) \tag{1}$$

and the redistribution term is proportional to

$$\rho_{33} \approx C\left(\frac{k}{k'}\right)\left(\frac{ku}{\Delta}\right)^2\left(\frac{2\tilde{\gamma}_{12}}{\gamma_{2eff}} - 1\right) Z_i\left(\frac{i\tilde{\eta}_{23}}{k'u}\right), \tag{2}$$

where $\tilde{\eta}_{13} = \tilde{\gamma}_{13} + i(\Delta + \Delta')$, $\tilde{\eta}_{23} = \tilde{\gamma}_{23} + i\Delta'$ and $\Delta = \Omega - \omega$, $\Delta' = \Omega' - \omega'$. The angular frequencies ω and ω' are the transition frequencies of the ground-to-intermediate and intermediate-to-final state, respectively. The wave vectors are $k' = \Omega'/c$ and $k = \Omega/c$, the subscripts 1, 2, and 3 refer to the ground, intermediate, and final states, respectively, and u is the most probable speed. The decay rates $\tilde{\gamma}_{ij}$ are the phenomenological decay constants of the density matrix elements ρ_{ij} and include the effects of phase-changing collisions. The quantity $Z_i(u)$ is the imaginary part of the plasma-dispersion function defined in Appendix A, and C is a constant of proportionality.[14] One may deduce the following useful information from these formulas: (i) the two-photon resonances are narrow, (ii) the redistribution peak (centered at

$\Delta' = 0$) is Doppler broadened, (iii) the ratio of the amplitudes of the broad to narrow resonances is independent of Δ and depends on pressure only, and (iv) the amplitude of the redistribution term vanishes in the limit of zero pressure where $2\tilde{\gamma}_{12} = \gamma_{2\text{eff}}$.

The effect of fine-structure state-changing collisions is quite important as it modifies the amplitude of the collisional-redistribution signals by a significant amount. The $3P_{1/2} \rightarrow 3P_{3/2}$ state-changing collisions must be included since they give rise to appreciable relaxation for atoms in the $3P_{1/2}$ state. By solving the rate equations for the steady-state we find these collisions produce an effective decay rate for the intermediate state (see Appendix B) of

$$\gamma_{2\text{eff}} = \gamma_2 \frac{\gamma_2 + 1.5\gamma_t}{\gamma_2 + 0.5\gamma_t}, \tag{3}$$

where γ_2 is the natural decay rate of the $3P_{1/2}$ state equal to 6.3×10^7 sec^{-1} and γ_t is the rate of transfer for $3P_{1/2} \rightarrow 3P_{3/2}$. This rate is proportional to pressure and is calculated from measured cross sections.[15,16] The effect of state-changing collisions on collisional redistribution in emission has recently been theoretically treated by Copper and Ballagh.[17]

Equations (1) and (2) are valid in the impact limit with $|\Delta| \gg ku$. To achieve greater accuracy in our calculations we have used more general expressions given in the Appendix A. This Appendix also contains a method for including the contributions of both hyperfine ground-state levels.

The points in Fig. 1 show our theoretically calculated values for the line shape. The relative amplitudes of the two narrow two-photon transitions were adjusted to exactly match the experimental data. This adjustment was required because of optical pumping effects which cause the population of the ground hyperfine states to vary slightly with pressure and laser intensity. Except for this adjustment no other free parameters are taken in the calculation. The values used for the collisional rate coefficients are given in Table I and are taken from the literature. The theory accurately predicts the amplitudes and widths of lines in the observed spectra at all pressures. To illustrate the importance of accounting for the fine-structure state-changing collisions, we indicate in Fig. 2 the theoretical result at 10.8 Torr of neon that would be obtained if these state changes were neglected. The effect of the state-changing collisions is to distribute the energy among all the fine-structure states with the result that the redistribution peak is lowered by a factor of 2.5. The correction varies up to a factor of 3 depending on the pressure, and for all pressures greater than about 1 Torr, gives rise to a substantial modification to the theory.

TABLE I. Broadening coefficients (MHz/Torr) at 200 °C.

Perturber	$\frac{1}{2\pi}\left(\frac{d\tilde{\gamma}_{12}}{dP}\right)$	$\frac{1}{2\pi}\left(\frac{d\tilde{\gamma}_{23}}{dP}\right)$	$\frac{1}{2\pi}\left(\frac{d\tilde{\gamma}_{13}}{dP}\right)$	$\frac{1}{2\pi}\left(\frac{d\gamma_t}{dP}\right)$
He	6.2 [a]	21 [c]	23 [d]	6.0 [e]
Ne	3.7 [a]	11 [c]	13 [d]	2.4 [e]
Kr	12 [b]	27 [c]	29 [d]	2.7 [e]

$\gamma_2/2\pi = 10$ MHz; $\gamma_3/2\pi = 3.2$ MHz; $\gamma_1/2\pi = 0.0$ MHz

$\tilde{\gamma}_{ij} = \frac{\gamma_i + \gamma_j}{2} + \frac{d\tilde{\gamma}_{ij}}{dP} P$

[a] D. G. McCartan and J. M. Farr, J. Phys. B 9, 985 (1976).

[b] This work.

[c] J. F. Kielkopf and R. B. Knollenberg, Phys. Rev. A 12, 559 (1975).

[d] F. Biraben, B. Cagnac, E. Giacobino, and G. Grynberg, J. Phys. B 10, 2369 (1977).

[e] Reference 15.

The results with other rare gases such as helium and krypton were similar to those obtained with neon. Figure 3 shows some typical line shapes obtained with helium and krypton. The agreement for collisions with helium is excellent with all relaxation rates calculated from published values. To our knowledge no published values for the pressure dependence of $\tilde{\gamma}_{12}$ exists for the sodium-krypton system so the theoretical points for krypton in Fig. 3 represent a fit to our experimental data. The pressure broadening coefficient obtained by this fit is

$$\frac{1}{2\pi}\left(\frac{d\tilde{\gamma}_{12}}{dP}\right) = 12.0 \pm 2 \frac{\text{MHz}}{\text{Torr}}.$$

The dependence of the amplitude of the redis-

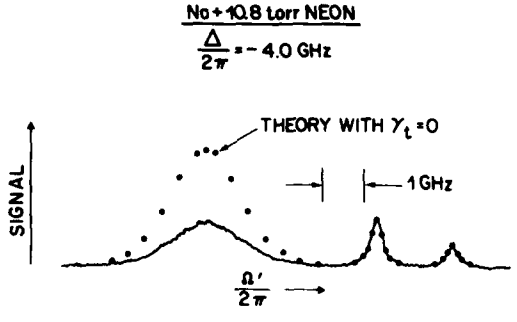

FIG. 2. Comparison of experimental excitation spectra with theoretical line shape that neglects fine-structure state-changing collisions in the $3P$ states.

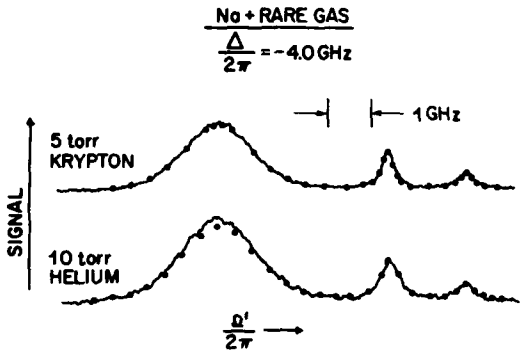

FIG. 3. Same as Fig. 1 except with helium and krypton perturbers. Detection sensitivity differs for these curves.

tributed component on laser detuning is shown in Fig. 4. The solid line is theoretical and assumed contributions from both ground hyperfine levels but does not account for optical pumping. The agreement is excellent. The ratio of the redistribution amplitude to the amplitudes of the narrow two-photon resonances was found to be essentially independent of detuning in accordance with theory.

We have experimentally verified the predictions of the theory of collisional redistribution and two-photon absorption in the impact regime. Comparisons of the experimental line shapes reveal good agreement with a theory having essentially no adjustable parameters. The importance of state-changing collisions on the redistribution has been demonstrated for the first time. We have used our measurements to obtain the broadening coefficient of the sodium resonance line for collisions with krypton. It should be noted that essentially all the relaxation parameters of an atomic system could have been obtained by these experiments. The widths of the two-photon resonances yield $\tilde{\gamma}_{13}$, the width of the redistribution component yields $\tilde{\gamma}_{23}$, and its amplitude is dependent on $\tilde{\gamma}_{12}$ and γ_t. The good agreement between the amplitudes and widths of the resonances in our experiment with the theory may be taken as confirmation of the broadening coefficients used in our calculation.

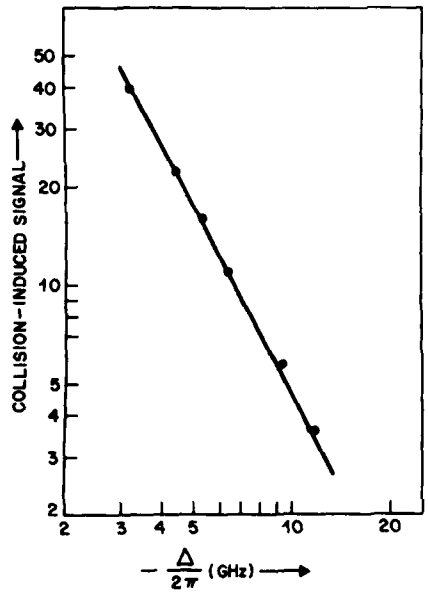

FIG. 4. Amplitude of collisional redistribution signal vs detuning, Δ. Points, experimental data; solid line, theory. Data taken with 10 Torr of neon buffer gas.

ACKNOWLEDGMENT

The research of one author (P.R.B.) was partially supported by the Office of Naval Research.

APPENDIX A: THREE-LEVEL SYSTEM LINE SHAPE

For the pump-field strength $(\chi/ku)=0.018$ (χ being the Rabi frequency at zero detuning) and detuning $|\Delta|/ku=4.0$ used in this experiment, the line shape is adequately described by the perturbation theory of Ref. 10. The result, derived for a three-level system, is

$$I=I_{TQ}+I_{SW}, \tag{A1}$$

where

$$I_{TQ}=-\frac{C}{\sqrt{\pi}}\frac{k}{k'}\frac{k}{(k'-k)}\,\mathrm{Im}\int\frac{W_0(X)dX}{(i\tilde{\eta}_{12}/ku+X)(i\tilde{\eta}_{23}/k'u-X)(i\tilde{\eta}_{13}/(k'-k)u-X)} \tag{A2}$$

and

$$I_{SW}=\frac{2C}{\sqrt{\pi}}\left(\frac{k}{k'}\right)\left(\frac{\tilde{\gamma}_{23}}{k'u}\right)\int\int\frac{\tilde{\gamma}_{12}W_0(X)G_{22}(X-X')dX\,dX'}{|i\tilde{\eta}_{12}/ku+X|^2|i\tilde{\eta}_{23}/k'u-X'|^2} \tag{A3}$$

represent the "two-quantum and "stepwise" contributions to the line shape. The variables appearing in Eqs. (A1) and (A2) are defined as follows: C is a constant proportional to the pump field intensity,

$$\tilde{\eta}_{12}=\tilde{\gamma}_{12}+i\tilde{\Delta}, \tag{A4a}$$

$$\tilde{\eta}_{23}=\tilde{\gamma}_{23}+i\tilde{\Delta}', \tag{A4b}$$

$$\tilde{\eta}_{13}=\tilde{\gamma}_{13}+i(\tilde{\Delta}+\tilde{\Delta}'), \tag{A4c}$$

with tildes indicating collisionally broadened and shifted values of the widths and detunings; the function

$$W_0(X)=\pi^{-1/2}e^{-X^2} \tag{A5}$$

is the thermal velocity distribution in dimensionless units; and $G_{22}(X-X')$ is a propagator[10] accounting for velocity-changing collisions in level 2. Equations (A2) and (A3) can be evaluated in terms of plasma-dispersion functions,[10] but asymptotic forms in the large-detuning limit are more easily obtained from the integral expressions.

One sees immediately from Eq. (A3) that the SW contribution depends on velocity-changing collisions through the propagator $G_{22}(X-X')$. However, for large detunings, $|\Delta|/ku \gg 1$, the denominator $i\tilde{\eta}_{12}/ku+X$ can be approximated by $i\Delta/ku$ over the range of X that contributes to the integral and the integral over X in Eq. (A3) is easily evaluated using the relation[10]

$$\int G_{22}(X-X')W_0(X)dX=\frac{W_0(X')}{\gamma_{2\text{eff}}}, \tag{A6}$$

where $\gamma_{2\text{eff}}$ is the effective lifetime of level 2. Equation (A6) expresses the fact that collisions do not change an equilibrium distribution. Hence, one obtains a *SW* contribution

$$I_{SW}=2C\left(\frac{k}{k'}\right)\left(\frac{\tilde{\gamma}_{12}}{\gamma_{2\text{eff}}}\right)\left(\frac{ku}{\Delta}\right)^2 Z_i\left(\frac{i\tilde{\eta}_{23}}{k'u}\right), \tag{A7}$$

where $Z_i(\mu)$ is the imaginary part of the plasma-dispersion function

$$Z(\mu)=-\pi^{-1/2}\int e^{-X^2}(\mu\pm X)^{-1}dX,$$

with $\mathrm{Im}(\mu)>0$.

Corrections to Eq. (A7) are of order $(ku/\Delta)^{-2} \approx 0.06$, and depend on the specific collision model adopted. In order to avoid specific models, we neglect all such corrections in this term. Consequently, the amplitude of the redistribution may be in error by an amount of the order of 6%. [Computer calculations using a fairly general collision model indicate that (A7) underestimates I_{SW} by 2% to 8%.]

For the TQ contribution in the limit $|\Delta|/ku \gg 1$, Eq. (A2) can be evaluated numerically for all values of Δ'. However, in the regions about the narrow resonance $\Delta' \approx -\Delta$ and the broad one $\Delta' \approx 0$, it suffices to use approximate forms. Near $\Delta' = -\Delta$, one finds, to order $(ku/\Delta)^2$,

$$I_{TQ}=\frac{Ck}{|k'-k|}\left(\frac{ku}{\Delta}\right)^2 Z_i\left(\frac{i\tilde{\eta}_{13}}{|k'-k|u}\right)\times\left[1+\left(\frac{ku}{\Delta}\right)^2\alpha\left(\frac{\tilde{\gamma}_{13}}{|k'-k|u}\right)\right] \text{ for } \Delta'\approx\Delta, \tag{A8}$$

where

$$\alpha(X)=3X^2\{[XZ_i(X)]^{-1}-1\}-\begin{cases}\frac{3}{2}(1-2/X^2) & \text{for } X\gg 1\\ 3\pi^{-1/2}X & \text{for } X\ll 1.\end{cases} \tag{A9}$$

Experimentally, $\tilde{\gamma}_{13}/(k'-k)u$ varies from 1.7 to 5.

Near $\Delta'=0$, the term is

$$I_{TQ}=-C\left(\frac{k}{k'}\right)\left(\frac{ku}{\Delta}\right)^2 Z_i\left(\frac{i\tilde{\eta}_{23}}{k'u}\right)\times\left[1+\left(\frac{ku}{\Delta}\right)^2\alpha\left(\frac{\tilde{\gamma}_{23}}{k'u}\right)\right] \text{ for } \Delta'\approx 0. \tag{A10}$$

Since $\tilde{\gamma}_{23}/ku \lesssim 1$ and $|ku/\Delta|=0.25$ for our experiment, the second term in square brackets represents a negligible correction and may be dropped.

Combining Eqs. (A8) and (A7) the line shape near $\Delta' \simeq -\Delta$ is given by

$$I=C\left(\frac{ku}{\Delta}\right)^2\left\{\frac{k}{k'-k}Z_i\left(\frac{i\tilde{\eta}_{13}}{(k'-k)u}\right)\times\left[1+\left(\frac{ku}{\Delta}\right)^2\alpha\left(\frac{\tilde{\gamma}_{13}}{(k'-k)u}\right)\right]+2\left(\frac{ku}{\Delta}\right)^2\frac{\tilde{\gamma}_{12}\tilde{\gamma}_{23}}{\gamma_{2\text{eff}}ku}\right\}, \tag{A11}$$

where we have used

$$Z_i(i\tilde{\eta}_{23}/k'u)\approx\tilde{\gamma}_{23}k'u/\Delta^2$$

in this region. Equation (A11) gives values generally a few percent less than computer evaluation of Eqs. (A2) and (A3).

In the region $\Delta' \approx 0$, one combines (A10) and (A7) to obtain the redistribution resonance

$$I=C\left(\frac{k}{k'}\right)\left(\frac{ku}{\Delta}\right)^2\left(\frac{2\tilde{\gamma}_{12}}{\gamma_{2\text{eff}}}-1\right)Z_i\left(\frac{i\tilde{\eta}_{23}}{k'u}\right). \tag{A12}$$

In the actual experimental situation, there are two hyperfine levels in the ground state separated by 1.77 GHz. The total line shape depends on contributions from both of these levels. The detuning for transitions originating from the $F=2$ state is Δ while that from the $F=1$ state is Δ_2, where

$\Delta_2/2\pi = \Delta/2\pi - 1.77$ GHz. The net modification of the line shape is the replacement of the factors $(ku/\Delta)^2$ appearing in *curly* brackets in Eqs. (A11) and (A12) by $(ku)^2(\Delta^{-2} + w\Delta_2^{-2})$, where w accounts for relative statistical weights and optical pumping of transitions originating from $F=1$ versus those originating from $F=2$. In fitting the data, w is the only adjustable parameter.

APPENDIX B: DERIVATION OF $\gamma_{2\text{eff}}$

The influence of the $3P_{3/2}$ state collisionally coupled to the $3P_{1/2}$ intermediate state can be included without much difficulty. In the perturbation limit *and* the large-pump-detuning limit, $|\Delta/ku| \gg 1$, the steady-state equations for the $P_{1/2}$ and $P_{3/2}$ population densities $n_{1/2}(v)$ and $n_{3/2}(v)$ for a ground-state density N_0 are

$$0 = -\gamma_2 n_{1/2} - \Gamma n_{1/2} + \Gamma' n_{3/2} + S, \tag{B1a}$$

$$0 = -\gamma_2 n_{3/2} - \Gamma' n_{3/2} + \Gamma n_{1/2}, \tag{B1b}$$

where

$$S = 2\chi^2 \tilde{\gamma}_{12} \Delta^{-2} u^{-1} W_0(v/u) N_0 \tag{B1c}$$

represents the pump field excitation of the $P_{1/2}$ state, and Γ and Γ' are the $\frac{1}{2} - \frac{3}{2}$ and $\frac{3}{2} - \frac{1}{2}$ collision rates, respectively. Equations (B1) reflect the fact that only the $P_{1/2}$ state is significantly pumped by the field. All effects of velocity-changing collisions are neglected in the large-detuning limit, since the intermediate-state velocity distribution is Maxwellian. Solving Eq. (B1b) for $n_{3/2}$ and substituting it into Eq. (B1a) one obtains the steady-state equation for $n_{1/2}$

$$0 = -\gamma_{2\text{eff}} n_{1/2} + S, \tag{B2}$$

where

$$\gamma_{2\text{eff}} = \gamma_2 \left(\frac{\gamma_2 + \Gamma' + \Gamma}{\gamma_2 + \Gamma'} \right). \tag{B3}$$

Thus, the net effect of the $P_{3/2}$ state can be included by replacing the decay rate γ_2 of the $P_{1/2}$ level by the $\gamma_{2\text{eff}}$ of Eq. (B3). For the $P_{1/2} - P_{3/2}$ levels, $\Gamma = 2\Gamma' \equiv \gamma_t$.

[1] D. L. Huber, Phys. Rev. 178, 93 (1969).
[2] A. Omont, E. W. Smith, and J. Cooper, Astrophys. J. 175, 185 (1972).
[3] J. L. Carlsten and A. Szöke, Phys. Rev. Lett. 36, 667 (1976); J. Phys. B 9, L231 (1976).
[4] J. L. Carlsten, A. Szöke, and M. G. Raymer, Phys. Rev. A 15, 1029 (1977).
[5] D. L. Rousseau, G. D. Patterson, and P. F. Williams, Phys. Rev. Lett. 34, 1306 (1975).
[6] R. D. Driver and J. L. Snider, J. Phys. B 10, 595 (1977).
[7] D. Mihalas, *Stellar Atmospheres* (Freeman, San Francisco, 1970), Chap. 10.
[8] C. Brechignac, R. Vetter, and P. R. Berman, Phys. Rev. A 17, 1609 (1978).
[9] P. F. Liao, J. E. Bjorkholm, and P. R. Berman (unpublished).
[10] P. R. Berman, Adv. At. Mol. Phys. 13, 57 (1977).
[11] D. Grischkowsky, Phys. Rev. A 14, 802 (1976).
[12] J. E. Bjorkholm and P. F. Liao, Phys. Rev. Lett. 33, 128 (1974); Phys. Rev. A 14, 751 (1976).
[13] E. Courtens and A. Szöke, Phys. Rev. A 15, 1588 (1977).
[14] The same constant of proportionality is used in Eqs. (1) and (2) because coherence effects are negligible. For other excitation polarizations and smaller detunings these constants may become functions of Δ and differ from each other— see, for example, B. R. Marx and L. Allen, J. Phys. B 11, 3023 (1978).
[15] J. C. Gay and W. B. Schneider, Z. Phys. A 278, 211 (1976).
[16] J. Apt and D. E. Pritchard, J. Phys. B 12, 83 (1979).
[17] J. Cooper and R. J. Ballagh, Phys. Rev. A 18, 1302 (1978).

PHYSICAL REVIEW A VOLUME 20, NUMBER 6 DECEMBER 1979

Theory of saturation spectroscopy including collisional effects

P. R. Berman
Physics Department, New York University, 4 Washington Place, New York, New York 10003

P. F. Liao and J. E. Bjorkholm
Bell Laboratories, Holmdel, New Jersey 07733

(Received 24 July 1979)

A theory of saturation spectroscopy in three-level gas-vapor systems, including collisional effects, is presented. Using a model of collisions in which they are phase interrupting in their effect on level coherences and velocity changing in their effect on level population densities, the authors calculate the absorption profile of a weak probe field on a given transition when an arbitrarily strong pump field acts on a coupled transition. Line shapes are derived for an arbitrary collision kernel describing the velocity-changing collisions, and these line shapes are evaluated for the collision kernel proposed by Keilson and Storer. Various limiting forms for the line shapes are derived and representative line shapes are displayed. Several new features of the line shapes, including collisionally induced increased probe absorption are discussed. The line shapes are seen to reflect the various collisional processes that may occur in atomic or molecular systems.

I. INTRODUCTION

The theory of saturation spectroscopy of gas vapors has received considerable attention[1-8] over the past several years, following the increased experimental activity in this field. In a typical experimental situation one uses a pump laser field to excite a given transition in an atom or molecule and then monitors the absorption of a copropagating or counterpropagating weak probe field on the same or a coupled transition. In general, only atoms having a limited range of longitudinal velocities can effectively interact with *both* the pump and the probe fields, leading to a saturation spectroscopy line shape that is essentially free of any Doppler width. The Doppler-free linewidths are of the order of the natural widths associated with atomic resonances.

Saturation spectroscopy has also proven useful for collisional studies, although this area of research is only beginning to experience significant growth. Pressure broadening and shift coefficients can be precisely determined in saturation spectroscopy experiments and these parameters are related to the total collision cross sections for the states involved in the transitions. Moreover, information on *differential* scattering cross sections may be obtained in saturation spectroscopy using a pump laser to selectively excite atoms having a specific longitudinal velocity and a second laser to probe this velocity distribution. Since collisions modify the velocity distribution, the probe absorption serves to monitor velocity-changing collision effects. In this manner, one obtains the differential scattering cross section averaged over perturber velocities and those transverse velocities of the active atoms not selected by the pump laser.

To explore fully the potential of saturation spectroscopy for collisional studies, it is useful to have a theory of the saturation spectroscopy line shape including collisional effects. Several theories exist,[6,9-16] but they have tended to be limited in one way or another. Some calculations are restricted to the weak-pump-field limit, some to the limit of decay widths and atom-field detunings much less than the Doppler width, some to the neglect of velocity-changing collisions, and some to extreme models for velocity-changing collisions. In this paper, we present a calculation of the saturation spectroscopy line shape in a three-level atomic system including collisional effects. A pump field of arbitrary strength drives a given transition and the absorption spectrum of a weak probe field on a coupled transition is derived. The calculation is based on a simple but often applicable collision model in which collisions are phase-interrupting in their effect on level coherences (off-diagonal density matrix elements) and velocity changing in their effect on level populations. The only restrictions on level widths, collision rates, and detunings are those implied by the impact approximation.[11]

In Secs. II and III, general equations are derived for the probe field absorption, and a specific calculation is carried out using the Keilson-Storer collision kernel in a large-angle-scattering limit. Limiting forms of the line shape for weak-pump fields, for large pump-field detunings, and for decay rates and detunings less than the Doppler width (Doppler limit) are given in Sec. V, and some representative line shapes are displayed in

Supported by the U.S. Office of Naval Research under Contract No. N00014-77-C-0553.

Sec. VI. An appendix generalizes the results to allow for an inelastic decay channel for the intermediate state.

The line shapes illustrated in Sec. VI contain some features that are either new or have not been emphasized in the past. Among these are (i) a relatively large dispersionlike contribution to the line shape that appears for pump-field detunings greater than the Doppler width, (ii) ac Stark splittings of the profiles in strong-pump fields for *both* copropagating and counterpropagating fields, and (iii) modifications of the strong-pump-field line profiles produced by velocity-changing collisions. An additional feature of the strong-pump-field line shapes discussed in Sec. VI is a collision-induced *increase* in both the maximum and integrated probe-field absorption. This result has implications for increasing yields in certain isotope-separation schemes utilizing lasers.

By necessity, this paper contains a large number of equations. The reader not interested in the details of the calculation can obtain the physical ideas by making reference to Secs. II A and II B and proceeding directly to Sec. VI. The theory has recently been used to explain the $3S_{1/2}$-$3P_{1/2}$-$4D_{3/2}$ excitation line shapes of Na in the presence of foreign-gas perturbers.[17]

II. PHYSICAL SYSTEM–EQUATIONS OF MOTION

A. Physical system neglecting collisions

The three-level atomic systems to be considered are shown in Fig. 1. The quantities $\beta = \pm 1$, $\beta' = \pm 1$ label each of the level configurations so that they may all be treated by a single formalism. For the upward cascade [Fig. 1(a)], $\beta = \beta' = 1$; for the inverted V [Fig. 1(b)], $\beta = 1$, $\beta' = -1$; and for the V configuration [Fig. 1(c)], $\beta = -1$, $\beta' = 1$. Each of the levels i is incoherently pumped with a rate density $\lambda_i(\vec{v})$ and each level decays at some rate γ_i, owing to spontaneous emission. The $\lambda_i(\vec{v})$ are assumed

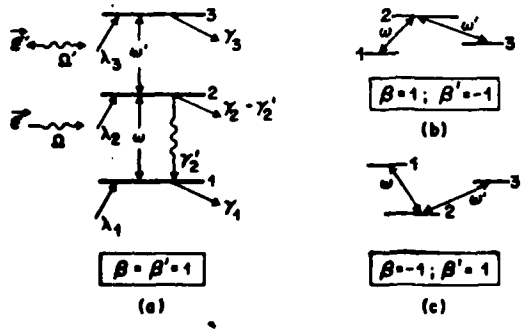

FIG. 1. Three-level systems considered in this work: (a) upward cascade, (b) inverted V, (c) V. Note that the total decay rate from level 2 is γ_2.

to produce equilibrium distributions in the absence of any fields, i.e., collisions do not alter the $\lambda_i(\vec{v})$. Levels 1 and 3 are assumed to have the same parity, which is opposite to that of level 2. The 1–2 and 2–3 transition frequencies are denoted by ω and ω', respectively. Note that it is possible to allow for any of the lowest-lying levels to be a ground state by taking the limit $\lambda_i(\vec{v}) \to 0$, $\gamma \to 0$, $\lambda_i(\vec{v})/\gamma \to N_i(\vec{v})$ (finite) for that level.

To include some effects of branching that occur in real physical systems, spontaneous emission from level 2 to level 1 at some rate γ_2' is included in the model [of course, $\gamma_2' = 0$ for the V configuration of Fig. 1(c)]. Extensions of the theory to allow for additional spontaneous-emission branching channels between the levels is straightforward.

The three-level systems are subjected to an arbitrarily strong monochromatic pump field

$$\vec{\mathcal{E}}(\vec{R}, t) = \hat{i}\,\mathcal{E}\cos(kZ - \Omega t) \tag{1a}$$

and a weak monochromatic probe field

$$\mathcal{E}'(\vec{R}, t) = \hat{i}\,\mathcal{E}'\cos(\epsilon k'Z - \Omega' t)\,, \tag{1b}$$

the fields having frequencies Ω, Ω' and propagation vectors

$$\vec{k} = \hat{Z}\Omega/c, \quad \vec{k}' = \hat{Z}\Omega'/c\,, \tag{2}$$

respectively. Our discussion is limited to the case of copropagating ($\epsilon = 1$) or counterpropagating ($\epsilon = -1$) laser fields. It is assumed that fields $\vec{\mathcal{E}}$ and $\vec{\mathcal{E}}'$ are nearly resonant with the 1–2 and 2–3 transitions, respectively. Furthermore, it is assumed that the difference $\omega - \omega'$ is large enough to insure that field $\vec{\mathcal{E}}$ drives only the 1–2 transition and $\vec{\mathcal{E}}'$ only the 2–3 transition.

The calculation is most conveniently performed using equations for density matrix elements. In the absence of collisions, the master equation for density matrix elements $\rho_{ij}(\vec{R}, \vec{v}, t)$ associated with an atomic wave packet centered at $\vec{R}$ moving with average velocity $\vec{v}$ at time t is[18]

$$\frac{\partial \rho_{ij}(\vec{R}, \vec{v}, t)}{\partial t} + \vec{v}\cdot\vec{\nabla}\rho_{ij}(\vec{R}, \vec{v}, t)$$
$$= (i\hbar)^{-1}[H(\vec{R}, t), \rho(\vec{R}, \vec{v}, t)]_{ij} - \gamma_{ij}\rho_{ij}(\vec{R}, \vec{v}, t)$$
$$+ \gamma_2'\delta_{i1}\delta_{j1}\rho_{22}(\vec{R}, \vec{v}, t) + \lambda_i(\vec{v})\delta_{ij}\,, \tag{3}$$

where

$$\gamma_{ij} = \tfrac{1}{2}(\gamma_i + \gamma_j)\,. \tag{4}$$

Matrix elements of Hamiltonian H are given by

$$H_{ij}(\vec{R}, t) = E_i\delta_{ij} - \mathcal{O}_{ij}[\mathcal{E}(\vec{R}, t) + \mathcal{E}'(\vec{R}, t)]\,, \tag{5}$$

where E_i is the energy of level i and $\mathcal{O}_{ij}$ is the x component of the dipole matrix element between states i and j.

B. Collision model

The three-level active atoms undergo collisions with ground-state perturbers. The following assumptions, pertaining to the nature of the collisions and the duration τ_c of a collision, are incorporated into the model: (i) The active-atom and perturber densities are such that one can neglect all but binary active-atom–perturber collisions. (ii) Resonant excitation-exchange collisions between active atoms and perturbers are excluded. (iii) Collisions are adiabatic in the sense that they cannot, in the absence of applied fields, induce transitions between levels 1, 2, and 3, shown in Fig. 1 (i.e., $\hbar\tau_c^{-1} \ll$ all level spacings). (iv) Collisions may be treated in the impact approximation, in which collisions can be thought to occur instantaneously with respect to various time scales in the problem (valid if $\tau_c^{-1} \gg$ atom-field detunings, Rabi frequencies, collision, and decay rates).

With these approximations, the net effect of collisions is the addition of a term $\left(\partial\rho_{ij}(\vec{R},\vec{v},t)/\partial t\right)_{\text{coll}}$ to the right-hand side of Eq. (3).[18] In general, collisions affect off-diagonal and diagonal density matrix elements differently. For diagonal elements, collisions result solely in velocity changes, and the collisional evolution of the population densities is governed by the usual transport equation:

$$\left(\frac{\partial\rho_{ii}(\vec{R},\vec{v},t)}{\partial t}\right)_{\text{coll}} = -\Gamma_i(\vec{v})\rho_{ii}(\vec{R},\vec{v},t) + \int d\vec{v}'\, W_i(\vec{v}'-\vec{v})\rho_{ii}(\vec{R},\vec{v}',t)\,, \tag{6}$$

where $W_i(\vec{v}'-\vec{v})$ is the kernel and

$$\Gamma_i(\vec{v}) = \int d\vec{v}'\, W_i(\vec{v}-\vec{v}') \tag{7}$$

is the rate for collisions in level i. One can use either classical or quantum-mechanical expressions[12] for the kernels and rates. The kernel is simply the differential scattering cross section in the center-of-mass system, averaged over the perturber velocity distribution consistent with energy and momentum conservation.

Collisional effects on off-diagonal density matrix elements are more complex. We adopt a model in which collisions are "phase interrupting" in their effect on off-diagonal density matrix elements, leading to a time rate of change

$$\left(\frac{\partial\rho_{ij}(\vec{R},\vec{v},t)}{\partial t}\right)_{\text{coll}} = -\left[\Gamma_{ij}^{ph}(\vec{v}) + iS_{ij}^{ph}(\vec{v})\right]\rho_{ij}(\vec{R},\vec{v},t), \quad i\neq j\,, \tag{8}$$

where $\Gamma_{ij}^{ph}(\vec{v})$ and $S_{ij}^{ph}(\vec{v})$ are broadening and shift parameters common to theories of pressure broadening.[9,16] The phase-interruption model is valid for either (a) a low perturber-to-active-atom mass ratio or (b) strongly state-dependent collisional interactions.[12]

In Sec. II D, a final assumption, limiting the calculation to large-angle scattering, is made. The reader not interested in the details of the lineshape calculation can proceed to Sec. III without loss of continuity.

C. Steady-state equations

Adding Eq. (6) or (8) to (3), introducing the field-interaction representations

$$\rho_{12}(\vec{R},\vec{v},t) = \tilde{\rho}_{12}(\vec{v},t)\exp\{-i\beta(kZ-\Omega t)\}\,, \tag{9a}$$

$$\rho_{23}(\vec{R},\vec{v},t) = \tilde{\rho}_{23}(\vec{v},t)\exp\{-i\beta'(\epsilon k'Z-\Omega' t)\}\,, \tag{9b}$$

$$\rho_{13}(\vec{R},\vec{v},t) = \tilde{\rho}_{13}(\vec{v},t)\exp\{-i[(\beta k+\epsilon\beta' k')Z - (\beta\Omega+\beta'\Omega')t]\}, \tag{9c}$$

$$\tilde{\rho}_{ij}(\vec{v},t) = \tilde{\rho}_{ji}(\vec{v},t)^*\,, \tag{9d}$$

$$\rho_{ii}(\vec{R},\vec{v},t) = \tilde{\rho}_{ii}(\vec{v},t)\,, \tag{9e}$$

making the rotating-wave approximation, and setting $\partial\tilde{\rho}_{ij}(\vec{v},t)/\partial t = 0$, one obtains the following steady-state equations:

$$\Gamma_1'(\vec{v})\tilde{\rho}_{11}(\vec{v}) = \int d\vec{v}'\, W_1(\vec{v}'-\vec{v})\tilde{\rho}_{11}(v') + i\chi[\tilde{\rho}_{21}(\vec{v})-\tilde{\rho}_{12}(\vec{v})] + \lambda_1(\vec{v}) + \gamma_2'\tilde{\rho}_{22}(\vec{v})\,, \tag{10a}$$

$$\Gamma_2'(\vec{v})\tilde{\rho}_{22}(\vec{v}) = \int d\vec{v}'\, W_2(\vec{v}'-\vec{v})\tilde{\rho}_{22}(v') - i\chi[\tilde{\rho}_{21}(\vec{v})-\tilde{\rho}_{12}(\vec{v})] - i\chi'[\tilde{\rho}_{23}(v)-\tilde{\rho}_{32}(\vec{v})] + \lambda_2(\vec{v})\,, \tag{10b}$$

$$\Gamma_3'(\vec{v})\tilde{\rho}_{33}(\vec{v}) = \int d\vec{v}'\, W_3(\vec{v}'-\vec{v})\tilde{\rho}_{33}(\vec{v}') + i\chi'[\tilde{\rho}_{23}(\vec{v})-\tilde{\rho}_{32}(\vec{v})] + \lambda_3(\vec{v})\,, \tag{10c}$$

$$\mu_{12}(\vec{v})\tilde{\rho}_{12}(\vec{v}) = i\chi[\tilde{\rho}_{22}(\vec{v})-\tilde{\rho}_{11}(\vec{v})] - i\chi'\tilde{\rho}_{13}(\vec{v})\,, \tag{10d}$$

$$\mu_{23}(\vec{v})\tilde{\rho}_{23}(\vec{v}) = i\chi'[\tilde{\rho}_{33}(\vec{v})-\tilde{\rho}_{22}(\vec{v})] + i\chi\tilde{\rho}_{13}(\vec{v})\,, \tag{10e}$$

$$\mu_{13}(\vec{v})\tilde{\rho}_{13}(\vec{v}) = i\chi\tilde{\rho}_{23}(\vec{v}) - i\chi'\tilde{\rho}_{12}(\vec{v})\,, \tag{10f}$$

$$\tilde{\rho}_{ij}(\vec{v}) = \tilde{\rho}_{ji}(\vec{v})^*\,, \tag{10g}$$

where

$$\mu_{12}(\vec{v}) = [\gamma_{12}+\Gamma_{12}^{ph}(\vec{v})] + i[\beta(\Delta-kv_a)+S_{12}^{ph}(\vec{v})]\,, \tag{11a}$$

$$\mu_{23}(\vec{v}) = [\gamma_{23}+\Gamma_{23}^{ph}(\vec{v})] + i[\beta'(\Delta'-\epsilon k'v_a)+S_{23}^{ph}(\vec{v})]\,, \tag{11b}$$

$$\mu_{13}(\tilde{\mathbf{v}}) = [\gamma_{13} + \Gamma_{13}^{(n)}(\tilde{\mathbf{v}})] + i[(\beta\Delta + \beta'\Delta') - (\beta k + \beta'\epsilon k')v_z + S_{13}^{(n)}(\tilde{\mathbf{v}})], \tag{11c}$$

$$\Gamma_i^t(\tilde{\mathbf{v}}) = \gamma_i + \Gamma_i(\tilde{\mathbf{v}}), \tag{12}$$

$$\chi = \mathcal{O}_{12}\mathcal{E}/2\hbar, \quad \chi' = \mathcal{O}_{23}\mathcal{E}'/2\hbar, \tag{13}$$

with the detunings Δ and Δ' defined as

$$\Delta = \Omega - \omega, \quad \Delta' = \Omega' - \omega'. \tag{14}$$

The normalization is such that $\int \rho_{ii}(\tilde{\mathbf{v}})\,d\tilde{\mathbf{v}}$ represents the total ensemble population in level i.

Typically one measures the probe-field absorption, which is equivalent to determining the value of

$$I(\Delta, \Delta') = \int d\tilde{\mathbf{v}} \left(\bar{\rho}_{33}(\tilde{\mathbf{v}}) - \frac{\lambda_3(\tilde{\mathbf{v}})}{\gamma_3}\right). \tag{15}$$

Using Eqs. (10c), (12), and (7), this equation can be rewritten

$$I(\Delta, \Delta') = -2(\chi'/\gamma_3)\,\mathrm{Im}\int d\tilde{\mathbf{v}}\,\bar{\rho}_{23}(\tilde{\mathbf{v}}). \tag{16}$$

It is sufficient to calculate $\bar{\rho}_{23}(\tilde{\mathbf{v}})$ to determine the line shape.

The solution of Eqs. (10) for $\bar{\rho}_{23}(\tilde{\mathbf{v}})$ to first order in χ' (weak probe field) and arbitrary order in χ (weak or strong pump field) is[1-3]

$$\bar{\rho}_{23}(\tilde{\mathbf{v}}) = \{-i\chi'/[\mu_{13}(\tilde{\mathbf{v}})\mu_{23}(\tilde{\mathbf{v}}) + \chi^2]\} \times \{\mu_{13}(\tilde{\mathbf{v}})[\bar{\rho}_{22}^{(0)}(\tilde{\mathbf{v}}) - \bar{\rho}_{11}^{(0)}(\tilde{\mathbf{v}})] + i\chi\bar{\rho}_{12}^{(0)}(\tilde{\mathbf{v}})\}, \tag{17}$$

where the $\bar{\rho}_{ij}^{(0)}(\tilde{\mathbf{v}})$ are solutions to Eqs. (10) with $\chi' = 0$.

It is convenient to rearrange the equations for $\bar{\rho}_{ij}^{(0)}(\tilde{\mathbf{v}})$ in order to isolate some of the strong-field effects. First, we write each $\bar{\rho}_{ii}^{(0)}(\tilde{\mathbf{v}})$ as a sum of its value $N_i(\tilde{\mathbf{v}})$ in the absence of fields plus a remainder $n_i(\tilde{\mathbf{v}})$. Explicitly, we have

$$\bar{\rho}_{ii}^{(0)}(\tilde{\mathbf{v}}) = N_i(\tilde{\mathbf{v}}) + n_i(\tilde{\mathbf{v}}), \tag{18}$$

where

$$N_1(\tilde{\mathbf{v}}) = \lambda_1(\tilde{\mathbf{v}})/\gamma_1 + \gamma_2\lambda_2(\tilde{\mathbf{v}})/\gamma_1\gamma_4,$$
$$N_2(\tilde{\mathbf{v}}) = \lambda_2(\tilde{\mathbf{v}})/\gamma_2, \tag{19}$$
$$N_3(\tilde{\mathbf{v}}) = \lambda_3(\tilde{\mathbf{v}})/\gamma_3.$$

Second, we substitute Eqs. (19) into Eqs. (10), set $\chi' = 0$, use the fact that

$$\int d\tilde{\mathbf{v}}'\,W_i(\tilde{\mathbf{v}}' - \tilde{\mathbf{v}})N_i(\tilde{\mathbf{v}}') = \Gamma_i(\tilde{\mathbf{v}})N_i(\tilde{\mathbf{v}}) \tag{20}$$

[since the $N_i(\tilde{\mathbf{v}})$ are assumed to be equilibrium distributions], and perform some algebraic manipulations on the resulting equations. Using this procedure, we obtain the following equations for $n_i(\tilde{\mathbf{v}})$ and $\rho_{ij}^{(0)}(\tilde{\mathbf{v}})$ $(i \neq j)$:

$$\Gamma_1^t(\tilde{\mathbf{v}})n_1(\tilde{\mathbf{v}}) - \int d\tilde{\mathbf{v}}'\,W_1(\tilde{\mathbf{v}}' - \tilde{\mathbf{v}})n_1(\tilde{\mathbf{v}}') = \left(\frac{2\chi^2\tilde{\gamma}_{12}(\tilde{\mathbf{v}})}{R_B(\tilde{\mathbf{v}})^2}\right)\left(1 - \frac{\gamma_2'}{\Gamma_2^t(\tilde{\mathbf{v}})}\right) \times [N_{21}(\tilde{\mathbf{v}}) + \mathfrak{F}(\tilde{\mathbf{v}})] + \left(\frac{\gamma_2'}{\Gamma_2^t(\tilde{\mathbf{v}})}\right) \times \int d\tilde{\mathbf{v}}'\,W_2(\tilde{\mathbf{v}}' - \tilde{\mathbf{v}})n_2(\tilde{\mathbf{v}}'), \tag{21a}$$

$$\Gamma_2^t(\tilde{\mathbf{v}})n_2(\tilde{\mathbf{v}}) - \int d\tilde{\mathbf{v}}'\,W_2(\tilde{\mathbf{v}}' - \tilde{\mathbf{v}})n_2(\tilde{\mathbf{v}}') = -\left(\frac{2\chi^2\tilde{\gamma}_{12}(\tilde{\mathbf{v}})}{R_B(\tilde{\mathbf{v}})^2}\right)[N_{21}(\tilde{\mathbf{v}}) + \mathfrak{F}(\tilde{\mathbf{v}})], \tag{21b}$$

$$\bar{\rho}_{12}^{(0)}(\tilde{\mathbf{v}}) = \left(\frac{i\chi\mu_{13}(\tilde{\mathbf{v}})^*}{R_B(\tilde{\mathbf{v}})^2}\right)[N_{21}(\tilde{\mathbf{v}}) + \mathfrak{F}(\tilde{\mathbf{v}})], \tag{21c}$$

$$n_3(\tilde{\mathbf{v}}) = \bar{\rho}_{23}^{(0)}(\tilde{\mathbf{v}}) = \bar{\rho}_{13}^{(0)}(\tilde{\mathbf{v}}) = 0, \tag{21d}$$

where

$$\tilde{\gamma}_{12}(\tilde{\mathbf{v}}) = \gamma_{12} + \Gamma_{12}^{(n)}(\tilde{\mathbf{v}}), \tag{22}$$

$$R_B(\tilde{\mathbf{v}})^2 = \gamma_B(\tilde{\mathbf{v}})^2 + [\Delta - kv_z + \beta S_{12}^{(n)}(\tilde{\mathbf{v}})]^2, \tag{23}$$

$$\gamma_B(\tilde{\mathbf{v}}) = \tilde{\gamma}_{12}(\tilde{\mathbf{v}})[1 + \mathcal{S}(\tilde{\mathbf{v}})]^{1/2}, \tag{24}$$

$$\mathcal{S}(\tilde{\mathbf{v}}) = \frac{2\chi^2}{\tilde{\gamma}_{12}(\tilde{\mathbf{v}})}\left[\frac{1}{\Gamma_2^t(\tilde{\mathbf{v}})} + \frac{1}{\Gamma_1^t(\tilde{\mathbf{v}})}\left(1 - \frac{\gamma_2'}{\Gamma_2^t(\tilde{\mathbf{v}})}\right)\right], \tag{25}$$

$$\mathfrak{F}(\tilde{\mathbf{v}}) = \frac{1}{\Gamma_2^t(\tilde{\mathbf{v}})}\left(1 - \frac{\gamma_2'}{\Gamma_1^t(\tilde{\mathbf{v}})}\right)\int d\tilde{\mathbf{v}}'\,W(\tilde{\mathbf{v}}' - \tilde{\mathbf{v}})n_2(\tilde{\mathbf{v}}') - \frac{1}{\Gamma_1^t(\tilde{\mathbf{v}})}\int d\tilde{\mathbf{v}}'\,W_1(\tilde{\mathbf{v}}' - \tilde{\mathbf{v}})n_1(\tilde{\mathbf{v}}'), \tag{26}$$

$$N_{ij}(\tilde{\mathbf{v}}) = N_i(\tilde{\mathbf{v}}) - N_j(\tilde{\mathbf{v}}). \tag{27}$$

Moreover, Eq. (17) may be written

$$\bar{\rho}_{23}(\tilde{\mathbf{v}}) = \{-i\chi'/[\mu_{13}(\tilde{\mathbf{v}})\mu_{23}(\tilde{\mathbf{v}}) + \chi^2]\} \times \{\mu_{13}(\tilde{\mathbf{v}})[-N_{32}(\tilde{\mathbf{v}}) + n_2(\tilde{\mathbf{v}})] + i\chi\bar{\rho}_{12}^{(0)}(\tilde{\mathbf{v}})\}. \tag{28}$$

The line shape, as determined by Eqs. (16) and (21)–(28), contains some features that may be noted at this point:

(i) Velocity-changing collisions in level 3 do not affect the line shape, a result which may be explained by the following reasoning. The probe field is weak, so that one need consider only a single probe-field-absorption process. If velocity-changing collisions in level 3 occur *before* the probe-field absorption, they do not alter the equilibrium distribution $N_3(\tilde{\mathbf{v}})$. If they occur *after* the probe-field absorption, they redistribute the velocities in level 3, but do not change the integrated population $\int \rho_{33}(\tilde{\mathbf{v}})\,d\tilde{\mathbf{v}}$, on which the line shape is dependent.

(ii) In the absence of collisions [$\mathfrak{F} = 0$, $W_i(\tilde{\mathbf{v}}$

$-\tilde{\nu})\to 0$, $\Gamma_{ij}^{ph}(\tilde{\nu})\to 0$, $S_i^{ph}(\tilde{\nu})\to 0$, $\Gamma_i'(\tilde{\nu})\to\gamma_i$], Eqs. (21) reduce to well-known equations of saturation spectroscopy.[1-8] The strong-field modification of the 1–2 absorption is contained in Eqs. (23)–(25), in which the homogeneous width γ_{12} is replaced by a power-broadened γ_B. The factor $\chi^2\tilde{\gamma}_{12}(\tilde{\nu})N_{21}(\tilde{\nu})|R_B(\tilde{\nu})|^{-2}$ appearing in Eqs. (21) represents holes or bumps created in the velocity distribution by the pump field.

(iii) One can understand the collision-induced modification of the 1–2 strong-field absorption on the basis of simply physical arguments. Phase-changing collisions are directly incorporated with the substitution $\gamma_{12}\to\tilde{\gamma}_{12}(\tilde{\nu})$, $\Delta_{12}\to\beta\Delta+S_{12}^{ph}(\tilde{\nu})$, representing the traditional pressure broadening and shifting of spectral profiles. Velocity-changing collisions in levels 1 and 2 lead to flow into and out of the velocity holes created in these population densities by the pump field. New velocity equilibrium distributions are established, as given by the solutions of Eqs. (21a) and (21b). The outward flow is contained in the $\Gamma_i'(\tilde{\nu})n_i(\tilde{\nu})$ terms in Eqs. (21a) and (21b); it is also implicitly contained in the saturation parameter $S(\tilde{\nu})$ through the presence of $\Gamma_i'(\tilde{\nu})$. The inward flow is given by the $\int d\tilde{\nu}'\,W_i(\tilde{\nu}'-\tilde{\nu})n_i(\tilde{\nu}')$ terms and the $\mathcal{F}(\tilde{\nu})$ terms in Eqs. (21a)–(21c).

D Large-angle scattering

Equations (21) are independent of the specific nature of the scattering (velocity-changing collisions) in levels 1 and 2 and could, in principle, be solved numerically for an arbitrary kernel. However, it is customary to seek approximate solutions to the equations. For weak velocity-changing collisions, $k\Delta u\gg\gamma_B$ (Δu = rms velocity change per collision), one can approximate the collision kernels as functions of $(\tilde{\nu}-\tilde{\nu}')$ and obtain solutions by Fourier-transform techniques.[5,6,9,10] Exact solutions are also obtainable[11] in the so-called "strong-collision model" in which a single collision, on average, thermalizes the velocity distribution.

For typical interatomic potentials, the collision kernels can be separated into a small-angle-scattering part accounting for the long-range part of the potential plus a large-angle-scattering (LAS) part accounting for scattering from deep attractive potential wells and/or a repulsive core. As a specific model, we will consider only the LAS part of the kernel, assuming weak collisional effects are negligible or can otherwise be incorporated into the line-shape formulas.

The kernel is defined to be a LAS one, provided

$$k\Delta u\gg\gamma_B\,. \tag{29}$$

In this limit, a single collision is sufficient to remove atoms from the velocity holes or bumps created by the fields. There is no velocity diffusion *within* a hole or bump. The $\mathcal{F}$ terms in Eqs. (21a)–(21c) represent the modifications of the bumps or holes owing to velocity-changing collisions; consequently, they should vanish in this model. An estimate of the value of $\mathcal{F}(\tilde{\nu})$ relative to $N_{21}(\tilde{\nu})$ at $\tilde{\nu}=(\Delta/k)\hat{z}$ is

$$\mathcal{F}/N_{21}\leq\pi^{1/2}\gamma_B/(k\Delta u)\,, \tag{30}$$

which will be small provided $\gamma_B/k\Delta u\ll 1$. Calculations using a more-general collision model[19] indicate that the LAS kernel provides a good approximation as long as $\gamma_B\ k\Delta u\lesssim 1$.

Thus, in the LAS model, the equations determining $n_2(\tilde{\nu})$ and $\tilde{\rho}_{12}^{(0)}(\tilde{\nu})$ needed in Eq. (28) are

$$\Gamma_2'(\tilde{\nu})n_2(\tilde{\nu})-\int d\tilde{\nu}'\,W_2(\tilde{\nu}'-\tilde{\nu})n_2(\tilde{\nu}')$$
$$=-\left(\frac{2\chi^2\tilde{\gamma}_{12}(\tilde{\nu})}{R_B(\tilde{\nu})^2}\right)N_{21}(\tilde{\nu})\,, \tag{31a}$$

$$\tilde{\rho}_{12}^{(0)}(\tilde{\nu})=\left(\frac{i\chi\mu_{12}(\tilde{\nu})^*}{R_B(\tilde{\nu})^2}\right)N_{21}(\tilde{\nu})\,. \tag{31b}$$

These equations differ from those of the weak-field case only by the presence of γ_B rather than $\tilde{\gamma}_{12}(\tilde{\nu})$ in the term for $R_B(\tilde{\nu})$.

One final separation is useful regardless of the kernel. A solution for $n_2(\tilde{\nu})$ can always be written in the form

$$n_2(\tilde{\nu})=n_2^{(0)}(\tilde{\nu})+\delta n_2(\tilde{\nu})\,, \tag{32a}$$

where

$$n_2^{(0)}(\tilde{\nu})=\frac{-2\chi^2\tilde{\gamma}_{12}(\tilde{\nu})N_{21}(\tilde{\nu})}{R_B(\tilde{\nu})^2\Gamma_2'(\tilde{\nu})} \tag{32b}$$

and $\delta n_2(\tilde{\nu})$, representing the velocity redistribution of the holes or bumps created by the pump field, satisfies

$$\Gamma_2'(\tilde{\nu})\delta n_2(\tilde{\nu})-\int d\tilde{\nu}'\,W_2(\tilde{\nu}'-\tilde{\nu})\delta n_2(\tilde{\nu}')$$
$$=\int d\tilde{\nu}'\,W_2(\tilde{\nu}'-\tilde{\nu})n_2^{(0)}(\tilde{\nu}')\,. \tag{32c}$$

III SATURATION-SPECTROSCOPY LINE SHAPE

Within the confines of the collision model adopted in Sec. II A, the probe absorption line profile is given by Eqs. (16), (28), (11), (27), (18), and (21). In saturation spectroscopy, one can arrange to detect only that part of the probe field absorption influenced by the presence of the laser-pump field. More precisely, one measures the probe-field absorption *minus* the probe-field absorption in the absence of the laser pump (i.e., $\chi=0$). De-

noting this quantity by $I_s(\Delta, \Delta')$, we find from Eqs. (16) and (18) that

$$I_s(\Delta, \Delta') = I(\Delta, \Delta') + \frac{2(\chi')^2}{\gamma_3} \mathrm{Re} \int d\vec{v} \frac{N_{12}(\vec{v})}{\mu_{23}(\vec{v})}. \quad (33)$$

To arrive at our final line-shape formula, three additional assumptions are made. First, the velocity or speed dependence of $\Gamma_{ij}^{ph}(\vec{v})$, $S_{ij}^{ph}(\vec{v})$, and $\Gamma_i(\vec{v})$ is neglected. Generally, this approximation is not drastic since these quantities are slowly varying functions of $\vec{v}$ that may be evaluated at some appropriate fixed value of $\vec{v}$ without introducing much error. *Second, it is assumed that velocity-changing collisions in level 2 are characterized by the large-angle-scattering limit discussed in Sec. II D.* Consequently, $n_2(\vec{v})$ and $\rho_{12}^{(0)}(\vec{v})$ are determined from Eqs. (31) rather than (21). Finally, the $N_{ij}(\vec{v})$ are taken to be Maxwellian:

$$N_{ij}(\vec{v}) = N_{ij}(\pi u^2)^{-3/2} \exp(-v^2/u^2). \quad (34)$$

The saturation-spectroscopy line shape is determined from Eqs. (33), (16), (28), (11), (27), (18), (31), (32), and (34). The integrals can be evaluated[7] in terms of plasma-dispersion functions and the result is conveniently separated into four terms as follows:

$$I_s(\Delta, \Delta') = I_{12}^{TQ} + I_{avc}^{SW} + I_{vc}^{SW} + I_{23}^{TQ}, \quad (35)$$

where

$$I_{12}^{TQ} = \frac{-2(\chi\chi')^2 N_{21}\theta_{12}\theta_{23}\theta_{13}}{\gamma_3 kuk'uk''u} \mathrm{Im} \sum_{j=1}^{4} A_j \tilde{Z}(r_j), \quad (36a)$$

$$I_{avc}^{SW} = \frac{4(\chi\chi')^2 N_{21}\tilde{\gamma}_{12}\theta_{23}}{\gamma_3 \Gamma_2^2 (ku)^2 k'u} \mathrm{Im} \sum_{j=1}^{4} D_j \tilde{Z}(r_j), \quad (36b)$$

$$I_{vc}^{SW} = \frac{2(\chi')^2}{\gamma_3} \mathrm{Re} \int d\vec{v} \frac{\mu_{13}(\vec{v})\delta n_2(\vec{v})}{\mu_{13}(\vec{v})\mu_{23}(\vec{v}) + \chi^2}, \quad (36c)$$

$$I_{23}^{TQ} = \frac{2(\chi')^2 N_{32}\theta_{23}}{\gamma_3 k'u} \mathrm{Im}\left(\sum_{j=1}^{2} B_j \tilde{Z}(r_j) - \tilde{Z}(r_7)\right); \quad (36d)$$

$$r_1 = r_6 + C, \quad (37a)$$

$$r_2 = r_7 - C, \quad (37b)$$

$$r_3 = i\eta_B/(k_{12}u), \quad (37c)$$

$$r_4 = -i\eta_B/(k_{12}u) = r_3^*, \quad (37d)$$

$$r_5 = i\eta_{12}^*/(k_{12}u), \quad (37e)$$

$$r_6 = -i\eta_{13}/(k_{13}u), \quad (37f)$$

$$r_7 = -i\eta_{23}/(k_{23}u), \quad (37g)$$

$$C = \frac{1}{2}\left[r_7 - r_6 - \left((r_7 - r_6)^2 + \frac{4\chi^2}{k_{13}uk_{23}u}\right)^{1/2}\right]; \quad (37h)$$

$$\eta_{12} = \bar{\gamma}_{12} + i\Delta_{12}, \quad (38a)$$

$$\eta_{23} = \bar{\gamma}_{23} + i\Delta_{23}, \quad (38b)$$

$$\eta_{13} = \bar{\gamma}_{13} + i\Delta_{13}, \quad (38c)$$

$$\eta_B = \gamma_B + i\Delta_{12}; \quad (38d)$$

$$\Delta_{12} = \beta\Delta + S_{12}^{ph}, \quad (39a)$$

$$\Delta_{23} = \beta'\Delta' + S_{23}^{ph}, \quad (39b)$$

$$\Delta_{13} = \beta\Delta + \beta'\Delta' + S_{13}^{ph}; \quad (39c)$$

$$\bar{\gamma}_{ij} = \gamma_{ij} + \Gamma_{ij}^{ph}, \quad (40a)$$

$$\gamma_B = \gamma_{12}(1+\mathcal{S})^{1/2}, \quad (40b)$$

$$\mathcal{S} = \frac{2\chi^2}{\bar{\gamma}_{12}}\left[\frac{1}{\Gamma_2^2} + \frac{1}{\Gamma_1^2}\left(1 - \frac{\gamma_2'}{\Gamma_2^2}\right)\right], \quad (40c)$$

$$\Gamma_i^2 = \gamma_i + \Gamma_i; \quad (40d)$$

$$\chi = \mathcal{P}_{12}\mathcal{E}/2\hbar; \quad \chi' = \mathcal{P}_{23}\mathcal{E}/2\hbar; \quad (41)$$

$$k_{12} = \beta k \equiv \theta_{12}k, \quad \theta_{12} = \beta, \quad (42a)$$

$$k_{23} = \epsilon\beta' k \equiv \theta_{23}k', \quad \theta_{23} = \epsilon\beta', \quad (42b)$$

$$k_{13} = \beta k + \epsilon\beta' k' \equiv \theta_{13}k'', \quad k'' = |k_{13}|, \quad \theta_{13} = k_{13}/k''; \quad (42c)$$

$$A_i = (r_5 - r_i)\left(\prod_{j=1,3;\, j\neq i} (r_j - r_i)\right)^{-1}, \quad (43a)$$

$$B_1 = (r_6 - r_1)/(r_2 - r_1), \quad B_2 = (r_6 - r_2)/(r_1 - r_2), \quad (43b)$$

$$D_i = (r_6 - r_i)\left(\prod_{j=1,4;\, j\neq i} (r_j - r_i)\right)^{-1}; \quad (43c)$$

subject to

$$\sum_{j=1}^{4} A_j = \sum_{j=1}^{4} D_j = 0, \quad B_1 + B_2 = 1. \quad (44)$$

$$N_{ij} \approx \mathrm{PD}, \quad (45)$$

where PD is the population difference between levels i and j in the absence of external fields;

$$\tilde{Z}(r) = \begin{cases} Z(r), & \mathrm{Im}\, r > 0, \\ -Z(-r), & \mathrm{Im}\, r < 0, \end{cases} \quad (46)$$

where $Z(r)$ is the plasma-dispersion function

$$Z(r) = -\pi^{-1/2} \int_{-\infty}^{\infty} dx\, e^{-x^2} (r \pm x)^{-1} \quad (47)$$

defined for $\mathrm{Im}(r) > 0$.

The terms appearing in Eq. (35) are designated as follows: (i) I_{12}^{TQ} is a two-quantum contribution to the line shape proportional to the inversion N_{21} (the label "two-quantum" is used to specify that such contributions vanish unless pump and probe fields are simultaneously present); (ii) I_{avc}^{SW} is a contribution resulting from the "stepwise" absorption of pump and probe photons by atoms that have

not undergone velocity-changing collisions in level 2; (iii) I_{vc}^{SW} is the corresponding contribution from atoms that *have* undergone velocity-changing collisions in level 2 (this term reflects the way in which the velocity holes or bumps in level 2 created by the pump field are redistributed by collisions); (iv) I_{23}^{TQ} is a two-quantum contribution to the line shape proportional to N_{32}. The labeling and interpretation of each of these terms have been given elsewhere.[11]

Equations (36a), (36b), and (36d) are easily evaluated using an efficient program for the plasma-dispersion function.[21] However, one must specify a collision kernel, $W_2(\vec{v}' - \vec{v})$ before Eq. (36c) can be calculated.

Independent of kernel, Eq. (36c) can be put in a more transparent form. It follows from Eqs. (32) that a propagator $\delta G_2(\vec{v}' - \vec{v})$, defined by

$$\delta n_2(\vec{v}) = \int d\vec{v}'\, \delta G_2(\vec{v}' - \vec{v}) n_2^{(0)}(\vec{v}') \tag{48}$$

satisfies the equation

$$\Gamma_2' \delta G_2(\vec{v}' - \vec{v}) - \int d\vec{v}''\, W_2(\vec{v}'' - \vec{v}) \delta G_2(\vec{v}' - \vec{v}'') = W_2(\vec{v}' - \vec{v}). \tag{49}$$

Using Eqs. (36c), (11), (48), (32b), (23), and (37), one can rewrite I_{vc}^{SW} in the form

$$I_{vc}^{SW} = \frac{4(\chi\chi')^2 \tilde{\gamma}_{12}\theta_{21} u^6}{\gamma_3 (ku)^2 k' u \Gamma_2'} \times \mathrm{Im} \int\int d\vec{x}\, d\vec{y}\, \frac{(x_z - r_5)\delta G_2(u\vec{y} - u\vec{x}) N_{21}(u\vec{y})}{(x_z - r_1)(x_z - r_2)(y_z - r_3)(y_z - r_4)}, \tag{50}$$

where one can readily identify (a) the original velocity distribution $N_{21}(u\vec{y})$, (b) resonance denominators with width $\mathrm{Im} r_3 = \gamma_B$ representing the 1–2 absorption by atoms having velocity $u\vec{y}$, (c) the propagator $\delta G_2(u\vec{y} - u\vec{x})$ representing the collisional redistribution of velocities from $u\vec{y}$ to $u\vec{x}$, and (d) terms representing the probe absorption from level 2 by atoms having velocity $u\vec{x}$. To evaluate Eq. (50), one must solve Eq. (49) for $\delta G_2(\vec{v}' - \vec{v})$. Although a formal quantum-mechanical expression for $W_2(\vec{v}' - \vec{v})$ is available, its evaluation presents many problems. For this reason one often attempts to approximate the true kernel by an analytically tractable phenomenological one.

IV. KEILSON-STORER KERNEL (KSK)

In this paper, we explicitly evaluate Eq. (50) for the collision kernel proposed by Keilson and Storer[22]

$$W_2(\vec{v}' \to \vec{v}) = \sqrt{2}\,(\pi\tilde{u}^2)^{-3/2} \exp(-|\vec{v} - \alpha\vec{v}'|^2/\tilde{u}^2), \tag{51a}$$

$$\tilde{u}^2 = (1 - \alpha^2)^{1/2} u, \tag{51b}$$

where Γ_2 is the collision rate and α and $\tilde{u}$ are constants. For atoms having velocity $\vec{v}'$, the average velocity following a collision is $\alpha\vec{v}'$ (this condition restricts α to values between 0 and 1) and the one-dimensional rms spread in velocities following a collision is $\tilde{u} = \sqrt{2}\,\Delta u$. For our LAS model, Eq. (29) further restricts α to values such that

$$(1 - \alpha^2)^{1/2} > \gamma_B/ku. \tag{52}$$

The Keilson-Storer kernel (KSK) adequately describes small-angle scattering.[22] Provided $v' < u$, it also describes LAS reasonably well, but is in error for both LAS and $v' \gtrsim u$.[17] The kernel has the additional advantage that it obeys detailed balance, and allows analytical solutions to be obtained.

If the KSK is inserted in Eq. (49) for the propagator, one can obtain the solution

$$\delta G_2(\vec{v}' - \vec{v}) = \sum_{n=1}^{\infty} \left(\frac{\Gamma_2}{\Gamma_2'}\right)^n \frac{1}{[\pi(\sigma_n u)^2]^{3/2}} \times \exp\left[-\left|\frac{\vec{v} - \alpha^n\vec{v}'}{\sigma_n u}\right|^2\right], \tag{53a}$$

$$\sigma_n = (1 - \alpha^{2n})^{1/2}. \tag{53b}$$

Substituting Eq. (53a) into Eq. (50), one obtains the SWvc contribution

$$I_{vc}^{SW} = \frac{4(\chi\chi')^2 N_{21}\tilde{\gamma}_{12}\theta_{21}}{\gamma_3 \Gamma_2'(ku)^2 k' u \pi^{1/2}} \sum_{n=1}^{\infty} \sum_{j=1}^{2} \left(\frac{\Gamma_2}{\Gamma_2'}\right)^n \frac{1}{\sigma_n} \mathrm{Im} \begin{cases} -B_j \left(\frac{ku}{\gamma_B}\right) \int_{-\infty}^{\infty} dx\, \frac{\exp(-x^2)}{r_j - x} Z_1\left(\frac{i\eta_B/ku + \alpha^n x}{\sigma_n}\right), & (54a) \\ \text{or} \\ B_j \int_{-\infty}^{\infty} dx\, \frac{\exp(-x^2)}{|x + i\eta_B/ku|^2} \bar{Z}\left(\frac{r_j - \alpha^n x}{\sigma_n}\right), & (54b) \end{cases}$$

where

$$Z_1(x) = \mathrm{Im}[Z(x)]; \quad Z_2(x) = \mathrm{Re}[Z(x)]. \tag{55}$$

In practice the sum may be terminated at some N for which $\alpha^N \ll 1$, and the sum from $n = N$ to ∞ explicitly evaluated. In this manner the sum from 1 to ∞ may be written

$$\sum_{n=1}^{\infty}\{\cdots\}=\sum_{n=1}^{N-1}\{\cdots\}$$

$$+\mathrm{Im}\sum_{j=1}^{2}\pi^{1/2}\left(\frac{ku}{\gamma_B}\right)B_j\mathcal{R}_N\tilde{Z}(r_j)Z_1\left(\frac{i\eta_B}{ku}\right), \tag{56a}$$

where

$$\mathcal{R}_N=(\Gamma_{22}/\Gamma_2^t)^N\Gamma_2^t/\gamma_2, \tag{56b}$$

$$\alpha^N\ll 1, \tag{56c}$$

with the sum from $n=1$ to $(N-1)$ evaluated by numerical integration. Thus, the LAS line shape for the KSK is given by Eqs. (36a), (36b), (36d) and (54), and for an arbitrary kernel by Eqs. (36a), (36b), (36d), (50), and (49).

V. LIMITING FORMS FOR THE LINE SHAPE

It is possible to obtain limiting forms for the line shape in several cases of practical interest. In this section, we give line-shape expressions valid for (a) weak-pump field, (b) large pump detuning, (c) arbitrarily strong pump field in the Doppler limit, and (d) weak pump field in the Doppler limit. The results are discussed in Sec. VI, where representative line shapes are displayed. Some of these results are not new, but are included for completeness.

A. Weak pump field

The weak-pump-field limit ($\chi\ll$ all $\tilde{\gamma}$'s) has been treated previously,[11] and may also be obtained from Eqs. (35), (36), (50), and (54) by straightforward algebra. To order χ^2, the line shape is given by

$$I_s(\Delta,\Delta')=I_{12}^{TQ}+I_{svc}^{SW}+I_{vc}^{SW}+I_{svc}^{TQ}, \tag{57a}$$

$$I_{12}^{TQ}\sim-\frac{2(\chi\chi')^2N_{21}}{\gamma_3 kuk'uk''u}\,\mathrm{Im}J_2\left(\frac{i\eta_{23}}{k'u},\frac{i\eta_{12}}{ku},\frac{i\eta_{13}}{k''u},\theta_{12}\theta_{23},\theta_{13}\theta_{23}\right), \tag{57b}$$

$$I_{svc}^{SW}\sim\frac{2(\chi\chi')^2N_{21}}{\gamma_2\Gamma_2^t kuk'u}\,\mathrm{Re}\left[I_1\left(\frac{i\eta_{23}}{k'u},\frac{i\eta_{12}^*}{ku},-\theta_{12}\theta_{23}\right)+I_1\left(\frac{i\eta_{23}}{k'u},\frac{i\eta_{12}}{ku},\theta_{12}\theta_{23}\right)\right], \tag{57c}$$

$$I_{vc}^{SW}\sim-\frac{4(\chi\chi')^2\tilde{\gamma}_{12}\tilde{\gamma}_{23}u^6}{\gamma_3\Gamma_2^t(ku)^2(k'u)^2}\int\int d\tilde{x}\,d\tilde{y}\,\frac{\delta G_2(u\tilde{y}-u\tilde{x})N_{21}(u\tilde{y})}{[(\gamma_B/ku)^2+(y_2-\theta_{12}\Delta_{12}/ku)^2]\{(\gamma_{23}/k'u)^2+(x_2-\theta_{23}\Delta_{23}/k'u)^2\}}, \quad \text{(arbitrary kernel)}, \tag{57d}$$

$$I_{vc}^{SW}\sim-\frac{4(\chi\chi')^2N_{21}}{\gamma_3\Gamma_2^t kuk'u\pi^{1/2}}\sum_{n=1}^{\infty}\left(\frac{\Gamma_2}{\Gamma_2^t}\right)^n\frac{1}{\sigma_n}\begin{cases}\displaystyle\int_{-\infty}^{\infty}dx\left(\frac{\tilde{\gamma}_{23}}{ku}\right)\frac{e^{-x^2}Z_1[(i\eta_{12}/ku+\alpha^n x\theta_{12})/\sigma_n]}{(\tilde{\gamma}_{23}/k'u)^2+(x-\theta_{23}\Delta_{23}/k'u)^2}, \\ \text{or} \\ \displaystyle\int_{-\infty}^{\infty}dx\left(\frac{\tilde{\gamma}_{12}}{ku}\right)\frac{e^{-x^2}Z_1[(i\eta_{23}/k'u+\alpha^n x\theta_{13})/\sigma_n]}{(\tilde{\gamma}_{12}/ku)^2+(x-\theta_{12}\Delta_{12}/ku)^2},\end{cases} \quad \text{(KSK)} \tag{57d'}$$

$$I_{23}^{TQ}\sim\frac{2(\chi\chi')^2N_{32}}{\gamma_3(k'u)^2k''u}\,\mathrm{Im}J_3\left(\frac{i\eta_{23}}{k'u},\frac{i\eta_{13}}{k''u},\theta_{13}\theta_{23}\right), \tag{57e}$$

where the functions I_1, I_2, and I_3 are defined by

$$I_1(\mu_1,\mu_2,\epsilon)=-M(\mu_1,\mu_2,\epsilon)[Z(\mu_1)-\epsilon Z(\mu_2)], \tag{58a}$$

$$I_2(\mu_1,\mu_2,\mu_3,\epsilon,\epsilon')=M(\mu_1,\mu_2,\epsilon)\times[I_1(\mu_1,\mu_3,\epsilon')-\epsilon I_1(\mu_2,\mu_3,\epsilon/\epsilon')], \tag{58b}$$

$$I_3(\mu_1,\mu_2,\epsilon)=-M(\mu_1,\mu_2,\epsilon)\times\{\epsilon I_1(\mu_1,\mu_2,\epsilon)+2[1+\mu_1 Z(\mu_1)]\}, \tag{58c}$$

with

$$M(\mu_1,\mu_2,\epsilon)=(\mu_2-\epsilon\mu_1)^{-1} \tag{58d}$$

and $\delta G_2(\tilde{v}'-\tilde{v})$ in Eq. (57d) is to be determined from Eq. (49).

B. Large pump detuning

In the limit of large pump detuning ($|\Delta|\gg$ all γ's, $|\Delta|\gg ku$), the SW contribution is greatly simplified. The population density $n_2(\tilde{v})$ is proportional to $N_{21}(\tilde{v})$ since each velocity subgroup is excited with equal (albeit small) probability by the off-resonant pump field. Collisions do not alter $N_{21}(\tilde{v})$; consequently the line shape in this limit is independent of velocity-changing collisions in level 2. The line shape is found to possess resonances in the regions $\Delta_{13}\approx 0$, $\Delta_{23}\approx 0$ and, in the region of these resonances, one finds[11,23]

$$I_s(\Delta,\Delta')\sim\frac{-2(\chi\chi')^2N_{21}}{\gamma_3 k''u(\Delta_{12})^2}Z_1\left(\frac{i\eta_{13}}{k''u}\right)\quad(\Delta_{13}\approx 0) \tag{59a}$$

$$\sim\frac{-2(\chi\chi')^2}{\gamma_3 k'u(\Delta_{12})^2}\left\{N_{21}\left(\frac{2\tilde{\gamma}_{12}}{\gamma_2}-1\right)Z_1\left(\frac{i\eta_{23}}{k'u}\right)+\frac{2N_{32}\Delta_{12}}{k'u}\left[\frac{\Delta_{23}}{k'u}Z_1\left(\frac{i\eta_{23}}{k'u}\right)-\frac{\tilde{\gamma}_{23}}{k'u}Z_1\left(\frac{i\eta_{23}}{k'u}\right)\right]-N_{32}\theta_{13}\theta_{23}\left(\frac{k''}{k'}\right)Z_1\left(\frac{i\eta_{23}}{k'u}\right)\right\}\quad(\Delta_{23}\approx 0). \tag{59b}$$

As has been discussed elsewhere,[11,17,24] the line shape includes collisionally aided radiative excitation of level 2. It contains a Doppler-broadened resonance at $\Delta' \approx 0$, in addition to the "direct" two-quantum resonance (which may be broad or narrow) centered near $\Delta' = -\beta\beta'\Delta$. In addition, I_{32}^{TQ} contributes a dispersionlike term near $\Delta' \approx 0$. Note that the limits on $|\Delta|$ imply that the large-pump-detuning case also satisfies the weak-pump-field criteria.

C. Arbitrarily strong pump field in the Doppler limit

The "Doppler limit" refers to the limit in which velocity-selected atoms provide the major contribution to the line shape. This limiting form for the line shape has been examined for arbitrarily strong pump fields and no collisions[1-7] or for weak pump fields including collisions,[11] but general expressions including effects of velocity-changing collisions and arbitrarily strong pump fields have not been previously obtained. The Doppler limit is achieved if *both* the homogeneous widths are smaller than the Doppler widths, i.e., $\gamma_B \ll ku$; $\gamma_{23} \ll k'u$, *and* the detunings are within the Doppler profiles, i.e., $|\Delta| < ku$; $|\Delta'| < k'u$. In the Doppler limit, only atoms having $v_z' \approx \Delta/k$, $v_z \approx \epsilon\Delta'/k'$ contribute appreciably to the line shape, and slowly varying functions of v_z' or v_z, such as the atomic-velocity distribution, can be evaluated at these values of v_z' and v_z, respectively. The Doppler-limit expressions are most conveniently calculated from Eqs. (33), (16), (28), and (32) for I_{12}^{TQ}, I_{nvc}^{SW}, and I_{23}^{TQ}, and from Eqs. (50) and (54) for I_{vc}^{SW}. One obtains the line shape in the Doppler limit for arbitrarily strong pump fields as

$$I_s(\Delta, \Delta') = I_{12}^{TQ} + I_{nvc}^{SW} + I_{vc}^{SW} + I_{23}^{TQ}, \tag{60a}$$

$$I_{12}^{TQ} \sim -[2(\chi\chi')^2 N_{21}\theta_{12}\theta_{23}\theta_{13}\pi^{1/2}/\gamma_3 kuk'uk''u]\exp[-(\Delta_{12}/ku)^2]\,\mathrm{Re}\sum_{j=1}^{4}\theta_j A_j, \tag{60b}$$

$$I_{nvc}^{SW} \sim [4(\chi\chi')^2 N_{21}\tilde{\gamma}_{12}\theta_{23}\pi^{1/2}/\gamma_3\Gamma_2'(ku)^2k'u]\exp[-(\Delta_{12}/ku)^2]\,\mathrm{Re}\sum_{j=1}^{4}\theta_j D_j, \tag{60c}$$

$$I_{vc}^{SW} \sim \frac{4(\chi\chi')^2 N_{21}\tilde{\gamma}_{12}\theta_{23}}{\gamma_3\Gamma_2'(ku)^2k'u\pi^{1/2}}\exp\left[-\left(\frac{\Delta_{12}}{ku}\right)^2\right]$$

$$\times \mathrm{Im}\begin{cases} u\int\int_{-\infty}^{\infty} dx\,dy\ \dfrac{\delta G_{2z}(uy-ux)(x-r_6)}{(x-r_1)(x-r_2)(y-r_3)(y-r_4)}, & \binom{\text{arbitrary}}{\text{kernel}}, \qquad (60d) \\ \displaystyle\sum_{j=1}^{2}\sum_{n=1}^{\infty}\int_{-\infty}^{\infty} dy\,B_j\left(\frac{\Gamma_2}{\Gamma_2'}\right)^n \frac{1}{\sigma_n}\ \frac{\tilde{Z}[(r_j-\alpha^n y)/\sigma_n]}{(\gamma_B/ku)^2+(y-\Delta_{12}\theta_{12}/ku)^2}, & \text{(KSK)}, \qquad (60d') \end{cases}$$

$$I_{23}^{TQ} \sim \frac{2(\chi')^2 N_{32}\theta_{23}\pi^{1/2}}{\gamma_3 k'u}\exp\left[-\left(\frac{\Delta_{23}}{k'u}\right)^2\right]\mathrm{Re}\left(\sum_{j=1}^{2}\theta_j B_j + \theta_{23}\right), \tag{60e}$$

where

$$\delta G_{2z}(v_z'-v_z) = \iiint\int_{-\infty}^{\infty} dv_x\,dv_y\,dv_x'\,dv_y'(\pi u^2)^{-1}\exp\left(\frac{-[(v_x')^2+(v_y')^2]}{u^2}\right)\delta G_2(\tilde{v}'-\tilde{v}), \tag{61}$$

$$\theta_j = \mathrm{sgn}[\mathrm{Im}(r_j)], \tag{62a}$$

$$\mathrm{sgn}(x) = \begin{cases} +1, & x>0, \\ -1, & x<0. \end{cases} \tag{62b}$$

Owing to Eqs. (44), it appears that I_{12}^{TQ} and I_{nvc}^{SW} can vanish if all the θ_j are equal. However, it follows from Eqs. (62), (37c), and (37d) that $\theta_1 = -\theta_1$; consequently I_{12}^{TQ} and I_{nvc}^{SW} are both nonzero in the strong-pump-field Doppler limit for *arbitrary* level schemes (i.e., arbitrary β, β', ϵ). The fact that I_{12}^{TQ} does *not* vanish in the Doppler limit for level schemes corresponding to $\theta_{12}\theta_{23} = 1$ is unique to the strong field case; as is well known,[1-8,11] it vanishes in the weak-field Doppler limit under such conditions. On the other hand, for strong pump fields (but not so strong that the Doppler limit is violated), I_{23}^{TQ} is small if $\theta_1 = \theta_2 = -\theta_{23}$, as is the case in the weak-field Doppler limit.

A further reduction of Eqs. (60d) and (60d') is possible if the *kernel* is also a slowly varying function of velocity compared with the hole width γ_B/k; i.e., if $k(\Delta u) \gg \gamma_B$ [note, our LAS model already requires $k(\Delta u) > \gamma_B$]. In that limit, the Im{··· terms in Eqs. (60d) and (60d') become

$$\mathrm{Im}\{\cdots\} = \mathrm{Im}\begin{cases} \pi \dfrac{ku}{\gamma_B}\, u \displaystyle\int_{-\infty}^{\infty} dx\, \frac{\delta G_{2s}(\Delta_{12}\theta_{12}/k - xu)(x - r_6)}{(x - r_1)(x - r_2)}, & \text{(arbitrary kernel)}, \quad (60f) \\ \pi \dfrac{ku}{\gamma_B} \displaystyle\sum_{j=1}^{2} \sum_{n=1}^{\infty} B_j \left(\frac{\Gamma_2}{\Gamma_2^t}\right)^n \frac{1}{\sigma_n} \tilde{Z}\left(\frac{r_j - \alpha^n \Delta_{12}\theta_{12}/ku}{\sigma_n}\right), & \text{(KSK)}. \quad (60f') \end{cases}$$

Moreover, if the kernel width Δu is also large compared with $\tilde{\gamma}_{23}/k'$ and $\tilde{\gamma}_{13}/k''$, this contribution further reduces to

$$\mathrm{Im}\{\cdots\} = \mathrm{Im}\left\{\pi^{3/2} \frac{ku}{\gamma_B} \sum_{j=1}^{2} B_j \theta_j \begin{cases} \pi^{1/2} u \delta G_{2s}\left(\dfrac{u\Delta_{12}\theta_{12}}{k} - u\,\mathrm{Re}(r_j)\right) & \text{(arbitrary kernel)}, \quad (60g) \\ \left(\dfrac{\Gamma_2}{\Gamma_2^t}\right)^n \sigma_n^{-1} \exp -\left(\dfrac{\mathrm{Re}\,(r_j) - \alpha^n \Delta_{12}\theta_{12}/ku}{\sigma_n}\right)^2, & \text{(KSK)}, \quad (60g') \end{cases}\right.$$

D. Weak pump field in the Doppler limit

If both the limits discussed in Secs. V A and V C are applicable, Eqs. (57) take the familiar form[1-8,11]

$$I_s(\Delta, \Delta') = I_{12}^{\mathrm{TQ}} + I_{\mathrm{nvc}}^{\mathrm{SW}} + I_{\mathrm{vc}}^{\mathrm{SW}} + I_{23}^{\mathrm{TQ}}, \quad (63a)$$

$$I_{12}^{\mathrm{TQ}} \sim -\frac{4(\chi\chi')^2 N_{21} \pi^{1/2}}{\gamma_3 kuk'uk''u} \exp\left[-\left(\frac{\Delta_{12}}{ku}\right)^2\right]\left(\frac{\tilde{\eta}_a^R \tilde{\eta}_b^R - \tilde{\eta}_a^I \tilde{\eta}_b^I}{|\tilde{\eta}_a|^2 |\tilde{\eta}_b|^2}\, \delta_{\theta_{13}\theta_{23},-1} + \frac{\tilde{\eta}_a^R \tilde{\eta}_c^R - \tilde{\eta}_a^I \tilde{\eta}_c^I}{|\tilde{\eta}_a|^2 |\tilde{\eta}_c|^2}\, \delta_{\theta_{13}\theta_{12},-1}\right)\delta_{\theta_{12}\theta_{23},-1}, \quad (63b)$$

$$I_{\mathrm{nvc}}^{\mathrm{SW}} \sim -\frac{4(\chi\chi')^2 N_{21} \pi^{1/2}}{\gamma_3 \Gamma_2^t kuk'u} \exp\left[-\left(\frac{\Delta_{12}}{ku}\right)^2\right] \frac{\tilde{\eta}_a^R}{|\tilde{\eta}_a|^2}, \quad (63c)$$

$$I_{\mathrm{vc}}^{\mathrm{SW}} \sim -\frac{4(\chi\chi')N_{21}}{\gamma_3 \Gamma_2^t kuk'u\pi^{1/2}} \exp\left[-\left(\frac{\Delta_{12}}{ku}\right)^2\right]$$

$$\times \begin{cases} \dfrac{\tilde{\gamma}_{23}}{k'u} u \displaystyle\iint_{-\infty}^{\infty} dx\, dy\, \frac{\delta G_{2s}(uy - ux)}{[(\tilde{\gamma}_{23}/k'u)^2 + (x - \theta_{23}\Delta_{23}/k'u)^2][(\tilde{\gamma}_{12}/ku)^2 + (y - \theta_{12}\Delta_{12}/ku)^2]}, & \text{(arbitrary kernel)}, \quad (63d) \\ \displaystyle\sum_{n=1}^{\infty} \left(\frac{\Gamma_2}{\Gamma_2^t}\right)^n \sigma_n^{-1} \int_{-\infty}^{\infty} dy\, \frac{Z_i(i\eta_{23}/k'u + \alpha^n \theta_{23} y)}{(\tilde{\gamma}_{12}/ku)^2 + (y - \Delta_{12}\theta_{12}/ku)^2}, & \text{(KSK)}, \quad (63d') \end{cases}$$

$$I_{23}^{\mathrm{TQ}} = \frac{4(\chi\chi')^2 N_{32} \pi^{1/2}}{\gamma_3 (k'u)^2 k''u} \exp\left[-\left(\frac{\Delta_{12}}{ku}\right)^2\right] \frac{(\tilde{\eta}_b^R)^2 - (\tilde{\eta}_b^I)^2}{|\tilde{\eta}_b|^4}\, \delta_{\theta_{13}\theta_{23},-1}, \quad (63e)$$

where

$$\tilde{\eta}_{a,b,c}^R = \mathrm{Re}\,\tilde{\eta}_{a,b,c}, \quad \tilde{\eta}_{a,b,c}^I = \mathrm{Im}\,\tilde{\eta}_{a,b,c}, \quad (64a)$$

$$\tilde{\eta}_a^R = \tilde{\gamma}_{23}/k'u + \tilde{\gamma}_{12}/ku, \quad \tilde{\eta}^I = \Delta_{23}/k'u - \mathrm{sgn}(\theta_{12}\theta_{23})\Delta_{12}/ku, \quad (64b)$$

$$\tilde{\eta}_b = \eta_{13}/k''u + \eta_{23}/k'u, \quad (64c)$$

$$\tilde{\eta}_c = \eta_{13}/k''u + \eta_{12}/ku. \quad (64d)$$

If $k(\Delta u) > \gamma_B$, the $\{\cdots$ terms in Eqs. (63d) and (63d') become

$$\{\cdots\} = \pi \frac{ku}{\tilde{\gamma}_{12}} \begin{cases} \dfrac{\tilde{\gamma}_{23} u}{k'u} \displaystyle\int_{-\infty}^{\infty} dx\, \frac{\delta G_{2s}(\Delta_{12}\theta_{12}/k - ux)}{(\tilde{\gamma}_{23}/k'u)^2 + (x - \Delta_{23}\theta_{23}/k'u)^2}, & \text{(arbitrary kernel)}, \quad (63f) \\ \displaystyle\sum_{n=1}^{\infty} \left(\frac{\Gamma_2}{\Gamma_2^t}\right)^n \sigma_n^{-1} Z_i\left[\frac{i\eta_{23} + \alpha^n \theta_{12}\theta_{23}\Delta_{12}k'/k}{k'u\sigma_n}\right], & \text{(KSK)}, \quad (63f') \end{cases}$$

and if, in addition, $k'\Delta u > \tilde{\gamma}_{23}$, they reduce to

$$\{\cdots\} = \pi^{3/2} \frac{ku}{\tilde{\gamma}_{12}} \begin{cases} \pi^{1/2} u \delta G_{2s}(\Delta_{12}\theta_{12}/k - \Delta_{23}\theta_{23}/k'), & \text{(arbitrary kernel)}, \quad (63g) \\ \displaystyle\sum_{n=1}^{\infty} \left(\frac{\Gamma_2}{\Gamma_2^t}\right)^n \sigma_n^{-1} \exp\left[-\left(\frac{\Delta_{23} - \alpha^n \theta_{12}\theta_{23}\Delta_{12}k'/k}{k'u\sigma_n}\right)^2\right], & \text{(KSK)}. \quad (63g') \end{cases}$$

VI. REPRESENTATIVE LINE SHAPES

In this section, a few representative probe-absorption-line profiles are displayed and discussed. Results are always given with either $N_{32}=0$ (giving $I_{12}^{TQ}+I_{nvc}^{SW}+I_{vc}^{SW}$, the probe absorption proportional to N_{21}) or $N_{21}=0$ (giving I_{23}^{TQ}, the probe absorption proportional to N_{32} with the linear probe absorption subtracted out). One must add the $N_{32}=0$ and $N_{21}=0$ contributions, properly weighted, to characterize the most general experimental situation, in which $N_{32}\neq 0$, $N_{21}\neq 0$. In all cases, we take $\gamma_1=0$, $\gamma_2'=\gamma_2$, $\beta=\beta'=1$ to simulate an upward cascade in which level 1 is the ground state.[25] Unless noted otherwise the following parameters are used:

$$N_{21}=-1,\quad N_{32}=0,\quad \text{or}\quad N_{21}=0,\quad N_{32}=-1,$$

$$\gamma_1=0,\quad \gamma_2=0.02,\quad \gamma'=0.02,\quad \gamma_3=0.01,$$

$$\bar{\gamma}_{12}=0.01+0.007P,$$

$$\bar{\gamma}_{23}=0.015+0.015P,$$

$$\bar{\gamma}_{13}=0.005+0.016P,$$

$$S_{12}^{ph}=S_{23}^{ph}=S_{13}^{ph}=0,$$

$$k'/k=0.4,$$

$$\Gamma_1=0.004P,\quad \Gamma_2=0.006P.$$

All frequencies are given in units of ku and P is the pressure in Torr. These parameters are typical of atom-atom collisions when levels 1, 2, and 3 are different electronic states. By restricting the discussion to $k'/k<1$, we are omitting some interesting effects[4-7] (vanishing of I_{23}^{TQ} for weak fields, modification of line splitting in strong fields). The ratio $k'/k=0.4$ is chosen to enhance the visibility of ac Stark splittings.[7]

Velocity-changing collisions are described by a KSK with

$$\alpha=0.4,\quad \bar{u}=0.93u,$$

which corresponds roughly to hard-sphere large-angle scattering by atoms of equal mass. The only remaining parameters to specify are Δ, ϵ, P and χ. The line shape $I_s(\Delta,\Delta')$, normalized to χ^2, is then displayed in the same arbitrary units.

In Fig. 2, the Doppler-limit line shapes with $N_{32}=0$ are shown as a function of χ for copropagating ($\epsilon=1$, broken line) and counterpropagating ($\epsilon=-1$, solid line) fields, $\Delta=-1$ and $P=0$. For counterpropagating fields, at low field strengths, the line is a narrow Lorentzian centered at $\Delta'=\epsilon(k'/k)\Delta=0.4$ with a half-width at half-maximum (HWHM) of η_0^R; as the field strength χ is increased such that $\chi>\gamma_{ij}$, the line splits owing to the ac Stark effect.[1-6] For copropagating fields and $\chi\ll\gamma$'s, the line is a Lorentzian centered at $\Delta'=\epsilon(k'/k)\Delta=-0.4$ with a HWHM of η_0^R that is greater

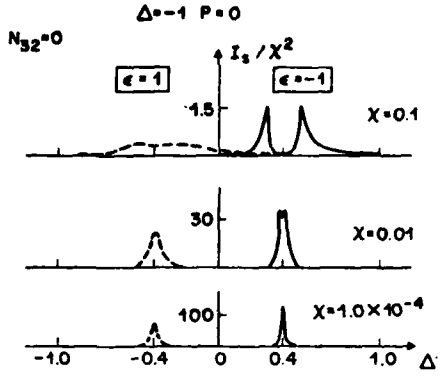

FIG. 2. Line shape $I_s(\Delta,\Delta')/\chi^2$ in arbitrary units for the case $N_{32}=0$, $\Delta=-1$, $P=0$, $\epsilon=1$ (broken line) or $\epsilon=-1$ (solid line), and several χ. All frequencies are in units of ku and P is in Torr. For values of other parameters, see the text. Note that, in all displayed line shapes, $\beta=\beta'=1$ (upward cascade).

than that of the $\epsilon=-1$ case (there is some Doppler-phase cancellation for counterpropagating fields). For sufficiently large χ, the $\epsilon=1$ line shape also exhibits ac Stark splitting. This splitting effect, which was also noted in Ref. 4, is dependent on the fact that $\gamma_2'\approx\gamma_2$; it vanishes if branching to level 1 is negligible ($\gamma_2'\ll\gamma_2$).

The $N_{21}=0$ Doppler-limit line shape is shown in Fig. 3 as a function of χ for $P=0$, $\Delta=-1$, and $\epsilon=-1$. The line shapes shown with $\chi=1.0\times10^{-4}$ and $\chi=0.01$ are typical for the case $\chi\ll ku$ which has been discussed by previous authors.[2-8] The $\chi=0.2$ line shape indicates a new feature characteristic of the case $\chi\gtrsim ku$. In this strong-field limit,

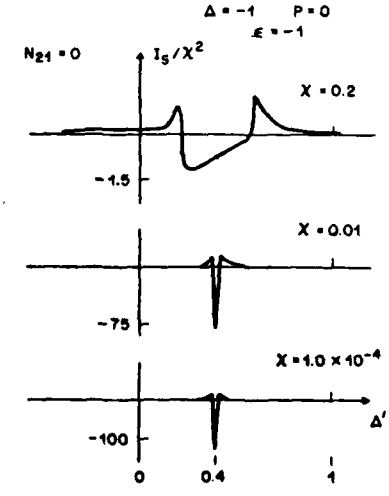

FIG. 3. Line shape for $N_{21}=0$, $\Delta=-1$, $P=0$, $\epsilon=-1$, and several χ. Units are as in Fig. 2. The same arbitrary units for I_s/χ^2 are used in all the figures.

I_{23}^{TQ} [i.e., component of $I_s(\Delta, \Delta') \propto N_{32}$] may be thought to consist of two parts. First there is an ac Stark-split profile, similar to I_{inv}^{SW} of the $N_{32} = 0$ case giving the *total* probe absorption. Then there is the linear-absorption component that must be subtracted off to give the saturation-spectroscopy profile. The linear absorption appears as the negative part of the line shape between the two peaks. As is easily derived, $\int I_{23}^{TQ}(\Delta, \Delta')\, d\Delta' = 0$.

The case of large detuning, $\Delta = -10$, is depicted in Figs. 4 and 5 for counterpropagating waves [see Eqs. (59)]. In Fig. 4, $N_{32} = 0$ and results are plotted as a function of P for $\chi = 0.01$. There is always a "direct" two-quantum resonance centered at $\Delta' = -\Delta = 10$. This component is Doppler broadened, since $k''u = (k - k')u = 0.6$. In addition, there is the broad-collisional-redistribution term centered at $\Delta' = 0$ which increases with increasing P and vanishes for $P = 0$ (the vanishing at $P = 0$ is a consequence of taking $\gamma_1 = 0$). We have recently undertaken a systematic experimental study of this effect and found good agreement with theory.[17]

In Fig. 5, $N_{21} = 0$, and one sees the dispersionlike contribution of I_{23}^{TQ}, centered near $\Delta' = 0$, predicted by Eq. (59). With increasing pressure this contribution broadens somewhat. Note that, for $\Delta = -10$, the amplitude of the dispersion term is 30 times that from the "direct" transition.

The effect of velocity-changing collisions is seen in Figs. 6 and 7 for weak and strong pump fields, respectively, with $\Delta = -1$, $\epsilon = -1$. With increasing pressure, the population density $n_2(\bar{v})$ approaches an equilibrium distribution, and the corresponding probe absorption approaches a Voigt profile centered at $\Delta' = 0$. By monitoring the line shape as a function of pressure, one can obtain information on the collision kernel giving rise to the velocity-changing collisions.

Figure 6 is applicable to the weak-pump-field limit.[11] Velocity-changing collisions remove atoms from the velocity bump created by the pump field, leading to absorption over an increased range of probe frequencies. The integrated line

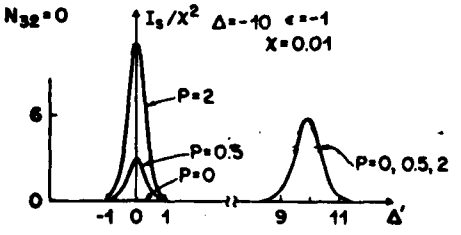

FIG. 4. Line shape for $N_{32} = 0$, $\Delta = -10$, $\epsilon = -1$, $\chi = 0.01$, and several P. The resonances centered about $\Delta' = 10$ vary only slightly in the pressure range studied.

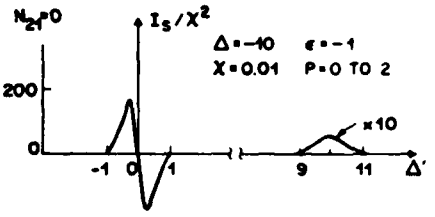

FIG. 5. Line shape for $N_{21} = 0$, $\Delta = -10$, $\epsilon = -1$, $\chi = 0.01$, and several P. The line shape changes only slightly in the pressure range $P = 0$ to 2.

shape remains constant.

Figure 7 illustrates two interesting features of collision effects in strong-pump-field saturation spectroscopy. First, the integrated probe absorption, which is proportional to $\bar{\gamma}_{12}\gamma_B$, grows with increasing perturber pressure; it would saturate at $\bar{\gamma}_{12} \gtrsim \chi(\gamma_B \approx \bar{\gamma}_{12})$. Second, the peak probe absorption also begins to increase for sufficiently high perturber pressure. Probe absorption from the excited-state velocity distribution becomes more efficient since collisions (a) increase the pump absorption and (b) redistribute atoms into a velocity range where they can interact more effectively with the probe. Although not displayed, the corresponding integrated and peak probe absorption for $\chi = 0.2$, $\Delta = -1$, $\epsilon = 1$ also increase with increasing perturber pressure. (The splitting

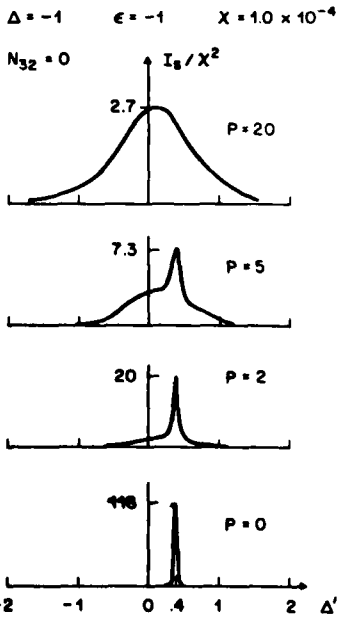

FIG. 6. Line shape for $N_{32} = 0$, $\Delta = -1$, $\epsilon = -1$, $\chi = 1.0 \times 10^{-4}$, and several pressures P.

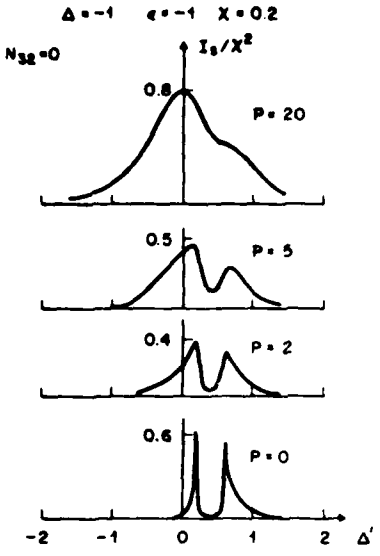

FIG. 7. Line shape for $N_{32}=0$, $\Delta=-1$, $\epsilon=-1$, $\chi=0.2$, and several pressures P.

seen in Fig. 2 disappears at low perturber pressures.) Thus, to maximize probe absorption, as is desirable in schemes using lasers for isotope separation, one should use perturber pressures that give $\tilde{\gamma}_{12}\approx\chi$ (provided that any quenching channels are not enhanced by collisional effects).

VII. SUMMARY

We have presented a theory of saturation spectroscopy in three-level systems, including collisional effects. Using a model of collisions in which they are phase interrupting in their effect on level coherences and velocity changing in their effect on level population densities, we have calculated the probe-absorption line shape in the presence of a strong pump field acting on a coupled transition. Line shapes for such systems enable one to extract data concerning the collision kernels and rates giving rise to the scattering effects. Specific results were obtained for a Keilson-Storer kernel in the large-angle-scattering limit. An analysis of foreign-gas broadening of the saturation-spectroscopy line shape of Na $3S_{1/2}-3P_{1/2}-4D_{3/2}$, based on the above theory, is presented in other papers.[17]

ACKNOWLEDGMENTS

This research was supported in part by the U. S. Office of Naval Research. One of us (P.R.B.) would like to thank Dr. J. Lam, M. J. L. LeGouët, and Dr. S. D. Yeh and Dr. E. J. Robinson for helpful discussions concerning this problem.

APPENDIX

Here, the theory is extended to include a situation often encountered experimentally, an inelastic collisional decay channel for level 2. That is, we assume that level 2 is collisionally coupled to a new level (denoted by "4"). Level 4 may spontaneously decay to the ground state with some rate γ_4'. However, it is assumed that level 4 is sufficiently separated in energy from level 2 that one can neglect field-induced transitions between levels 1 and 4 and levels 4 and 3 for the external-field frequencies under consideration which are in near-resonance with the 1–2 and 2–3 transition frequencies, respectively. There *will* be probe absorption near ω_{34} but this is a separate effect that is well separated from probe absorption near ω_{32}.

The 2–4 collisional coupling may be incorporated into the problem by the addition of the following term to the right-hand side of Eq. (10a),

$$\gamma_4'\tilde{\rho}_{44}(\vec{v}); \tag{A1a}$$

and the following terms to the right-hand side of Eq. (10b),

$$-\Gamma_{24}(\vec{v})\tilde{\rho}_{22}(\vec{v})+\int d\vec{v}'\,W_{42}(\vec{v}'-\vec{v})\tilde{\rho}_{22}(\vec{v}'); \tag{A1b}$$

where $W_{ij}(\vec{v}'-\vec{v})$ is the inelastic kernel for $i-j$ collisional coupling and $\Gamma_{ij}(\vec{v})$ is the rate for $i-j$ collisions. One must also add the following equation for the population density of level 4,

$$\Gamma_4^t(\vec{v})\tilde{\rho}_{44}(\vec{v})=\int d\vec{v}'\,W_4(\vec{v}'-\vec{v})\tilde{\rho}_{44}(\vec{v}')-\Gamma_{42}(\vec{v})\tilde{\rho}_{44}(\vec{v})+\int d\vec{v}'\,W_{24}(\vec{v}')\tilde{\rho}_{22}(\vec{v}')+\lambda_4(\vec{v}). \tag{A2}$$

It is assumed that collisions cannot create any coherence between level 4 and any of the other levels—i.e., $\tilde{\rho}_{4j}=0$ for $j\neq 4$.

The line shape is still given by Eqs. (33), (16), (28) with $n_2(\vec{v})$ and $\rho_{12}^{(0)}(\vec{v})$ determined from the following equations:

$$\Gamma_1^t(\vec{v})n_1(\vec{v})=\int d\vec{v}'\,W_1(\vec{v}'-\vec{v})n_1(\vec{v}')+i\chi[\tilde{\rho}_{21}^{(0)}(\vec{v})-\tilde{\rho}_{12}^{(0)}(\vec{v})]+\gamma_2'n_2(\vec{v})+\gamma_4'n_4(\vec{v}), \tag{A3a}$$

$$\Gamma_2^t(\vec{v})n_2(\vec{v})=\int d\vec{v}'\,W_2(\vec{v}'-\vec{v})n_2(\vec{v}')-i\chi[\tilde{\rho}_{21}^{(0)}(\vec{v})-\tilde{\rho}_{12}^{(0)}(\vec{v})]-\Gamma_{24}(\vec{v})n_2(\vec{v})+\int d\vec{v}'\,W_{42}(\vec{v}'-\vec{v})n_4(\vec{v}'), \tag{A3b}$$

$$\Gamma_4^t(\vec{v})n_4(\vec{v}) = \int d\vec{v}'\, W_4(\vec{v}'-\vec{v})n_4(\vec{v}') - \Gamma_{42}(\vec{v})n_4(\vec{v}) + \int d\vec{v}'\, W_{24}(\vec{v}'-\vec{v})n_2(\vec{v}'), \tag{A3c}$$

$$\mu_{12}(\vec{v})\tilde{\rho}_{12}^{(0)}(\vec{v}) = i\chi[N_{21}(\vec{v}) + n_2(\vec{v}) - n_1(\vec{v})], \tag{A3d}$$

$$\tilde{\rho}_{21}^{(0)}(\vec{v}) = [\tilde{\rho}_{12}^{(0)}(\vec{v})]^*, \tag{A3e}$$

$$N_{ij}(\vec{v}) = N_i(\vec{v}) - N_j(\vec{v}), \tag{A3f}$$

where the $N_i(\vec{v})$ are the equilibrium population densities in the absence of external fields. The $N_i(\vec{v})$ are defined as solutions to

$$\Gamma_1^t(\vec{v})N_1(\vec{v}) = \int d\vec{v}'\, W_1(\vec{v}'-\vec{v})N_1(\vec{v}') + \gamma_2' N_2(\vec{v}) + \gamma_4' N_4(\vec{v}) + \lambda_1(\vec{v}), \tag{A4a}$$

$$\Gamma_2^t(\vec{v})N_2(\vec{v}) = \int d\vec{v}'\, W_2(\vec{v}'-\vec{v})N_2(\vec{v}') - \Gamma_{24}N_2(\vec{v}) + \int d\vec{v}'\, W_{42}(\vec{v}')N_4(\vec{v}') + \lambda_2(\vec{v}), \tag{A4b}$$

$$\Gamma_4^t(\vec{v})N_4(\vec{v}) = \int d\vec{v}'\, W_4(\vec{v}'-\vec{v})N_4(\vec{v}') - \Gamma_{42}(\vec{v})N_4(\vec{v}) + \int d\vec{v}'\, W_{24}(\vec{v}'-\vec{v})N_2(\vec{v}') + \lambda_2(\vec{v}), \tag{A4c}$$

$$N_3(\vec{v}) = \lambda_3(\vec{v})/\gamma_3. \tag{A4d}$$

Equations (A3) must, in general, be solved numerically once the kernels are specified.

There is, however, a limiting case of some practical interest for which analytic solutions of Eqs. (A3) may be found. If the energy separation of levels 2 and 4 is $< 0.1\times$ (thermal energy), then collisions can transfer population between levels 2 and 4 without resulting in a significant velocity change. We consider such a case, for which

$$W_{42}(\vec{v}'-\vec{v}) = \Gamma_{42}(\vec{v})\delta(\vec{v}-\vec{v}'), \qquad W_{24}(\vec{v}'-\vec{v}) = \Gamma_{24}(\vec{v})\delta(\vec{v}-\vec{v}'). \tag{A5}$$

Furthermore, we neglect the velocity dependence of all γ's, adopt the *same* Keilson-Storer kernel [Eq. (51)] for velocity-changing collisions in levels 2 and 4, assume that the $N_i(\vec{v})$ are Maxwellians with most probable speeds u, and take $\gamma_4 = \gamma_2$, $\gamma_4' = \gamma_2'$. In this limit, Eq. (A3) for $n_2(\vec{v})$, $n_4(\vec{v})$, and $\rho_{12}^{(0)}(\vec{v})$ reduce to

$$\Gamma_1^t n_1(\vec{v}) - \int d\vec{v}'\, W_1(\vec{v}'-\vec{v})n_1(\vec{v}') = \left(\frac{2\chi^2\tilde{\gamma}_{12}}{R_g(\vec{v})^2}\right)\left(1-\frac{\gamma_2'}{\Gamma_2^t}\right)[N_{21}(\vec{v}) + \mathfrak{F}_g(\vec{v})] + \left(\frac{\gamma_2'}{\Gamma_2^t}\right)\int d\vec{v}'\, W_2(\vec{v}'-\vec{v})[n_2(\vec{v}') + n_4(\vec{v}')], \tag{A6a}$$

$$\Gamma_2^t n_2(\vec{v}) - \int d\vec{v}'\, W_2(\vec{v}'-\vec{v})n_2(\vec{v}') = -\left(\frac{2\chi^2\tilde{\gamma}_{12}}{R_g(\vec{v})^2}\right)[N_{21}(\vec{v}) + \mathfrak{F}_g(\vec{v})] - \Gamma_{24}n_2(\vec{v}) + \Gamma_{42}n_4(\vec{v}), \tag{A6b}$$

$$\Gamma_2^t n_4(\vec{v}) - \int d\vec{v}'\, W_2(\vec{v}'-\vec{v})n_4(\vec{v}') = -\Gamma_{42}n_4(\vec{v}) + \Gamma_{24}n_2(\vec{v}), \tag{A6c}$$

$$\tilde{\rho}_{12}^{(0)}(\vec{v}) = [i\chi\mu_{12}^*(\vec{v})/R_g(\vec{v})^2][N_{21}(\vec{v}) + \mathfrak{F}_g(\vec{v})]; \tag{A6d}$$

where

$$N_i(\vec{v}) = N_i(\pi u^2)^{-3/2}\exp(-v^2/u^2), \tag{A7}$$

$$\lambda_i(\vec{v}) = \lambda_i(\pi u^2)^{-3/2}\exp(-v^2/u^2), \tag{A8}$$

$$N_1 = [(\lambda_2+\lambda_4)(\gamma_2'/\gamma_2) + \lambda_1]/\gamma_1, \tag{A9a}$$

$$N_2 = [(\lambda_2+\lambda_4)(\Gamma_{42}/\gamma_2) + \lambda_2]/(\gamma_2 + \Gamma_{42} + \Gamma_{24}), \tag{A9b}$$

$$N_3 = \lambda_3/\gamma_3; \tag{A9c}$$

$$R_g(\vec{v})^2 = \gamma_g^2 + (\Delta_{12} - kv_z)^2, \tag{A10a}$$

$$\gamma_g = \tilde{\gamma}_{12}[1+\delta_g]^{1/2}, \tag{A10b}$$

$$\delta_g = (2\chi^2/\tilde{\gamma}_{12})[1/\Gamma_2^g + (1/\Gamma_1^t)(1-\gamma_2'/\Gamma_2^t)]; \tag{A10c}$$

$$\Gamma_g = \Gamma_2^t\Gamma_2^T/(\Gamma_2^t + \Gamma_{42}), \tag{A11}$$

$$\Gamma_2^T = \Gamma_2^t + \Gamma_{42} + \Gamma_{24}, \tag{A12}$$

$$\mathfrak{F}_g(\vec{v}) = \frac{1}{\Gamma_2^g}\int d\vec{v}'\, W_2(\vec{v}'-\vec{v})\left(n_2(\vec{v}') + \frac{\Gamma_{42}}{\Gamma_2^t+\Gamma_{42}}n_4(\vec{v}')\right) - \left(\frac{\gamma_2'}{\Gamma_1^t\Gamma_2^t}\right)\int d\vec{v}'\, W_2(\vec{v}'-\vec{v})[n_2(\vec{v}') + n_4(\vec{v}')] - \left(\frac{1}{\Gamma_1^t}\right)\int d\vec{v}'\, W_1(\vec{v}'-\vec{v})n_1(\vec{v}'). \tag{A13}$$

The only difference between Eqs. (21) and Eqs. (A6) is that R_B is replaced by R_E, $\mathcal{F}$ by $\mathcal{F}_E$, and $n_2(\vec{v})$ is determined from the coupled Eqs. (A6b) and (A6c) rather than from Eq. (21a). Defining

$$n(\vec{v}) = n_2(\vec{v}) + n_4(\vec{v}), \tag{A14}$$

and dropping the $\mathcal{F}_E$ term (LAS limit), one can rewrite Eqs. (A6b, c) in the form

$$\Gamma_2^T n_2(\vec{v}) - \int d\vec{v}'\, W_2(\vec{v}' - \vec{v}) n_2(\vec{v}') = A_E(\vec{v}) + \Gamma_{12} n(\vec{v}), \tag{A15a}$$

$$\Gamma_2^t n(\vec{v}) - \int d\vec{v}'\, W_2(\vec{v}' - \vec{v}) n(\vec{v}') = A_E(\vec{v}), \tag{A15b}$$

where

$$A_E(\vec{v}) = -[2\chi^2 \tilde{\gamma}_{12}/R_E(v)^2] N_{21}(\vec{v}) \tag{A16}$$

and Γ_2^T is defined by Eq. (A12). To arrive at results analogous to those of Secs. III, IV, and V, we set

$$n_2(\vec{v}) = n_{2E}^{(0)}(\vec{v}) + \delta n_{2E}(\vec{v}), \quad n(\vec{v}) = n_E^{(0)}(\vec{v}) + \delta n_E(\vec{v}), \tag{A17}$$

$$n_{2E}^{(0)}(\vec{v}) = A_E(\vec{v})/\Gamma_2^E, \quad n_E^{(0)}(\vec{v}) = A_E(\vec{v})/\Gamma_2^t, \tag{A18}$$

where δn_{2E} and δn_E satisfy the following equations:

$$\Gamma_2^T \delta n_{2E}(\vec{v}) - \int d\vec{v}'\, W_2(\vec{v}' - \vec{v}) \delta n_2(\vec{v}') = \int d\vec{v}'\, W_2(\vec{v}' - \vec{v}) n_{2E}^{(0)}(\vec{v}') + \Gamma_{42} \delta n_E(\vec{v}), \tag{A19a}$$

$$\Gamma_2^t \delta n_E(\vec{v}) - \int d\vec{v}'\, W_2(\vec{v}' - \vec{v}) \delta n_E(\vec{v}') = \int d\vec{v}'\, W_2(\vec{v}' - \vec{v}) n_E^{(0)}(\vec{v}'). \tag{A19b}$$

As in Eq. (48), we can introduce propagators defined by

$$\begin{Bmatrix} \delta n_{2E}(\vec{v}) \\ \delta n_E(\vec{v}) \end{Bmatrix} = \int d\vec{v}' \begin{Bmatrix} \delta G_2^E(\vec{v}' - \vec{v}) n_{2E}^{(0)}(\vec{v}') \\ \delta G^E(\vec{v}' - \vec{v}) n_E^{(0)}(\vec{v}') \end{Bmatrix}, \tag{A20}$$

which satisfy

$$\Gamma_2^T \delta G_2^E(\vec{v}' - \vec{v}) - \int d\vec{v}''\, W_2(\vec{v}'' - \vec{v}) \delta G_2^E(\vec{v}' - \vec{v}'') = W_2(\vec{v}' - \vec{v}) + \left(\frac{\Gamma_{12}\Gamma_E}{\Gamma_2^t}\right) \delta G^E(\vec{v}' - \vec{v}), \tag{A21a}$$

$$\Gamma_2^t \delta G^E(\vec{v}' - \vec{v}) - \int d\vec{v}''\, W_2(\vec{v}'' - \vec{v}) \delta G^E(\vec{v}' - \vec{v}) = W_2(\vec{v}' - \vec{v}). \tag{A21b}$$

We can now take over all of the equations of the text in Secs. III, IV, and V [Eqs. (35), ff] if the following substitutions are made:

$$\begin{aligned} &\eta_B \to \eta_E = \gamma_E + i\Delta_{12}, \\ &\delta \to \delta_E, \\ &\gamma_B \to \gamma_E, \\ &\delta n_2(\vec{v}) \to \delta n_2^E(\vec{v}); \\ &\Gamma_2^t \to \Gamma_2^E, \end{aligned} \tag{A22}$$

except in factors γ_2'/Γ_2^t, $(\Gamma_2/\Gamma_2^t)^n$;

$$\begin{aligned} &\delta G_2(\vec{v}' - \vec{v}) \to \delta G_2^E(\vec{v}' - \vec{v}), \\ &(\Gamma_2/\Gamma_2^t)^n \to (\Gamma_2/\Gamma_2^t)^n f_n, \end{aligned}$$

where

$$f_0 = 1, \quad f_n = \left(\frac{\Gamma_{42}\Gamma_2^E}{\Gamma_2^t\Gamma_2^t} + \frac{\Gamma_2^t}{\Gamma_2^t} f_{n-1}\right), \quad n > 1,$$

$$\mathfrak{R}_N \to \left(\frac{\Gamma_2}{\Gamma_2^t}\right)^N \frac{\Gamma_2^T}{\gamma_2 + \Gamma_{42} + \Gamma_{24}} \left(\frac{\Gamma_{42}\Gamma_2^E}{\gamma_2\Gamma_2^t} + \frac{\Gamma_2^t}{\Gamma_2^t} f_{n-1}\right).$$

With the above substitutions, the equations of the text are generalized to allow for coupling between states 2 and 4 produced by inelastic collisions. Velocity-changing collisions occur in *both* levels 2 and 4 (characterized by the same collision kernel), but the collisionally induced transfers $2 \rightleftharpoons 4$ occur without significant change of velocity. Such a model has been recently used to explain the saturation spectroscopy of Na–rare-gas systems for the $3S_{1/2} - 3P_{1/2} - 4D_{3/2}$ upward cascade.[17] In that system, level "4" is the $3P_{3/2}$ state which is collisionally coupled to $3P_{1/2}$. A discussion of the importance of accounting for the $P_{1/2} \rightleftharpoons P_{3/2}$ coupling is given in Refs. 17 and 26.

[1] G. E. Notkin, S. G. Rautian, and A. A. Feoktistov, Zh. Eksp. Teor. Fiz. 52, 1673 (1967) [Sov. Phys. JETP 25, 1112 (1967)].
[2] M. S. Feld and A. Javan, Phys. Rev. 177, 540 (1969).
[3] T. W. Hänsch and P. E. Toschek, Z. Phys. 236, 213 (1970).
[4] T. Y. Popova, A. K. Popov, S. G. Rautian, and R. I. Sokolovskii, Zh. Eksp. Teor. Fiz. 57, 850 (1969) [Sov. Phys. JETP 30, 466, 1208 (1970)].
[5] B. J. Feldman and M. S. Feld, Phys. Rev. A 5, 899 (1972); N. Skribanowitz, M. J. Kelly, and M. S. Feld, *ibid.* 6, 2302 (1972).

[6]I. M. Beterov and V. P. Chebotaev, Prog. Quantum Electron. 3, 1 (1974), and references therein.
[7]R. Salomaa and S. Stenholm, J. Phys. B 8, 1795 (1975); 9, 1221 (1976); R. Salomaa, *ibid.* 10, 3005 (1977).
[8]Additional references may be found in *Laser Spectroscopy III*, edited by J. L. Hall and J. L. Carlsten (Springer-Verlag, New York, 1977); *Nonlinear Laser Spectroscopy*, edited by V. S. Letokhov and V. P. Chebotaev (Springer-Verlag, New York, 1977); *High Resolution Laser Spectroscopy*, edited by K. Shimoda (Springer-Verlag, New York, 1976); *Laser Spectroscopy of Atoms and Molecules*, edited by H. Walther (Springer-Verlag, New York, 1976); *Frontiers in Laser Spectroscopy*, edited by R. Balian, S. Haroche, and S. Liberman (North-Holland, Amsterdam, 1977).
[9]K. Shimoda, in *High Resolution Laser Spectroscopy*, edited by K. Shimoda (Springer-Verlag, New York, 1976), p. 11.
[10]S. Stenholm, J. Phys. B 10, 761 (1977).
[11]P. R. Berman, in *Advances in Atomic and Molecular Physics*, edited by D. R. Bates and B. Bederson (Academic, New York, 1977), Vol. 13, p. 57.
[12]P. R. Berman, Phys. Rep. 43, 101 (1978).
[13]A. P. Kolchenko, A. A. Pukhov, S. G. Rautian, and A. M. Shalagin, Zh. Eksp. Teor. Fiz. 63, 1173 (1972) [Sov. Phys. JETP 36, 619 (1973)].
[14]V. P. Kochanov, S. G. Rautian, and A. M. Shalagin, Zh. Eksp. Teor. Fiz. 72, 1358 (1977) [Sov. Phys. JETP 45, 714 (1977)].
[15]L. Klein, M. Giraud, and A. Ben-Reuven, Phys. Rev. A 16, 289 (1977).
[16]Extensive additional references may be found in Ref. 11 and in a review article by P. R. Berman [Appl. Phys. (Germany) 6, 283 (1975)].
[17]P. F. Liao, J. E. Bjorkholm, and P. R. Berman (unpublished).
[18]P. R. Berman, Phys. Rev. A 5, 927 (1972).
[19]J. L. LeGouët (unpublished).
[20]S. G. Rautian and A. A. Feoktistov, Zh. Eksp. Teor. Fiz. 56, 227 (1969) [Sov. Phys. JETP 29, 126 (1969)].
[21]S. R. Drayson, J. Quant. Spectroc. Radiat. Transfer 16, 611 (1976).
[22]J. Keilson and K. E. Storer, Quart. Appl. Math 10, 243 (1952).
[23]Equation (59b) is a somewhat better asymptotic form than that given in Ref. 11.
[24]P. R. Berman, Phys. Rev. A 13, 2191 (1976).
[25]To avoid indeterminate factors in the saturation parameter at zero pressure, we actually take $\gamma_1 = 0.0001$ and $\gamma_2 = \gamma_2' + 0.0001$. These small additions to γ_1 and γ_2 may be thought to simulate transit-time effects.
[26]P. F. Liao, J. E. Bjorkholm, and P. R. Berman, Phys. Rev. A 20, 1489 (1979).

PHYSICAL REVIEW A VOLUME 21, NUMBER 6 JUNE 1980

Effects of velocity-changing collisions on two-photon and stepwise-absorption spectroscopic line shapes

P. F. Liao and J. E. Bjorkholm
Bell Laboratories, Holmdel, New Jersey 07733

P. R. Berman
Physics Department, New York University, New York, New York 10003

(Received 5 September 1979)

We report the results of an experimental study of the effects of velocity-changing collisions on two-photon and stepwise-absorption line shapes. Excitation spectra for the $3S_{1/2} \rightarrow 3P_{1/2} \rightarrow 4D_{3/2}$ transitions of sodium atoms undergoing collisions with foreign gas perturbers are obtained. These spectra are obtained with two cw dye lasers. One laser, the pump laser, is tuned 1.6 GHz below the $3S_{1/2} \rightarrow 3P_{1/2}$ transition frequency and excites a nonthermal longitudinal velocity distribution of excited $3P_{1/2}$ atoms in the vapor. Absorption of the second (probe) laser is used to monitor the steady-state excited-state distribution which is a result of collisions with rare gas atoms. The spectra are obtained for various pressures of He, Ne, and Kr gases and are fit to a theoretical model which utilizes either the phenomenological Keilson-Störer or the classical hard-sphere collision kernel. The theoretical model includes the effects of collisionally aided excitation of the $3P_{1/2}$ state as well as effects due to fine-structure state-changing collisions. Although both kernels are found to predict line shapes which are in reasonable agreement with the experimental results, the hard-sphere kernel is found superior as it gives a better description of the effects of large-angle scattering for heavy perturbers. Neither kernel provides a fully adequate description over the entire line profile. The experimental data is used to extract effective hard-sphere collision cross sections for collisions between sodium $3P_{1/2}$ atoms and helium, neon, and krypton perturbers.

I. INTRODUCTION

Using tunable narrow-band lasers, one can selectively excite a narrow nonthermal longitudinal velocity distribution in an atomic or molecular vapor. Collisions between these atoms or molecules and other atoms in the gas cause this distribution to thermalize. A study of the manner in which the collisions modify the distribution leads to an increased understanding of the collisions. In this paper we report the results of a systematic study of the effects of collisions on line shapes obtained in sodium using two-photon spectroscopy with a resonant intermediate state. These measurements, which are made with two cw dye lasers, yield values for the equivalent hard-sphere elastic-scattering cross sections for collisions between sodium atoms in the $3P_{1/2}$ state and rare gas perturbers. Comparisons of the experimental line shapes are made with a theory which utilizes either a classical hard-sphere collision kernel or the Keilson-Störer collision kernel. The theory accounts for the presence of fine-structure state-changing collisions as well as velocity-changing collisions. The validity of these collision models is discussed in light of the experimental data.

Measurements of the effects of velocity-changing collisions on laser spectroscopic line shapes have been made for some time.[1,2] In a typical experiment, one monitors the steady-state velocity distribution of atomic levels subjected to nonthermal excitation by a narrow-band laser. The degree of velocity thermalization achieved in these states as a result of collisions is determined by the number of collisions occurring within the lifetime of the states and the strength of the collisions. Most previous experiments have been analyzed under the assumptions that the collisions are either of a "weak" or "strong" nature. In the case of "weak" collisions, the collisions which occur during an atom's lifetime have only a small effect on the atomic velocity,[3] whereas, in the "strong" collision limit, those atoms which have experienced collisions are assumed to have a thermal distribution. Recently the problem of collisions intermediate to the two limits has received increased attention.[2] In this case, atoms which experience collisions reach a thermal velocity distribution only if they have several collisions within their lifetime. Because of the short lifetime of the excited atoms in our experiment (16 nsec), the excited sodium atoms never reach a thermal distribution so that the measured steady-state velocity distribution shows a "persistence of velocity."

The manner in which the atoms change velocities as a result of collisions is directly dependent on the strength and form of the interaction between the active atom and the perturber atom.

Supported by the U.S. [illegible] under Contract No. [illegible].

Hence, measurements of the thermalization process yield information about the interaction potentials. At the present time we have analyzed our experimental results to obtain the equivalent hard-sphere cross sections for sodium in collision with helium, neon, or krypton rare gas atoms. This choice of perturber atoms allows us to observe the effect of different active atom to perturber atom mass ratios.

Our measurements are made by selectively exciting a particular velocity distribution of sodium atoms to the $3P_{1/2}$ excited state. This excitation is accomplished by tuning a cw dye laser to the wing of the Doppler-broadened $3S_{1/2}-3P_{1/2}$ transition. A second laser is then scanned to produce $3P_{1/2}$-$4D_{3/2}$ transitions. The resulting line shape directly reflects the longitudinal velocity distribution of the $3P_{1/2}$ state.

In the absence of velocity-changing collisions, one might expect only those atoms which have longitudinal velocities such that they are Doppler shifted into resonance with the laser frequency would be excited. However, the presence of phase-interrupting collisions results in an excitation of all the velocity groups. In this nonresonant excitation, the energy defect or excess between the atomic transition energy and the laser photon energy is provided or removed by a collision.[4,5] This nonresonant collisionally assisted excitation results in population of velocity groups other than those desired and must be accounted for properly in the final analysis of the line shape.

State-changing collisions such as those which produce transitions between the $3P_{1/2}$ and $3P_{3/2}$ fine-structure states are also found to play an important role. Our analysis is therefore made to account for the effects of such collisions.

In the following section we briefly discuss our experimental setup and the underlying principles involved in obtaining a description of the collision-induced modification of spectroscopic line shapes. In Sec. III we compare two kernels (Keilson-Störer[6] and classical hard sphere) that can be used to describe velocity-changing collisions. Our experimental results and a comparison with theory using these collision kernels are then discussed in Sec. IV.

II. BASIC PRINCIPLES AND EXPERIMENTAL SETUP

The effect of collisions on the line shapes associated with three-level systems has been treated recently[7] and the following discussion will be based largely on those results. Our experimental situation is, in fact, somewhat more complicated than the simple three-level case due to the presence of additional levels. While these additional levels are not coupled by the laser radiation fields to the other states, collisions can cause transitions between these levels and the states of interest. Furthermore, the theory given in Ref. 7 is valid only in the limit of low intensities. Our actual experiment utilized intensities which often exceed the saturation intensity of a transition and require a more accurate theory to completely describe it. A detailed discussion of this more complete theory is given elsewhere.[8] In what follows, we give only an outline of the basic principles of the experiment and present the major theoretical results.

Our experimental data are obtained using the experimental setup shown in Fig. 1. We use two cw single-mode dye lasers, one (the pump) is set at a fixed angular frequency Ω which is tuned to the wing of the Doppler-broadened $3S_{1/2}$-$3P_{1/2}$ transition, and the other (the probe), of frequency Ω', is scanned to complete transitions to the $4D_{3/2}$ state. Transitions to $4D_{5/2}$ are weak in comparison with those to $4D_{3/2}$, because of dipole selection rules which forbid $3P_{1/2}-4D_{5/2}$ transitions, and are neglected. The unfocused beams from the two lasers propagate in opposite directions through a cell at 200 °C containing sodium vapor. Typical laser intensities are 0.5 W/cm^2, and each beam is linearly polarized in the same direction. The sodium vapor density is held between 10^{10}–10^{11} cm^{-3} so that resonant reabsorption of atomic fluorescence was not significant and sodium-sodium collisions could be neglected. We monitor the population of the $4D_{3/2}$ state by measuring the intensity of fluorescence at ~330 nm which occurs when the $4D_{3/2}$ state decays via the $4P$ state back to the ground state. Our results give

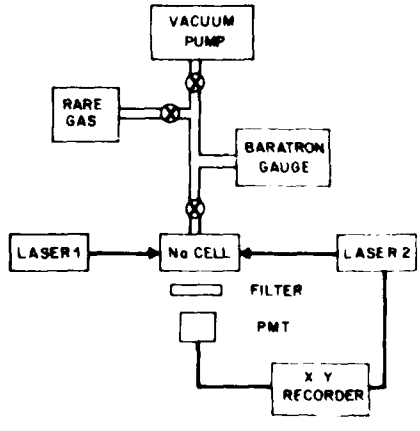

FIG. 1. Schematic diagram of the experimental setup. Although not shown, the light from laser 1 was chopped and the output of the photomultiplier (PMT) was processed with a lock-in amplifier.

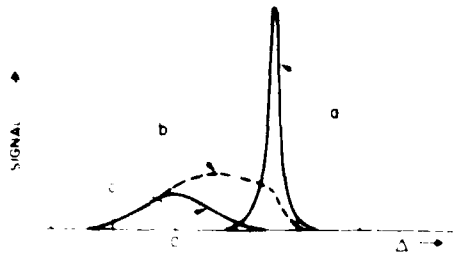

[illegible] Schematic representation of the observed line shape in terms of three components. Component (a) is the "two-photon" line; components (b) and (c) are the collisionally induced components, as discussed in the text.

the $3S_{1/2} \rightarrow 3P_{1/2} \rightarrow 4D_{3/2}$ two-photon excitation spectrum.

The line shape can be roughly viewed as composed of three parts which are illustrated schematically in Fig. 2. Although the three components are not completely independent, one can roughly describe them as arising in the following manner. The narrow component marked *a* would be present even in the absence of collisions and is composed of two-quantum and stepwise transitions of those atoms which have not undergone velocity-changing collisions in the $3P_{1/2}$ intermediate state. We shall refer to this component as the "two-photon" line. The characteristics of this line have been experimentally[7] and theoretically[8] studied in great detail. The line is essentially Doppler free owing to the velocity selectivity of the excitation and the use of oppositely propagating beams. The component labeled *b* arises from those atoms which, once excited into the $3P_{1/2}$ state, experience velocity-changing collisions. The collisions modify the initial narrow velocity distribution which was excited by the laser at frequency ω and cause the distribution to broaden and shift toward equilibrium; this thermalization is mirrored in component *b* of the probe absorption. In our experiments ω is not set at the atomic resonance frequency and hence the initial longitudinal velocity distribution is not centered at $v_z = 0$ but at a fairly high $v_z \simeq 10^5$ cm/sec. The final component, labeled *c*, is due to collisionally aided excitation of the $3P_{1/2}$ excited state. This excitation is essentially non-velocity-selective and therefore is completely Doppler broadened; the probe absorption from this state has nearly the shape of the equilibrium Voigt profile. It differs from the velocity-changing collision component, *b*, as it would be present even in the absence of velocity-changing collisions, e.g., if the perturber atoms were much less massive than the sodium atoms. It may be viewed as arising from phase-changing collisions

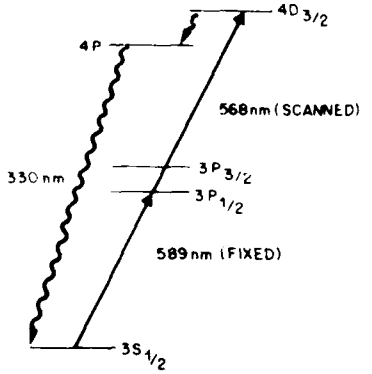

FIG. 3. The energy levels of the sodium atom relevant for our experiment. Not shown is the 1.77-GHz hyperfine splitting of the 3S ground state.

which effectively broaden the atomic resonance of each atom. The exact shape of the excitation spectrum depends on the relative amplitudes of the three components. The components *b* and *c* each increase relative to *a* as the perturber pressure is increased. The ratio of *b* to *c* amplitudes depends on Ω. Component *b* decreases rapidly when ω is adjusted away from the atomic resonance because the number of atoms which have the correct velocity so as to be Doppler shifted into resonance decreases exponentially. Hence at detunings much greater than the Doppler width, component *c* will dominate, while at small detunings component *b* will dominate. We have recently made a detailed study of the collisional redistribution by phase-changing collisions for the case where ω is tuned far from the resonance so that component *b* is negligible.[9]

The level scheme which is appropriate for our experiments is shown in Fig. 3. We generally follow the notation of Refs. 7 and 8 so that state 1 is the $3S_{1/2}$ ground state, state 3 is the $4D_{3/2}$ final state, and state 2 is the $3P_{1/2}$ intermediate state. We also allow for state-changing collisions between the $3P_{1/2}$ and $3P_{3/2}$ (state 4) fine-structure states. The laser field at ω' is assumed to couple only the $2 \rightarrow 3$ transition, while that at ω is assumed to act on only the $1 \rightarrow 2$ transition.

A complete theory for the excitation line shape is given in Ref. 8 assuming the probe field to be weak. We shall attempt to fit our data using this theory and hard-sphere collision models. For such models, collisions produce relatively large velocity changes for the active atoms [i.e., velocity changes Δu such that $\Omega(\Delta u \ldots)$ all homogeneous widths]. In this limit the line shape is given by[8]

$$I(\Omega') \propto I_{\text{TPA}}(\Omega') + I_{\text{SW}}(\Omega'), \qquad (1)$$

where

$$I_{TW}(\Omega') = \frac{2(\chi'\chi)^2}{\gamma_3 k k' k'' u^3} \operatorname{Im} \sum_{j=1}^{4} A_j \tilde{Z}(r_j), \tag{2}$$

$$I_{SW}(\Omega') = \frac{2(\chi')^2}{\gamma_3 k'} \operatorname{Im} \int \frac{n_2(ux)}{(x - r_2)} dx, \tag{3}$$

$$\tilde{Z}(r) = -\pi^{-1/2} \int_{-\infty}^{\infty} e^{-x^2} (r - x)^{-1} dx$$

[$\tilde{Z}(r)$ is the plasma dispersion function $Z(r)$ for $\operatorname{Im}(r) > 0$ and is $-Z(r)$ for $\operatorname{Im}(r) < 0$], where $\chi(\chi')$ is the Rabi frequency of the transition $1-2$ $(2-3)$, u is the most probable sodium velocity, $k = \Omega/c$, $k' = \Omega'/c$, and $k'' = |k' - k|$. The other quantities are defined as

$$r_1 = a + c,$$

$$r_2 = b - c,$$

$$r_3 = i\eta_B/ku,$$

$$r_4 = -i\eta_B/ku,$$

$$r_5 = i\eta_{12}^*/ku,$$

where

$$a = \frac{+i\eta_{13}}{k''u}, \quad b = \frac{i\eta_{23}}{k'u},$$

$$c = \tfrac{1}{2}\{b - a - [(b-a)^2 + 4\chi^2/k'k''u^2]^{1/2}\},$$

and

$$A_i = (r_5 - r_i) \Big/ \prod_{j=1,4;\, j\neq i} (r_j - r_i),$$

$$\eta_{12} = \tilde{\gamma}_{12} + i\Delta,$$

$$\eta_{13} = \tilde{\gamma}_{13} + i(\Delta + \Delta'),$$

$$\eta_{23} = \tilde{\gamma}_{23} + i\Delta',$$

$$\eta_B = \gamma_B + i\Delta, \quad (\gamma_B)^2 = \tilde{\gamma}_{12}^2 + 2\tilde{\gamma}_{12}\chi^2/\Gamma_S,$$

$$\Gamma_S^{-1} = \frac{\gamma_2 + \Gamma_2(v) + 0.5\gamma'}{[\gamma_2 + \Gamma_2(v)][\gamma_2 + \Gamma_2(v) + 1.5\gamma']} + \frac{1}{\Gamma_1(v)}\left(1 - \frac{\gamma_2'}{\gamma_2 + \Gamma_2(v)}\right).$$

The detunings are defined as $\Delta = \Omega - \omega$, $\Delta' = \Omega' - \omega'$, where the angular frequencies ω and ω' are the transition frequencies of the ground-to-intermediate and intermediate-to-final states, respectively. The decay rates $\tilde{\gamma}_{ij}$ are the phenomenological decay constants of the density matrix elements ρ_{ij} and include the effects of phase-changing collisions. The rate γ_2 is the total natural decay rate out of the intermediate state, γ_2' is the natural decay rate from level 2 to 1, $\Gamma_i(v)$ is the rate of velocity-changing collisions for atoms in level i, and γ' is the $3P_{1/2}$ to $3P_{3/2}$ fine-structure state-changing collision rate. Note that the theory allows for power broadening of the $1-2$ transition. The population distribution $n_2(v)$ of the intermediate state appearing in Eq. (3) is determined by the atom-pump field interaction and the effects of velocity-changing collisions. Equation (3) is an approximation valid for the case $|k| \approx |k'|$ as in our experiment.

The effect of fine-structure state-changing collisions introduces additional complexities. First, it modifies the power broadening of the $1-2$ transition. Second, it may modify the velocity-changing process. Finally, it decreases the effective excitation of state 2 since atoms are transferred from the $3P_{1/2}$ to the $3P_{3/2}$ state. To minimize the complexities we make the simplifying assumption that the velocity-changing cross section is the same for the two fine-structure states, and that no velocity change occurs in the fine-structure state-changing processes. We have verified that the latter assumption is nearly correct by tuning Ω to the wing of the $3S_{1/2} - 3P_{3/2}$ transition and thereby exciting a particular velocity class of atoms into the $3P_{3/2}$ state. Collisions cause some of these atoms to transfer to the $3P_{1/2}$ state. The velocity distribution of the atoms in the $3P_{1/2}$ state is then recorded by scanning Ω' across the region of the $3P_{1/2} - 4D_{3/2}$ transition. The resulting excitation spectrum is shown in Fig. 4. As can be seen in Fig. 4, the spectrum and hence the velocity distribution is concentrated in a small region which corresponds to the initial velocity of the atoms. The small splitting in the line is due to the hyperfine structure of the $3P_{1/2}$ state. The fine-structure state change appears to happen with little or no change in velocity, justifying our assumption.

To calculate the signal amplitude we must determine $n_2(v)$, the velocity distribution of the $3P_{1/2}$ state. The equations describing this distribution and the longitudinal velocity distribution $n_4(v)$ of

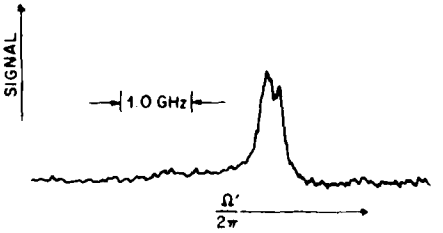

FIG. 4. Probe laser excitation spectrum of the $3P_{1/2} - 4D_{3/2}$ transition with the pump laser tuned to the $3S_{1/2} - 3P_{3/2}$ transition. This signal is the result of fine-structure state-changing collisions produced by 0.5 Torr of neon perturber gas. The narrow line width demonstrates that fine-structure state changes occur with negligible velocity change.

the $3P_{1/2}$ state are[11]

$$\frac{dn_2(v)}{dt} = -[\gamma_2 + \Gamma_2(v) + \gamma_{24}^t]n_2(v) + \gamma_{42}^t n_4(v) + \int W(v',v)n_2(v')dv' + T(v), \quad (4)$$

$$\frac{dn_4(v)}{dt} = -[\gamma_2 + \Gamma_2(v) + \gamma_{42}^t]n_4(v) + \gamma_{24}^t n_2(v) + \int W(v',v)n_4(v')dv', \quad (5)$$

where $T(v)$ is the velocity distribution of atoms excited to the $3P_{1/2}$ state by the pump laser. The collision kernel $W(v,v')$ is defined such that the $W(v,v')dv\,dt$ is the probability that a collision will cause an atom in level 2 moving with a longitudinal velocity between v and $v+dv$ to change to be between v' and $v'+dv$ during a time interval dt. The rate $\Gamma_2(v)$ is given by

$$\Gamma_2(v) = \int W(v,v')dv'$$

and $\gamma_{24}^t = \gamma^t$ and $\gamma_{42}^t = 0.5\gamma^t$ are the $3P_{1/2} \to 3P_{3/2}$ and $3P_{3/2} \to 3P_{1/2}$ collisional transfer rates, respectively.

The equation which gives $n(v) = n_2(v) + n_4(v)$, the longitudinal velocity distribution function for the sum of the population densities of the two $3P$ states, is

$$\frac{dn(v)}{dt} = -\left(\gamma_2 + \int W(v,v')dv'\right)n(v) + \int W(v',v)n(v')dv' + T(v). \quad (6)$$

Equation (6) is easily solved to yield the steady-state solution

$$n(v) = \sum_{i=0}^{\infty} n^i(v), \quad (7)$$

where

$$n^0(v) = T(v)/[\gamma_2 + \Gamma_2(v)],$$

$$n^{i+1}(v) = \int W(v',v)n^i(v')dv'/[\gamma_2 + \Gamma_2(v)].$$

The quantity $n^i(v)$ is the population density of atoms having experienced exactly i collisions since initially excited into the $3P$ states.

By substituting $n_4 = n - n_2$ into Eq. (4) and using Eq. (7), we solve Eq. (4) to obtain

$$n_2(v) = \sum_{i=0}^{\infty} n_2^i(v), \quad (8)$$

where

$$n_2^0(v) = \frac{0.5\gamma^t n(v) + T(v)}{\gamma_2 + \Gamma_2(v) + 1.5\gamma^t} \quad (9)$$

and

$$n_2^i(v) = \int W(v',v)n_2^{i-1}(v')dv'/[\gamma_2 + \Gamma_2(v) + 1.5\gamma^t]. \quad (10)$$

In this paper we consider two collision kernels for insertion into Eq. (10), the Keilson-Störer and the classical hard-sphere kernels. Owing to the simple mathematical form of the Keilson-Störer kernel an analytic expression for $n_2(v)$ can be obtained. However, for the hard-sphere kernel it is necessary to calculate $n_2(v)$ numerically. These collision kernels will be discussed in the following section. The distribution $n_2(v)$, given by Eqs. (8)–(10), is inserted into Eq. (3) and the total line shape is then given by Eqs. (1)–(3).

III. COLLISION KERNELS

All the properties of the velocity-changing collision process are contained in the collision kernel. The most commonly used kernel is the phenomenological kernel of Keilson and Störer[6]

$$W(v,v') = \Gamma[\pi(\Delta u)^2]^{-1/2}\exp[-(v' - \alpha v)^2/(\Delta u)^2],$$

where Γ is the (speed-independent) rate of collisions, α is a parameter which depends on the active and perturber atom mass ratio, and

$$\Delta u = (1-\alpha^2)^{1/2}u$$

is $\sqrt{2}$ times the rms velocity change per collision. Borenstein and Lamb[12] compared the Keilson-Störer kernel with Monte Carlo calculations of hard-sphere collisions and found fairly close agreement between the two. However, they were concerned mainly with the cases of light perturbers and small initial velocities (velocities small compared with Doppler width). Recently, more detailed comparisons have been made[13,14] although again for cases of light perturbers and low velocities.

In this section we shall compare some of the properties of the Keilson-Störer kernel with the exact analytic expression for the kernel which describes classical collisions between atoms having a hard-sphere interatomic potential ($V = 0$ for $r > r_0$ and $V = \infty$ for $r < r_0$).

The Keilson-Störer kernel has the form of a displaced Gaussian whose width and shift are determined by the parameter α. The method for the determination of α which we utilize is that suggested by LeGouët,[13] in which α is chosen such that the Keilson-Störer model gives the same rms velocity change per collision as the analytic hard-sphere kernel. This method gives $\alpha = 0.8$,

0.4, and 0.0 for collisions between sodium and helium, neon and krypton atoms, respectively. A major feature of the Keilson-Störer kernel is its mathematical simplicity which allows analytic expressions to be obtained.

The hard-sphere kernel is considerably more complicated. It is given by the following expression:

$$W(v',v)=\frac{\pi r_0^2}{4}\left(\frac{1+\beta^2}{\beta^2}\right)\left(\left\{1-\mathrm{erf}\left[\left(\frac{1+\beta^2}{2\beta}\right)|S|+\beta\,\frac{v'}{u}\,\frac{S}{|S|}\right]\right\}\right.$$
$$\left.+\exp\left[-S\left(S+\frac{2v'}{u}\right)\right]\left\{1-\mathrm{erf}\left[\left(\frac{1-\beta^2}{2\beta}\right)|S|-\beta\,\frac{v'}{u}\,\frac{S}{|S|}\right]\right\}\right),$$

where

$$\beta^2=m_p/m_a,\quad S=(v-v')/u\,.$$

The mass of the active atom (Na) is m_a, and the mass of the perturber atom is m_p. This kernel has been obtained by Kol'chenko,[15] however, for completeness we have included its derivation in the Appendix.

To compare the kernels, we plot in Figs. 5–7 $n^i(v)$ [Eq. (7)] for sodium calculated with both kernels for helium, neon, and krypton perturbers assuming $T(v)$ is a delta function at $v/u=1.6$. In the case of a very light perturber such as helium (Fig. 5), the two kernels are quite similar. Each gives distributions $n^i(v)$ which shift more toward equilibrium with each collision, and both models produce distributions with approximately the same shifts and widths. To allow for easy comparison of the distributions we have normalized the peak of each to unity. In fact, at the pressure (2.5 Torr) used for the calculation, each sucessive $n^i(v)$ decreases in amplitude by about a factor of 6 or more.

The calculated distributions for the most massive perturber, krypton, show some significant differences. Krypton is 3.7 times heavier than sodium. As in the case of helium, the distributions predicted by the two kernels are quite similar for $i \geq 2$ although the widths of the distributions now predicted by the hard-sphere models are significantly larger than those given by the Keilson-Störer model owing to the speed dependence of $\Gamma(v)$ in the hard-sphere model. The greatest difference appears in the distribution $i=1$. Krypton hard-sphere collisions produce a relatively flat-topped distribution. The amplitude at $v=0$ is nearly the same as at the initial velocity (taken to be $v_0=1.6$ u). The Keilson-Störer distribution, on the other hand, is a factor of 12 larger at $v=0$ than at v_0. Note that the velocity distributions produced by the heavier perturber initially broaden and then narrow in the hard-sphere model, whereas for the Keilson-Störer kernel, complete thermalization occurs after one collision.

Comparisons of the distributions calculated using these two kernels indicate the following. First, for heavier perturbers it is at low pressures that the differences are most significant since it is at low perturber pressure that the contribution of $n^1(v)$ to $n(v)$ dominates. Second, for high perturber pressures the two kernels give nearly the same line shapes. Our experiments have therefore concentrated on fairly low per-

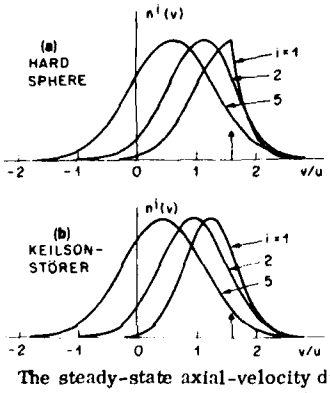

FIG. 5. The steady-state axial-velocity distributions $n^i(v)$ for sodium atoms in the $3P$ states which have experienced exactly i collisions since being initially excited. The calculations were carried out for 2.5 Torr of helium perturber gas, using both the (a) hard-sphere and (b) the Keilson-Störer kernels. All curves have been normalized to the same height.

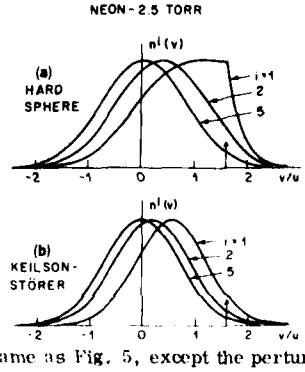

FIG. 6. Same as Fig. 5, except the perturber gas is neon.

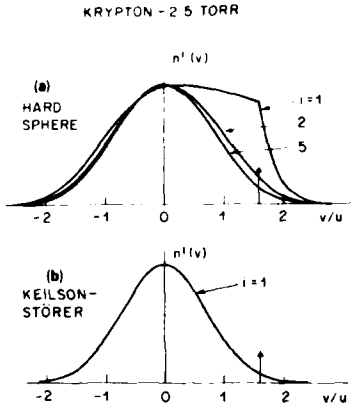

FIG. 7. Same as Fig. 5, except the perturber gas is krypton.

turber pressures. In the case of helium we expect the two models to give nearly identical results.

IV. EXPERIMENTAL RESULTS

Excitation spectra were taken of the $3S_{1/2} - 3P_{1/2} - 4D_{3/2}$ transition of atomic sodium vapor for various pressures of helium, neon, and krypton buffer gases. In each case, the laser at Ω was adjusted to be 1.6 GHz below the $3S_{1/2}(F=2) - 3P_{1/2}$ transition. Examples of the spectra obtained by sweeping Ω' are given in Figs. 8–12. In each case, the two narrow line-shape features are the result of the combination of two-quantum and stepwise transitions originating from the two hyperfine levels of the ground state. The broader feature is the collision-induced signal and, as discussed earlier, arises from velocity-changed

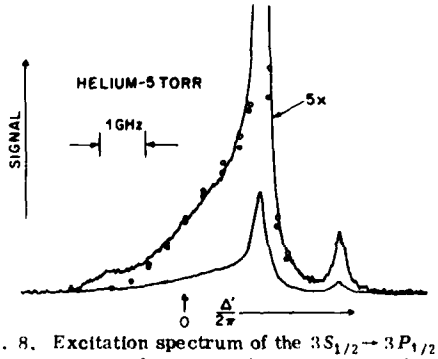

FIG. 8. Excitation spectrum of the $3S_{1/2} \rightarrow 3P_{1/2} \rightarrow 4D_{3/2}$ transition of atomic sodium in 5 Torr of helium perturber gas. The pump laser was tuned such that $\Delta/2\pi = -1.6$ GHz. The solid (open) circles show the theoretical fit obtained using the hard-sphere (Keilson-Störer) collision kernel.

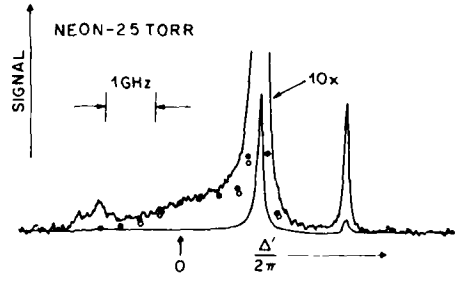

FIG. 9. Same as Fig. 8, except for 2.5 Torr of neon perturber gas.

atoms and atoms excited via phase-interrupting collisions. This feature is not present when the perturber gas is removed.

The excitation was made with counter-propagating beams. This geometry was utilized to minimize the line width of the two narrow two-photon and stepwise resonances. It is essential that these resonances be narrow so that the collision-induced signals are unobscured. If we use copropagating beams the narrow resonances are split by 390 MHz because of the hyperfine structure of the $3P_{1/2}$ state.[9] With the use of oppositely propagating beams, this splitting collapses[9] to 7 MHz. Some of the spectra contain evidence of resonances due to copropagating beams. These are symmetrically located about $\Delta' = 0$ from the counter-propagating resonances and apparently are the result of stray reflections into the sodium cell. We were unable to eliminate them completely.

We choose to set $\Omega/2\pi$ to be 1.6 GHz below the

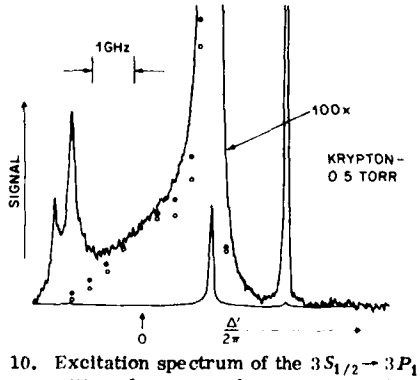

FIG. 10. Excitation spectrum of the $3S_{1/2} \rightarrow 3P_{1/2} \rightarrow 4D_{3/2}$ transition of atomic sodium in a perturber gas of krypton. The pump laser was tuned such that $\Delta/2\pi = -1.6$ GHz. The krypton pressure was 0.5 Torr. The solid (open) circles show the theoretical fit obtained using the hard-sphere (Keilson-Störer) collision kernel. The sharp resonances occurring for negative Δ' are due to the residual copropagating light, as discussed in the text.

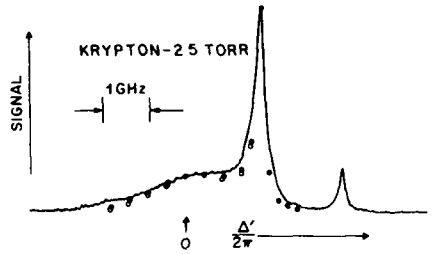

FIG. 11. Same as Fig. 10, except the krypton pressure was 2.5 Torr.

$3S_{1/2}(F=2)-3P_{1/2}$ transition. With this rather large detuning, the difference between the Keilson-Störer and hard-sphere kernel which we discussed in Sec. III is emphasized. Furthermore, the spurious copropagating resonances mentioned above are less troublesome since they occur at the edge of the line shape of interest. At this detuning the collisional redistribution and velocity-changing contributions to the line shape (components b and c of Fig. 2) are comparable in amplitude.

The data were fit to Eqs. (1)–(3) and (8)–(10) using experimental values of γ_{ij} and γ^t obtained from the literature,[16] and a value $\chi/ku=0.018$ determined from measurements of pump intensity. The line shape was assumed to arise as an independent sum of contributions originating from both hyperfine ground states. The relative amplitudes of the two-narrow resonances were found to be pressure and intensity dependent. This dependence is due to optical-pumping effects which modify the population of the ground-state hyperfine levels. To account for the optical pumping, the initial relative population of the two states was taken as a free parameter which was adjusted so that the theory correctly predicted the relative amplitudes of the two narrow resonances.

The only remaining parameter to be determined is the velocity-changing collision cross section. We obtain values for these cross sections at each perturber pressure by fitting the ratio of the signal at $\Delta'=0$ to that at $\Delta'/2\pi=1.6$ GHz. Having fit these two ratios, the overall comparison between the theoretical and experimental profiles can be used to test various collision models. One should note that, for our procedure, the nature of the fit is relatively insensitive to the saturation parameter. This result was verified experimentally by varying the pump power. In our analysis we set the branching ratio $\gamma_2'/\gamma_2=1$ for both $3P_{1/2}-3S_{1/2}$ $(F=1)$ and $3P_{1/2}-3S_{1/2}$ $(F=2)$ transitions and $\Gamma_1(v)$ to gas kinetic values. The net effect of such an arbitrary choice is to modify the saturation parameter, but, as noted above, this modification has little effect on our fitting procedure. Finally, the assumption of a weak probe field is reasonably well satisfied; signal strength was found to vary linearly with probe power.

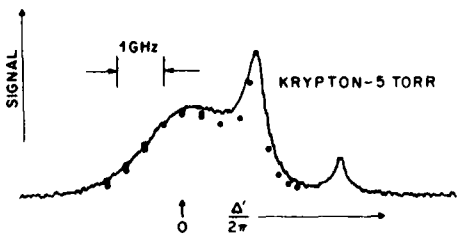

FIG. 12. Same as Fig. 10, except the krypton pressure was 5 Torr.

Representative data obtained with helium and neon buffer gases are shown in Figs. 8 and 9. The results of the theory using both the Keilson-Störer kernel (open circles) and the classical hard-sphere kernel (solid points) are given. As expected, for these lighter perturbers both kernels do nearly equally well in producing fairly accurate line shapes. However, for the data with krypton perturbers (Figs. 10–12) the hard-sphere model does better in predicting the line shape at the lowest pressure. The theoretical line shape using the hard-sphere kernel is slightly wider and gives more intensity in the region $\Delta'/2\pi=1$ GHz than does the Keilson-Störer kernel and hence is in better agreement with the experimental data. Both models fail in the region very close to the narrow resonances.

To obtain curves which are more closely related to the velocity-changing collision kernel, we have attempted to extract from the experimental spectra only that component arising from velocity-changing collisions (component b of Fig. 2). To extract this component we subtract from the experimental data the theoretical contributions from all other sources. The results of this subtraction are shown in Figs. 13 and 14 as n_{vc}. The smooth curve represents the experimental points after this subtraction. The solid points give the theoretical velocity-changing contribution using the hard-sphere kernel and the open circles give the same for the Keilson-Störer kernel. In Fig. 13 we show results for the case of helium perturbers at 9.5 Torr. As expected from our earlier discussion, both collision kernels give similar distributions and these are in good agreement with the experimental data. The data for krypton at 1 Torr are given in Fig. 14. In this case, the hard-sphere model is clearly superior to the Keilson-Störer approximation, which produces a line shape which is too sharply peaked at $\Delta'=0$.

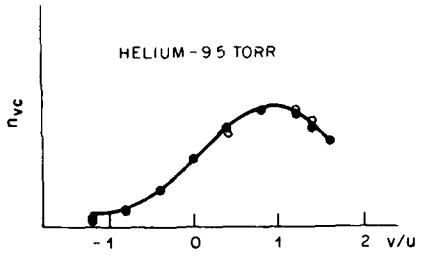

FIG. 13. The contribution of velocity-changing collisions to the excitation spectrum as a function of normalized velocity for 9.5 Torr of helium perturber gas. The smooth curve is the difference between the experimental excitation spectrum and the theoretical contributions to the excitation spectrum from all sources except velocity-changing collisions. The solid circles give the contribution due to velocity-changing collisions as calculated using the hard-sphere kernel; the open circles give the same for the Keilson-Störer kernel.

Although the hard-sphere calculation is in excellent agreement in the wing, it also fails for frequencies very near to the narrow resonance. Owing to the low pressure the theoretical line shapes in Fig. 14 are dominated by the $i=1$ contribution shown in Fig. 7.

The good agreement between theory and experiment in the line wings is evidence that large-angle scattering is correctly described by a hard-sphere model. This result is consistent with large-angle scattering occurring for very close collisions where the alkali–rare-gas potentials can be approximated by an infinite repulsive barrier. The failure of the theory near the narrow resonance for the heavier perturbers (Ne and Kr) is indicative of an interatomic potential that is other than hard sphere. Most likely there exist attractive wells in the Na*-Kr and Na*-Ne potentials that give rise to the additional scattering near the resonances.

The fact that the widths of the narrow resonance near $\Delta'/2\pi = 1.6$ GHz is generally larger than that predicted by the line-shape theory using empirically determined experimental values for all broadening parameters may be due to either (a) additional small-angle velocity-changing collisions or (b) larger values of the broadening parameters caused by the laser selection of fast Na atoms. We should also note that our theory of the $3P_{1/2} \rightarrow 3P_{3/2}$ exchange is oversimplified and can lead to some additional errors.

The values for the hard-sphere collision cross sections which we obtain exhibit the pressure dependence shown in Fig. 15. The slow increase of the cross sections with increasing pressures is another indication that the theory is failing to account properly for the true collisional interaction. This variation implies that with increasing pressure the amplitude of the resonance at $\Delta'/2\pi = 1.6$ GHz becomes increasingly overestimated by the theory leading to anomalously large values for the calculated collision cross sections. Whether this variation is due to our model for $3P_{1/2} \rightarrow 3P_{3/2}$ collisions, to effects of weak velocity-changing collisions, or to our failure to use speed-dependent broadening parameters is unknown at present. It would seem reasonable to consider the cross sections we obtained as upper bounds for the true cross sections.

The cross sections for collisions with neon and krypton are approximately 30 and 55 Å^2, respectively, and are similar to the values which can be deduced from ground-state gas kinetic radii.[17] The fact that the krypton cross section is larger is reasonable in light of its larger size and greater polarizability. The helium cross section of ~60 Å^2, on the other hand, does not fit this picture. The apparent helium cross section is the largest of the three measured cross sections within the estimated accuracy of our measurements of 30 to 40 percent despite the fact that the helium core is surely the smallest and the atom is the least polarizable. It should be noted, however, that we

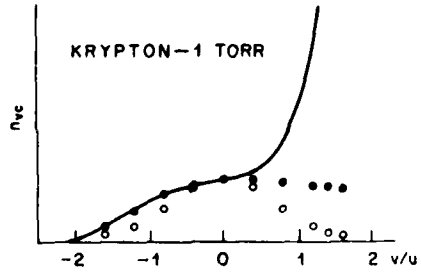

FIG. 14. Same as Fig. 13, except for 1 Torr of krypton perturber gas. The hard-sphere and Keilson-Störer kernels now lead to significantly different profiles.

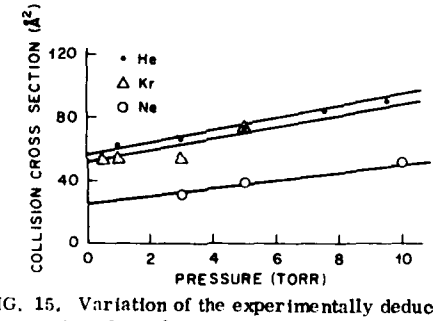

FIG. 15. Variation of the experimentally deduced cross sections for velocity-changing collisions between Na ($3P_{1/2}$) and He, Ne, and Kr perturbers as a function of perturber pressure.

have arbitrarily chosen to fit the data at $\Delta=0$, where, because of the small velocity change produced by sodium-helium collisions, the contribution of the velocity changing signal (component b in Fig. 2) is extremely small. Small errors in the calculation of component c will then result in substantial error in our result for the cross section. If instead, we fit the lowest-pressure helium data at $\Delta'/2\pi = 1$ GHz, we find $\sigma = 35$ Å^2, in better relative agreement with our expectations. However, the optimum cross section is still found to increase with pressure since the cross sections calculated at higher pressures are independent of where we fit the data.

V. CONCLUSION

We have examined the effects of velocity-changing collisions on the $3S_{1/2}-3P_{1/2}-4D_{3/2}$ excitation spectra of sodium vapor. The observed line shapes are reasonably well described by a theory in which collisions are characterized by either the phenomenological Keilson-Störer kernel or a classical hard-sphere kernel. For collisions between excited sodium atoms and heavy rare-gas atoms, the hard-sphere kernel is superior to the Keilson-Störer kernel. It gives a better description of the effects of large-angle scattering, although neither kernel provides a fully adequate description over the entire profile. The two kernels give essentially the same line shape for low active atom to perturber atom mass ratio. They also agree at high pressures independent of the mass ratio. Our data indicate that improved models are required to accurately describe sodium–rare-gas collisions. By fitting our data we extract effective hard-sphere collision cross sections for collisions between sodium $3P_{1/2}$ atoms and helium, neon, and krypton perturbers.

ACKNOWLEDGMENT

The work of one author (PRB) was supported by the U. S. Office of Naval Research.

APPENDIX

In this appendix, collision kernels and rates for classical hard-sphere scattering are derived. The collision kernel $W(\vec{v}',\vec{v})$ gives the probability density per unit time for a collision with the perturber bath to change the velocity of an "active atom" particle from $\vec{v}'$ to $\vec{v}$ and is given by[7]

$$W(\vec{v}',\vec{v}) = N\left(\frac{m_a}{\mu}\right)\int d\vec{v}_p' d\vec{v}_r' W_p(\vec{v}_p') v_r^{-1} \times \delta\left(\vec{v}_r + \frac{m_a}{m_p}\vec{v}' - \frac{m_a}{\mu}\vec{v} + \vec{v}_p'\right) \times \delta(v_r - v_r')\left|f(\vec{v}_r', \vec{v}_r)\right|^2 \quad \text{(A1)}$$

with

$$\vec{v}_r = \vec{v} - \vec{v}_p, \quad \vec{v}_r' = \vec{v}' - \vec{v}_p',$$

where m_a is the active atom mass, m_p is the perturber mass, μ is the reduced mass, $\vec{v}$ (or $\vec{v}'$) is the active atom velocity, $\vec{v}_p$ (or $\vec{v}_p'$) is the perturber velocity, $|f_i(\vec{v}_r',\vec{v}_r)|^2$ is the differential scattering cross section, N is the perturber density, and $W_p(\vec{v}_p)$ the perturber velocity distribution assumed to be of the form

$$W_p(\vec{v}_p) = (\pi u_p^2)^{-3/2}\exp(-v_p^2/u_p^2), \quad \text{(A2a)}$$

$$u_p^2 = 2kT_p/m_p, \quad \text{(A2b)}$$

where T_p is the temperature associated with the perturbers. The delta functions in Eq. (A1) guarantee conservation of momentum and energy in the collisions.

For classical hard-sphere scattering,

$$|f_i(\vec{v}_r',\vec{v}_r)|^2 = r_0^2/4, \quad \text{(A3)}$$

where r_0 is the sum of active atom and perturber hard-sphere radii. Substituting Eq. (A3) into Eq. (A1) and performing the integrations over $\vec{v}_p'$ and $\vec{v}_r$, one can obtain the kernel

$$W(\vec{v}',\vec{v}) = \frac{N\pi r_0^2 u_p}{\pi^{3/2}\alpha^2 u^2 S}\exp\left\{-\left[\left(S + \frac{\mu\vec{S}\cdot\vec{v}'}{m_a S}\right)^2/\alpha^2 u^2\right]\right\}, \quad \text{(A4)}$$

where

$$\vec{S} = \vec{v} - \vec{v}', \quad \text{(A5)}$$

$$u = 2kT_a/m_a, \quad \text{(A6)}$$

$$\alpha = 2(\mu/m_a)(u_p/u), \quad \text{(A7)}$$

and T_a is the temperature characterizing the active atoms. The rate associated with this kernel is

$$\Gamma(\vec{v}) = \int d\vec{v}' W(\vec{v},\vec{v}') = N\pi r_0^2\left\{\frac{u_p}{\sqrt{2}}\exp\left[-\left(\frac{v}{u_p}\right)^2\right] + \left[1 + \tfrac{1}{2}\left(\frac{u_p}{v}\right)^2\right] v\Phi\left(\frac{v}{u_p}\right)\right\}, \quad \text{(A8)}$$

where Φ is the error function. Note that, as expected, for $v \gg u_p$, $\Gamma(v) \sim N\pi r_0^2 v$ and, for $v \ll u_p$, $\Gamma(v) \sim N\pi r_0^2 (2/\pi^{1/2}) u_p$.

In the text, we use a one-dimensional kernel

obtained from Eq. (A1) by averaging over an initial transverse velocity distribution

$$W_t(\vec{v}_t') = (\pi u^2)^{-1} \exp[-(v_t'^2/u^2)], \tag{A9}$$

with

$$\vec{v}_t' = \vec{v}' - v_z'\hat{z} \tag{A10}$$

and summing over all final transverse velocities

$$\vec{v}_t = \vec{v} - v_z\hat{z}\,. \tag{A11}$$

Thus, the one-dimensional kernel is defined by

$$W(v_z', v_z) = \int dv_t dv_t' W_t(\vec{v}_t')\, W(\vec{v}', \vec{v})\,. \tag{A12}$$

Substituting Eqs. (A1) and (A9) into (A12) and carrying out the tedious but straightforward integrations, one may obtain

$$W(v_z', v_z) = \tfrac{1}{4}\pi r_0^2 N \frac{(1+\beta^2)}{\beta^2}\left\{1 - \Phi\left(\frac{1+\beta^2}{2\beta} r|S_z| + \frac{v_z'}{u}\beta\frac{S_z}{|S_z|}\right) + \exp\left[-rS_z\left(rS_z + \frac{2v_z'}{u}\right)\right]\right.$$
$$\left.\times\left[1 - \Phi\left(\frac{1-\beta^2}{2\beta} r|S_z| - \frac{v_z'}{u}\beta\frac{S_z}{|S_z|}\right)\right]\right\}, \tag{A13}$$

where

$$\beta = u/u_b\,,$$
$$r = (\beta^2 + T_a/T_b)/(\beta^2+1)\,.$$

If $T_a = T_b$, then $r = 1$ and one arrives at Eq. (12) of the text.

The rate $\Gamma(v_z)$ defined by

$$\Gamma(v_z) = \int dv_z' W(v_z, v_z')$$

may be calculated as

$$\Gamma(v_z) = \pi r_0^2 N u_b\left(\left(\frac{v_z}{u_b}\right)\Phi\left(\frac{v_z}{u_b}\right) + \pi^{-1/2}\exp\left[-\left(\frac{v_z}{u_b}\right)^2\right]\right.$$
$$\left.\times\left\{1 + \pi^{1/2}\int_0^\infty \exp\left(-\frac{\beta^2 x^2}{(1+\beta^2)^2}\right)\cosh\left(\frac{2v_z x}{u_b(1+\beta^2)^{1/2}}\right)\left[1 - \Phi\left(\frac{x}{1+\beta^2}\right)\right]dx\right\}\right). \tag{A14}$$

Equations (A4), (A8), and (A13) have been derived previously by Kol'chenko.[15] As noted in the text,[11] the use of one-dimensional kernels in the theory of saturation spectroscopy is not strictly valid when the collision rates are speed dependent.

[1] T. W. Hänsch and P. E. Toschek, IEEE, J. Quant. Elect. 5, 61 (1969); P. W. Smith and T. W. Hänsch, Phys. Rev. Lett. 26, 740 (1971); R. Keil, A. Schabert, and P. Toschek, Z. Phys. 261, 71 (1973); I. M. Beterov, Y. A. Matyugin, and V. P. Chebotaev, Zh. Eksp. Teor. Fiz. 64, 1495 (1973) [Sov. Phys.—JETP 37, 756 (1973)].

[2] W. K. Bischel and C. K. Rhodes, Phys. Rev. A14, 176 (1976); C. Brechignac, R. Vetter, and P. R. Berman, Phys. Rev. A 17, 1609 (1978); J. Phys. Lett. (Paris) 39, L231 (1978); T. Mossberg, A. Flusberg, R. Kachru, and S. R. Hartman, Phys. Rev. Lett. 42, 1665 (1979).

[3] C. N. Bagaev, E. V. Baklanov, and V. P. Chebotaev, Pis'ma Zh. Eksp. Teor. Fiz. 16, 15 (1972) [JETP Lett. 16, 9 (1972)]; T. W. Meyer, C. K. Rhodes, and H. A. Haus, Phys. Rev. A12, 1993 (1975); P. Cahuzac, O. Robaux, and R. Vetter, J. Phys. B 9, 3165 (1975); A. T. Mattick, N. A. Kurnit, and A. Javan, Chem. Phys. Lett. 38, 176 (1976); P. Cahuzac, F. Marie, O. Robaux, R. Vetter, and P. R. Berman, J. Phys. B 11, 645 (1978).

[4] D. L. Huber, Phys. Rev. 178, 93 (1969); A. Omont, E. W. Smith, and J. Cooper, Astrophys. J. 175, 185 (1972); J. L. Carlsten and A. Szöke, Phys. Rev. Lett. 36, 667 (1976); J. Phys. B 9, L231 (1976); J. L. Carlsten, A. Szöke, and M. G. Raymer, Phys. Rev. A 15, 1029 (1977); D. L. Rousseau, G. D. Patterson, and P. F. Williams, Phys. Rev. Lett. 34, 1306 (1975); R. D. Driver and J. L. Snider, J. Phys. B 10, 595 (1977).

[5] P. F. Liao, J. E. Bjorkholm, and P. R. Berman, Phys. Rev. A 20, 1489 (1979).

[6] J. Keilson and K. E. Störer, Q. Appl. Math. 10, 243 (1952).

[7] P. R. Berman, Adv. At. Mol. Phys. 13, 57 (1977).

[8] P. R. Berman, P. F. Liao, and J. E. Bjorkholm, Phys. Rev. A 20, 2389 (1979).

[9] See, for example, J. E. Bjorkholm and P. F. Liao, Phys. Rev. A14, 751 (1976) and references therein.

[10]See, for example, I. M. Beterov and V. P. Chebotaev, Prog. Quant. Electr. 3, 1 (1974); R. Salomaa and S. Stenholm, J. Phys. B 8, 1795 (1975); 9, 1221 (1976).

[11]The use of a one-dimensional kernel is not strictly valid in cases where the collision rates are speed dependent. In order to reduce the equations to those of an effective one-dimensional problem in velocity space, one must be able to factor the density matrix into parts depending on the longitudinal and transverse velocity components. This factorization procedure fails for saturation spectroscopy with speed-dependent rates; the pump laser field excites a nonthermal longitudinal velocity distribution which is transferred, in part, to the transverse velocity distribution *via* the speed dependence in the collision rate (i.e., if one excites a "hot" longitudinal atom, part of this heat is transferred to the transverse velocity distribution *via* collisions). The errors introduced by using a one-dimensional kernel are probably not severe, considering the overall accuracy of the calculation.

[12]M. Borenstein and W. E. Lamb, Phys. Rev. A5, 1311 (1972).

[13]J. L. LeGouët, J. Phys. B 11, 3001 (1978).

[14]C. R. Borde, private communication.

[15]A. P. Kol'chenko, S. G. Rautian, and A. M. Shalagin, Nucl. Physics Institute Semiconductor Physics Internal report, 1972 (unpublished).

[16]See Table I of Ref. 5.

[17]C. W. Allen, *Astrophysical Quantities*, 2nd ed. (Univ. of London, London, 1963), p. 45.

J. Phys. B: Atom. Molec. Phys. 13 (1980) 2359–2365. Printed in Great Britain

Solvable model for optical and radiative collisions†

E J Robinson

Physics Department, New York University, 4 Washington Place, New York, NY 10003, USA

Received 6 August 1979, in final form 2 November 1979

Abstract. The related problems of optical and radiative collisions are examined theoretically. The actual R^{-n} potentials found in nature are simulated by powers of the hyperbolic secant, which enables one to obtain closed-form solutions for the transition probabilities in the weak-field regime.

Recently much attention has been given to the related problems of 'optical' and 'radiative' collisions (Cahuzac and Toschek 1978, Brechignac *et al* 1979, Falcone *et al* 1976a, b, Gallagher and Holstein 1977, Geltman 1976, Gudzenko and Yakovlenko 1972, Harris and Lidow 1974, 1975, Harris and White 1977, Knight 1977, Lisitsa and Yakovlenko 1974, Payne *et al* 1977, Payne and Nayfeh 1976, Robinson 1979, Yeh and Berman 1979). In the optical case, foreign-gas collisions enhance the probability of photoabsorption by an atom interacting with a radiation field detuned from resonance by more than the Doppler width. (For strong fields, the detuning is presumed to be in excess of the power-broadened homogeneous width.) Thus, without the collision, the transition probability is negligible.

A radiative collision is one in which excitation is transferred between two unlike atomic species due to the simultaneous effect of the collision between the atoms and their interaction with the radiation field. The photon is nearly resonant with the difference in excitation energy between the two atoms. Since the transition involves a change in state of both of the atoms, it is rigorously forbidden without the collision.

In this paper, we present solutions for a model version of these problems in the weak-field limit. The models replace the true potentials that characterise the dynamics with powers of the hyperbolic secant. These retain the essential physics but enable one to obtain closed-form expressions for transition probabilities.

The theoretical treatments are similar for the two problems. The relative nuclear motion is taken to be a classical straight-line path, so that the atom–atom interaction generates a time-dependent potential for the electrons, whose motion is then described via the Schrödinger equation. Making the dipole approximation for the electron–field interaction, the electronic Hamiltonian for either problem is

$$H = H_a + V_c + e\boldsymbol{E}\cdot(\boldsymbol{r}_A + \boldsymbol{r}_B)\cos\Omega t \tag{1}$$

where H_a is the separated atom Hamiltonian, V_c the atom–atom interaction, $\boldsymbol{E}$ the amplitude of the electric field (we assume linearly polarised light), $\boldsymbol{r}_A$ and $\boldsymbol{r}_B$ the sum of

† Work supported by the US Office of Naval Research.

the coordinates of the electrons in each atom with respect to its respective nucleus, and Ω the frequency of the field.

For optical collisions, if one makes the further simplification that the effect of V_c may be adequately represented by its asymptotic van der Waals' R^{-6} energy, and that only two levels, the initial and final states of active atom A, designated $|1\rangle$ and $|2\rangle$, need be included in the expansion for the wavefunction, the Schrödinger equation becomes a pair of coupled equations for a two-level system. Making the rotating-wave approximation, the effective two-level Hamiltonian is, in the 'dressed atom' representation (Yeh and Berman 1979)

$$H = \sum_{j=1}^{2} \left(\frac{\Delta C_{6j}}{2\nu R^6}\right) |j\rangle\langle j| + (\chi C_6/R^6)[|1\rangle\langle 2| \exp(\mathrm{i}\nu t) + |2\rangle\langle 1| \exp(-\mathrm{i}\nu t)] \tag{2}$$

where C_{6j} is the van der Waals' constant of $|j\rangle$, $C_6 = C_{61} - C_{62}$, ν the Rabi frequency, χ the field strength in frequency units, and Δ the detuning from exact resonance.

One may approximately reduce the radiative collision problem to a two-level system as well. Here states $|1\rangle$ and $|2\rangle$ are composites—in state $|1\rangle$ atom A is excited to A* and B in ground state B_0, while in $|2\rangle$, A is in ground state A_0 and B excited to B**. The transition proceeds via virtual intermediate states of the composite system. If one sums over these and assumes that the relevant frequency range is sufficiently small to treat the summations as essentially frequency independent, we obtain, after angle averaging, the effective two-level Hamiltonian

$$H = \sum_{j=1}^{2} \left(\frac{C_{6j}}{R^6} + Q_j E^2\right) |j\rangle\langle j| + \frac{KE}{R^3}[|1\rangle\langle 2| \exp(\mathrm{i}\Delta t) + |2\rangle\langle 1| \exp(-\mathrm{i}\Delta t)] \tag{3}$$

where we have again represented the atom–atom interaction by its leading term at large separations. Here C_{6j}, Q_j are the van der Waals and AC Stark coefficients for state $|j\rangle$, K is the indicated intermediate-state factor, and Δ the detuning. The time-dependent Schrödinger equation for state amplitudes a_1 and a_2 become, in an interaction representation, for optical collisions

$$\mathrm{i}\dot{a}_1 = \frac{A}{R^6}\left\{\exp\left[\mathrm{i}\left(C_6' \int_0^t \mathrm{d}t'\, R^{-6}(t') + \nu t\right)\right]\right\} a_2 \tag{4a}$$

$$\mathrm{i}\dot{a}_2 = \frac{A}{R^6}\left\{\exp\left[-\mathrm{i}\left(C_6' \int_0^t \mathrm{d}t'\, R^{-6}(t') + \nu t\right)\right]\right\} a_1 \tag{4b}$$

where $A = (\chi/\nu)\, C_6$ and $C_6' = (\Delta/2\nu)\, C_6$.

The corresponding equations for the radiative collision problem are

$$\mathrm{i}\dot{a}_1 = a_2 \frac{KE}{R^3}\left\{\exp\left[\mathrm{i}\left(C_6 \int_0^t \mathrm{d}t'\, R^{-6}(t') + \Delta_g t\right)\right]\right\} \tag{5a}$$

$$\mathrm{i}\dot{a}_2 = a_1 \frac{KE}{R^3}\left\{\exp\left[-\mathrm{i}\left(C_6 \int_0^t \mathrm{d}t'\, R^{-6}(t') + \Delta_g t\right)\right]\right\} \tag{5b}$$

where Δ_g is a 'generalised' central detuning, defined to incorporate the AC Stark effect, i.e., $\Delta_g = \Delta + (Q_1 - Q_2)\, E^2$. These equations are to be solved subject to the initial conditions $a_1 = 1$, $a_2 = 0$ for $t \to -\infty$. In the weak-field limit, $a_1 \simeq 1$ for all t, and the

transition amplitude, $a_2(+\infty)$, becomes

$$a_2(\infty) = -iF\int_{-\infty}^{\infty} R^{-3m}(t)\exp\left[-i\left(\lambda\int_0^t R^{-}(\quad)\,dt' + st\right)\right]dt \tag{6}$$

where $m = 1$, $\lambda = C_6$, $s = \Delta$, $F = K$ in the radiative problem, and $m = 2$, $\lambda = C_6'$, $s = \nu$, $F = A$, in optical collisions. (In this low-power limit, the AC Stark effect is naturally neglected.)

Thus, for weak fields, the problem reduces to the evaluation of the integral in equation (6). For the actual R^{-n} potentials found in nature, exact analytic expressions for this integral are not known, although various approximations have been tried which do yield closed forms for radiative collisions. Geltman (1976) and Knight (1977) use a method that is equivalent to neglecting the level-shifting term in the exponential of equation (6), and obtain a result proportional to the modified Bessel function K_1. Robinson extended their results by approximating the R^{-6} level-shifting potential by a delta function in time, obtaining, in addition to a term that behaves like the K_1 function, a term dependent on modified Bessel and Struve functions I_1 and L_{-1}. In the present work, we replace the R^{-3} and R^{-6} interactions by model potentials which closely resemble their time dependence but for which the integrals may be exactly evaluated in terms of special functions.

We begin with the case of radiative collisions. R^{-3} is replaced by $(\operatorname{sech} \pi t/T)/\rho^3$, R^{-6} by $(B/\rho^6)(\operatorname{sech}^2 \pi t/T)$, where ρ is the impact parameter, $T = 2\rho/v$, where v is the relative velocity.

B is chosen so that the phase induced by the model and true potentials are the same. In tables 1 and 2 we present values for the model and true coupling and level-shifting potentials for values of t expected to make the dominant contribution to the transition probability, and note that the correspondence is close except where the potential drops to less than 10% of its peak value. Our choice of parameters has the property that when $C_6 \to 0$ and $\Delta = 0$, the model and exact problems predict the same transition probabilities.

Table 1. A comparison of the true and model coupling potentials, $V_T = R^{-3}$ and $V_M = \rho^{-3}\operatorname{sech}(\pi t/T)$. The time t is expressed in units of $T = 2\rho/v$. The potentials are normalised to be equal at $t = 0$ and to have the value 8.

t	V_T	V_M	V_T/V_M
0	8·00	8·00	1·00
0·1	7·54	7·62	0·99
0·2	6·40	6·64	0·96
0·3	5·04	5·41	0·93
0·4	3·81	4·21	0·90
0·5	2·83	3·19	0·89
0·6	2·10	2·37	0·88
0·7	1·57	1·75	0·90
0·8	1·19	1·29	0·93
0·9	0·92	0·94	0·97
1·0	0·72	0·69	1·03
1·1	0·57	0·50	1·12
1·2	0·46	0·37	1·23
1·3	0·37	0·27	1·37

Table 2. A comparison of the true and model level-shifting potentials, $V_T = R^{-6}$ and $V_M = (3\pi^2/32\rho^6)\,\mathrm{sech}^2(\pi t/T)$. The potentials are normalised so that $V_T = 64$ at $t = 0$ and so that the integrated phase is the same for each. The time t is expressed in units of $T = 2\rho/v$.

t	V_T	V_M	V_T/V_M
0·0	64·0	59·2	1·08
0·1	56·9	53·7	1·06
0·2	41·0	40·8	1·00
0·3	25·4	27·1	0·94
0·4	14·5	16·4	0·88
0·5	8·0	9·4	0·85
0·6	4·4	5·2	0·84
0·7	2·5	2·8	0·87
0·8	1·4	1·5	0·92
0·9	0·84	0·82	1·02
1·0	0·51	0·44	1·16
1·1	0·32	0·24	1·36

For the model potentials, equation (6) becomes

$$\mathrm{i}a_2(\infty) = \frac{K}{\rho^3}\int_{-\infty}^{\infty} \mathrm{sech}\left(\frac{\pi t}{T}\right)\exp\left\{\mathrm{i}\left[\mu\,\tanh\left(\frac{\pi t}{T}\right)+\Delta t\right]\right\}\mathrm{d}t$$

$$= \frac{KT}{\pi\rho^3}\int_{-\infty}^{\infty} \mathrm{sech}\,x\,\exp[\mathrm{i}(\mu\,\tanh x+\beta x)]\,\mathrm{d}x \tag{7}$$

where $x = \pi t/T$ and $\beta \equiv \Delta T/\pi$. The author was unable to locate this integral in the general tables available to him, although once he had succeeded in evaluating it, did find it in the more specialised literature (Buchholz 1969). There is some epistomological value in presenting the evaluation of the integral in equation (6), so we do so, rather than merely presenting the formula of Buchholz. We write

$$F = \int_{-\infty}^{\infty} \mathrm{sech}\,x\,\exp[\mathrm{i}(\mu\,\tanh x+\beta x)]\,\mathrm{d}x. \tag{8a}$$

If we differentiate F with respect to μ, we have

$$\frac{\mathrm{d}F}{\mathrm{d}\mu} = \mathrm{i}\int_{-\infty}^{\infty} \mathrm{sech}\,x\,\tanh x\,\exp[\mathrm{i}(\mu\,\tanh x+\beta x)]\,\mathrm{d}x \tag{8b}$$

and

$$\frac{\mathrm{d}^2F}{\mathrm{d}\mu^2} = -\int_{-\infty}^{\infty} \mathrm{sech}\,x\,\tanh^2 x\,\exp[\mathrm{i}(\mu\,\tanh x+\beta x)]\,\mathrm{d}x. \tag{8c}$$

Performing parts integrations of equations (8*b*) and (8*c*), and rearranging terms, we obtain the differential equation

$$\mu F'' + F' + (\mu + B)F = 0 \tag{9}$$

where a prime denotes differentiation with respect to μ. This equation is to be solved

subject to the boundary condition that at $\mu = 0$

$$F = \int_{-\infty}^{\infty} \operatorname{sech} x \, e^{i\beta x} \, dx = \pi \operatorname{sech}(\pi\beta/2).$$

If equation (9) is reduced to normal form, we have, with $\phi = \mu^{1/2}F$

$$\phi'' + [\tfrac{1}{4}\mu^{-2} + 1 + \beta\mu^{-1}]\phi = 0 \tag{10}$$

which has the same form as the radial Schrödinger equation for a charged particle in a Coulomb field of coupling constant $-\frac{1}{2}\beta$ and 'angular momentum' $L = \frac{1}{2}$. The lack of symmetry that prevails in the radiative collision problem according to the sign of the detuning may be inferred directly from the great difference between the wavefunctions in the Coulomb problem for attractive and repulsive potentials. If we consider the radiative collision problem where the final state has a van der Waals potential that is more attractive than that of the initial state, negative detuning corresponds to a repulsive Coulomb potential, and positive detuning to an attractive Coulomb potential.

With the given boundary condition, we thus find the transition amplitude proportional to a confluent hypergeometric function

$$ia_2(\infty) = \left(\frac{KE}{\rho^2 v}\right) e^{-i\alpha} \operatorname{sech}\left(\frac{\pi\beta}{2}\right) {}_1F_1\left(\frac{1}{2} + i\frac{\Delta\rho}{\pi v}, 1, i\frac{3\pi C_6}{8\rho^5 v}\right). \tag{11}$$

This reduces at exact resonance to the Bessel function J_0,

$$ia_2(\infty) = \left(\frac{KE}{\rho^2 v}\right) J_0\left(\frac{3\pi C_6}{16\rho^5 v}\right). \tag{12}$$

Equation (12) could be obtained directly by noting that the change of variable $\tanh x = \sin y$ casts equation (8*a*) into the form of a well known representation of the Bessel function (Abramowitz and Stegun 1964).

The total cross section may be calculated by integrating the transition probability over impact parameter, yielding

$$Q = 2\pi \int_0^\infty |a_2(\infty)|^2 \rho \, d\rho. \tag{13}$$

Off resonance, this requires numerical integration or other approximate methods. The resonant case may be evaluated exactly, however (Gradshteyn and Ryzhik 1965). Thus, for zero detuning, we have

$$Q = \frac{2K^2E^2}{2^{3/5}\pi v^{8/5}} \left(\frac{3\pi C_6}{16}\right)^{-2/5} \frac{\Gamma(\frac{3}{5})\Gamma(\frac{1}{5})}{(\Gamma(\frac{4}{5}))^3}. \tag{14}$$

For small impact parameters, μ becomes large, and one may use the asymptotic form of the confluent hypergeometric function. We find that the transition probability goes to zero as $\rho \to 0$, oscillating with increasing rapidity as ρ diminishes. These oscillations are a well known characteristic of this problem (Harris and White 1977). However, our observation that the envelope of the transition probability vanishes linearly near the origin is in disagreement with the extrapolated curve of Harris and White. Those authors present a curve whose envelope approaches a constant non-zero value as ρ decreases. This is hard to understand, since a steepest descent evaluation of the integral in equation (6), with the true potentials in the integrand, yields a result

qualitatively similar to our own. (One does obtain a constant envelope factor at small impact parameter in the optical collision case.)

The discussion of the previous paragraph refers only to the puzzle of differing mathematical results, and should not be taken to mean that we claim our solution to be valid for small values of ρ. The original formulation of the problem in terms of R^{-m} potentials and straight-line paths is invalid in this region, and our model, which does not correct for these simplifications, cannot be expected to hold there either.

That the formulation is truly applicable only for large is not a serious defect, since the major portion of the total cross section is contributed by impact parameters where the approximations are good. It may also be possible, by modifying the scheme used for parametrising the hyperbolic secants, to incorporate some small separation effects into a generalisation of the model presented here. We are examining recent experimental results for clues as to how this might be accomplished.

Sample numerical values of total cross sections are close to the 'universal' curve of Payne *et al* (1977), who evaluated equations (6) and (13) numerically, in terms of dimensionless variables.

As we have indicated, an entirely analogous procedure can be applied to the optical collision case, with $\operatorname{sech}^2 \pi t/T$ replacing $R^{-6}(t)$ in both the exponential and the prefactor. For this problem, we wish to evaluate

$$F = \int_{-\infty}^{\infty} \operatorname{sech}^2 x \exp[\mathrm{i}(\mu \tanh x + \beta x)]\,\mathrm{d}x. \tag{15}$$

A differential equation in μ is again obtained, this time

$$\mu F'' + 2F' + (\mu + \beta)F = 0 \tag{16}$$

which, to within a trivial transformation, is the same as the confluent hypergeometric equation. The relevant solution this time is

$$F = \pi\beta \operatorname{cosech}(\tfrac{1}{2}\pi\beta)\, \mathrm{e}^{-\mathrm{i}\mu} \quad {}_1F_1(1 + \tfrac{1}{2}\mathrm{i}\beta, 2, 2\mathrm{i}\mu). \tag{17}$$

In normal form, this becomes a Coulomb radial equation for angular momentum $L = 0$. Equation (16) is solved subject to the boundary condition at $\mu = 0$

$$F = \pi\beta \operatorname{cosech}(\tfrac{1}{2}\pi\beta).$$

For the impact limit $\nu = 0$ and the solution once more reduces to a Bessel function, this time $J_{1/2}(\mu)$. We note that this impact limit is exact, i.e., it is identical to the weak-field impact limit of the original R^{-6} problem. That the model gives the same result as the true potential in this case is not surprising, since the impact limit assumes that 'nothing happens' during the collision, i.e., that the result depends only upon the phase induced by the collision, not upon the shape in time of the potential function. Since the true and model potentials induce the same phase by construction, there can be no difference between their results.

In future work, we shall apply the model developed here to specific systems of experimental interest. We also note that this model may be solved analytically for fields of arbitrary strength. The solutions one obtains are not among those special functions familiar to physicists. We shall report on this work also in a subsequent article.

References

Abramowitz M and Stegun I A 1964 *Handbook of Mathematical Functions* (Washington, DC: National Bureau of Standards)

Brechignac C, Cahuzac P and Toschek P E 1979 Preprint

Buchholz H 1969 *The Confluent Hypergeometric Function* (Berlin, Heidelberg, New York: Springer)

Cahuzac P and Toschek P E 1978 *Phys. Rev. Lett.* **40** 1087

Falcone R W, Green W R, White J C, and Harris S E 1976a *Phys. Rev. Lett.* **36** 462

—— 1976b *Phys. Rev. Lett.* **37** 1590

Gallagher A and Holstein T 1977 *Phys. Rev.* A **16** 2413

Geltman S 1976 *J. Phys. B: Atom. Molec. Phys.* **9** L569

Gradshteyn I S and Ryzhik I M 1965 *Table of Integrals, Series, and Products* (New York, San Francisco, London: Academic)

Gudzenko L I and Yakovlenko S I 1972 *Sov. Phys.-JETP* **35** 877

Harris S E and Lidow D B 1974 *Phys. Rev. Lett.* **33** 1974

—— 1975 *Phys. Rev. Lett.* **34** 172

Harris S E and White J C 1977 *IEEE J. Quant. Electron.* **QE-13** 972

Knight P L 1977 *J. Phys. B: Atom. Molec. Phys.* **10** L19

Lisitsa V S and Yakovlenko S E 1974 *Sov. Phys.-JETP* **39** 759

Payne M G, Choi C W and Nayfeh M H 1977 *Proc. Conf. on Multiphoton Processes, Rochester, NY* Abstracts p 190

Payne M G and Nayfeh M H 1976 *Phys. Rev.* A **13** 596

Robinson E J 1979 *J. Phys. B: Atom. Molec. Phys.* **12** 1451

Yeh S and Berman P R 1979 *Phys. Rev.* A **19** 1106

Supported by the U.S. Office of Naval Research
under Contract No. N00014-77-C-0553.

J. Phys. B: Atom. Molec. Phys. **13** (1980) 2243–2250. Printed in Great Britain

Pulse area effects in resonant multiphoton ionisation†

E J Robinson

Department of Physics, New York University, 4 Washington Place, New York, NY 10003, USA

Received 1 August 1979, in final form 20 November 1979

Abstract. A theory of resonant multiphoton ionisation by smooth pulses is developed. It is shown that the spectrum of the effect may exhibit structure associated with time domain correlations.

Among the effects of non-linear optics, multiphoton ionisation and detachment were among the earliest to be investigated after the invention of the laser (Geltman 1963, 1965, Hall *et al* 1965, Hall 1966, Robinson and Geltman 1967, Zernik 1964, Zernik and Klopfenstein 1965, Bebb 1966, 1967, Bebb and Gold 1966, Chin and Isenor 1967, Chin *et al* 1969, Young *et al* 1969, Fox *et al* 1971, Kogan *et al* 1971, Agostini *et al* 1971, Luger and Robinson 1970, Luvain and Mainfray 1972). These are bound–free electronic transitions in atomic systems generated by the smultaneous absorption of more than one quantum. The calculation of rates for these processes typically requires the evaluation of summations over intermediate states. In the crudest approximation, the theory assumes that the radiation field is monochromatic and is switched on adiabatically. If the intensity is low and there are no nearly resonant intermediate states, the transition rate is given by the lowest order of time-dependent perturbation theory consistent with the number of photons of energy $h\nu$ needed to compensate for the binding energy. Much work has been done on this problem, and it remains an active area of research (Flank *et al* 1976, Flank and Rachman 1975, Teague *et al* 1976).

In recent times, with the availability of tunable lasers, the study of multiphoton ionisation where one or more intermediate states are close to resonance has come to the fore (Beers and Armstrong 1975, Geltman 1979, Dixit and Lambropoulous 1979, Gontier and Trahin 1979, Granneman and van der Wiel 1975, Eberly and ONeil 1979). (Negative ions have few, if any, bound excited states, so that these systems are excluded.) The simple perturbation theory, acceptable in the non-resonant case, becomes invalid when the population of the initial level is depleted and/or its phase is significantly affected by coupling to the intermediate states. Theories which take this into account have been developed and predict interesting effects such as structure in the photoionisation spectrum due to the AC Stark effect, the departure of the transition probability from a simple linear function of time and bandwidth effects. The richness of this field has stimulated great activity.

† Work supported by the US Office of Naval Research.

0022-3700/80/112243+08$01.50

The purpose of the present paper is to point out that under special, but potentially achievable circumstances, the combined temporal behaviour of a pulsed laser and an atomic system undergoing population oscillations can conspire to produce a spectrum (transition probability versus frequency) in multiple photon ionisation which has a minimum at exact intermediate state resonance (ISR), exhibits maxima as the laser is detuned above and below, and then falls off rapidly. This superficially resembles the AC Stark effect in experiments where there are three resonantly coupled bound levels, but has a very different origin. It involves the radiation from only one pulsed laser, not two. In addition, the power dependence of the effect differs markedly from that associated with Stark structure, being present only for pulses whose areas are close to $2\pi n$, n integral. (Our 'pulse area' is twice the area used in the sense of photon echoes.) In principle, n may be any integer, but it is unlikely that the effect could readily be seen for any value but $n = 1$. This is discussed in detail below. We designate this splitting as 'mock structure' because of its misleading resemblance to Stark structure.

This structure occurs because the probability of inducing the final state is a function of the product of the pulse envelope and the intermediate state population. The latter oscillates in time, and if it should pass through a minimum coincidentally with the maximum in the envelope function of the field strength, the transition probability will be lower than at neighbouring frequencies where this anticorrelation is absent or less pronounced.

We consider an isolated atom interacting with a pulsed laser, undergoing multiple photon ionisation from the ground state via a single resonant intermediate state. For simplicity, effects due to the other, non-resonant, intermediate states are ignored in this article. The ground and intermediate states are strongly coupled, with the latter also connected to the final states in the continuum. The coupling to the continuum is weak, and is treated perturbatively, with the effect of the continuum on the populations and phases of the intermediate and ground states ignored. Final-state amplitudes are to be computed via a quadrature over the intermediate-state amplitude.

Let the pulse coupling the two-level bound complex have the form $f(t)\cos\Omega t$, where $f(t)$ is a smooth function of time, vanishing at $t = \pm\infty$. No assumption about the 'adiabaticity' or 'suddenness' is made. The time-dependent Schrödinger equation for the amplitudes of this pair of states becomes, in the rotating-wave approximation,

$$\mathrm{i}\dot{a}_1 = V_{12}(t)a_2\exp(\mathrm{i}\Delta t) \tag{1a}$$

$$\mathrm{i}\dot{a}_2 = V_{12}(t)a_1\exp(-\mathrm{i}\Delta t) \tag{1b}$$

where Δ is the detuning of the central frequency of the pulse from exact ISR. The amplitude of a particular continuum state is given perturbatively by

$$a_k(t) = -\mathrm{i}\int_{\infty}^{t} a_2(t')V_{2k}(t')\exp(-\mathrm{i}\Delta_k t')\,\mathrm{d}t' \tag{2a}$$

so that the probability of finding the system is state $|k\rangle$ as $t \to +\infty$ becomes

$$P_k = |a_k(t = +\infty)|^2$$

$$= \int_{-\infty}^{\infty} a_0(t)V_{2k}(t)\exp(-\mathrm{i}\Delta_k t)\,\mathrm{d}t\int_{\infty}^{\infty} V_{2k}(t')\exp(\mathrm{i}\Delta_k t')a_2^*(t')\,\mathrm{d}t'. \tag{2b}$$

The total probability of ionisation is then obtained by integrating over the continuum

$$P = \int_0^\infty P_k \, \mathrm{d}E_k$$

$$= \int_0^\infty \mathrm{d}E_k \int_{-\infty}^\infty V_{2k}(t) \exp(-\mathrm{i}\Delta_k t) a_2(t) \, \mathrm{d}t$$

$$\times \int_{-\infty}^\infty V_{2k}(t') \exp(\mathrm{i}\Delta_k t') a_2^*(t') \, \mathrm{d}t' \tag{3}$$

where we have incorporated the density of continuum states into the definition of V_{2k}. If the overall process is a two-quantum effect, V_{2k} has the same time dependence as V_{12}. If states $|1\rangle$ and $|2\rangle$ differ by one photon, and states $|2\rangle$ and $|k\rangle$ by $N-1$ photons (for a total absorption of N photons in ionising the ground state), V_{2k} is an effective operator whose time dependence is $f^{(N-1)}(t)$. Making the usual mild approximations of neglecting the variation of $V_{2k} = V_0^e f^{N-1}(t)$ with final-state energy and extending the lower limit of the energy integration to $-\infty$ (Geltman 1979), the integrated transition probability becomes

$$P = \int_{-\infty}^\infty \mathrm{d}\Delta_k (V_0^e)^2 \int_{-\infty}^\infty f^{N-1}(t) \exp(-\mathrm{i}\Delta_k t) a_2(t) \, \mathrm{d}t$$

$$\times \int_{-\infty}^\infty f^{N-1}(t') \exp(\mathrm{i}\Delta_k t') a_2^*(t') \, \mathrm{d}t' \tag{4}$$

or, since the detuning integral is proportional to $\delta(t-t')$,

$$P = 2\pi (V_0^e)^2 \int_{-\infty}^\infty f^{2N-2}(t) |a_2(t)|^2 \, \mathrm{d}t. \tag{5}$$

We note that while $a_2(t)$ is a function of the detuning between states $|1\rangle$ and $|2\rangle$, the integral in equation (5) is independent of Δ_k, the detuning between the intermediate and final states. The population $|a_2(t)|^2$ undergoes Rabi-type oscillations, whose amplitude in the strong-field region is roughly independent of detuning, but where the positions of extrema do depend on Δ, the first detuning. Hence, if the time duration of $f^{(2N-2)}(t)$ is short, one may expect to see an oscillatory variation of P with laser frequency. This is most clearly demonstrated in the limiting case of large N, where f^{2N-2} is approximated by the delta function $C\delta(t)$, C constant, so that

$$P = 2\pi C^2 |a_2(0)|^2. \tag{6}$$

We see that in this extreme situation, the photoionisation spectrum is simply the population variations of level $|2\rangle$ transformed into the frequency domain.

We now examine the question of where and whether one may find a sufficiently narrow f^{2N-2} to be possibly observable in actual systems with realistic pulses. We require the coupling between levels $|1\rangle$ and $|2\rangle$ to be sufficiently strong to render the amplitude of the population oscillations at least roughly independent of detuning, without causing the oscillation frequency to be rapid enough to wash out the effect. The details will, of course, depend upon the pulse shape. To simplify the work, we resort to a model in which $f(t)$ is a hyperbolic secant in time. This provides a smooth envelope which might well resemble true pulses. It also enables one to solve the two-level part of

the problem analytically (Rosen and Zener 1932, Robiscoe 1978). Equations (1) become

$$i\dot{a}_1 = V_0 \operatorname{sech}(\pi t/T) \exp(i\Delta t) a_2 \tag{7a}$$

$$i\dot{a}_2 = V_0 \operatorname{sech}(\pi t/T) \exp(-i\Delta t) a_1. \tag{7b}$$

In terms of the parameters a, b, c, Z, given by

$$a = V_0 T/\pi \qquad b = -V_0 T/\pi \qquad c = \tfrac{1}{2} + i\Delta T/2\pi$$

$$Z = \tfrac{1}{2}[\tanh(\pi t/T) + 1]$$

with the initial conditions $a_1 = 1$ and $a_2 = 0$ at $t = -\infty$, equation (5) becomes

$$P = 4T(V_0^e)^2 \int_0^1 [4Z(1-Z)]^{N-2} |a_2(Z)|^2 \, dZ \tag{8}$$

with a_2 given in terms of the variable Z by (Robiscoe 1978, Rosen and Zener 1932)

$$a_2 = \frac{V_0 T}{\pi(|1-c|)} Z^{1-c} {}_2F_1(c-a+1, c-b+1, 2-c, Z) \tag{9}$$

where ${}_2F_1$ is a hypergeometric function.

The appropriate parameters to characterise the problem in this regime of small V_0^e are T, N and V_0T, where the pulse area V_0T determines whether the transition from level $|1\rangle$ to level $|2\rangle$ is saturated, and, if so, the number of oscillations that the population of the intermediate state undergoes for all times.

To gain a quantitative understanding of how the frequency spectrum for multiphoton ionisation varies with the parameters of the problem, we integrated equation (8) numerically, varying N between 3 and 13, and let V_0T assume values in the vicinity of $2\pi n$, with $n = 1, 2, 3$. (At exact resonance, this condition assures that the amplitude a_2 passes through zero at $t = 0$.) We also explored the regions where the pulse area was very different from an integral multiple of 2π. We found the following results. For $V_0T < 5$, the spectra peaked at $\Delta = 0$ and diminished monotonically with increasing detuning for all values of N in the range investigated, i.e., no structure is predicted. For $V_0T \simeq 2\pi$, and $N \leqslant 4$, no structure was perceived, but for $N > 4$, we found that the calculated ionisation probability had a local minimum at $\Delta = 0$, rose to a maximum for small but finite detuning, and then decreased monotonically with still greater detuning. As N increased, the value of Δ for which the maximum occurred tended to increase slowly. The ratio, $1 + R$, of the maximum ionisation probability to the value at $\Delta = 0$, increased more rapidly with increasing N. The excess probability R varied from a few per cent at $N = 5$ to nearly unity at $N = 13$, i.e., for high-order processes, as one might expect, the effect is more pronounced. It was not necessary that the pulse area be exactly 2π to see the mock structure. We found that the splitting was perceivable in the range from about $V_0T \simeq 5{\cdot}5$ to $V_0T \simeq 7$, peaking, of course, at 2π. For $V_0T > 7$, the effect washes out. It reappears in the limit of large N for pulse areas near 4π (see below). Table 1 shows, for $V_0T = 2\pi$, the position of the maximum and the ratio $1 + R$ of the maximum ionisation probability to the resonant probability, for increasing N. Figure 1 represents a photoionisation spectrum for the case of $N = 13$.

For $N = 13$, we found that some small structure (R is a few per cent) could be seen in the vicinity of $V_0T = 4\pi$. It appears that this 'second harmonic' will be obtainable experimentally only with great difficulty.

Table 1. Position and amplitude of mock structure maxima.

N	$(\Delta T)_{max}$	$1+R$
5	2·0	1·02
6	3·0	1·10
7	3·5	1·20
8	4·0	1·31
9	4·0	1·43
10	4·3	1·55
11	4·3	1·66
12	4·5	1·79
13	4·5	1·91

N is the number of photons needed to ionise the ground state. $(\Delta T)_{max}$ is the position of the mock structure maximum in dimensionless units. T is the characteristic time that appears in the hyperbolic secant envelope function. $1+R$ is the ratio of transition probability at maximum to probability at exact resonance.

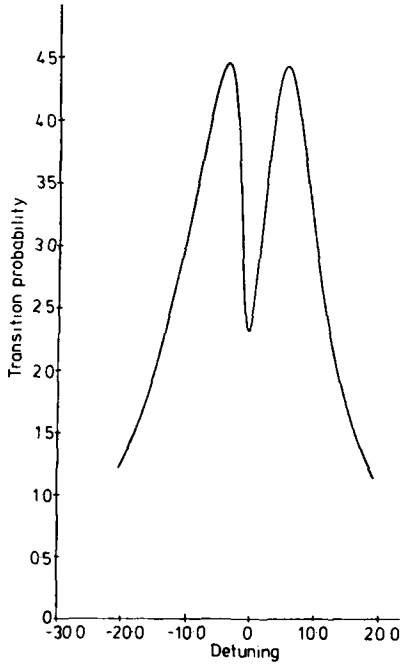

Figure 1. Mock structure for a pulse area of 2π and $N = 13$. The ordinate is the transition probability for ionisation, in arbitrary units, the abscissa is the detuning in units of T^{-1}.

While our quantitative predictions are strictly valid only for the hyperbolic secant pulse, we believe that qualitatively similar results should obtain for general pulse shapes and be observable with mode-locked lasers.

The present treatment assumes that the coupling between the intermediate state (IS) and the continuum is weak, implying that $N\hbar\Omega$ is above, and $(N-1)\hbar\Omega$, below the threshold for ionisation. Thus, since the calculated results indicate that N must be at

least 5 before mock structure can be observed, we require that the IS excitation energy be less than one quarter of the ionisation potential of the initial state. This condition cannot be satisfied for the ground states of most atomic systems if the bound–bound transition is constrained to be allowed by E1 selection rules.

Nevertheless, it is possible to find systems which are realistic candidates for experimental studies of the theory presented here. The simplest of these are the metastable 1s2s $^1S_0$ levels of the He isoelectronic series. Table 2 presents the ionisation potentials and 2s–2p excitation energies for the first three members of this sequence (Wiese *et al* 1966). Taking the photon energy to be nearly resonant with the indicated transition, the photoionisation of metastable He, Li^+ and Be^{2+} requires 7, 12 and 19 quanta, respectively. N will increase as one proceeds to more highly ionised members of the group, since, to lowest order in the nuclear charge Z, the ionisation potential scales as Z^2 while the 2s–2p separation is only linear in Z.

Table 2. Ionisation and minimum excitation energies of the 1s2s $^1S_0$ metastable states of the first three members of the He isoelectronic series.

System	Ionisation energy (cm^{-1})	2p excitation energy (cm^{-1})
He	32 027	4 857
Li^+	118 718	10 445
Be^{2+}	260 068	16 279

Source: Wiese *et al* (1966).

A further useful property of the He series is that accurate *ab initio* calculations of matrix elements are possible. In addition, the 2p levels are well separated from the $L = 1$ states of greater n, with the matrix elements also possessing much greater magnitude than those that are neglected. Consequently, the approximation of considering only a single intermediate state should be an excellent one for these systems.

If one were to relax the condition that only E1-allowed nearly resonant IS should be considered, one would be able to use ground states for the initial levels, since the periodic table abounds in atoms which have low-lying excited states in the ground configuration. The relative contribution of such states to the total ionisation, as compared with E1-allowed non-resonant IS, is of order $(M_F\Delta_A/M_A\Delta_F)^2$, where M_F, M_A are the forbidden and allowed matrix elements, and Δ_F, Δ_A the forbidden and allowed detunings. (The respective contributions of the forbidden and allowed intermediate states to the total ionisation do not interfere.) Taking published numbers for Cl as typical (Wiese *et al* 1969), the forbidden $^2P_{3/2}$–$^2P_{1/2}$ transition within the $3p^5$ configuration dominates strongly over absorption to $3p^4ns$ and $3p^4nd$, as long as one is within $\pm 10\,cm^{-1}$ of resonance. Furthermore, as Wiese *et al* (1969) point out, the theoretical value of the matrix element for this transition is expected to be accurate, since its value is affected by errors in the wavefunction to a much lower degree than are calculated allowed transition probabilities.

The influence of pulse areas on the spectrum of multiphoton ionisation has previously been considered by Crance and Feneuille (1977a, b). These authors also include the effect of non-resonant (NR) intermediate states via an effective operator approach. Interference between the NR amplitude and that of the ISR has the effect of

shifting the maximum of the spectrum, and removing its symmetry with respect to detuning. It should also distort, but not eliminate, any mock structure effects that might be present. Crance and Feneuille analysed not only rectangular pulses, for which they solved the two-level part of the problem in closed form, and where the doubling predicted in the present article cannot occur, but also several different smooth pulses (not hyperbolic secants), for which they used numerical methods in the two-level portion. Their results for smoothly varying pulses do not predict mock structure, apparently because the N values chosen were below the required minimum, according to the present calculation.

That the effect is appreciable only for pulses whose area is near 2π suggests that it may be useful in measuring the integrated intensity of focused short pulses, provided the resonant matrix element is accurately known. The presence of this doublet would then establish the product V_0T to within rather narrow limits. One could determine whether the effect was indeed mock structure by observing if the splitting disappeared with increased and decreased intensity.

For the hyperbolic secant pulse, one may also solve for the amplitude a_1 of the initial state (Robiscoe 1978). In terms of the parameters given after equations ($7a$) and ($7b$), this amplitude is simply the hypergeometric function ${}_2F_1(a, b, c^*, Z)$, so that an obvious alternative expression for $|a_2|^2$ is $1-|{}_2F_1(a, b, c, Z)|^2$. The advantage of this form is that for pulse areas that are integral multiples of π, the series for the function ${}_2F_1(a, b, c, Z)$ reduces to a polynomial in Z, enabling one to evaluate the integral appearing in equation (8) in closed form. This procedure would not have been especially useful in the present work, since we explored non-integral as well as integral pulse areas. We mention this point only on the chance that it may prove to be of value to some readers.

To summarise, we have formulated a theory of resonant multiphoton ionisation by pulses which predicts a spectrum whose maximum is split into a doublet by purely temporal factors. It appears similar to the AC Stark effect, but occurs under conditions where the latter does not cause structure to appear, and exhibits a totally different intensity dependence.

References

Agostini P, Luvain M and Mainfray G 1971 *Phys. Lett.* **36A** 21
Bebb H B 1966 *Phys. Rev.* **149** 25
—— 1967 *Phys. Rev.* **153** 23
Bebb H B and Gold A 1966 *Phys. Rev.* **143** 1
Beers B L and Armstrong L Jr 1975 *Phys. Rev.* A **12** 2447
Chin S L and Isenor N R 1967 *Phys. Rev.* **158** 93
Chin S L, Isenor N R and Young M 1969 *Phys. Rev.* **188** 7
Crance M and Feneuille S 1977a *J. Physique* **37** L333
—— 1977b *Phys. Rev.* A **16** 1587
Dixit S N and Lanbropoulos P 1979 *Phys. Rev.* A **19** 1576
Eberly J H and ONeil S V 1979 *Phys. Rev.* A **19** 1161
Flank Y and Rachman A 1975 *Phys. Lett.* **53A** 247
Flank Y, Laplanche G, Jaouen M and Rachman A 1976 *J. Phys. B: Atom. Molec. Phys.* **9** L409
Fox R A, Kohan R M and Robinson E J 1971 *Phys. Rev. Lett.* **26** 1416
Geltman S 1963 *Phys. Lett.* **4** 168
—— 1965 *Phys. Lett.* **19** 616
—— 1979 *Bull. Am. Phys. Soc.* **24** 66
Gontier Y and Trahin M 1979 *Phys. Rev.* A **19** 264
Granneman E H A and van der Wiel M J 1975 *J. Phys. B: Atom. Molec. Phys.* **8** 1617

Hall J L 1966 *IEEE J Quant. Electron.* **QE-2** 361
Hall J L, Robinson E J and Branscomb L M 1965 *Phys. Rev. Lett.* **14** 1013
Kogan R M, Fox R A Robinson E J and Burnham G T 1971 *Bull. Am. Phys. Soc.* **16** 1411
Luger A D and Robinson E J 1970 *Phys. Lett.* **31A** 247
Luvain M and Mainfray G 1972 *Phys. Lett.* **39A** 1
Robinson E J and Geltman S 1967 *Phys. Rev.* **153** 4
Robiscoe R T 1978 *Phys. Rev.* A **17** 247
Rosen N and Zener C 1932 *Phys. Rev.* **40** 502
Teague M R, Lambropoulos P, Goodmanson D and Norcross D W 1976 *Phys. Rev.* A **14** 1057
Wiese W L, Smith M W and Glennon B M 1966 *Atomic Transition Probabilities* vol 1 (Washington, DC: National Bureau of Standards)
Wiese W L, Smith B W and Miles B M 1969 *Atomic Transition Probabilities* vol 2 (Washington, DC: National Bureau of Standards)
Young M, Chin S L and Isenor N R 1968 *Can. J. Phys.* **46** 1537
Zernik W 1964 *Phys. Rev.* **135** A51
Zernik W and Klopfenstein R W 1965 *J. Math. Phys.* **6** 262

To Appear in
Annales de Physique

Application of Laser Spectroscopy to Collisional Studies*

P. R. Berman

Physics Department, New York University
4 Washington Place
New York, New York 10003, U. S. A.

I should like to thank the Comité d'Organisation for their kind invitation to participate in this Conference. I apologize for writing this summary of my talk in English rather than French, and ask the readers' indulgence on this point.

The traditional method for studying atomic or molecular collisions is the use of crossed atomic or molecular beams. Owing to the low beam densities one encounters, such studies have generally been restricted to atoms or molecules in ground or metastable states; however, it is now possible to use lasers to achieve substantial excited state atomic populations so that scattering from excited states may also be studied in crossed beam experiments.[1] Typically, one obtains the differential scattering cross section as a function of center-of-mass energy in crossed beam experiments. These experiments, although often

* Supported by the U.S. Office of Naval Research.

difficult to perform, provide a "direct" measure of the scattering process.

A somewhat less direct method for studying collisional processes in gases has been available for many years under the heading "pressure broadening." Since the absorptive properties of a vapor are affected by collisions occuring within the vapor, collisional information is implicitly contained in the absorption or emission profiles associated with various atomic transitions in the vapor. Using linear spectroscopy, one can measure the broadening (or narrowing) of the spectral profile associated with a given transition of "active" atoms as a function of perturber gas pressure. From such data, one can reach some conclusion regarding the total cross section for scattering between active atoms (in the states involved in the transition) and ground state perturbers. Using saturation spectroscopy or coherent transient techniques, one can also obtain information about differential scattering cross sections involving excited-state active atoms (see below), albeit of a somewhat different nature than that obtained in beam experiments.

Owing to time limitations, I shall not discuss linear spectroscopy,[2] and shall, instead, concentrate on the saturation spectroscopy of three-level systems. I shall also mention some coherent transient experiments that are particularly well-suited to collisional studies and a recent experiment employing a combination of atomic beam and laser spectroscopic techniques.

Before beginning to discuss three-level systems, it is perhaps useful to describe the type of collisional data one can

Supported by the U.S. Office of Naval Research under Contract No. N00014-77-C-0553.

hope to obtain from laser spectroscopic studies involving cells rather than beams. In a typical experiment, one uses a laser to excite active atoms having a specific longitudinal velocity and then probes the manner in which collisions with perturber atoms cause this velocity distribution to return towards equilibrium. Thus, in such an experiment, one measures the differential scattering cross section averaged over the perturber velocity distribution and the transverse active-atom velocity distribution. I have referred to this as a "poor man's" differential scattering cross section, since it contains less information than the corresponding cross sections obtained in beam experiments. Still, the "poor man's" differential cross section is rich enough to draw conclusions concerning the interatomic potential giving rise to the scattering. Moreover, the variety of cross-sections (elastic, inelastic, exchange, magnetic relaxation, etc.) that are easily probed using laser spectroscopic techniques guarantees, in my opinion, a promising future for this mode of collisional study.

Three-level Systems

Three-level systems have received considerable attention[3-18] for both high resolution and collisional studies. Figure 1 illustrates three types of three-level systems. The quantities β and β' label the different level schemes so that all may be treated by a single formalism; $\beta = \beta' = 1$ in Fig. 1a (upward cascade); $\beta = 1, \beta' = -1$ in Fig. 1b (inverse V); $\beta = -1$ $\beta' = 1$ in Fig. 1c (V). The three levels are incoherently pumped at some rate density $\lambda_i(v)$ ($i = 1,2,3$) and each level decays at some rate γ_i. External fields having frequency Ω and Ω' drive the 1 - 2 transition (frequency ω)

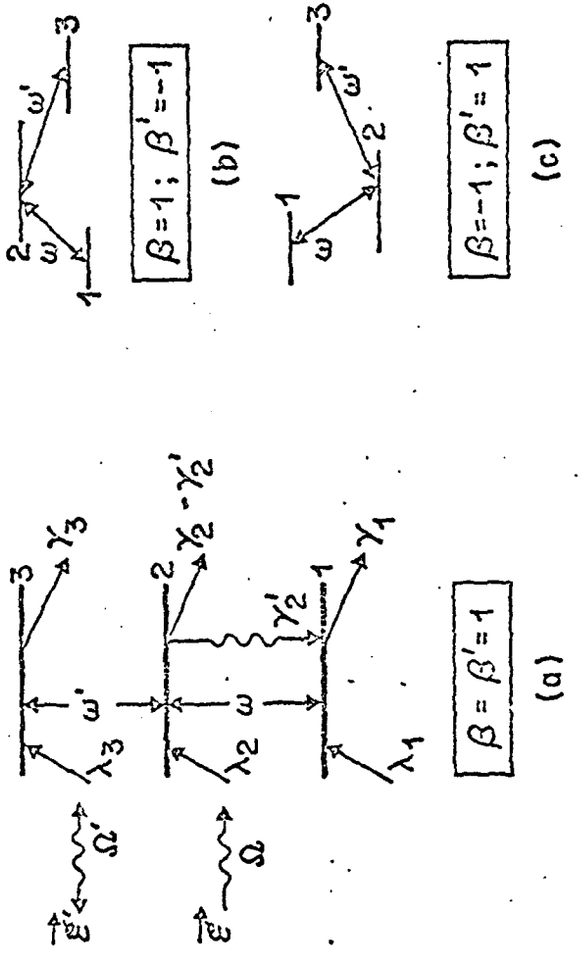

Fig. 1 Three-level systems: (a) upward cascade, (b) inverted V, (c) V.

and 2 - 3 transition (frequency ω'), respectively. The field propagation vectors are $k\hat{z}$ and $\epsilon k'\hat{z}$ ($k = \Omega/c$, $k' = \Omega'/c$) with ϵ equal to either +1 (copropagating) or - 1 (counterpropagating). Spontaneous emission between level 2 and 1 is allowed at rate γ_2'. The Rabi frequencies associated with the 1 - 2 and 2 - 3 transitions are denoted by X and X', respectively. I shall limit the discussion to the upward cascade (Fig. 1a) and take $\lambda_2 = \lambda_3 = 0$; $\lambda_1 = 0$, $\gamma_1 = 0$ λ_1/γ_1 = constant, to simulate level 1 being the ground state. The field at frequency Ω (pump) is of arbitrary strength and that at frequency Ω' (probe) is assumed to be weak.

The binary, elastic collisions between active atoms and ground state foreign gas perturbers are treated in the impact approximation.[2] Collisions are assumed to be "phase-interrupting" in their effect on level coherences (giving rise to broadening and shift parameters) and velocity-changing in their effect on population densities (i.e. collisions result in the relaxation of any velocity-selected population excited by the pump field). This rather simple collision model is generally valid for electronic transitions.

The pump field is detuned a fixed amount Δ from the 1-2 transition and the probe absorption is monitored as a function of its detuning Δ' from the 2-3 transition. If u is the most probable active atom speed, then two cases of interest are $|\Delta| >> ku$., $|\Delta| < ku$.

$|\Delta| >> ku$

If the pump detuning is equal to several Doppler widths, the only resonance in the absence of collisions occurs at $\Delta' = -\Delta + (k + \epsilon k')v_z$. When averaged over the active atom velocity distribution, the resulting line shape is a Voigt profile centered at $\Delta' = -\Delta$ with a width obtained from the convolution of a Lorentzian of of width (HWHM) $\gamma_3/2$ and a Gaussian of width $0.83(k + \epsilon k')u$, If $k \simeq k'$ and $\epsilon = -1$, this two-photon resonance can be very narrow.

With collisions present, a new resonance centered at $\Delta' = 0$ can result from a collisionally-aided radiative excitation[19] of level two via the reaction.

$$A_1 + P + \hbar\Omega \rightarrow A_2 + P$$

where A_i is the active-atom in state i and P is the perturber. The difference in energy between $\hbar\Omega$ and $\hbar\omega$ is now compensated by a corresponding change in the atoms' kinetic energy following a collision. With collisionally-aided excitation of level 2, probe absorption on the 2-3 transition centered at $\Delta' = 0$ can occur.

Thus, in the absence of collisions, there is only one resonance centered at $\Delta' = -\Delta$. In the presence of foreign gas perturbers, a new resonance appears at $\Delta' = 0$ which grows with increasing pressure. The width and shift of the $\Delta' = -\Delta$ resonance can be used to obtain the 1-3 broadening and shift coefficients, that of the $\Delta' = 0$ resonance to obtain the 2-3 broadening and shift coefficients. Moreover, the amplitude of the $\Delta' = 0$ resonance is proportional to the 1-2 broadening coefficient. Recent

experimental data[20] on Na($3S_{1/2} \rightarrow 3P_{1/2} \rightarrow 4D_{3/2}$) perturbed by Ne is shown in Fig. 2. The effects of collisions for this large detuning case ($\Delta = -4.0$ ku, $k'/k = 1.0375$, $\varepsilon = -1$) are clearly seen (the second narrow resonance centered at $\Delta' = 5.77$ku arises from ground state hyperfine structure).

$|\Delta| < ku$

The above type of experiment can provide total cross section data (total cross sections may be extracted from the broadening coefficients). However, to obtain information concerning differential cross sections, one must tune within the Doppler width. In this case, the pump laser selects a specific longitudinal velocity group having $v_z = \Delta/k$, leading to a resonance condition $\Delta' = -\Delta + (k + \varepsilon k')v_z = \varepsilon(k'/k)\Delta$. . The resonance width is on the order of the natural widths of the transition levels, owing to the fact that only a small longitudinal velocity class of atoms is being used. The resonance is broadened and may even be split in strong pump fields, reflecting power broadening and the ac Stark effect, respectively. Probe absorption in the absence of collisions is shown in Fig. 3 for $k'/k = 0.4$. There is ac Stark splitting for counterpropagating waves in strong fields. For the case shown of complete branching to the ground state ($\gamma_1' = \gamma_2$) there is also some splitting for the copropagating case.

In the presence of collisions, the following interactions can occur:

$$A_1 + P + \hbar\Omega \rightarrow A_2(v_z' = \Delta/k) + P$$

$$A_2(v_z' = \Delta/k) + P \rightarrow A_2(v_z) + P$$

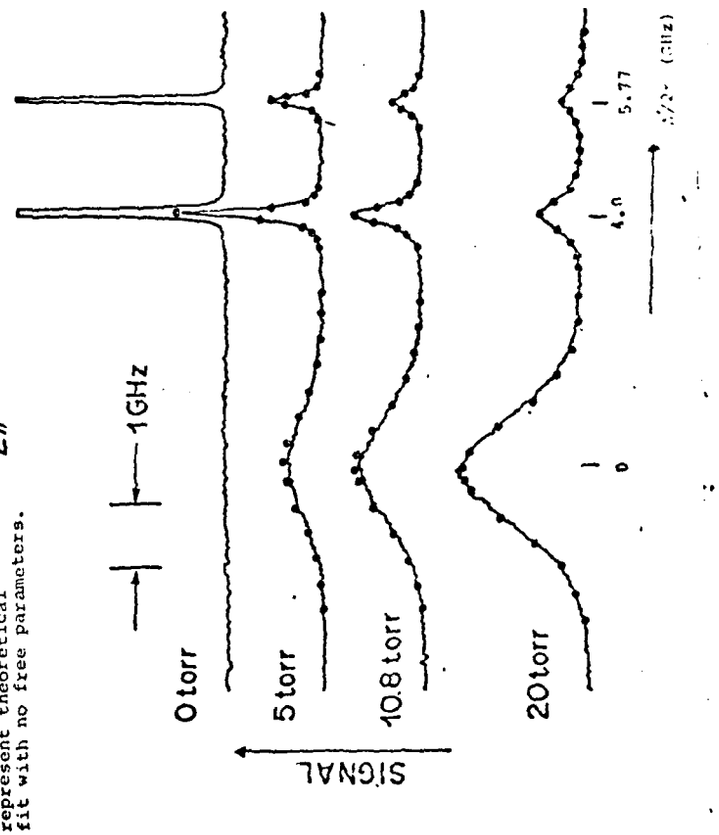

Fig. 2 Experimental excitation spectra for Na (3S+3P+4D) perturbed by various pressures of Ne for a pump detuning $\Delta/2\pi = -4.0$GHz. (Doppler width = 1.66ku/2π = 1.66 GHz.). Dots represent theoretical fit with no free parameters.

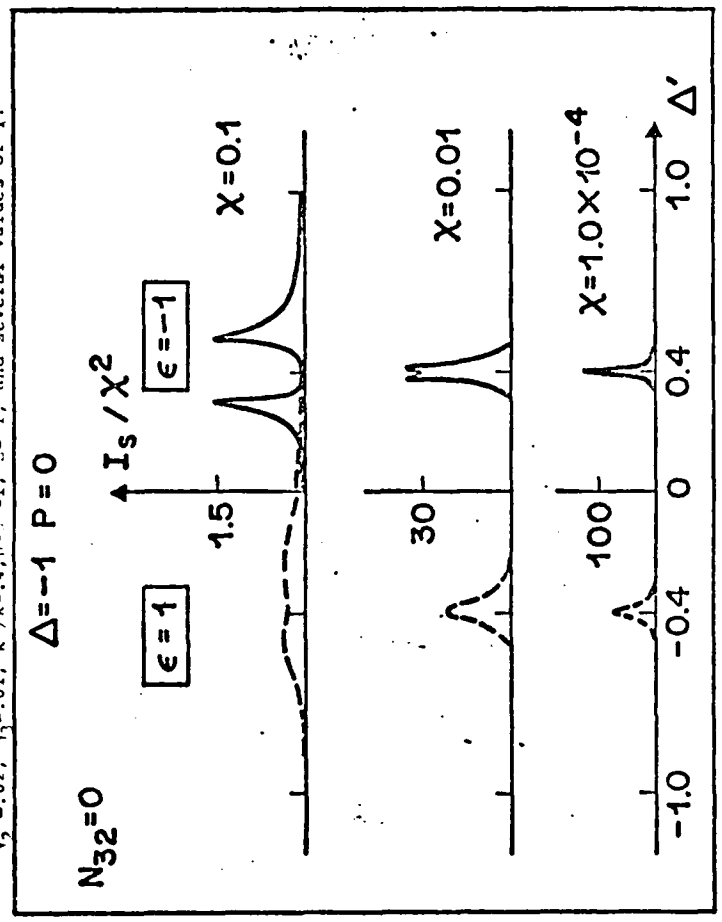

Fig. 3 Probe absorption I_s in the absence of collisions. I_s is normalized to χ^2, but is in arbitrary units. All frequencies are in units of ku, P is the pressure in Torr, and N_{32} (population difference of levels 3 and 2 in the absence of any applied fields) equals zero. The broken curve is for copropagating fields (ε=1) and the solid curve for counterpropagating ones (ε = -1). Profiles are drawn for γ_1=0, γ_2=.02, γ_2'=.02, γ_3=.01, k'/k=1.4, k=k', Δ=-1, and several values of χ.

Collisions result in an excitation of level 2 and a partial thermalization of the velocity distribution from the initial value $v_z' = \Delta/k$ selected by the pump field to values describing a thermal distribution. The degree of thermalization is determined by the number of collisions $n = \Gamma_2 / \gamma_2$ (Γ_2 = collisions rate) occurring within the lifetime of level 2 and the rms change in velocity per collision Δu. In addition, the structure of the velocity redistribution may be used to infer something about the interatomic potential giving rise to the scattering.

Theoretical probe absorption profiles for weak and strong pump fields are shown in Figs. 4 and 5, respectively, using the Keilson-Storer[21] collision kernel. One may note the gradual thermalization with increasing perturber pressure. In the strong field case both the integrated and peak probe absorption can increase with increasing pressure whereas, in the weak field case, the areas under the curves are constant.

Systematic experiments of this nature were recently carried out by Bréchignac et al[22] in Kr perturbed by rare gases and by Liao et al[23] for Na perturbed by rare gases. The data for Na($3S_{1/2}$-$3P_{1/2}$-$4D_{3/2}$) perturbed by Ne is shown in Fig. 6 for a detuning $\Delta/ku = -1.6$. The overall qualitative features are similar to those shown in Fig. 4 (for the three-level Na system chosen, $k'/k = 1.0375$ so that ac Stark splitting is suppressed). One can see the thermalization of the $3P_{1/2}$ level of Na with increasing Ne pressure.

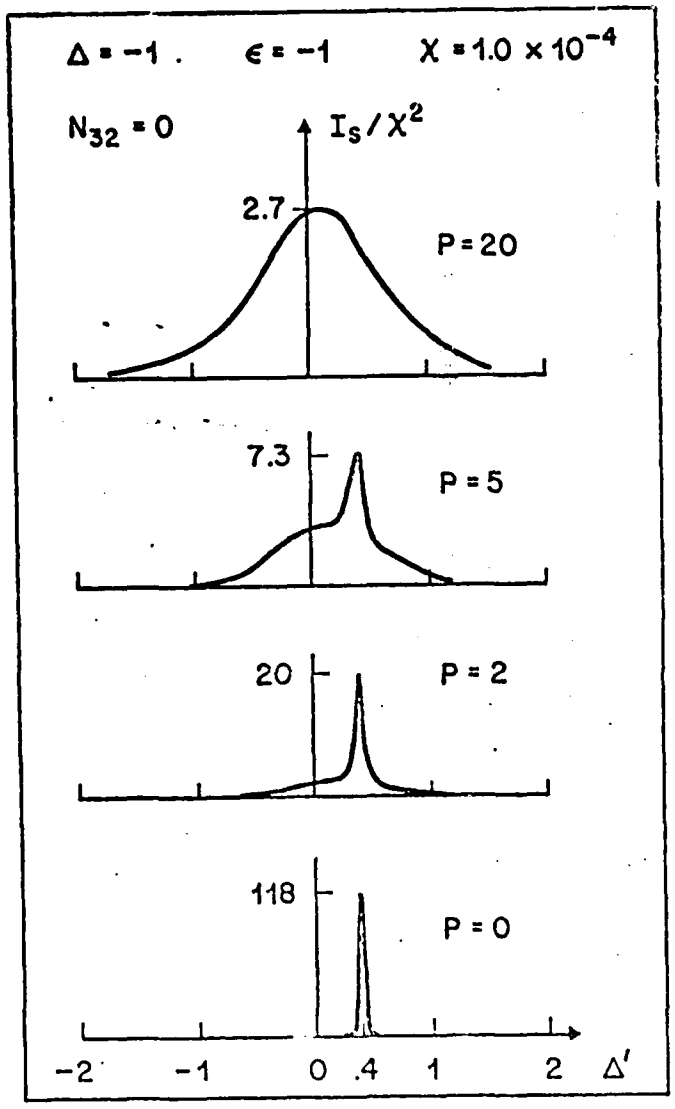

Fig. 4 Probe absorption in the weak pump field limit for various perturber pressures. Parameters not explicitly displayed are the same as in Fig. 3. Collision parameters (in units of ku) are as follows: phase-interrupting broadening rates Γ_{12}=.007P, Γ_{23}=.015P, Γ_{13}= .016P; velocity-changing collision rates Γ_1=.004P, Γ_2=.006P. A Keilson-Storer kernel with Δu=.66u is used to describe velocity-changing collisions.

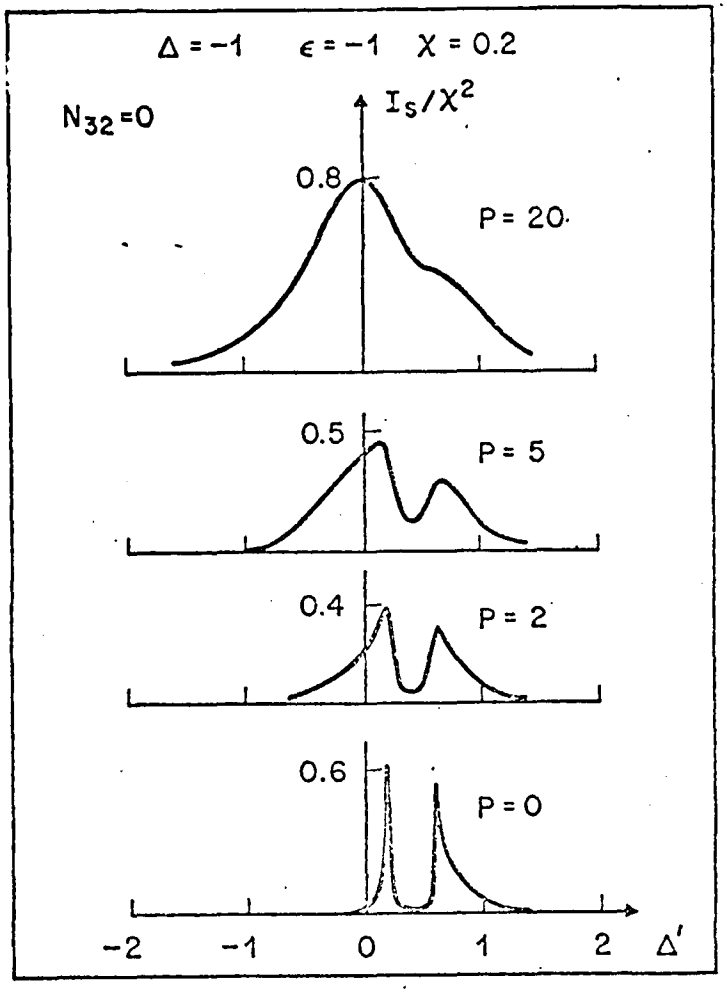

Fig. 5 Probe absorption for a strong pump field (χ=.2). Other parameters are as in Fig. 4.

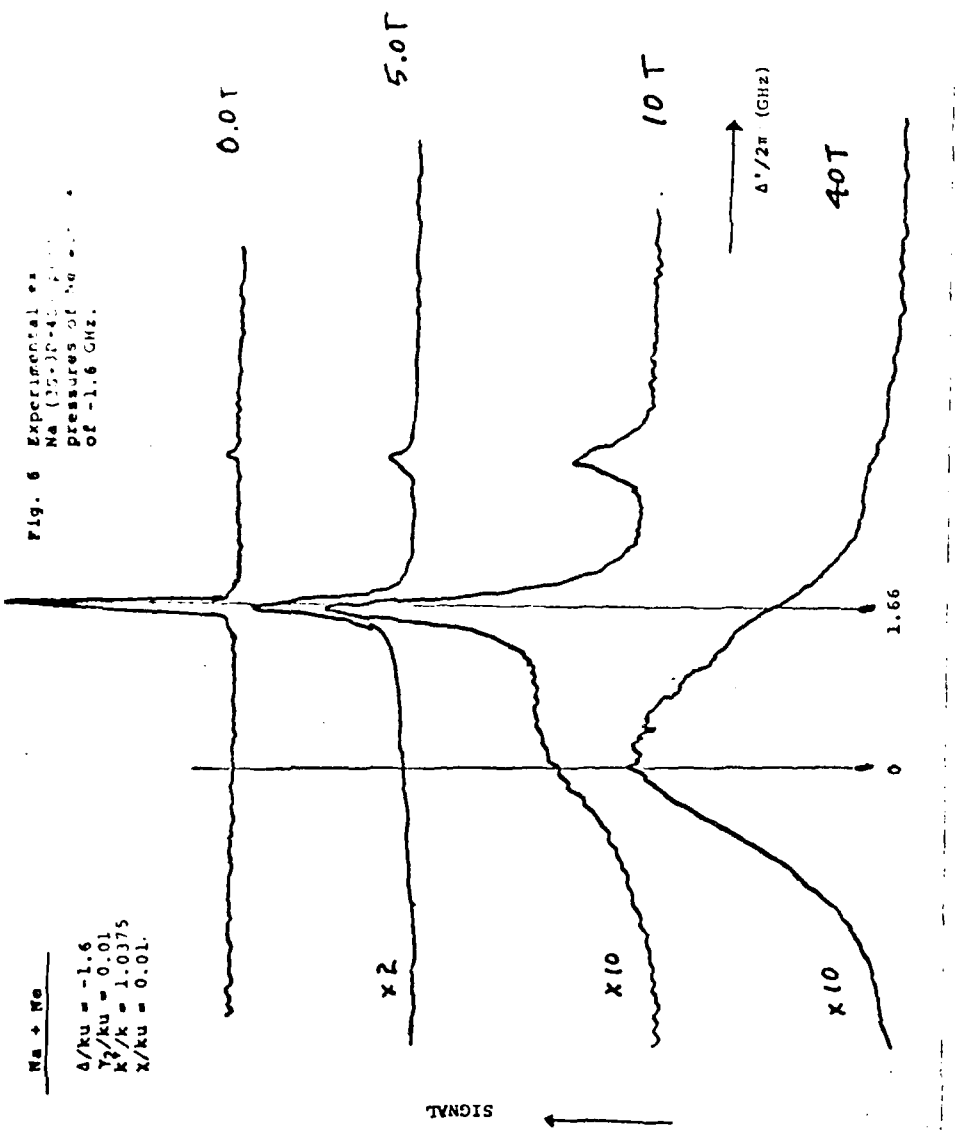

Fig. 6 Experimental ex... Na (3S-3P-4D ...) pressures of Ne ... of ~1.6 GHz.

The data of Liao et al[23] could also be used to test different collision kernels that are used to describe scattering in level 2. It was found that both the Keilson-Storer and classical Hard-Sphere kernels correctly characterized Na-He collisions, that the hard-sphere kernel was superior to Keilson-Storer for Na-Ne and Na-Kr collisions, and that neither kernel adequately described the entire profile for Na-Ne and Na-Kr collisions. These results imply that large-angle scattering of $Na(3P_{1/2})$ with heavy foreign gases can not be characterized as totally hard-sphere in nature; it would not be surprising if some large-angle scattering could be attributed to attractive wells in the interatomic potentials. It appears to me that this type of experiment reflects an increased interest in both the experimental and theoretical[24] determination of atomic collision kernels.

Coherent Transients

It is also possible to carry out laser spectroscopic collisional studies using time resolved techniques. Some of these methods are particularly well suited to collisional studies. I shall mention two such types of experiments.

In time-delayed saturation spectroscopy, one uses a narrow band, pulsed laser to excite atoms having a given longitudinal velocity. A second laser, time delayed from the first, is then applied to the same or a coupled transition in order to monitor the velocity relaxation as a function of either time delay or perturber pressure. An advantage of this technique to steady-state

methods is that two-photon processes do not occur in the time-resolved experiment since the fields are applied at different times. Thus, the probe absorption occurs only from "stepwise" excitation, greatly simplifying the analysis. A limited number of experiments of this type have been performed.[25]

A second class of experiments which holds promise for collisional studies may be broadly characterized as photon echo experiments. In these experiments, a system is exposed to two or more pulses. The pulses lead to a dephasing and rephasing of atomic dipoles in the sample such that, at some time following the last applied pulse, the dipoles rephase and emit an "echo." Collisions disturb this dephasing-rephasing process and cause a decrease in echo amplitude. Thus, the echo amplitude can be used to monitor collisional processes in gases. This method is especially useful in determining whether collisions are "phase-interrupting" or "velocity-changing" in their effect on level coherences.[13, 14, 26]

By using standing waves as the excitation pulses, one excites higher-order harmonics in both populations and level coherences. The photon echoes following such excitation can reflect collisional effects on both population densities and level coherences.[27] Moreover, one can also observe population echoes as various population spatial harmonics rephase following the second pulse.[28] Studies of velocity-changing collisions on level populations can also be made using "stimulated" echoes,[29] which is simply a variation of the standing-wave echo method. Photon echo experiments offer an

interesting possibility for future collisional investigations.[28, 29]

Beam-Laser Experiment

Finally, I should like to mention the experiment of Phillips et al.[30] This experiment employed crossed atomic beams and a laser excitation-detection scheme. As in the steady-state experiment, a pump laser excites a particular velocity class of atoms to some intermediate state. A second laser, directed along the active atom-perturber relative velocity axis, is then scanned to probe a coupled transition. At each probe laser frequency, only those active atoms which have been scattered through a particular scattering angle θ (these atoms form a cone of angle θ about the laser axis) in the center-of-mass system resonantly interact with the probe. Thus, measuring the probe absorption is equivalent to measuring the differential scattering cross section. This method has high sensitivity and can be used for short-lived excited states; it was used to determine the differential cross section for $3P_{1/2} \rightarrow 3P_{3/2}$ fine structure state changing collisions in Na undergoing collisions with Ar perturbers.[30]

References

1. See, for example, I.V. Hertel and W. Stoll in Advances in Atomic and Molecular Physics, D.R. Bates and B. Bederson, editors (Academic Press, New York, 1977) vol. 13, p. 113.

2. For discussions of linear spectroscopy with many additional references, see P.R. Berman, Appl. Phys. (Germany) 6 283(1975) and K. Shimoda in High Resolution Laser Spectroscopy (K. Shimoda, ed., Springer-Verlag, New York, 1976) p. 11.

3. G.E. Notkin, S.F. Rautian and A.A. Feoktistov, Zh. Eksp. Teor. Fiz. 52, 1673 (1967) [Sov. Phys.-JETP 25, 1112 (1967)] .

4. M.S. Feld and A. Javan, Phys. Rev. 177, 540 (1969).

5. T.W. Hansch and P.E. Toschek, Z. Phys. 236, 213 (1970).

6. T.Y. Popova, A.K. Popov, S.G. Rautian and R.I. Sokolovskii, Zh. Eksp. Teor. Fiz. 57, 850 (1969). [Sov. Phys.-JETP 30, 466, 1208 (1970)] .

7. B.J. Feldman and M.S. Feld, Phys. Rev. A5, 899 (1972); N. Skribanowitz, M.J. Kelly and M.S. Feld, Phys. Rev. A6 , 2302 (1972).

8. I.M. Beterov and V.P. Chebotaev, Prog. Quantum Elec. 3,1 (1974) and references therein.

9. R. Salomaa and S. Stenholm, J. Phys. B8, 1795 (1975); 9, 1221 (1976); R. Salomaa, ibid 10, 3005 (1977).

10. Additional references may be found in Laser Spectroscopy III edited by J.L. Hall and J. L. Carlsten (Springer-Verlag, New York, 1977); Nonlinear Laser Spectroscopy, V.S. Letokhov V.P. Chebotaev (Springer-Verlag, New York, 1977); High Resolution Laser Spectroscopy edited by K. Shimoda (Springer-Verlag, New York, 1976); Laser Spectroscopy of Atoms and Molecules edited by H. Walther (Springer-Verlag, New York, 1976); Frontiers in Laser Spectroscopy edited by R. Balian, S. Haroche and S. Liberman (North-Holland, Amsterdam, 1977).

11. S. Stenholm, J. Phys. B10, 761 (1977).

12. C.J. Borde in Laser Spectroscopy III (J. Hall and J.L. Carlsten, eds., Springer-Verlag, New York, 1977) p. 121.

13. P.R. Berman, in Advances in Atomic and Molecular Physics edited by D.R. Bates and B. Bederson (Academic Press Inc., New York, 1977) Vol. 13, p. 57.

14. P.R. Berman, Phys. Reports 43, 101 (1978).

15. A.P. Kolchenko, A.A. Pukhov, S.G. Rautian and A.M. Shalagin, Zh. Eksp. Teor. Fiz. 63, 1173 (1972) [Sov. Phys.-JETP 36, 619 (1973)] .

16. V.P. Kochanov, S.G. Rautian and A.M. Shalagin, Zh. Eksp. Teor. Fiz. 72, 1358 (1977) [Sov. Phys.-JETP 45, 714 (1977)] .

17. L. Klein, M. Giraud, and A. Ben-Reuven, Phys. Rev. A16, 289 (1977).

18. Extensive additional references may be found in Refs. 2 and 13.

19. S. Yeh and P.R. Berman, Phys. Rev. A19, 1106 (1979) and references therein.

20. P. F. Liao, J.E. Bjorkholm and P.R. Berman, Phys. Rev. A (in Press).

21. J. Keilson and K.E. Storer, Q. Appl. Math. 10, 243 (1952).

22. C. Brechignac, R. Vetter and P.R. Berman, Phys. Rev. A17, 1609 (1978); Journal de Physique Lettres 39, L231 (1978).

23. P. F. Liao, J.E. Bjorkholm and P.R. Berman (unpublished).

24. S. Avrillier, thesis, Universite Paris-Nord (1978).

25. T.W. Hansch, I.S. Shahin and A.L. Schawlow, Phys. Rev. Letters 27, 707 (1971) J. Brochard and P. Cahuzac, J. Phys. B9, 2027 (1976); P. Cahuzac and X. Drago, Opt. Comm. 24, 63 (1978).

26. Three-level systems in which the 1-2 population difference vanishes in the absence of applied fields are also ideal for studying this aspect of collisions. See P. Cahuzac, J.L. LeGouet, P.E. Toschek and R. Vetter (unpublished).

27. J.L. LeGouet and P.R. Berman, Phys. Rev. A, (in Press) and references therein.

28. R. Kachru, T.W. Mossberg, E. Whittaker and S.R. Hartmann (unpublished); T.W. Mossberg, R. Kachru, E. Whittaker and S.R. Hartmann (unpublished).

29. T. Mossberg, A. Flusberg, R. Kachru and S.R. Hartmann, Phys. Rev. Letters 42, 1665 (1979).

30. W. D. Phillips, J.A. Serri, D. J. Ely, D.E. Pritchard, K.R. Way and J.L. Kinsey, Phys. Rev. Letters 41, 937 (1978).

To Appear in Comments on Atomic and Molecular Physics

Line Shapes in Laser Experiments

R. Vetter and P.R. Berman[*,+]
Laboratoire Aimé Cotton, C.N.R.S. II, Batiment 505
91405 Orsay, France

Abstract

A brief review of recent developments in line shape studies using laser spectroscopy is presented. Experiments are discussed in which the absorption or emission line profiles associated with various transitions in a vapor can be used to provide useful information concerning the atomic sample being tested. In particular, ways in which collisional effects manifest themselves in line shapes are described and the manner in which collision cross section can be extracted from these line shapes is discussed. Illustrative experiments using methods of linear spectroscopy, two-photon spectroscopy and saturation spectroscopy are presented.

I. Introduction

With the rapid development of tunable lasers, there has been a renewed interest in the field of atomic spectroscopy. Not only has traditional spectroscopy been carried out with increased precision using laser sources, but also new spectroscopic techniques for probing atomic systems have been developed. Historically, one has studied absorption or emission lineshapes to determine atomic transition frequencies, lifetimes, and oscillator strengths. Moreover, line shape studies have been used to provide information pertaining to collisional processes occurring in vapors. With the laser revolution, one can now expect to obtain new and valuable data concerning both atomic structure and collisional effects by studying laser spectroscopic line shapes.

In this brief review it is not possible to discuss all the recent developments in laser spectroscopy. Therefore, we limit the discussion to a few cases of current interest. In particular we emphasize the experimental aspects of linear and saturation spectroscopy using weak laser fields (Rabi frequency much less than homogeneous widths) in which collisional processes are probed. We assume that collisions can be described by relatively simple models. The collisions are taken to be thermal and describable by the impact theory of pressure broadening - - we consider only binary collisions between atoms and detunings between laser and atomic transition frequencies which are small compared with the inverse duration of a collision.

Supported by the U.S. Office of Naval Research under Contract No. N00014-77-C-0553.

Several reviews of collisional studies using laser spectroscopy have recently appeared[1-6] but these reviews did not emphasize the experimental aspects of the problem as we shall do in this work. Section II is devoted to a study of linear spectroscopy, Section III to two-photon spectroscopy, Section IV to saturated absorption and Section V to saturation spectroscopy of three-level systems.

II Linear Absorption

Linear spectroscopy is a classic technique for studying atomic systems that can be easily carried out using laser sources. One monitors the absorption of a given transition as a function of the frequency of the applied laser field. The laser field is assumed to be weak enough so as not to significantly alter atomic state populations. Profiles in linear absorption are characterized by the following features.

1. Profile intensities are proportional to the difference of populations in the two levels involved in the transition.

2. The line shape is given by the convolution of a Doppler-shifted Lorentzian representing the absorption profile of a given longitudinal velocity sub-class of atoms with the velocity distribution of these atoms.

3. With laser sources, the apparatus function is negligible compared with other sources of broadening.

4. High signal-to-noise ratios are easily obtained.

Collisions within the vapor add new features to the line shapes. The most common effect of collisions is to introduce a pressure and speed-dependent width and shift into the Lorentzian component of the profile. The width can be related to the total cross-section for scattering of the active atoms in the states of the transition by ground state perturbers. It is also possible in certain cases to observe a narrowing of the total profile (Dicke narrowing) with increasing perturber pressure, provided that the collisional interaction for the two states of the transition is nearly identical.[2] We do not consider this narrowing effect in this review since it rarely occurs for electronic transitions. We therefore take line shapes of the form

$$\int \frac{\gamma(\vec{v})}{\gamma^2(\vec{v}) + (\Delta + S(\vec{v}) - \vec{k}\cdot\vec{v})^2}\, G(\vec{v})\, d\vec{v} \qquad (1)$$

where $2\gamma(\vec{v})$ is the speed-dependent homogeneous width (FWHM, natural plus collisional width), $S(\vec{v})$ is the speed-dependent collisional shift, Δ the detuning of the laser frequency from the absorption transition frequency, $\vec{k}$ the laser propagation vector and $G(\vec{v})$ the velocity distribution of the active atoms.

If the speed dependence of γ and S is neglected, and if $G(\vec{v})$ is Gaussian, the resultant line shape is termed a Voigt profile.

As an example of linear spectroscopy with lasers, we describe an absorption experiment on the 3.51 μm line of XeI.[7] A xenon laser oscillating at 3.51 μm and finely tunable across its gain curve provides a weak laser beam which propagates inside a discharge tube filled with

^{130}Xe. The absorbed or amplified part of the laser flux is recorded as its frequency is scanned. Background signal is eliminated by using a square wave excitation of the discharge and phase sensitive detection.[8] The line profile is analyzed at several pressures according to equation (1) where $G(\vec{v})$ is assumed Gaussian and the speed-dependence of γ and S is neglected. The shift is determined by the position of the symmetry axis of the line profile relative to that of the same transition measured using a reference tube. One fits the profile of the lineshape with two free parameters, the homogeneous and Doppler widths. Although the deconvolution procedure is not unique, consistent results are obtained by assuming profiles of the form (1). The width of the Lorentzian component is shown in Fig. 1 as a function of pressure of either the He, Ne or Ar perturbers. The width of the Gaussian remains constant with pressure, slightly above the temperature of the bath. The different widths plotted in Fig. 1 are linear functions of pressure and converge to the value 4.7 MHz as the pressure approaches zero, in agreement with the expected value of 4.6 MHz.[7] Data taken from reference 7 indicate that shifts are also linear functions of pressure and converge to zero as the pressure approaches zero.

The situation is somewhat more complicated with Xe atoms as perturbers. Fig. 2 shows the width of the Voigt profile, of the Gaussian component, and of the Lorentzian one obtained after profile analysis.[7] The data clearly show that the Gaussian width no longer remains constant with pressure and that there is a corresponding effect on the width of the Voigt profile. However, the width of the Lorentzian remains

a linear function of pressure within experimental accuracy. The cause of the deviation of the Gaussian may be due to a non-resonant transfer of excitation.[7] With Kr atoms as perturbers, a non-resonant excitation transfer leads to severely distorted profiles.[9] Similar experiments have been performed with He and Ne as active atoms.[10,11]

The creation of non-Maxwellian initial state velocity distributions occurs in certain of the above discharge tube experiments and can be strictly avoided only in absorption experiments on transitions originating from the ground atomic state. Although the existence of non-Maxwellian distributions complicates the analysis, there are certain transitions in the rare gases that can be readily studied spectroscopically only by using discharges. It may be noted that one can readily vary the temperature of discharges to study the temperature dependence of collision rates and shifts.[12] The data shown in Fig. 1 and Fig. 2 are restricted to the core of the line (frequency range on the order of several Doppler widths). In this range one is sensitive mainly to collisions with large impact parameters, typically greater than 5Å. In order to probe the short range part of the interatomic potential one must study the far wings of the line.[13,14]

III. Two-photon Absorption

In linear spectroscopy one is always faced with the problem of deconvoluting a profile into its components. A great emphasis over the past several years has been placed in obtaining spectroscopic techniques

which are essentially Doppler-free; that is, profiles in which the Doppler component is suppressed. One such method that has been developed is that of two-photon Doppler-free spectroscopy.[15-19] The principle involved is easily understood if one writes the condition for absorption of two photons in the atomic rest frame. If the separation of the two levels of the same parity is 2ω and the excitation photons of frequency Ω are provided by copropagating ($\varepsilon = 1$) or counterpropagating ($\varepsilon = -1$) laser beams, the resonance condition is: $\Omega(1 - v_z/c) + \Omega(1 - \varepsilon v_z/c) = 2\omega$. One sees immediately that for $\varepsilon = -1$ the Doppler shifts cancel. As Ω is varied, an absorption profile characterized by the natural width of the initial and final states of the transition is obtained. In this method each atom contributes to the signal regardless of its velocity. The Doppler-free nature of this signal is provided by a cancellation of Doppler shifts. The profile also may contain a broad background signal arising from absorption of two copropagating photons from one of the laser beams. It can be eliminated by suitable polarization of the beam. It should be noted that by "two-photon" spectroscopy, we are referring to the absorption of two photons of the same frequency between two levels of the same parity with a non-resonant intermediate level.

In the absence of collisions, the two photon absorption operator determines the line shape. It has been shown that this operator is the sum of a scalar operator and a quadrupolar one, leading to two contributions to the line shape. However, in most cases of interest, only one operator couples the two levels and the line shape reduces to a single Lorentzian[20] having the homogeneous width of the two transition

levels. In principle, it is possible to obtain extremely narrow lines, especially if the initial and final states are metastable. There have been many high resolution experiments carried out using this technique.[21]

As in the case of linear spectroscopy, collisions can be incorporated by using a speed-dependent width and shift in the line profile. The line is no longer a true Lorentzian and can be asymmetric. If one neglects the speed dependence of width and shift, one recovers a Lorentzian line shape that is collision broadened and shifted.

Experiments specifically designed to study collisional effects have been carried out initially by Cagnac's group[22], and subsequently by other groups (References 23, 24). In particular, in Reference 22, one is able to find the variation of the width and shift of two photon excitation of Na (3S-5S and 3S-4D) transitions as a function of the pressure of various noble gases. The lines have a similar appearance to those of Fig. 1, with typical broadening coefficients on the order of 25 MHz/Torr (of the same order as that observed in linear spectroscopy). A similar experiment has been carried out with Ne as active atoms.[25] In this case, absorption takes place from a metastable level. More recently, two photon absorption has been used also to study collisional processes in Rydberg states.[23,24]

Although two-photon absorption offers unique possibilities for high precision spectroscopic studies, the signal strengths are limited by the small excitation probability one generally encounters. The excitation probability can be enhanced if there is a nearly resonant intermediate state.

IV Saturated Absorption

As a more versatile alternative one can use saturation spectroscopy to obtain Doppler free line shapes.[21] The principle involved is quite simple and differs from that of two photon spectroscopy. In saturation spectroscopy, one uses a laser beam ("pump") to excite a given longitudinal velocity subclass of atoms and probes these atoms with a second laser beam [illegible]. Since atoms having only a narrow range of axial velocities contribute to the signal in the absence of collisions, the width of the resonance can be on the order of the natural width. The Doppler free character of the response arises from the selection of a narrow Lorentzian velocity class, whereas in two photon spectroscopy, it is due to a cancellation of Doppler phases.

The resonance condition for saturated absorption is easily understood. The pump excites only those atoms having velocities $kv_z = \Delta$ where Δ is the pump detuning. On the other hand the probe (counterpropagating with respect to the pump) interacts only with those atoms having $kv_z = -\Delta$, hence the saturated absorption signal is non-zero only for $\Delta \approx 0$ (within $\pm$ the homogeneous width). A linear absorption background can be eliminated by simple experimental techniques. The term "saturation spectroscopy" is used to indicate that the signal one observes is proportional to the cube of the applied field amplitude; this cubic power is composed of a quadratic term $|E|^2$ representing the change of population induced by the pump and of a factor E representing the linear absorption of the probe. One can still speak of a "weak field" limit since one is obtaining a term corresponding to the lowest nonvanishing contribution to the signal. Narrow profiles of this type have been obtained in many atomic systems.[21]

In the presence of collisions the line shapes are modified.[26,27] The process can be viewed as follows: the pump field excites a particular velocity sub-class of atoms, collisions cause this narrow distribution to relax towards thermal equilibrium and the probe absorption from these partially thermalized atoms gives rise to the overall line shape. Collisions enter the lineshape in two ways. First, there is the effect of collisions on optical coherence (off-diagonal density matrix elements). These effects manifest themselves as a broadening and a shift of the Lorentzian component of the absorption profile, just as in linear absorption. However, in saturated absorption there is a second effect. Collisions result in a relaxation of the non-thermal velocity distribution of the populations (diagonal density matrix elements) created by the pump field. The saturated absorption profile reflects the various collisional processes occurring in the vapor and may be used to gain information about the interatomic potential giving rise to scattering within the vapor.

In order to describe velocity changes in collisions, one generally uses a collision kernel $W(\vec{v}' \to \vec{v})$ giving the probability density per unit time for an active atom to undergo a change from $\vec{v}'$ to $\vec{v}$, as a result of collisions with the perturber bath. Although the precise form of the line shape is dependent on the specific nature of the collision kernel, general comments can be made without reference to a particular kernel. However, one must introduce the parameter Δu = rms velocity change per collision and $\Gamma = \int W(\vec{v}' \to \vec{v})\, dv$ = rate of velocity changing collisions = v.c.c. The amount of thermalization is then determined by the number of collisions $\bar{n}$ occurring within the lifetime of the transition levels and the

strength of the collision which is characterized by Δu. Two cases of interest occur.

. If k Δu > γ (γ is the homogeneous width (FWHM associated with the transition), collisions are strong enough to remove atoms from the velocity "holes" or "bumps" created by the pump field. In this case, collisions lead to a broad background in the saturated absorption profile and the line shape can be used to monitor these v.c.c. As the perturber pressure is increased, the line shape tends towards a Voigt profile whose Lorentzian component is provided by collisionally thermalized active atoms.

. If k Δu < γ, v.c.c. are so weak that they do not significantly alter the line shape. An interesting effect can arise at low pressures. At such pressures, γ is determined by the natural width and one can have k Δu > γ for relatively small Δu. This condition leads to distorted profiles, which nevertheless may appear Lorentzian in nature. As the pressure is increased γ is determined by the collision broadened homogeneous width and the limit k Δu < γ is achieved. At these pressures, the line is a Lorentzian with FWHM γ. A non-linear variation of the line width with pressure can occur for these relatively weak collisions.

All these effects can be seen in the data shown in Fig. 2 and Fig. 4. In Fig. 3, the saturated absorption profile of the 557 nm Kr I line is shown, for Kr active atoms perturbed by He.[28] One can identify three components in the profile: (1) A narrow Lorentzian arising from atoms not having undergone v.c.c. (2) A component arising from Kr^{*}-Kr collisions leading to a broad, completely thermalized Gaussian background. (3) A background arising from Kr^{*}-He collisions having k Δu > γ. In Fig. 3

is also shown the variation with pressure of the width of the components arising from v.c.c. with He and Kr atoms, respectively. One notes that both widths approach the thermal one with increasing pressure and that Δu for Ar perturbers is greater than Δu for He perturbers.

In Fig. 4, the variation with pressure of the "Lorentzian" component width 2γ for saturated absorption in the 3.51 μm Xe I line is shown, for Xe active atoms perturbed by Xe.[29] For comparison the corresponding width $2\gamma_o$ of linear absorption is also displayed.[7] The saturated absorption data are strongly suggestive of the presence of the weak v.c.c. described above. Similar non-linear variations have been obtained in other systems.[30-36]

Experimental values for cross sections and rates of v.c.c. (representing collisions with larger impact parameters) can be orders of magnitude larger than hard sphere values.

It should be noted that saturated absorption can also be performed using two independent counterpropagating laser beams, the pump having a fixed frequency and the probe a variable one. The line shape in this case is similar to that encountered in three-level systems discussed in the next section. One can use modifications of saturated absorption experiments that have the potential of yielding higher signal-to-noise ratios. The most popular of these techniques is polarization spectroscopy.[21,39]

V. Three-Level Systems

One slight disadvantage of saturated absorption collisional studies is that the v.c.c. effects occur in the populations of both states of the transition and it is sometimes difficult to isolate the effect on a given level. This situation can be rectified if one studies collisions using three-level systems[40-42, 21], although many of these experiments require an additional laser. In a typical experiment, one starts with population in level 1 (Fig. 5), applies a field of frequency Ω, amplitude $\mathcal{E}$ to drive the 1-2 transition which has a frequency ω and in addition, applies a second field of frequency Ω', amplitude $\mathcal{E}'$ to complete transitions to level 3 (the 2-3 transition frequency being ω'). The λ_i represent incoherent pumping rates for the various levels and the γ_i-s decay rates from those levels. In general, the pump detuning $\Delta = (\Omega-\omega)$ is fixed and the population of level 3 is monitored as a function of the probe detuning $\Delta' = (\Omega'-\omega')$. There are many variations of this three-level system (TLS) but, to be specific, we shall consider the case of the upward cascade in Fig. 5a with $\lambda_2 = \lambda_3 = 0, \lambda_1 \sim 0, \gamma_1 \sim 0, \lambda_1/\gamma_1 =$ constant to simulate the case where level 1 is the ground state. One might note, however, that high resolution line shapes can also be obtained when levels other than level 1 are incoherently pumped.[6]

In the absence of collisions, there is only one resonance condition for excitation to level 3 for each velocity subclass of atoms. This condition is simply a "two-photon" resonance requirement $\Delta' = -\Delta + (k+k'\epsilon)v_z$ where $\epsilon = 1$ for copropagating and $\epsilon = -1$ for counterpropagating fields.

There remains some freedom in satisfying this resonance condition by the choice of the velocity subclass v_z. If $|\Delta| \gg ku$ (large detunings) one obtains maximum excitation by choosing v_z at the center of the Doppler profile ($v_z = 0$). This leads to the resonance condition $\Delta' = -\Delta$. In this case the line shape is the convolution of a Lorentzian of width $2\gamma_{13}$ ($\gamma_{ij} = (\gamma_i + \gamma_j)/2$) and a Gaussian of width $1.66\,(k + \epsilon k')u$ where u is the most probably active atom velocity. One notes that if $\epsilon = -1$ and $k \approx k'$ the width of the resonance is approximately equal to the natural width $2\gamma_{13}$ associated with the two photon transition. This width can be extremely narrow, especially if level 3 is metastable. The Doppler free nature of the line under such conditions arises from the cancellation of the Doppler phases associated with the 1-2 and 2-3 transitions.

If $|\Delta| < ku$ (small detunings) one obtains a maximum excitation by choosing those atoms having velocity $v_z = \Delta/k$ such that they are resonant with the pump field Ω. Substituting this value of v_z into the resonance condition one obtains $\Delta' = (\epsilon k'/k)\Delta$ as the position for maximum probe absorption. The line width is always on the order of the natural width of the states involved in the transitions. The Doppler free nature of this line, however, arises from the fact that only atoms having a narrow range of longitudinal velocities are contributing to the signal (there can be an additional narrowing of the line if counterpropagating waves are used, owing to Doppler phase cancellation). For either small or large detunings the probe absorption is proportional to $\mathcal{E}^2\mathcal{E}'^2$. For the case of intermediate detunings it is possible to observe resonances at both

$\Delta' = -\Delta$ and $\Delta' = (\epsilon k'/k)\delta$.[43]

To include collisional effects it is more convenient to look at large and small detunings separately.

1. $|\Delta| \gg ku$ With collisions present, a new resonance[44-50] centered at $\Delta' = 0$ can result from a collisionally aided radiative excitation of level 2 by means of the reaction $A_1 + P + \hbar\Omega \rightarrow A_2 + P$ where A_1 is the active atom in state 1 and P is the perturber. The difference in energy between $\hbar\Omega$ and $h\omega$ is now compensated by a corresponding change in the atoms' kinetic energy following a collision. With collisionally aided excitation of level 2, probe absorption on the 2-3 transition centered at $\Delta' = 0$ can occur. In the absence of collisions, there is only one resonance centered at $\Delta' = -\Delta$ and in the presence of foreign gas perturbers, a new resonance appears at $\Delta' = 0$ which grows with increasing pressure. The width and shift of the $\Delta' = -\Delta$ resonance can be used to obtain the 2-3 broadening and shift coefficients. Moreover, the amplitude of the $\Delta' = 0$ resonance is proportional to the 1-2 broadening coefficient. Recent experimental data[50] on Na ($3^2S_{1/2} - 3^2P_{1/2} - 4^2D_{3/2}$) perturbed by the Ne are shown in Fig. 6. The effects of collisions for this large detuning case ($\Delta = -4.0$ ku, $k/k' = 1.0375$, $\epsilon = -1$) are clearly seen (the second narrow resonance centered at $\Delta' = 5.77$ ku arises from ground state hyperfine structure).

2. $|\Delta| \leq ku$. The pump laser excites a given velocity subclass of level 2 population which collisions tend to thermalize. By studying the profiles as a function of pressure, it is possible to obtain information on the interatomic potential giving rise to the relaxation.[51-56] The following interactions occur when collisions are present

$$A_1 + P + \hbar\Omega \rightarrow A_2\,(v_z' = \Delta/k) + P$$

$$A_2\,(v_z' = \Delta/k) + P \rightarrow A(v_z) + P \quad .$$

Collisions result in an excitation of level 2 and a partial thermalization of the velocity distribution. The degree of thermalization is determined by the number of collisions $\bar{n} = \Gamma_2/\nu_c$ (Γ_2: collision rate) occurring within the lifetime of level 2 and the rms change in velocity per collision Δu. In addition, the structure of the velocity redistribution may be used to infer something about the interatomic potential giving rise to scattering within the sample.

Theoretical probe absorption profiles for a weak pump field are shown in Fig. 7 for several pressures using the Keilson-Storer collision kernel.[57] One may note the gradual thermalization with increasing perturber pressure. The area under the curve remains constant. Systematic experiments of this nature were recently carried out by Brechignac et al[58] in Kr perturbed by He (Fig. 8), and by Liao et al[59] in Na perturbed by noble gases (Fig. 9). In both figures, one can see a collision-induced partial thermalization of the sample.

A complementary experiment performed using Kr and Xe was published recently.[60] In that system transfer from an excited state of Kr to an excited state of Xe can be achieved by quasi-resonant collisional excitation transfer. The Kr excited state is pumped in a velocity selective

manner and the excited state is probed. Results show that the Xe atoms retain some memory of the Kr velocity, despite the fact that the Xe atoms were characterized by a Gaussian distribution before the transfer.

By careful studies of the line shapes associated with TLS, one ultimately hopes to be able to test various models for the interatomic potentials. There is some evidence from the data of Liao et al[59], for example, that suggests a hard sphere model is not sufficient to explain large angle scattering between Na (3P) and Kr or Ne perturbers. One expects that future studies involving TLS will provide additional insight into one's understanding of collisional processes occurring in atomic systems.

VI. Conclusion

We have briefly discussed some of the ways in which the study of laser spectroscopic line shapes associated with atomic states can be used to provide collisional data. By necessity, many interesting aspects of collisional processes and line shape formations have not been discussed at all. Among these are inelastic collisions, resonant exchange collisions, collision-induced magnetic relaxation, polarization spectroscopy, laser assisted collisional excitation, collisionally-aided radiative excitation, resonance fluorescence, strong field effects (a.c. Stark splitting), coherent transient methods, and laser spectroscopy using atomic beams. Nevertheless we hope to have conveyed a sense of the type of information one can hope to obtain from experimental line shapes of laser spectroscopy.

Footnotes and References

* Permanent address: Physics Department, New York University, New York, N.Y. 10003

* Supported by the U.S. Naval Research Office. Fulbright Research Scholar Fund for the period October - November, 1979.

References

1. I.M. Beterov and V.P. Chebotaev, Prog. Quant. Elect. 3, 1 (1974).
2. P.R. Berman, Appl. Phys. (Germany) 6, 283 (1975).
3. K. Shimoda, High Resolution Laser Spectroscopy, Ed. K. Shimoda (Springer-Verlag, New York), p. 11 (1976).
4. S. Stenholm, J. Phys. B. 9, 761 (1977).
5. P.R. Berman, Advances in Atomic and Molecular Physics, Eds.D.R. Bates and B. Bederson (Academic Press, New York) 13, 57 (1977).
6. P.R. Berman, Physics Reports 43, 101 (1978).
7. R. Vetter and E. Marié, J. Phys. B 11, 2845 (1978).
8. J. Brochard and R. Vetter, J. Phys. B 7, 315 (1974).
9. J. Brochard and R. Vetter, J. de Physique 38, 121 (1977).
10. Ph. Cahuzac and R. Damaschini, J. Phys. B
11. P.R.C. Hariri, K. Burnett, R. Damaschini, D.N. Stacey, and R.C. Thompson, J. Phys. B 12, L143 (1979).
12. O. Wallee, E. Marié, N. Tran Minh, and R. Vetter, J. Phys. B
13. R.E.M. Hedges, D.L. Drummond and A. Gallagher, Phys. Rev. A6, 1519 (1979). W.P. West and A. Gallagher, Phys. Rev. A17, 1431 (1978).
14. K. Niemax, Proc. of the 4th Int. Conf. on Spectral Line Shapes, Ed. W.E. Baylis (Univ. of Windsor, Ontario) (1978).
15. D.E. Roberts and E.N. Fortson, Phys. Rev. Lett. 31, 1593 (1973).
16. D. Pritchard, J. Apt. and T.W. Ducas, Phys. Rev. Lett. 32, 641 (1974).
17. F. Biraben, B. Cagnac and G. Grynberg, Phys. Rev. Lett. 32, 643 (1974).

References - Con't.

18. M.D. Levenson and N. Bloembergen, Phys. Rev. Lett. 32, 645 (1974).
19. Th. W. Hänsch, K.C. Harvey, G. Meisel, and A.L. Schawlow, Opt. Commun. 11, 50 (1974).
20. B. Cagnac, G. Grynberg and F. Biraben, J. de Physique 34, 845 (1973); G. Grynberg, Thesis, Paris CNRS A.O. 12497 (1976).
21. For extensive references, see Laser Spectroscopy III, Eds.J.L. Hall and J.L. Carlsten (Springer Verlag, New York), (1977), Nonlinear Laser Spectroscopy, Eds.V.S. Letokhov and V.P. Chebotayev (Springer Verlag, New York) (1977); Laser Spectroscopy of Atoms and Molecules, Ed. H. Walther, (Springer Verlag, New York) (1976); Frontiers in Laser Spectroscopy, Ed. R. Balian, S. Haroche, and S. Liberman (North Holland, Amsterdam) (1977). See also Reference 3.
22. F. Biraben, B. Cagnac, E. Giacobino and G. Grynberg, J. Phys. B 10, 2369 (1977).
23. K.H. Weber and K. Niemax, Opt. Commun. 18, 317 (1979).
24. T.F. Gallagher, W.E. Cooke and S.A. Edelstein, Phys. Rev. A17, 125 (1978) and ibid. 904 (1978).
25. M.M. Salour, Phys. Rev. A17, 614 (1978).
26. P.W. Smith and Th. Hänsch, Phys. Rev. Lett. 26, 740 (1971).
27. T. Kan and G.J. Wolga, I.E.E.E. J. Quant. Elect. 7, 141 (1971).
28. C. Brechignac, R. Vetter and P.R. Berman, Phys. Rev. A17, 1669 (1978).
29. Ph. Cahuzac, E. Marié, O. Robaux, R. Vetter and P.R. Berman, J. Phys. B 11, 645 (1978).

AD-A090 528 NEW YORK UNIV N Y DEPT OF PHYSICS F/G 7/4
THEORETICAL STUDIES RELATING TO THE INTERACTION OF RADIATION WI--ETC(U)
OCT 80 N00014-77-C-0553
UNCLASSIFIED NL

2 OF 2
AD A090528

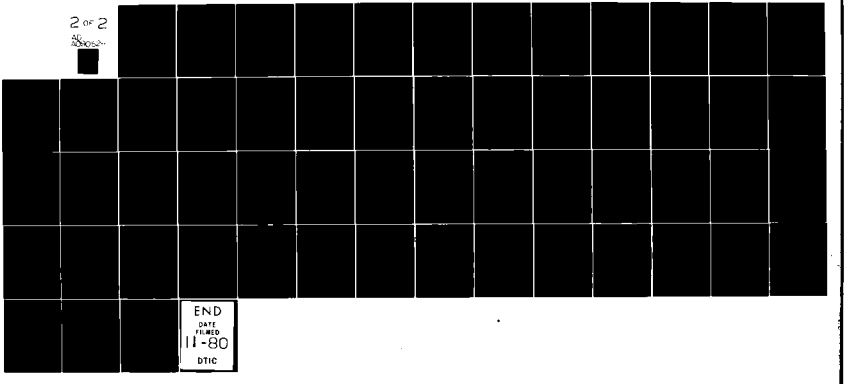

END
DATE FILMED
11-80
DTIC

30. C.E. Bagaev, E.V. Baklanov, and V.P. Chebotaev, J.E.T.P. Lett. 16 9 (1972).

31. T.W. Meyer, C.K. Rhodes, and H.A. Haus, Phys. Rev. A12, 1993 (1975).

32. Ph. Cahuzac, O. Robaux and R. Vetter, J. Phys. B9, 3165 (1976)

33. A.T. Mattick, N.A. Kurnit, and A. Javan, Chem. Phys. Lett. 38, 176 (1976).

34. C.J. Borde in Laser Spectroscopy III, Eds. J.L. Hall and J.L. Carlsten (Springer Verlag, New York) (1977).

35. I. Colomb and M. Dumont, Opt. Commun. 21, 143 (1977); I. Colomb, These du 3e cycle, Paris-Nord (1977).

36. J.L. LeGouet, J. Phys. B11, 3001 (1978).

37. M. Bornstein and W.E. Lamb, Phys. Rev. A5, 1311 (1972).

38. B. Avrillier, Thesis, Université de Paris-Nord (1978)

39. C. Wieman and Th. W. Hänsch, Phys. Rev. Lett. 36, 1170 (1976).

40. G.E. Notkin, S.F. Rautian, and A.A. Feoktistov, Zh. Eksp. Teor. Fiz. 52, 1673 (1967) [Sov. Phys. J.E.T.P. 25, 1112 (1967)].

41. M.S. Feld and A. Javan, Phys. Rev. 177, 540 (1969).

42. Th. W. Hänsch and P.E. Toschek, Z. Phys. 236, 213 (1970).

43. J.E. Bjorkholm and P.F. Liao, Phys. Rev. A14, 751 (1976).

44. D.L. Huber, Phys. Rev. 178, 93 (1969).

45. A. Omont, E.W. Smith and J. Cooper, Astrophys. J. 175, 185 (1972).

46. J.L. Carlsten and A. Szöke, Phys. Rev. Lett. 36, 667 (1976) and J. Phys. B9, L231 (1976).

47. J.L. Carlsten, A. Szoke, and M.G. Raymer, Phys. Rev. A15, 1029 (1977).

48. D.L. Rousseau, G.D. Patterson and P.F. Williams, Phys. Rev. Lett. 34, 1306 (1975).

49. R.D. Driver and J.L. Snider, J. Phys. B10, 595 (1977).

50. P.F. Liao, J.E. Bjorkholm and P.R. Berman, Phys. Rev. A20, 1489 (1979).

51. Th. W. Hänsch and P.E. Toschek, I.E.E.E. J. Q. Elec. 5, 61 (1969).

52. I.M. Beterov, Y.A. Mattuygin and V.P. Chebotaev, Sov. Phys. J.E.T.P. 37, 756 (1973).

53. W.K. Bischel, P.J. Kelly and C.K. Rhodes, Phys. Rev. Lett. 34, 300 (1975); Phys. Rev. A13, 1817 (1976), and ibid. 1829 (1976).

54. A. Kiel, A. Schabert, and P.E. Toscheck, Z. Phys. 261, 71 (1973).

55. W.K. Bischel, C.K. Rhodes, Phys. Rev. A14, 176 (1976).

56. Ph. Cahuzac, J.L. LeGouet, P.E. Toschek and R. Vetter, Appl. Phys. (Germany) 20, 83 (1979).

57. J. Keilson and K. Storer, Q. Appl. Math. 10, 243 (1952).

58. C. Brechignac, R. Vetter and P.R. Berman, J. de Physique Lett. 39, L231 (1978).

59. P.F. Liao, J.E. Bjorkholm and P.R. Berman, Phys. Rev. A21, 1927 (1980).

60. J.L. Picqué and R. Vetter, Phys. Rev. Lett. 43, 508 (1979).

Figure Captions

1. Width L of the Lorentzian component of the 3.51 μm line of Xe I vs. perturber pressure obtained in linear spectroscopy. The insert shows the low pressure domain (data from Ref. 7).

2. FWHM of the Lorentzian component L, the Gaussian component G, and the total Voigt profile V of the 3.51 μm Xe I line vs. pressure. One notices a marked variation of the Gaussian width at low pressure; the corresponding temperatures associated with the widths are indicated on the ordinate of the G vs. P curve. The variation of the Lorentzian width is nearly linear with a slope of (10.9 ± 1.3) MHz/Torr (data from Reference 7).

3. Saturated absorption of the 557 nm line of KrI. The upper curve shows the experimental profile (solid line) for a perturber pressure of 110 mTorr of He and the curves 1, 2, 3 represent respectively the components of this line arising from Kr^* atoms that have not experienced v.c.c., from Kr^* atoms that have undergone v.c.c. with Kr, and from Kr^* atoms that have undergone v.c.c. with He atoms. The lower graph represents the width of the v.c.c. component "3" perturbed by He perturbers (dots) or Ar ones (crosses). The dashed line is the thermal equilibrium value (data from Reference 28).

4. Width of the 3.51 μm line of Xe I as a function of Xe pressure in both linear ($2\gamma_o$) and saturation (2γ) spectroscopy. Point "A" is the natural line width of 4.6 MHz. One observes a marked non-linear variation of the width, owing to v.c.c. (data from Reference 29).

Figure Captions - Con't.

5. Three-level systems used in saturation spectroscopy. (a) upward cascade, (b) inverted "V", (c) "V". The λ_i are values for incoherent pumping and γ_i the decay rates for the states i. In this work, we consider case (a) in the limit $\lambda_2 = \lambda_3 = 0$, $\lambda_1 \neq 0$, $\gamma_1 \neq 0$ and $\lambda_1/\gamma \sim$ constant, simulating a system in which level 1 is the ground state.

6. Experimental profiles of probe absorption for the excitation of the $3^2S_{1/2} - 3^2P_{1/2} - 4^2D_{3/2}$ transition in Na for various pressures of Ne perturbers. The pump detuning is $\Delta/2\pi = -4\text{GHz} = -4ku/2\pi$. The two narrow resonances represent "direct" two photon excitation of the 4^2D state from the two hyperfine components of the ground state. The collision induced broad resonance is centered at the $3^2P_{1/2} - 4^2D_{3/2}$ transition frequency. Solid lines, experiment; points, theoretical fit (date from Reference 50).

7. Theoretical profiles for probe absorption I_s (in arbitrary units) in a TLS with $k'/k = 0.4$, counterpropagating waves ($\varepsilon = -1$), a detuning $\Delta/ku = -1$, and a weak pump field. The population inversion N_{22} between levels 3 and 2 in the absence of collisions is taken to be zero. The abcissa is the probe detuning Δ' in units of ku. The curves are calculated for different perturbers using a Keilson-Storer collision kernel with $\Delta u = 0.66u$ and a v.c.c. rate $\Gamma_2/ku = 0.006\,P$, where P is the perturber pressure in Torr. The lifetime of the intermediate state is $\gamma_2/ku = 0.02$. These curves show the thermalization of

Figure Captions - Con't.

the intermediate state population velocity distribution with increasing P.

8. Profiles for linear and saturation spectroscopy of the 557 nm line of KrI. Curve I, linear absorption profile in pure Kr, centered at ν_0. Curves II and III represent saturated absorption profiles obtained with two counterpropagating laser beams, the pump being detuned by $\Delta/2\pi$ = 600 MHz from ν_0. Curve II is recorded for pure Kr at a pressure of 10 mTorr and curve III is recorded for a mixture of Kr (10 mTorr) and He (450 mTorr). Curve III is analyzed in terms of components arising from Kr^* atoms which have not experienced v.c.c. (curve (a)), Kr^* atoms that have undergone thermalizing events with Kr atoms (curve (b)) and Kr^* atoms that have undergone v.c.c. with He atoms (curve (d)). The lower graph shows the contribution to curve (c) from Kr^* atoms that have undergone 1, 3, 5, ... collisions with He, indicating the gradual thermalization of Kr^* as a function of the number of Kr^* - He collisions (data from Reference 58).

9. Experimental probe absorption as a function of $\Delta'/2\pi$ for the same transition in Na shown in Fig. (6), but for a pump detuning $\Delta/2\pi = -1.6$ ku/$2\pi = -1.6$ GHz. The partial thermalization resulting from v.c.c. is evident. The solid circles represent a theoretical fit using a hard sphere collision kernel and the open circles a fit using the Keilson-Storer collision kernel (data from Reference 59).

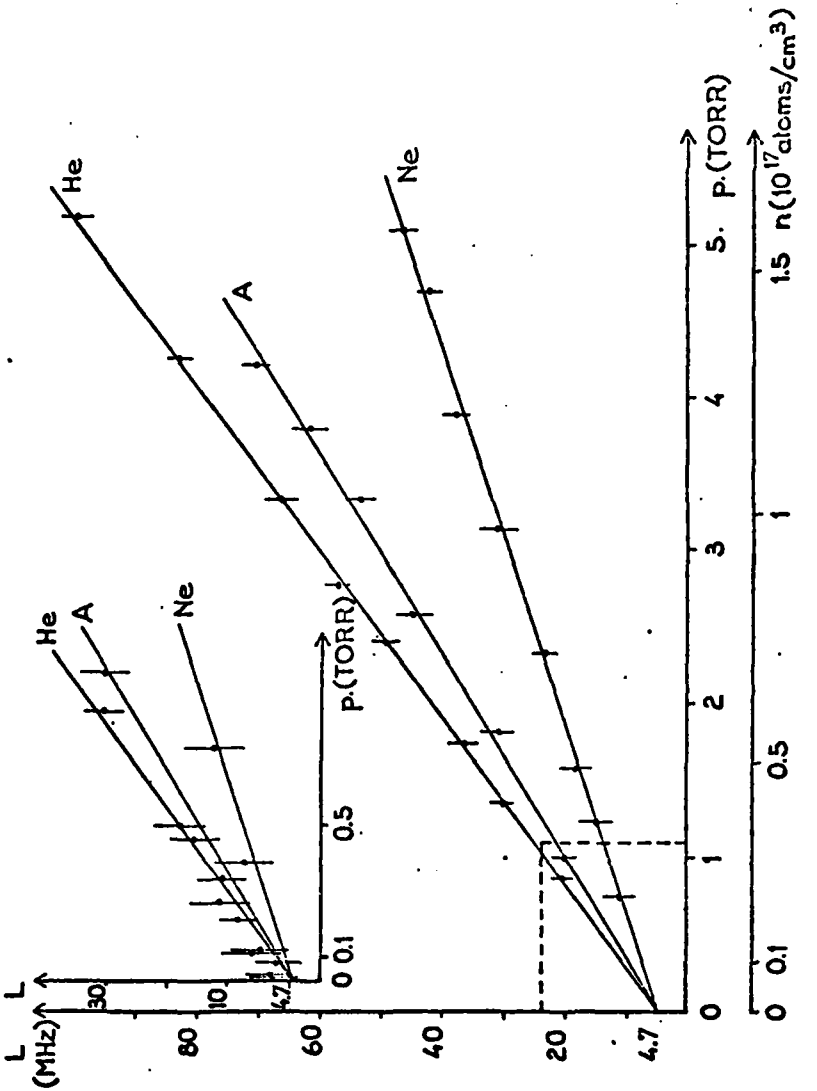

Fig. 1

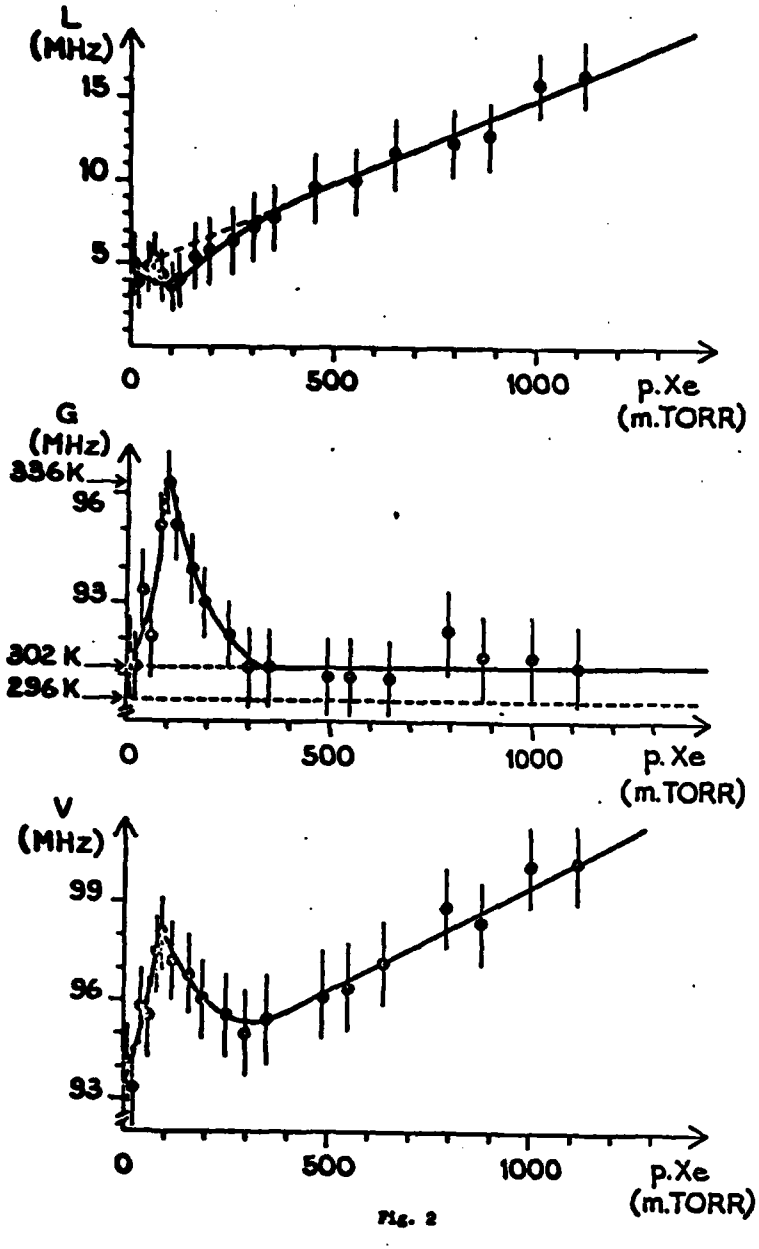
L
(MHz)
15
10
5
0
500
1000
p.Xe
(m.TORR)
G
(MHz)
336K
96
93
302 K
296 K
0
500
1000
p. Xe
(m.TORR)
V
(MHz)
99
96
93
0
500
1000
p.Xe
(m.TORR)

Fig. 2

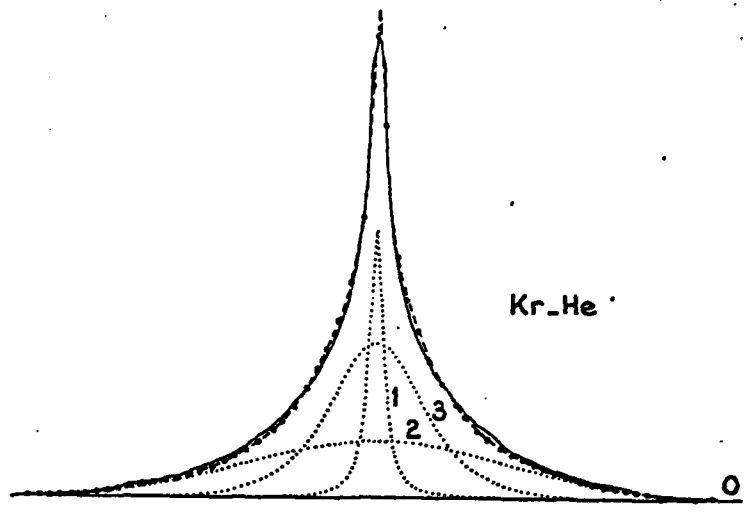
Kr_He
1
2
3
0

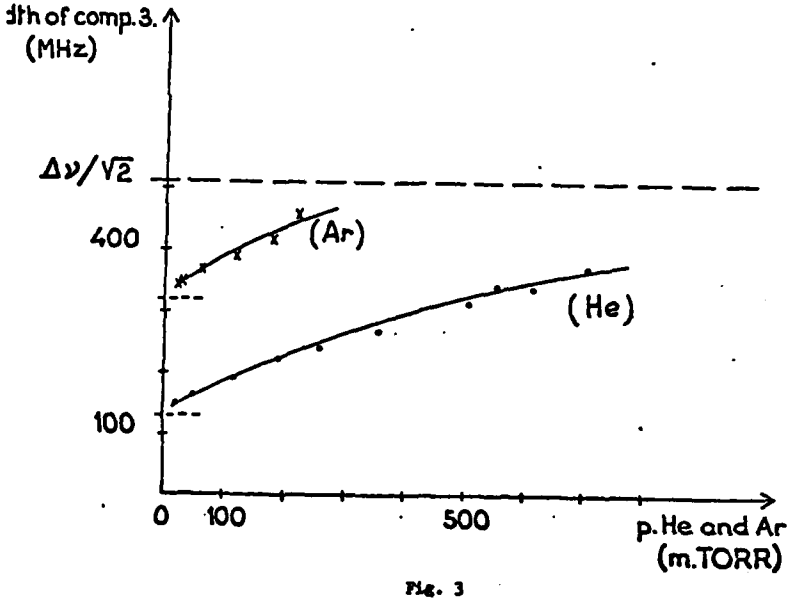
dth of comp. 3.
(MHz)
Δν/√2
400
100
(Ar)
(He)
0
100
500
p. He and Ar
(m.TORR)

Fig. 3

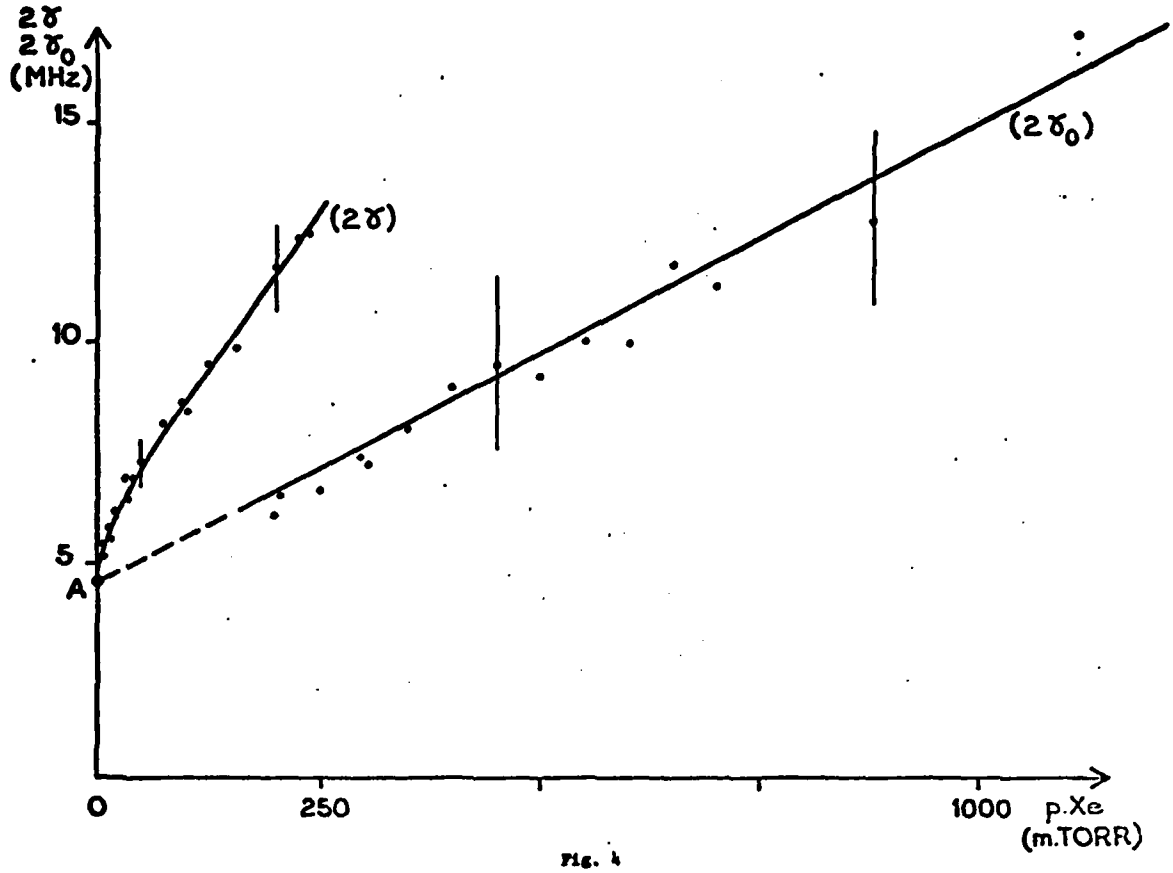
2γ
2γ0
(MHz)
15
10
5
A
(2γ)
(2γ0)
0
250
1000
p.Xe
(m.TORR)

Fig. 4

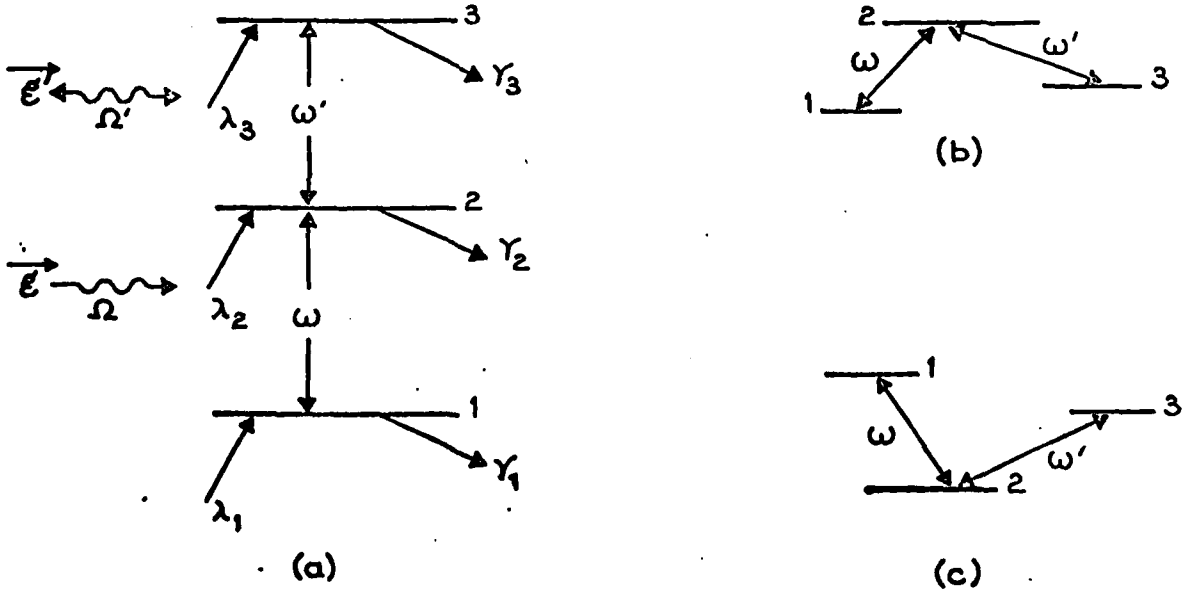
3
2
1
ε'
Ω'
λ3
ω'
γ3
ε
Ω
λ2
ω
γ2
λ1
γ1
(a)
2
ω
ω'
1
3
(b)
1
ω
2
ω'
3
(c)

Fig. 5

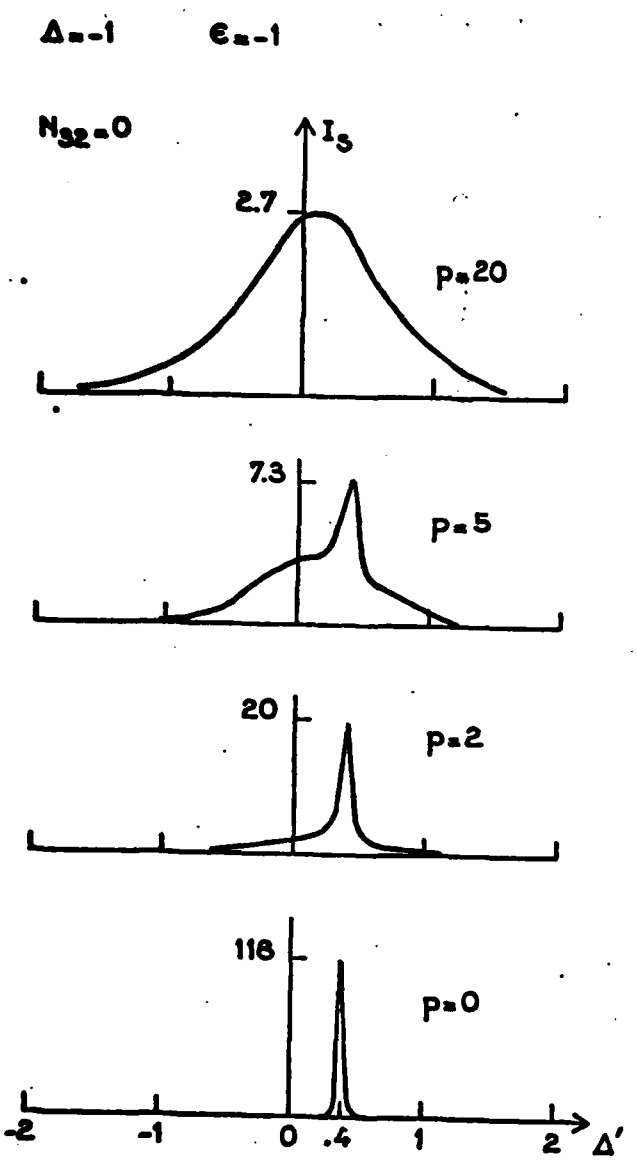
Δ=-1
ε=-1
N32=0
IS
2.7
p=20
7.3
p=5
20
p=2
116
p=0
-2
-1
0
.4
1
2
Δ'

Fig. 7

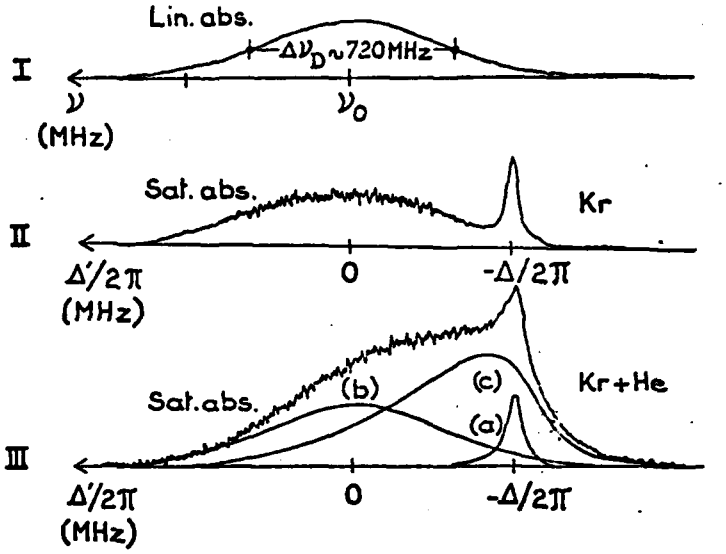
Lin. abs.
Δν_D ~ 720 MHz
I
ν
ν0
(MHz)
Sat. abs.
Kr
II
Δ'/2π
0
-Δ/2π
(MHz)
Sat. abs.
(b)
(c)
(a)
Kr+He
III
Δ'/2π
0
-Δ/2π
(MHz)

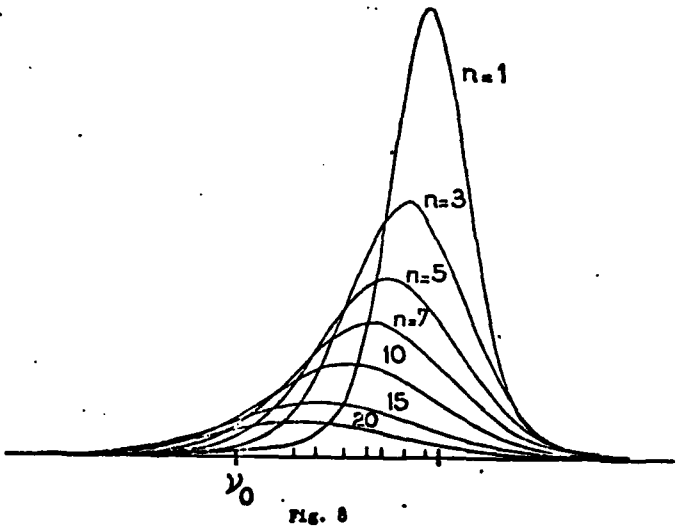
n=1
n=3
n=5
n=7
10
15
20
ν0

Fig. 8

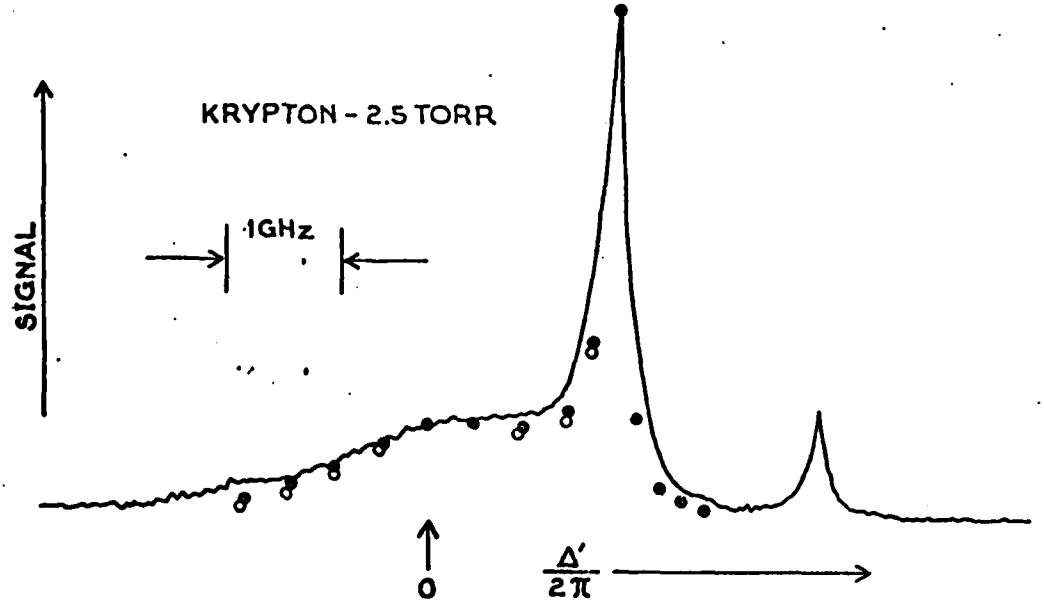

Fig. 9

SSSIII 65 PLRAA,801100AQ1354,2 PRA11003

47-A5

Coherence effects in radiatively assisted inelastic collisions: General theory

Paul R. Berman

*Laboratoire Aimé Cotton, Centre National de la Recherche Scientifique II, Bâtiment 505, 91405 Orsay-Cedex, France and Physics Department, New York University, 4 Washington Place, New York, New York 10003**

(Received 21 March 1980)

A radiatively assisted inelastic collision (RAIC) is one in which two atoms collide in the presence of a radiation field to produce a reaction of the form $A^* + B + \hbar\Omega \rightarrow A + B^*$. In this paper, a general theory of RAIC is developed with special attention given to the final-state coherences produced by RAIC. These final-state coherences can be monitored by standard experimental techniques (polarization of fluorescence, quantum beats), enabling one to use such studies to gain information on the interatomic potentials that are relevant to the RAIC under consideration.

PACS numbers: 32.90. + a, 34.90. + q, 34.50. − s, 32.70. − n

I. INTRODUCTION

There has been considerable recent interest in reactions of the form

$$A_i + A'_{i'} + \hbar\Omega \rightarrow A_f + A'_{f'} \tag{1}$$

in which two atoms (A and A') undergo a collision while simultaneously absorbing a photon of energy $\hbar\Omega$ from an external radiation field to take the atoms from some initial state $A_i A'_{i'}$ to a final state $A_f A'_{f'}$. In many cases, the direct transition $A_i + A'_{i'} \rightarrow A_f + A'_{f'}$ is energetically forbidden; consequently, the transition can take place only in the presence of the radiation field, with the photon providing the energy mismatch $(E_f + E_{f'}) - (E_i + E_{i'})$.[1] Such processes have been referred to as radiative collisions[2] (RC), laser-induced collisional energy transfer[3] (LICET), or radiatively assisted inelastic collisions[4] (RAIC) and have been the subject of a large number of theoretical[5] and a lesser number of experimental[3,6] investigations. By studying the RAIC cross section as a function of frequency Ω, one can gain important information about the initial- and final-state AA' interatomic potentials.

Typically, the RAIC cross section can be measured by monitoring the fluorescence from one of the final states ($A'_{f'}$, for example) since the total RAIC cross section can be simply related to the *total* fluorescence rate. It is apparent, however, that additional information is contained in the polarization of the fluorescence, i.e., in the coherence properties of the final states. It is the purpose of this paper to present a general theory of RAIC which allows one to calculate the final-state coherence properties as well as the total RAIC cross section. Experimentally, the final-state coherence can be probed by standard methods (absorption, emission, or quantum beats originating from one of the final states).

A few calculations[7,8] have already appeared which include magnetic degeneracy effects in RAIC and in the related problem of collisionally assisted radiative excitation (CARE). However, these calculations were restricted to specific J values for the various levels and to specific forms for the interatomic potentials; moreover, only total cross sections were obtained.

A more global picture of the collisional process is achieved if levels of arbitrary J and interatomic potentials of a quite general nature are considered. The calculations, including an averaging over different collisions orientations, are conveniently carried out using techniques involving irreducible tensor operators. The final-state coherence resulting from RAIC can then be interpreted in terms of the symmetry properties of the interatomic potential and the characteristic properties (polarization, frequency, intensity) of the external light field participating in the RAIC reaction.

A general formalism for RAIC is given in this paper. The physical system is described in Sec. II, the equations of motion are given in Sec. III (and derived in Appendix A), and a formal solution is obtained in Sec. IV. A discussion of the results is given in Sec. V. In Appendix B, I present a diagrammatic interpretation of the operators that appear in the equations of motion.

Solutions of the RAIC equations in the limit where the external field is weak and the collision-induced level shifts of the atomic energy levels can be neglected will be presented in a following paper. In future work, solutions of the RAIC equations will be sought that are valid for arbitrary field strengths and include level-shifting effects.

II. PHYSICAL SYSTEM

The physical system consists of a low density (≈ several hundred Torr) atomic vapor containing two types of atoms, A and A', to which a light pulse is applied. The atomic energy levels for

Supported by the U.S. Office of Naval Research under Contract No. N00014-77-C-0553.

atoms A and A' are shown in Fig. 1. Levels of atom A are designated by unprimed variables and those of atom A' by primed ones. It is assumed that the levels of each atom can be separated into subgroups of levels (see Fig. 1), with the energy separation between sublevels in a given group having some upper bound $\hbar\omega_E$ (to be established below). Specifically, the sublevels within a group are generally different fine structure, hyperfine structure, or Zeeman sublevels of a given electronic state. The atoms are prepared in a linear superposition of states $|ii'\rangle$, where i and i' represent any of the sublevels in the i and i' groups, respectively.

The light pulse is taken to be of the form

$$\vec{E}(\vec{R},t)=\tfrac{1}{2}[\vec{\mathcal{E}}(\vec{R},t)e^{-i\Omega t}+\vec{\mathcal{E}}(\vec{R},t)^{*}e^{i\Omega t}], \qquad (2)$$

where the envelope function $|\vec{\mathcal{E}}(\vec{R},t)|$ is characterized by a duration T and a maximum amplitude $|\mathcal{E}_0|$ (Fig. 2). It is assumed that the pulse envelope varies very slowly in an optical period ($\Omega T \gg 1$) and that the frequency Ω is very far detuned from any transition frequency in atom A or in atom A'. On the other hand, the field is assumed to be in near resonance with the transition in the *composite* AA' system from some initial state $|ii'\rangle$ to a final state $|ff'\rangle$. In other words

$$\hbar\Omega \approx E_f + E_{f'} - (E_i + E_{i'}), \qquad (3)$$

where E_α is the energy of a given level α.

Thus, the field can induce transitions only in the composite system AA', implying that excitation can occur only if there is an $A-A'$ collision during the on-time of the light pulse. Let us suppose that such a collision occurs, centered at time $t=t_c$, position $\vec{R}=\vec{R}_c$, and is characterized by a collision duration $\tau_c = b/v$, where b is the impact

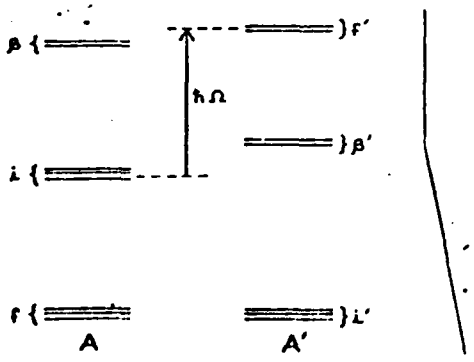

FIG. 1. Energy levels for the atoms A and A' under consideration. The groups of levels represented by a single letter are degenerate or near degenerate, with a maximum frequency separation ω_E such that $\omega_E\tau_c \ll 1$ (τ_c = duration of a collision). The field frequency Ω is such that $\hbar\Omega \approx E_f + E_{f'} - (E_i + E_{i'})$.

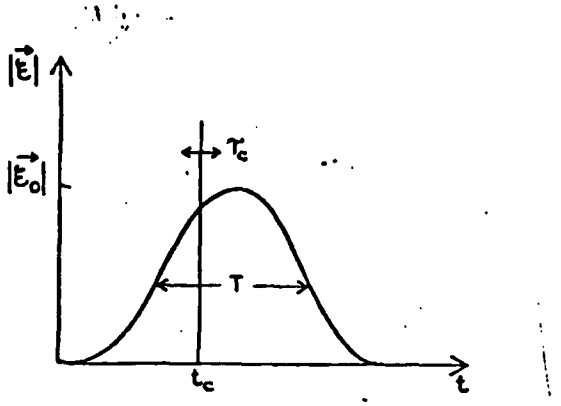

FIG. 2. Field-pulse envelope as a function of time. A collision occurs, centered in time at $t=t_c$, with a duration $\tau_c \ll T$.

parameter and v_r the relative atomic speed associated with the collision. Collision durations are on the order of 10^{-12} sec so that is is reasonable to assume that

$$\tau_c \ll T, \qquad (4)$$

since pulse durations $T \gtrsim 1.0$ nsec are typical. Thus, excitation occurs on the time scale τ_c; on this time scale, the field amplitude $\vec{\mathcal{E}}(\vec{R},t)$ is essentially constant and may be evaluated as $\vec{\mathcal{E}}(\vec{R}_c,t_c)$ (Fig. 2). In calculating excitation probabilities, it is generally necessary to average over all possible t_c and $\vec{R}_c$ during the light pulse and to average over all collision impact parameters, orientations, and relative speeds. The average over $\vec{R}_c$ is equivalent to an average over the spatial profile of the light pulse.

The following assumptions are adopted: (1) Collisional excitation exchange between atoms A and A' does not occur in the absence of the light field (i.e., all such exchange processes are assumed to be nonresonant). (2) The frequency ω_E is chosen such that

$$\omega_E\tau_c \ll 1, \qquad (5)$$

ensuring that all sublevels in a given group are, in effect, degenerate during a collision. (3) There is no population decay or buildup of Doppler phase during a collision; that is,

$$\gamma\tau_c \ll 1, \quad ku\tau_c \ll 1, \qquad (6)$$

where γ is a decay rate associated with the initial or final states, $\vec{k}$ is a wave vector associated with the field, and u is an atomic speed. (4) Each atom undergoes, at most, one collision, on average, during the pulse time T, enabling one to ignore multiple-collision effects [valid for densities $\ll 10^{19}$ atoms/cm^3 T (nsec)]. (5) The collision trajectory is treated classically, which implies that the change in kinetic energy resulting from

RAIC is small, i.e., that

$$|\omega_{fi}+\omega_{f'i'}-\Omega|\tau_c \lesssim 1, \tag{7}$$

where

$$\omega_{\alpha\beta}=\omega_\alpha-\omega_\beta, \quad \omega_\alpha=E_\alpha/\hbar. \tag{7a}$$

If condition (7) were not satisfied, one could not assign a unique classical trajectory to the collision.

To summarize, I am considering the radiatively assisted collisional reaction

$$A_i+A'_{i'}+\hbar\Omega \rightarrow A_f+A'_{f'}$$

from initial states $|ii'\rangle$ to final states $|ff'\rangle$, in which the photon is provided by an electromagnetic pulse. Several assumptions relating to the time scales in the problem have been made which are valid for many systems of practical interest. All information on final-state coherence is contained in the density matrix following the RAIC. The final-state density matrix for one of the atoms can be obtained by taking the trace of the final-state density matrix for the composite system over the final-state variables of the other atom. Experimentally, it is generally such a single-particle density matrix that is monitored (e.g., by fluorescence from the final state of one of the atoms).

III. EQUATIONS OF MOTION

By assumption, the collision trajectory is treated classically. That is, relative to a fixed laboratory frame, a collision is characterized by an impact parameter b, relative speed $v_r=|\vec{v}-\vec{v}'|$ ($\vec{v}$ and $\vec{v}'$ being, respectively, the velocities of atoms A and A'), and orientation O relative to the fixed frame. The Hamiltonian for the RAIC can be written

$$H(t;b,v_r,\Theta,\vec{R}_c,t_c)=H_0(\vec{r})+H'_0(\vec{r}') - \tfrac{1}{2}(\vec{\mu}+\vec{\mu}')\cdot[\vec{\mathcal{E}}(\vec{R}_c,t_c)e^{-i\Omega t}+\text{c.c.}] +\mathcal{U}(\vec{r},\vec{r}',\vec{R}(t)), \tag{8}$$

where H_0 and H'_0 are the free-atom Hamiltonians for atoms A and A', respectively, $\vec{\mu}$ and $\vec{\mu}'$ are the dipole-moment operators for atoms A and A', respectively (the atom-field interaction is treated in the dipole approximation), and $\mathcal{U}$ is the A-A' interaction Hamiltonian. The collision is centered in time at $t=t_c$ and $\vec{R}_c$ is the position of the center of mass of the atoms when $t=t_c$. All effects of atomic motion are contained implicitly in the interatomic separation $\vec{R}(t)$, calculated for a classical trajectory. In writing the approximate Hamiltonian (8), conditions (4), (6), and (7) were used.

According to the assumptions of Sec. II, states $|ii'\rangle$ can be coupled only to states $|i_1i'_1\rangle$ (i_1 is another state in the i group) or to states $|ff'\rangle$. The corresponding equations of motion for the probability amplitudes $a_{ii'}(t)$, $a_{ff'}(t)$ (in the interaction representation), as derived in Appendix A starting from the Schrödinger equation with the Hamiltonian (8), are given by

$$i\hbar\dot{a}_{ii'}=\sum_{i_1i'_1}\langle ii'|\hat{S}(ii';t,b,v_r,\Theta,\vec{R}_c,t_c)|i_1i'_1\rangle a_{i_1i'_1} + \sum_{ff'}\langle ii'|\hat{T}(ff',ii';t,b,v_r,\Theta,\vec{R}_c,t_c)|ff'\rangle e^{i\Delta t}a_{ff'},$$

$$i\hbar\dot{a}_{ff'}=\sum_{f_1f'_1}\langle ff'|\hat{S}(ff';t,b,v_r,\Theta,\vec{R}_c,t_c)|f_1f'_1\rangle a_{f_1f'_1} + \sum_{ii'}\langle ff'|\hat{T}(ii',ff';t,b,v_r,\Theta,\vec{R}_c,t_c)|ii'\rangle e^{-i\Delta t}a_{ii'}, \tag{9b}$$

where the detuning Δ is defined by

$$\Delta=\Omega-(\omega_{fi}+\omega_{f'i'}), \tag{10}$$

and the operators $\hat{S}$ and $\hat{T}$ are defined below.

The operator $\hat{S}(\alpha\alpha';t,b,v_r,\Theta,\vec{R}_c,t_c)$ is an operator that acts *only* in the $\alpha\alpha'$ subspace ($\alpha\alpha'=ii'$ or ff'); it shifts and couples levels within that subspace. Explicitly (see Appendix A),

$$\hat{S}(\alpha\alpha';t,b,v_r,\Theta,\vec{R}_c,t_c)=\hat{S}_L+\hat{S}_c, \tag{11}$$

$$\hat{S}_L=\frac{-1}{4i}\sum_{\beta\beta'}\left(\frac{\vec{\mu}_T\cdot\vec{\mathcal{E}}(\vec{R}_c,t_c)^*|\beta\beta'\rangle\langle\beta\beta'|\vec{\mu}_T\cdot\vec{\mathcal{E}}(\vec{R}_c,t_c)}{\omega_{\beta\alpha}+\omega_{\beta'\alpha'}-\Omega}+\frac{\vec{\mu}_T\cdot\vec{\mathcal{E}}(\vec{R}_c,t_c)|\beta\beta'\rangle\langle\beta\beta'|\vec{\mu}_T\cdot\vec{\mathcal{E}}(\vec{R}_c,t_c)^*}{\omega_{\beta\alpha}+\omega_{\beta'\alpha'}+\Omega}\right), \tag{11a}$$

$$\hat{S}_c=-\hbar^{-1}\sum_{\beta\beta'}\frac{\mathcal{U}(\vec{R}(t))|\beta\beta'\rangle\langle\beta\beta'|\mathcal{U}(\vec{R}(t))}{\omega_{\beta\alpha}+\omega_{\beta'\alpha'}}, \tag{11b}$$

where

$$\vec{\mu}_T = \vec{\mu} + \vec{\mu}' . \tag{12}$$

The operator $\hat{S}$ may appear to be complicated, but it has a well-known physical interpretation. The term $\hat{S}_L$ involves only field variables and gives rise to the shifting (light shifts) and coupling of $\alpha\alpha'$ levels produced by an *off-resonant* external electromagnetic field. The summation over intermediate states $\beta\beta'$ represents the virtual excitation of these levels by the field. The term $\hat{S}_c$ [Eq. (11b)] involves only collision variables and gives rise to collisionally induced shifting and coupling of levels in the $\alpha\alpha'$ group. The shift of the levels is the origin of the pressure broadening and shifting of spectral lines, while the coupling within the $\alpha\alpha'$ group leads to collisionally induced relaxation of any alignment, orientation, etc., that may be present in that group of levels. Again one finds a summation over an infinite number of virtual excitations $|\beta\beta'\rangle$.

The transition operator $\hat{T}$ that couples groups of states $|ii'\rangle$ to $|ff'\rangle$ is given by (see Appendix A)

$$\hat{T}(ii', ff'; t, b, v_r, \Theta, \vec{R}_c, t_c) = \frac{1}{2i\hbar} \sum_{\beta\beta'} \left(\frac{\mathcal{U}(\vec{R}(t))|\beta\beta'\rangle\langle\beta\beta'|\vec{\mu}_T}{\omega_{\beta f} + \omega_{\beta' f'}} + \frac{\vec{\mu}_T|\beta\beta'\rangle\langle\beta\beta'|\mathcal{U}(\vec{R}(t))}{\omega_{\beta i} + \omega_{\beta' i'}} \right) \cdot \vec{\mathcal{E}}(\vec{R}_c, t_c) \tag{13}$$

and represents the combined effect of the (field + collision) in producing the transition from initial to final states. The corresponding transition operator which couples states $|ff'\rangle$ to $|ii'\rangle$ is given by[3]

$$\hat{T}(ff', ii'; t, b, v_r, \Theta, \vec{R}_c, t_c) = \frac{1}{2i\hbar} \sum_{\beta\beta'} \left(\frac{\vec{\mu}_T|\beta\beta'\rangle\langle\beta\beta'|\mathcal{U}(\vec{R}(t))}{\omega_{\beta f} + \omega_{\beta' f'}} + \frac{\mathcal{U}(\vec{R}(t))|\beta\beta'\rangle\langle\beta\beta'|\vec{\mu}_T}{\omega_{\beta i} + \omega_{\beta' i'}} \right) \cdot \vec{\mathcal{E}}(\vec{R}_c, t_c)^* . \tag{14}$$

Note that the matrix elements of $\hat{T}$ appearing in Eq. (9) are related by

$$\langle ii'|\hat{T}(ff', ii'; t)|ff'\rangle = \langle ff'|T(ii', ff'; t)|ii'\rangle^* . \tag{15}$$

A diagrammatic interpretation of $\hat{S}$ and $\hat{T}$ is given in Appendix B.

To obtain the RAIC excitation probability, one must solve Eqs. (9) for $a_{ff'}(t_c^+)$ subject to the initial conditions

$$a_{ii'}(t_c^-) \neq 0, \quad a_{ff'}(t_c^-) = 0 , \tag{16}$$

where t_c^- (t_c^+) are times before (after) the collision. Since $\tau_c \ll T$ [Eq. (4) or Fig. 2], the times $t_c^\pm$ can be set equal to $\pm\infty$ when integrating Eqs. (9) without introducing significant error.

The validity conditions for Eqs. (9) are discussed in detail in Appendix A. If

$$\bar{\omega}\tau_c \gg 1 , \tag{17}$$

where $\bar{\omega}$ is any of the frequency denominators appearing in the operators $\hat{T}$ and $\hat{S}$, and if Eqs. (3)–(7) are satisfied, then Eqs. (9) are valid over a wide range of field strengths.[10] Condition (17) ensures that the intermediate states act only as *virtual* levels in the RAIC problem. The virtual excitations are represented by the summations over β and β' in the $\hat{S}$ and $\hat{T}$ operators, and the problem is reduced to an effective two groups of levels problem for the states $|ii'\rangle$ and $|ff'\rangle$. It should be noted that Eqs. (9) reduce to the corresponding equations derived by other authors in various limiting cases.[5]

IV. FORMAL SOLUTION

It is useful to make use of Eq. (15) and to rewrite Eqs. (9) in matrix form as

$$i\hbar\dot{\vec{a}}_I = S(I, t)\vec{a}_I + [T(IF, t)]^\dagger e^{i\Delta t}\vec{a}_F , \tag{18a}$$

$$i\hbar\dot{\vec{a}}_F = S(F, t)\vec{a}_F + T(IF, t)e^{-i\Delta t}\vec{a}_I , \tag{18b}$$

$$\vec{a}_I(t_c^-) \neq 0, \quad \vec{a}_F(t_c^-) = 0 , \tag{18c}$$

where $\vec{a}_I$ ($\vec{a}_F$) is a vector containing all possible states $|ii'\rangle$ ($|ff'\rangle$) in the initial (final) group of levels and $S(I, t)$, $S(F, t)$, and $T(IF, t)$ are matrix representations of the corresponding operators appearing in Eqs. (9). A solution of the form

$$\vec{a}_K(t) = G_K(t, t_c^-)\vec{A}_K(t) , \quad K = I, F \tag{19}$$

is sought, where the matrix $G_K(t, t')$ is chosen to satisfy the equations

$$i\hbar\frac{\partial G_K(t, t')}{\partial t} = S(K, t)G_K(t, t') , \tag{20a}$$

$$G_K(t, t) = 1, \quad K = I, F \tag{20b}$$

and the symbols I and F represent the entire ii' and ff' subspaces, respectively. Substituting Eqs. (19) and (20) into Eqs. (18) and making use of the relations

$$\begin{aligned} &(G_K(t, t'))^{-1} = G_K(t', t) , \\ &G_K(t, t_1)G_K(t_1, t_2) = G_K(t, t_2) , \end{aligned} \tag{21}$$

which follow directly from Eqs. (19) and (20), one obtains

$$i\hbar\dot{\vec{A}}_I = G_I(t_c^-, t)(T(IF, t))^\dagger G_F(t, t_c^-)e^{i\Delta t}\vec{A}_F , \tag{22a}$$

$$i\hbar\dot{\bar{A}}_F = G_F(t_c^-, t)T(IF, t)G_I(t, t_c^-)e^{-i\alpha t}\bar{A}_I, \quad (22b)$$

$$\bar{A}_I(t_c^-) = \bar{a}_I(t_c^-), \quad \bar{A}_F(t_c^-) = 0. \quad (22c)$$

In this form, all effects of shifting and coupling within the ii' and ff' subspaces are contained in the matrices $G_I(t, t')$ and $G_F(t, t')$, respectively.

Once a solution to Eqs. (22) is found, final-state density matrix elements of the form

$$\bar{\rho}_{ff';f_1f_1'}(t_c^+; b, v_r, \Theta, \bar{R}_c, t_c) = a_{ff'}(t_c^+)[a_{f_1f_1'}(t_c^+)]^* = [G_F(t_c^+, t_c^-)\bar{A}_F(t_c^-)]_{ff'}[G_F(t_c^+, t_c^-)\bar{A}_F(t_c^-)]^*_{f_1f_1'} \quad (23)$$

may be constructed (the tilde is a reminder that results are expressed in the interaction representation). The (complex) rate at which RAIC create density matrix elements $\bar{\rho}_{ff';f_1f_1'}(t_c^+; v_r, t_c)$ at time t_c during the light pulse for atoms A and A' having relative speed v_r starting from an initial density matrix element $\bar{\rho}_{ii';i_1i_1'}(t_c^-)$ is given by

$$\Gamma^{II_1}_{FF_1}(v_r, t_c) = \mathfrak{N}_A\mathfrak{N}_{A'}v_r\int_0^\infty 2\pi b\,db\int(8\pi^2)^{-1}d\Theta\int d\bar{R}_c \times \frac{d[\bar{\rho}_{FF_1}(t_c^+; b, v_r, \Theta, \bar{R}_c, t_c)]}{d[\bar{\rho}_{II_1}(t_c^-)]}, \quad (24)$$

where $\mathfrak{N}_\alpha$ is the α-atom density (assumed to be independent of position) and the shorthand notation

$$I = ii', \quad F = ff', \quad I_1 = i_1i_1', \quad F_1 = f_1f_1', \quad (25)$$

etc., has been adopted. The integral over $\bar{R}_c$ in Eq. (24) is limited to the interaction region of the atoms and light field; it is essentially an integration over the spatial profile of the light beam.

Thus, *during the light pulse*, the density matrix evolves as

$$\frac{\partial\bar{\rho}_{FF_1}(\bar{v}, \bar{v}', t_c)}{\partial t_c} = \sum_{II_1}\Gamma^{II_1}_{FF_1}(v_r, t_c)\bar{\rho}_{II_1}(\bar{v}, \bar{v}', t_c) + [\bar{X}(t_c)\bar{\rho}(v, v', t_c)]_{FF_1}, \quad (26)$$

where $\bar{v}_r = \bar{v} - \bar{v}'$. The assumption that an atom undergoes at most one collision during the light pulse is contained implicitly in Eq. (26), otherwise, terms such as

$$\Gamma^{F_2F_3}_{FF_1}\bar{\rho}_{F_2F_3}$$

would be present; the term in brackets represents changes produced by processes *other* than RAIC (i.e., level decay, other external fields, etc.).[11] It is an equation of the form (26) *plus* a corresponding equation for times when the light pulse is *off* which must be solved in order to make connection with a given experimental situation (of course, there are no RAIC terms in the equations with the field off). For example, if the pulse time T is short enough so that the bracketed term in Eq. (26) may be neglected, then the final-state density matrix following the light pulse is simply

$$\bar{\rho}_{FF_1}(\bar{v}, \bar{v}', T^+) = \sum_{II_1}\left(\int_{T^-}^{T^+}\Gamma^{II_1}_{FF_1}(v_r, t_c)dt_c\right) \times \bar{\rho}_{II_1}(\bar{v}, \bar{v}', T^-), \quad (27)$$

where $T^-(T^+)$ indicates a time just before (after) the pulse. One can then monitor the final-state density matrix via absorption or emission experiments to obtain values for the various rates $\Gamma^{II_1}_{FF_1}$. For longer pulse times T, it may be necessary to integrate Eq. (26) to obtain the net effect of the light pulse.

To be consistent with other authors, I define a RAIC transfer rate per pulse from some initial state described by $\bar{\rho}_{II_1}$ to a final state described by $\bar{\rho}_{FF_1}$ as

$$\Gamma^{II_1}_{FF_1}(v_r) = \frac{1}{T^+ - T^-}\int_{T^-}^{T^+}\Gamma^{II_1}_{FF_1}(v_r, t_c)dt_c \quad (28)$$

and a RAIC transfer cross section per pulse by

$$\sigma^{II_1}_{FF_1}(v_r) = \Gamma^{II_1}_{FF_1}(v_r)\Big/\left(\mathfrak{N}_A\mathfrak{N}_{A'}v_r\int d\bar{R}_c\right), \quad (29)$$

where the $\bar{R}_c$ integration is over the interaction volume.[12] The rate and cross section for transfer of *population* from some initial state $|I\rangle$ to a final state $|F\rangle$ is obtained by setting $I_1 = I$, $F_1 = F$ in Eqs. (28) and (29). Finally, one can define an average RAIC rate and cross section by

$$\bar{\Gamma}(v_r) = \frac{1}{N_I}\sum_{IF}\Gamma^{II}_{FF}(v_r), \quad (30a)$$

$$\bar{\sigma}(v_r) = \frac{1}{N_I}\sum_{IF}\sigma^{II}_{FF}(v_r), \quad (30b)$$

where N_I is the number of initial states. Equation (30b) defines a quantity that has been typically referred to as the RAIC cross section.[5]

V. DISCUSSION

In general, it is difficult to obtain solutions to Eqs. (22) and perform the necessary averaging

over collision orientations. However, certain general features of the solutions may be understood by examining some of the limiting forms of these equations.

A. Nondegenerate levels

In this limit, the matrices S and T in Eqs. (18) become scalars. Equation (20) is easily integrated and one finds that Eqs. (22) take the form

$$i\hbar\dot{A}_I = T(IF,t)^* \exp\{i[\Delta t - \varphi_c(t)]\}A_F, \tag{31a}$$

$$i\hbar\dot{A}_F = T(IF,t)\exp\{-i[\Delta t - \varphi_c(t)]\}A_I, \tag{31b}$$

where

$$\varphi_c(t) = \int_{t_c^-}^{t} [S(F,t') - S(I,t')]\,dt' \tag{32}$$

and I and F are nondegenerate states. The phase $\varphi_c(t)$ contains the effects of the level shifts produced by the off-resonant light field and the collisional interaction. Equations (31) have been studied by many authors using a variety of analytical and numerical techniques.[5,13] The resulting RAIC profile exhibits a marked asymmetry for large $|\Delta|$, resulting from the action of the level-shifting term. For one sign of Δ, the I-F transition can be brought into instantaneous resonance with the field during a collision, leading to enhanced excitation; for the other sign of Δ, no such instantaneous resonance is possible. Equations (31) also contains saturation effects which can appear for large field strengths or small impact parameters.

B. Perturbation theory limit

By neglecting the level-shifting terms in Eqs. (22) and taking $\Delta = 0$, one can estimate that a perturbation solution is valid provided

$$\frac{|\mathcal{U}(t=t_c)|\tau_c\chi}{\hbar\bar{\omega}} \ll 1, \tag{33}$$

where $\mathcal{U}(t=t_c)$ is the interatomic potential at the time of closest approach, $\tau_c = b/v_r$ is the collision time, χ is a Rabi frequency (e.g., $\chi = \langle\beta'|\mu'|\gamma\rangle|\mathcal{E}|/2\hbar$), and $\bar{\omega}$ is some characteristic frequency denominator appearing in the transition operator $\hat{T}$ [Eq. (13)]. For nonzero Δ, Eq. (33) is replaced by a less severe condition. Since $|\mathcal{U}(t=t_c)|\tau_c/\hbar \approx 1$ in the range of impact parameters that contributes to excitation,[14] the perturbation theory fails for field strengths $\chi \gtrsim \bar{\omega}$. Regardless of field strength, inequality (33) always fails to hold for sufficiently small impact parameters [$\mathcal{U}(t=t_c)$ varies typically as b^{-n}]; this domain can be treated by using a cutoff procedure.[5]

In the perturbation-theory limit, Eq. (22b) can be integrated directly after setting $\bar{A}_I(t) = \bar{a}_I(t_c^-)$. Using Eqs. (22), (19), and (21), one may obtain

$$\bar{a}_F(t_c^+) = (i\hbar)^{-1}\int_{t_c^-}^{t_c^+} G_F(t_c^+,t')T(IF,t') \times G_I(t',t_c^-)e^{-i\Delta t'}\bar{a}_F(t_c^-)\,dt'. \tag{34}$$

To be consistent with the perturbation-theory limit, the contributions to G_F and G_I arising from the light-shift operator should be neglected. Equation (34) may be given a simple interpretation. Starting in the state represented by $\bar{a}_I(t_c^-)$, one has a mixing and shifting of the initial levels from time $t = t_c^-$ to time $t = t'$ [represented by $G_I(t',t_c^-)$], a transition from initial to final state at time $t = t'$ [represented by $T(IF,t')$] and a mixing and shifting of final-state levels from time $t = t'$ to time $t = t_c^+$ [represented by $G_F(t_c^+,t')$]; an integration over all possible t' is included. Thus, it appears that reorientation effects in the initial and final states are correlated with both the shifting of these levels and the changes that occur in the $I-F$ transition. In particular, if there are times at which instantaneous resonances occur for a given detuning $|\Delta|\tau_c \gtrsim 1$, the T matrix can be evaluated at such times and the integral (34) evaluated by a stationary-phase method. This condition can help to simplify the calculations, although the average over collision orientations can still pose considerable problems. Experimentally, one should expect to find a variation of final-state coherence as a function of detuning.

C. Perturbation theory neglecting level shifts

Additional simplifications of Eq. (34) are possible for a range of impact parameters if one limits the detuning to the impact core of the RAIC profile ($|\Delta|\tau_c \ll 1$). If $|\Delta|\tau_c \ll 1$, the effects of instantaneous resonances are not important, since the phase factor $\exp(i\Delta t)$ is slowly varying; all times t' in the range (t_c^-, t_c^+) contribute to the integral in Eq. (34). Since the S matrix is quadratic in the collision interaction potential while the T matrix is linear in it, there exists a range of impact parameters where one can neglect the collisional contributions to S. Contributions to S from the light field have already been neglected owing to the perturbation-theory limit. Thus, in this limit where all level shifting and mixing in the initial and final states are ignored, $S(I,t) = S(F,t) = 0$ and, $G_I(t,t') = G_F(t,t') = 1$. Equation (34) reduces to

$$\bar{a}_F(t_c^+) = (i\hbar)^{-1}\int_{t_c^-}^{t_c^+} dt'\,T(IF,t')e^{-i\Delta t'}\bar{a}_I(t_c^-). \tag{35}$$

This expression is evaluated explicitly in the following paper, where the appropriate averaging over collision orientations and impact parameters is carried out. Since the interatomic potential appears linearly in Eq. (35) and, consequently, bilinearly in Eqs. (23) and (24), the averaging over collision orientations is easily performed using techniques involving irreducible tensor operators. One can show that the collsion produces the same type of final-state coherence properties that would be produced by replacing the collision by an unpolarized field having the same multipolar properties as the collision operator (e.g., a dipole collision operator is replaced by an unpolarized electric field). This result is not difficult to understand. Excitation is produced in a single collision; when averaged over all collision orientations, the *net* effect is similar to that produced by an unpolarized field of the corresponding multipolarity.

It is relatively easy in this case to predict the final-state coherence properties for various polarizations of the external field. The final-state coherence may be observed by monitoring the polarization of fluorescence or the quantum beats originating from one of the final states.

D. General case

If perturbation theory fails (power densities $\geq 10^{10}$ W/cm^2), the solutions of Eqs. (22) exhibit saturation effects. Unless a way can be found to perform the averaging over collision orientations and beam intensity profiles, one is faced with the costly task of integrating Eqs. (22) numerically as a function of collision orientation Θ and field amplitude $\mathcal{E}(\vec{R}_c, t_c)$. There has been limited work in this area, although a few related calculations have appeared.[7]

A general formalism for calculating the final-state coherences produced by radiatively-assisted inelastic collisions has been given. In the following paper, the RAIC transfer cross section is calculated in the perturbation-theory limit, neglecting level-shifting effects. In future work, it is hoped that the more general problem will be addressed.

ACKNOWLEDGMENT

This work was carried out while I was a guest at the Laboratoire Aimé Cotton, Orsay, France. The hospitality shown to me during my stay is gratefully acknowledged. I should also like to acknowledge financial support from the Fulbright Foundation. This research was also supported by the U. S. Office of Naval Research.

APPENDIX A

In this appendix, starting from the Hamiltonian (8) and using the assumptions of Sec. II, I derive Eqs. (9). The wave vector is written as

$$|\Psi(t)\rangle = \sum_M a_M(t) e^{-i\omega_M t} |M\rangle , \tag{A1}$$

where

$$|M\rangle = |nn'\rangle = |n\rangle |n'\rangle' ,$$
$$\omega_M = \omega_n + \omega_{n'} ,$$

and (ω_n and $\omega_{n'}$) and ($|n\rangle$ and $|n'\rangle'$) are eigenfrequencies and eigenkets of free atoms A and A', respectively [i.e., eigenfrequencies and eigenkets of the Hamiltonians $H_0(\vec{r})$ and $H_0'(\vec{r}')$, respectively, appearing in Eq. (8)]. I adopt the notation that a captial Roman letter represents a composite state of the AA' system [e.g., $|I\rangle = |ii'\rangle$, $\omega_{F_1} = \omega_{f_1} + \omega_{f_1'}$, etc.]. Using Schrödingers Equation with the Hamiltonian (8), one can derive the following equation for the probability amplitude (in the interaction representation) $a_M(t)$:

$$i\hbar \dot{a}_M = \{ -\tfrac{1}{2}\langle M|\vec{\mu}_T|B\rangle \cdot [\vec{\mathcal{E}} e^{-i\Omega t} + \vec{\mathcal{E}}^* e^{i\Omega t}] + \langle M|\mathcal{U}(t)|B\rangle \} e^{i\omega_{MB} t} a_B , \tag{A2}$$

where $\vec{\mu}_T = \vec{\mu} + \vec{\mu}'$, $\omega_{MB} = \omega_M - \omega_B$, and the summation convention is used.

According to the assumptions of Sec. II, the only states that are significnatly coupled are $|I\rangle$ and $|F\rangle$. However, this coupling does not yet appear directly in Eq. (A2) since the I-F coupling is via virtual intermediate states. To see the coupling directly, one writes Eq. (A2) for $\dot{a}_F$, replacing the a_B which appears on the right-hand side of this equation by the value obtained by formally integrating Eq. (A2) for $\dot{a}_B$. In this way, one finds

$$i\hbar \dot{a}_F = e^{i\omega_{FB} t} [-\tfrac{1}{2}\langle F|\vec{\mu}_T|B\rangle \cdot (\vec{\mathcal{E}} e^{-i\Omega t} + \vec{\mathcal{E}}^* e^{i\Omega t}) + \langle F|\mathcal{U}(t)|B\rangle]$$
$$\times \left(a_B(t_c^-) + (i\hbar)^{-1} \int_{t_c^-}^{t} dt' \, e^{i\omega_{BM} t'} [-\tfrac{1}{2}\langle B|\vec{\mu}_T|M\rangle \cdot (\vec{\mathcal{E}} e^{-i\Omega t'} + \vec{\mathcal{E}}^* e^{i\Omega t'}) + \langle B|\mathcal{U}(t')|M\rangle] a_M(t') \right) . \tag{A3}$$

The term proportional to $a_B(t_c^-)$ can be neglected using the assumption that the field and collision must act *simultaneously* to produce a transition. The validity conditions for the neglect of this term are

$$\bar{\omega}_e T \gg 1 , \quad \bar{\omega}_e \tau_c \gg 1 , \tag{A4}$$

where $\bar{\omega}_e$ and $\bar{\omega}_c$ are some appropriate frequency

mismatches for the atom-field and atom-atom interactions, respectively.[15]

The integral term in Eq. (A3) is treated as follows: (1) The only terms $a_\nu(t')$ of importance are assumed to be $a_{F_1}(t')$ and $a_I(t')$, where $|F_1\rangle$ is in the final-state group of levels. This assumption is equivalent to asserting that there is negligible population in all states outside the I and F groups (i.e., that there are only *virtual* excitations of the intermediate states). For this approximation to be valid one must again require conditions (A4) to hold. In addition, one must require that the cross section for transfer within a *given* atom from either its initial or final state to some intermediate state be negligible. This cross section is precisely that associated with collisionally-aided radiative excitation (CARE).[4] For $\bar{\omega}_c\tau_c \gg 1$ and $\chi \ll \bar{\omega}_c$, CARE is unimportant. However, CARE may become significant in the strong-field regime $\chi \approx \bar{\omega}_c$; in that case, one would have to expand the basis to include those states coupled to either $|I\rangle$ or $|F\rangle$ by CARE. (2) Antiresonance terms in Eq. (A3) varying as $\exp[\pm i(\omega_{F_1} + \Omega)t]$ or $\exp(\pm 2i\Omega t)$ are neglected. (3) The functions $\langle B|u(t')|M\rangle$ and $a_\nu(t')$ are assumed to be slowly varying with respect to the exponential factors and are evaluated at time $t' = t$. For this assumption to be valid, one must have

$$\bar{\omega}_c\tau_c \gg 1, \quad \omega_c\tau_c \gg 1. \tag{A5}$$

There is a supplementary condition which must also be satisfied related to the time variation of $a_I(t')$ (see below). (4) Frequency differences $\omega_{FF_1}, \omega_{II_1}$ are neglected with respect to $\bar{\omega}_c$ or $\bar{\omega}_c$ and factors such as $\exp(i\omega_{II_1}t)$ or $\exp(i\omega_{FF_1}t)$ are set equal to unity. These approximations are valid owing to Eqs. (5) and (A5).

With these assumptions, one can easily carry out the integration in Eq. (A3) and obtain

$$i\hbar\dot{a}_F = \left[-\frac{1}{4\hbar}\left(\frac{\langle F|\vec{\mu}_T|B\rangle\cdot\vec{\mathcal{E}}^*\langle B|\vec{\mu}_T|F_1\rangle\cdot\vec{\mathcal{E}}}{\omega_{BF}-\Omega} + \frac{\langle F|\vec{\mu}_T|B\rangle\cdot\vec{\mathcal{E}}\langle B|\vec{\mu}_T|F_1\rangle\cdot\vec{\mathcal{E}}^*}{\omega_{BF}+\Omega}\right) - \frac{1}{\hbar}\frac{\langle F|u(t)|B\rangle\langle B|u(t)|F_1\rangle}{\omega_{BF}}\right]a_{F_1}$$
$$+\frac{1}{2\hbar}\left(\frac{\langle F|\vec{\mu}_T|B\rangle\langle B|u(t)|I\rangle}{\omega_{BI}} + \frac{\langle F|u(t)|B\rangle\langle B|\vec{\mu}_T|I\rangle}{\omega_{BF}-\Delta}\right)\cdot\vec{\mathcal{E}}e^{-i\Delta t}a_I, \tag{A6}$$

where and there is no sum on F where Δ is defined by Eq. (10). The quantity Δ appearing in the frequency denominator can be neglected in comparison with ω_{BF} and it should be dropped for consistency (see below). Equation (A6) is then identical to Eqs. (9b), (11), and (13), using the notation $I = ii'$, $F = ff'$, $B = \beta\beta'$, and $F_1 = f_1 f_1'$. Similarly, Eq. (9a) can be verified.

Finally, one can check to see if $a_I(t)$ is slowly varying compared with $\exp(i\bar{\omega}t)$ as has been assumed ($\bar{\omega} = \bar{\omega}_c$ or $\bar{\omega}_c$). By examining Eqs. (9), one can deduce that $|\dot{a}_I/a_I|_{\max}$ is given by the largest of either $|\Delta|$, $\omega_c = 1/\tau_c$, or $\hbar^{-1}|u(t = t_c)|\chi/\bar{\omega}$, where χ is a Rabi frequency in the problem. Thus, in order to neglect all but the groups I and F, one must have

$$\bar{\omega}/|\Delta| \gg 1, \quad \bar{\omega}\tau_c \gg 1,$$
$$\left[\frac{|u(t = t_c)|\tau_c}{\hbar}\left(\frac{\chi}{\bar{\omega}}\right)\right]\frac{1}{\bar{\omega}\tau_c} \ll 1. \tag{A7}$$

Note that one may retain a consistent solution even in the strong-field limit [Eq. (33)], $\hbar^{-1}|u(t = t_c)|\tau_c\chi/\bar{\omega} \gtrsim 1$, provided that $\bar{\omega}\tau_c$ is large enough to assure the validity of the last inequality in conditions (A7).

APPENDIX B

A simple diagrammatic interpretation of the operators $\hat{T}$ and $\hat{S}$ appearing in Eqs. (9) can be given. The interaction between the field and the atoms is represented by

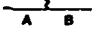

(B1)

The field takes the atom from the composite state $A = \alpha\alpha'$ to $B = \beta\beta'$. Actually this diagram may be thought of as the sum of two diagrams,

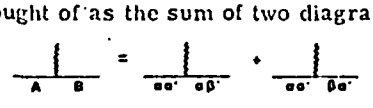

in which the field acts on each atom separately. The collisional interaction is represented by

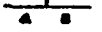

(B2)

taking the atoms from states A to B.

With these definitions, it is relatively easy to draw the diagrams corresponding to the operators $\hat{S}_L$, $\hat{S}_e$ and $\hat{T}(IF)$ appearing in Eqs. (11) and (13), and these are shown in Fig. 3. Figure 3(a) corresponds to the light-shift operator $\hat{S}_L(F)$ which acts

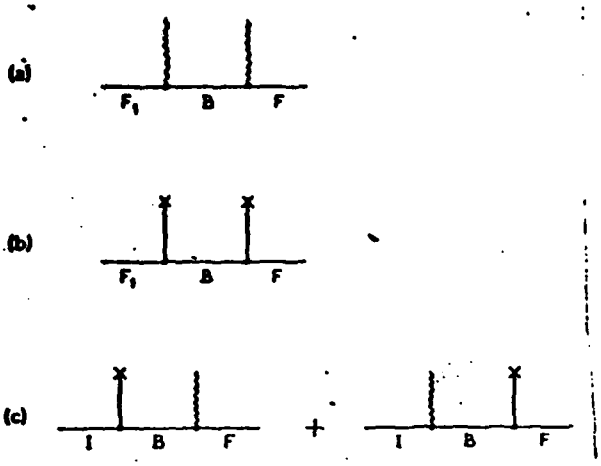

FIG. 3. Diagrammatic interpretation of the operators (a) $\hat{S}_L(F)$, (b) $\hat{S}_c(F)$, and (c) $\hat{T}(IF)$. In each diagram a wavy-line vertex refers to an atom-field interaction and a straight-line vertex to a collisional interaction.

in the final-state subspace [a similar diagram can be drawn for $\hat{S}_L(I)$]. The field excites either of the atoms to some intermediate virtual state and then de-excites the atom back to the final-state manifold. Figure 3(b) corresponds to the collisional operator $\hat{S}_c(F)$; the collision excites the atoms to some intermediate state $B=\beta\beta'$ and then de-excites them to the final-state manifold. Finally, Fig. 3(c) corresponds to the operator $\hat{T}(IF)$. The field and collision combine to excite the atoms from initial state I to final state F via the virtual intermediate state B. These diagrams immediately illustrate the nature of the operators appearing in the RAIC equations (i.e., $\hat{S}_L$ varies as $|\mathcal{E}|^2$, $\hat{S}_c$ as $\mathfrak{u}^2$, and $\hat{T}$ as $\mathfrak{u}\mathcal{E}$).

It is also possible to directly construct the operators from the diagrams. More precisely, the following rules enable one to calculate the matrix representation of the operators in the interaction representation.

(1) Assign a factor $(-1)^{N-1}$ (N = number of vertices) and a factor $e^{i\omega_{GH}t}$ (G = final state, H = initial state) to each diagram.

(2) Each vertex of the form (B1) is assigned the value $-\langle B|\vec{\mu}_T\cdot\vec{E}(t)|A\rangle$, where $\vec{E}(t)$ is given by Eq. (2). Each vertex of the form (B2) is assigned the value $\langle B|\mathfrak{u}(t)|A\rangle$.

(3) In the resulting expression, reject all rapidly varying terms (e.g., terms varying as $\exp(\pm 2i\Omega t)$ or $\exp[\pm i(\Omega+\omega_{FI})t]$).

(4) For a vertex of the form (B1) assign an energy denominator $\hbar(\omega_{BI}\pm\Omega)$, with the (+) sign used if $\vec{\mathcal{E}}$ appears in the B-A matrix element and the (−) sign if $\vec{\mathcal{E}}^*$ appears in the B-A matrix element. For a vertex of the form (B2) assign an energy denominator $\hbar\omega_{BA}$. Energy denominators are assigned for *all but the last vertex* in any diagram.

(5) Sum over all intermediate states.

As an example, I calculate Fig. 3(a) and the second diagram in Fig. 3(c). Following rules (1) and (2) for Fig. 3(a) gives

$$-\tfrac{1}{4}e^{i\omega_{FF_1}t}\langle B|\vec{\mu}_T\cdot(\vec{\mathcal{E}}e^{-i\Omega t}+\vec{\mathcal{E}}^*e^{i\Omega t})|F_1\rangle \times\langle F|\vec{\mu}_T\cdot(\vec{\mathcal{E}}e^{-i\Omega t}+\vec{\mathcal{E}}^*e^{i\Omega t})|B\rangle .$$

Keeping only the slowly varying terms [rule (3)] yields

$$-\tfrac{1}{4}e^{i\omega_{FF_1}t}[\langle F|\vec{\mu}_T\cdot\vec{\mathcal{E}}^*|B\rangle\langle B|\vec{\mu}_T\cdot\vec{\mathcal{E}}|F_1\rangle +\langle F|\vec{\mu}_T\cdot\vec{\mathcal{E}}|B\rangle\langle B|\vec{\mu}_T\cdot\vec{\mathcal{E}}^*|F_1\rangle] \tag{B3}$$

An energy denominator is assigned only to the first vertex and is $\hbar(\omega_{BF}-\Omega)$ for the first term in (B3) (since $\vec{\mathcal{E}}$ appears in the B-F_1 matrix element) and is $\hbar(\omega_{BF}+\Omega)$ for the second term in (B3) (since $\vec{\mathcal{E}}^*$ appears in the B-F_1 matrix element). Therefore,

$$\langle F|\hat{S}_L|F_1\rangle=-\frac{1}{4\hbar}e^{i\omega_{FF_1}t}\times\left(\frac{\langle F|\vec{\mu}_T\cdot\vec{\mathcal{E}}^*|B\rangle\langle B|\vec{\mu}_T\cdot\vec{\mathcal{E}}|F_1\rangle}{\omega_{BF_1}-\Omega}+\frac{\langle F|\vec{\mu}_T\cdot\vec{\mathcal{E}}|B\rangle\langle B|\vec{\mu}_T\cdot\vec{\mathcal{E}}^*|F_1\rangle}{\omega_{BF_1}+\Omega}\right)$$

in agreement with the first two terms of Eq. (A6) [recall that I set $\exp(i\omega_{FF_1}t)=1$ and $\omega_{BF}\approx\omega_{BF_1}$ in that equation].

Similarly, applying rules (1) and (2) to the second diagram of Fig. 3(c) yields

$$\tfrac{1}{2}e^{i\omega_{FI}t}\langle B|\vec{\mu}_T\cdot(\vec{\mathcal{E}}e^{-i\Omega t}+\vec{\mathcal{E}}^*e^{i\Omega t})|I\rangle\langle F|\mathfrak{u}|B\rangle .$$

Keeping the slowly varying term which varies as $\vec{\mathcal{E}}\exp[i(\omega_{FI}-\Omega)t]=\vec{\mathcal{E}}e^{-i\Delta t}$ and applying rules (3)–(5) gives

$$\frac{1}{2\hbar}e^{-i\Delta t}\frac{\langle F|\mathfrak{u}|B\rangle\langle B|\vec{\mu}_T\cdot\mathcal{E}|I\rangle}{\omega_{BI}-\Omega},$$

which agrees with the last term of Eq. (A6) since $\omega_{BI}-\Omega=\omega_{BF}-\Delta$.

[*]Permanent address.

[1]Part of the energy mismatch can also be compensated for by a change in the translational energy of the atoms.

[2]L. I. Gudzenko and S. I. Yakovlenko, Zh. Eksp. Teor. Fiz. 62, 1686 (1972) [Sov. Phys.—JETP 35, 877 (1972)].

[3]Ph. Cahuzac and P. E. Toschek, Phys. Rev. Lett. 40, 1087 (1978).

[4]S. Yeh and P. R. Berman, Phys. Rev. A 19, 1106 (1979).

[5]Extensive lists of references can be found in two recent articles which address the problem of RAIC. See S. I. Yakovlenko, Kvant. Elektron (Moscow), xx, xxx (19xx). [Sov. J. Quantum Electron. 8, 151 (1978)]; M. G. Payne, V. E. Anderson, and J.-E. Turner, Phys. Rev. A 20, 1032 (1979).

[6]S. E. Harris, J. F. Young, W. R. Green, R. W. Falcone, J. Lukasik, J. C. White, J. R. Willison, M. D. Wright, and G. A. Zdasiuk, in *Laser Spectroscopy IV*, edited by H. Walther and K. W. Rothe (Springer, Berlin, 1979), p. 349 and references therein; C. Bréchignac, Ph. Cahuzac, and P. E. Toschek, Phys. Rev. A 21, 1969 (1980).

[7]S. P. Andreev and V. S. Lisitsa, Zh. Eksp. Teor. Fiz. 72, 73 (1977) [Sov. Phys.—JETP 45, 38 (1977)]; J. Light and A. Szoke, Phys. Rev. A 18, 1363 (1978).

[8]S. E. Harris and J. C. White, IEEE J. Quantum Electron. 13, 972 (1977).

[9]The operator appearing in Eq. (14) appears to be the adjoint of the operator in Eq. (13). However, as defined, these operators act in different spaces [i.e., $\hat{T}(ii';ff')$ is defined to couple only states $|ii'\rangle$ to $|ff'\rangle$, implying $\langle ii'|\hat{T}(ii',ff')|ff'\rangle = 0$].

[10]See Eq. (A7) for a more precise statement of the validity conditions.

[11]In situations where one starts from initial states having a nonthermal velocity distribution, effects of velocity-changing collisions may have to be included in Eq. (26). In that case, the first term on the right-hand side of Eq. (26) would be replaced by an integral giving the transfer from initial states with velocities $\bar{v}_1$, $\bar{v}_1'$ to final states with velocities $\bar{v}$, $\bar{v}'$.

[12]As defined, the transfer rates and cross sections are generally complex quantities.

[13]E. J. Robinson, J. Phys. B 12, 1451 (1979); *ibid.* (in press).

[14]The impact parameter b_ω for which $|\mathcal{U}(t=t_c)|\tau_c/\hbar = 1$ is the so-called Weisskopf radius and represents a characteristic length in the problem.

[15]Since some energy mismatch can also be provided by a change in the atom's translational motion, the condition $\bar{\omega}_c\tau_c \gg 1$ can be replaced by the somewhat stronger condition $\hbar\bar{\omega}_c >$ (thermal energy).

SSSHI1063 PLRAA,801100AQ1355,2 PRA11003

Theory of coherences produced by radiatively assisted inelastic collisions: Weak-field impact-core limit

Paul R. Berman

*Laboratoire Aimé Cotton, Centre National de la Recherche Scientifique II, Bâtiment 505, 91405 Orsay-Cedex, France and Physics Department, New York University, 4 Washington Place, New York, New York 10003**

(Received 21 March 1980)

A theoretical calculation of the final-state coherences produced by a radiatively assisted inelastic collision (RAIC) is presented. Two atoms, A and A', collide in the presence of an external radiation field to produce the RAIC reaction $A_i + A_i' + \hbar\Omega \rightarrow A_f + A_f'$, where $|ii'\rangle$ is the initial state, $|ff'\rangle$ is the final state, and Ω is the frequency of the external field. It is assumed that the final states consist of a number of nearly degenerate levels and the coherences produced in these levels by the RAIC reaction is calculated. These final-state coherences can be monitored by standard techniques (polarization of fluorescence, quantum beats) enabling one to use the final-state coherences as a probe of the RAIC reaction. The calculation is limited to the weak-field (perturbation-theory) limit and is valid only in the impact core of the RAIC profile.

PACS numbers: 32.90. + a, 34.90. + q, 34.50. − s, 32.70. − a

I. INTRODUCTION

In a previous paper[1] (to be referred to as RAIC I), a general theory or radiatively assisted inelastic collisions (RAIC) was developed. These collisions represent processes of the form

$$A_i + A_i' + \hbar\Omega \rightarrow A_f + A_f',$$

in which two atoms (A and A') are excited from initial states $i\,i'$ to final states $f\,f'$ by the combined action of the collision and the absorption of a photon from an external pulsed radiation field. Whereas most previous theories of RAIC considered only one possible excitation channel (from nondegenerate state $i\,i'$ to nondegenerate state $f\,f'$), the theory presented in RAIC I allowed for the more general RAIC excitation from a group of initial levels characterized by some appropriate density matrix to a group of final levels. An expression was obtained for the final-state density matrix which completely described both the population and coherence properties of the excitation process. The final-state coherences can be monitored by standard experimental techniques (e.g., measurement of the polarization of fluorescence or quantum beats originating from the final states of one of the atoms); alternatively, one can monitor the final-state populations (e.g., by measuring the total fluorescence rate from one of the final states). It turns out, however, that measurements of final-state coherences provide a more sensitive probe of the RAIC interatomic potentials than do measurements of final-state populations. Thus, it appears useful to develop a theory of RAIC which permits one to calculate the induced-final-state coherences.

In this paper, a perturbative solution of the RAIC equations is obtained which is valid provided (1) the external field is sufficiently weak and (2) the detunings are restricted to the impact core of the RAIC profile. Starting with some arbitrary initial density matrix and assuming interatomic potentials and external-field polarizations of a quite arbitrary nature, the final-state density matrix for the system is calculated. The most general case leads to rather lengthy expressions which are presented in the Appendices. Specific results are given in the body of the paper for the reduced density matrix of atom A' in the limits of (1) dipole-dipole interatomic potential, (2) straight-line collisional trajectory, (3) linearly polarized external field, (4) central tuning, (5) unpolarized initial state, (6) final states of a given atom characterized by the same J quantum number, and (7) a summation over intermediate virtual states that reduces to one term, owing to a nearly satisfied resonance condition. It is shown that the fluorescence emitted from the final states of one of the atoms directly reflects the nature of the interatomic potential. Thus, in contrast with normal RAIC experiments where one must record an entire RAIC profile as a function of detuning to test interatomic potential models, a polarization measurement at central tuning (where the signal is largest) serves to probe the interatomic potential.

It may seem strange that collisions *induce* coherence, since it is generally thought that collisions *destroy* coherence. In fact, it will be seen that the collisional interaction may be viewed as two unpolarized (but possibly correlated) "fields" incident on the atoms from all directions. The fields are chosen to have the same multipolar properties as the collisional interactions they represent (e.g., a dipole operator is replaced by a dipole field). In this way the final-state coher-

Supported by the U.S. Office of Naval Research under Contract No. N00014-77-C-0553.

ence can be understood as the combined action of *three* fields; two unpolarized fields plus the external field. It is the external field which may be polarized and possesses a well-defined directionality in any case, that is the origin of the final-state coherence. The collisional interaction responsible for the RAIC reaction will, in general, modify the final-state coherence.

In Sec. II, the physical system is described and an expression for the final-state amplitude given. An outline of the calculation is presented in Sec. III, with the details given in the Appendices. The final-state density matrix is given in Sec. IV for the case outlined above. In Sec. V the RAIC excitation cross sections and the polarization of the fluoresence emitted from the final state of atom A' are calculated using a cutoff procedure to treat collisions with small impact parameters. A discussion and physical interpretation of the results are given in Sec. VI.

It should be noted that this paper is essentially self-contained. However, the reader is referred to RAIC I for a general overview of the problem, for a detailed derivation of the RAIC equations including validity conditions, and for references to previous work.

II. PHYSICAL SYSTEM AND TRANSITION AMPLITUDE

The physical system consists of two atoms, A and A', undergoing a collision in the presence of a pulsed radiation field. The time of closest approach during the collision is $t = t_c$ and the center-of-mass position of the atoms at this time is $\vec{R} = \vec{R}_c$. The amplitude of the pulsed field is assumed to vary slowly during the collision and is evaluated at $(\vec{R}_c, t_c)$; the field is taken to be of the form

$$\vec{E}(t; \vec{R}_c, t_c) = \tfrac{1}{2}\{\vec{\mathcal{E}}_c e^{-i\Omega t} + \vec{\mathcal{E}}_c^{*} e^{i\Omega t}\}, \tag{1}$$

where $|\vec{\mathcal{E}}_c|$ is the field amplitude at $(\vec{R}_c, t_c)$.

The energy levels of atoms A and A' are shown in Fig. 1. Each label in the figure represents a group of levels having a maximum frequency separation $\omega_c \ll \tau_c^{-1}$, where τ_c is the duration of a collision. Since

$$\omega_c \tau_c \ll 1, \tag{2}$$

levels within a given group may be considered as degenerate during the RAIC. The levels associated with atom A are represented by lower-case unprimed variables and those associated with atom A' by primed ones. A capital letter refers to a state of the composite system ($I = i\,i'$, $E = c\,c'$, $F_1 = f_1 f_1'$, etc.) and the convention

$$\omega_I = \omega_i + \omega_{i'}, \quad \omega_F = \omega_f + \omega_{f'}, \tag{3}$$

etc., is adopted, where $\omega_\alpha = E_\alpha/\hbar$ and E_α is the energy associated with state α.

Before the collision, the atoms are in an arbitrary linear superposition of the states $|I\rangle = |ii'\rangle = |i\rangle|i'\rangle$, where i and i' represent any of the levels in the i and i' groups, respectively. The field is assumed to be nearly resonant with the $I - F$ transition in the composite system, i.e., $\Omega \approx \omega_F - \omega_I$. More precisely, the detuning Δ defined by

$$\Delta = \Omega - \omega_{FI}, \tag{4}$$

$$\omega_{FI} = \omega_F - \omega_I \tag{4a}$$

is limited, in this work, to the impact core of the RAIC profile

$$|\Delta|\,\tau_c \ll 1. \tag{5}$$

All other atom-atom or atom-field interactions are assumed to be nonresonant; in other words, all levels outside the I and F groups enter the problem only as *virtual* levels. The contribution of these virtual levels can be included in effective operators that act in the IF subspace only. The problem is to determine the final-state density matrix following the collision since it provides a complete description of the final-state coherences and populations produced by RAIC.

The RAIC can be characterized by three operators which have been discussed in RAIC I. First, there is the "light-shift" operator $\hat{S}_L$ which couples and shifts the levels *within* both the initial and final groups of levels. This light-shift operator represents the virtual excitation and de-excitation of either of the atoms by the external field. The effects produced by $\hat{S}_L$, which are second order in the field, are neglected in this work, since the field is treated in a perturbation-theory limit.

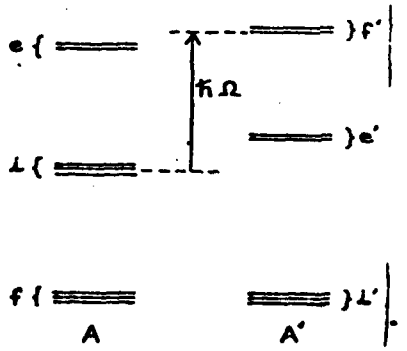

FIG. 1. Energy-level diagram of atoms A and A'. Each group of levels labeled by a single letter is nearly degenerate with a maximum frequency spacing between levels within a group less than an inverse collision time. The external-field frequency Ω is such that $\hbar\Omega \approx (E_f + E_{f'}) - (E_i + E_{i'})$.

Second, there is the collisional operator $\hat{S}_c$ which also couples and shifts the levels *within* the initial and final groups of levels. This operator is second order in the collisional interaction, representing the collision-induced virtual excitation and de-excitation of the composite AA' system in either its initial or final state. The operator $\hat{S}_c$ is the origin of the pressure broadening and shifting of spectral profiles. The relative importance of $\hat{S}_c$ is dependent on (i) the detuning Δ and (ii) the impact parameter associated with a given collision. Owing to condition (5), the collision possesses sufficient frequency components to effectively compensate for the detuning Δ. Thus, in contrast to the case $|\Delta|\,\tau_c > 1$, where collisional shifts can significantly enhance excitation cross sections by bringing the atomic transition frequency into instantaneous resonance with the field, all effects produced by the operator $\hat{S}_c$ related to the detuning may be neglected. The dependence of $\hat{S}_c$ on the impact parameter is discussed following the description of the transition operator.

The transition operator $\hat{T}(IF)$ represents the combined action of the (field + collision) in *coupling* the initial state $|I\rangle$ to final state $|F\rangle$ via a virtual excitation of intermediate states. This operator can be represented diagrammatically by the four terms shown in either Fig. 2 or Fig. 3. In Figs. 2(a) and 3(a), the collision (represented by non-wavy lines) acts to virtually excite the atoms from state $|ii'\rangle$ to state $|ef'\rangle$ and the field (represented by wavy lines) then acts on atom A to complete the excitation to the final state $|ff'\rangle$. In Figs. 2(b) and 3(b) the collision excites the virtual state $|fe'\rangle$ and the field acts on atom A' to complete the excitation. In Figs. 2(c) and 3(c) the field acts on atom A to excite the virtual state $|ei'\rangle$ and the collision completes the excitation to the final state $|ff'\rangle$. Finally, in Figs. 2(d) and 3(d), the field acts on atom A' to excite the virtual state $|ie'\rangle$ and the collision completes the excitation.

It may be seen from Fig. 2 that the transition operator is linear in both the field and collisional interaction. Explicitly,[1] one finds matrix elements of $\hat{T}(IF)$ to be

$$\langle F|\hat{T}(IF;t,b,v_r,\Theta,\vec{R}_c,t_c)|I\rangle = \frac{1}{2\hbar}\left(\frac{\langle F|\vec{\mu}_A|E\rangle\langle E|\mathcal{U}(\vec{R}(t))|I\rangle}{\omega_{EI}} + \frac{\langle F|\mathcal{U}(\vec{R}(t))|E\rangle\langle E|\vec{\mu}_A|I\rangle}{\omega_{EF}}\right)\cdot\vec{\mathcal{E}}_c\,, \quad (6)$$

where t is the time during the collision; b, v_r,

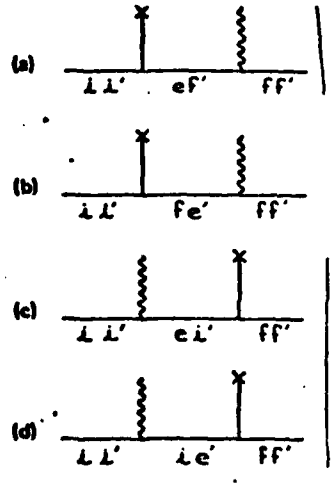

FIG. 2. Diagrams representing matrix elements of the transition operation from initial state $|ii'\rangle$ to final state $|ff'\rangle$. A straight-line vertex corresponds to a collision interaction and wavy-line vertex to an atom-field interaction. The states e and e' represent some arbitrary intermediate (virtual) states in atoms A and A', respectively.

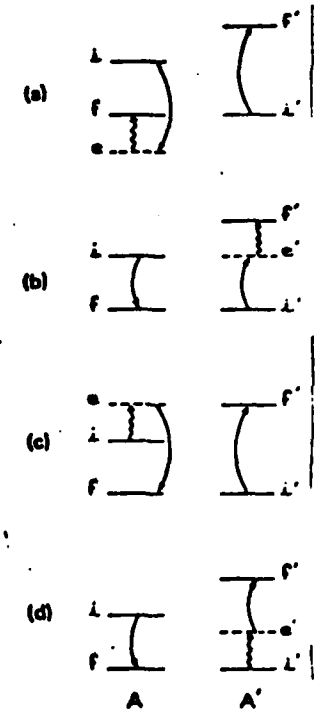

FIG. 3. A schematic representation of the contributions to the final-state RAIC amplitude complementary to that shown in Fig. 2. Each diagram corresponds to the similarly labeled diagram in Fig. 2. Solid lines with arrows represent the collisional interaction and wavy lines represent the atom-field interaction. States e and e' are virtual states excited in the RAIC reaction. Each level actually corresponds to a group of nearly degenerate levels.

and Θ are the impact parameter, relative speed, and collision orientation, respectively, associated with the collision

$$\vec{\mu}_T = \vec{\mu} + \vec{\mu}' \tag{7}$$

where $\vec{\mu}$ and $\vec{\mu}'$ are the electric-dipole operators for atoms A and A', respectively; and $\mathcal{U}(\vec{R}(t))$ is the collision interaction Hamiltonian calculated assuming a classical interatomic collision trajectory $\vec{R}(t)$. In writing Eq. (6), I have used the fact that $\omega_\epsilon \ll \omega_{EI}$, ω_{EF} (recall that ω_ϵ is the maximum frequency separation within a group of levels) and have adopted a summation convention in which any repeated state label (*not* including its appearance in a phase factor or frequency denominator) is summed over (e.g., in Eq. (6), there is a sum over E but not over I or F).[2] Since $\vec{\mu}_T$ is the sum of two terms, one can readily identify Eq. (6) with the four figures of Fig. 2. An analogous calculation for the operator $\hat{T}(FI)$ yields

$$\langle I|\hat{T}(FI;t)|F\rangle = \langle F|\hat{T}(IF;t)|I\rangle^* . \tag{8}$$

Since $\hat{T}(IF)$ varies linearly in $\mathcal{U}$ and $\hat{S}_\epsilon$ varies as $(\mathcal{U})^2$, and since $\mathcal{U}$ varies typically as b^{-n} ($n>0$), one can conclude that, for collisions with "large" impact parameters, the effects produced by $\hat{S}_\epsilon$ may be neglected in comparison with those produced by $\hat{T}(IF)$. For "smaller" impact parameters, the contribution of $\hat{S}_\epsilon$ can no longer be ignored. For the present, I consider only those collisions with $b>b_0$, where b_0 is the minimum impact parameter for which the contribution from $\hat{S}_\epsilon$ can be neglected. In Sec. V a simple model is developed for treating collisions with $b<b_0$.

Thus, during collisions with $b>b_0$, the probability amplitudes (in the interaction representation) for the initial and final states obey the equations of motion

$$i\hbar\dot{a}_F = \langle F|T(IF,t)|I\rangle e^{-i\Delta t}a_I , \tag{9a}$$

$$i\hbar\dot{a}_I = \langle F|\hat{T}(IF,t)|I\rangle^* e^{i\Delta t}a_F , \tag{9b}$$

where it has been assumed that changes in a_I or a_F resulting from level decay and atomic motion (Doppler effect) are negligible on the time scale of a collision. Furthermore, it is now assumed that the field strength is weak enough so that Eqs. (9) can be solved by perturbation theory with initial conditions $a_I(t_c^-)\neq 0$, $a_F(t_c^-)=0$, where t_c^- is a time just before the collision. Integrating Eqs. (9) in the perturbation-theory limit, one finds a final-state amplitude at time t_c^+ just following the collision given by

$$a_F(t_c^+) = (i\hbar)^{-1}\left(\int_{t_c^-}^{t_c^+}\langle F|\hat{T}(IF,t)|I\rangle e^{-i\Delta t}dt\right)a_I(t_c^-) . \tag{10}$$

Perturbation theory is valid provided that $|a_F(t)|^2 \ll 1$ for all t during a collision having $b=b_0$. Under typical experimental conditions, perturbation theory is valid for power densities $\lesssim 10^{10}\mathrm{W/cm^2}$.

It remains to carry out the integration in Eq. (10), to form final-state density-matrix elements, and to average over all appropriate collision parameters.

III. OUTLINE OF CALCULATION

Forming final-state density-matrix elements from the amplitude (10) and carrying out the average over collision orientations Θ, one obtains[3]

$$\rho_{FF_1}(t_c^+;b,v_r,\vec{R}_c,t_c) = R^{II_1}_{FF_1}(b,v_r,\vec{R}_c,t_c)\rho_{II_1}(t_c^-), \tag{11a}$$

where

$$R^{II_1}_{FF_1}(b,v_r,\vec{R}_c,t_c) = \hbar^{-2}(8\pi^2)^{-1}\int d\Theta\int_{t_c^-}^{t_c^+}\langle F|\hat{T}(IF,t)|I\rangle e^{-i\Delta t}dt\int_{t_c^-}^{t_c^+}\langle F_1|\hat{T}(IF,t')|I_1\rangle^* e^{i\Delta t'}dt' . \tag{11b}$$

The dependence of $\hat{T}$ on $(b,v_r,\Theta,\vec{R}_c,t_c)$ has been suppressed in Eqs. (10) and (11). In this section, a method for evaluating Eqs. (11) is outlined; details of the calculation are given in the Appendices. The averaging over b and $\vec{R}_c$ is deferred to Sec. V.[4]

The matrix elements of $\hat{T}$ needed in Eq. (11b) may be calculated using Eq. (6) once the interatomic potential $\mathcal{U}$ and the field $\vec{\mathcal{E}}_\epsilon$ are specified. An arbitrary potential can be written in the form

$$\mathcal{U}(t-t_c,\ b,v_r,\Theta) = A^{kk'}_{qq'}(t-t_c,b,v_r,\Theta)T^k_q\,T'^{k'}_{q'}, \tag{12}$$

where T^k_q and $T'^{k'}_{q'}$ are components of irreducible tensor operators of rank k and k' (assumed integral), respectively, which act on states of atoms A and A', respectively. In the form (12), the potential can be viewed as the sum of correlated multipolar fields acting on each of the atoms, the correlation provided by the coupling constants

$A^{qq'}_{ee'}$. The average over all collision orientations needed in Eq. (11b) is equivalent to including all possible directions of incidence and polarizations for these multipolar fields. In the same sense, therefore, the collisions can be viewed as producing the same effect as a sum of unpolarized, but correlated, multipolar fields acting on atoms A and A'. This picture of the collisional process can be useful in understanding the coherences produced by RAIC and is used in Sec. VI to help explain the results obtained for the various RAIC cross sections.

In order to carry out the average over Θ, it is convenient to rewrite Eq. (12) in the form

$$\mathcal{U}(t-t_c;b,v_r,\Theta)=\,^{kk'}A^K_Q(t-t_c;b,\bar{v}_r,\Theta)\,^{kk'}V^K_Q\,, \tag{13}$$

where

$$\,^{kk'}V^K_Q=\begin{bmatrix} k & k' & K \\ q & q' & Q\end{bmatrix}T^k_q\,T^{k'}_{q'}\,, \tag{14a}$$

$$\,^{kk'}A^K_Q=\begin{bmatrix} k & k' & K \\ q & q' & Q\end{bmatrix}A^{kk'}_{qq'}\,, \tag{14b}$$

and the quantity in brackets is a Clebsch-Gordon coefficient. Since the V^K_Q transform as the components of an irreducible tensor operator under rotation, the expansion coefficients A^K_Q transform as

$$\,^{kk'}A^K_Q(t-t_c;b,\bar{v}_r,\Theta)=\mathfrak{R}^{(K)}_{QQ'}(\Theta)\,^{kk'}A^K_{Q'} \times(t-t_c;b,v_r,0)\,, \tag{15}$$

where the $\mathfrak{R}^{(K)}_{QQ'}$ are matrix elements of the irreducible representation of order (K) of the rotation group and $\Theta=0$ is some arbitrary collision geometry. The Θ dependence is now contained totally in the $\mathfrak{R}^{(K)}_{QQ'}$, enabling one to easily perform the Θ integration required in Eq. (11b) (see below). In anticipation of the time integrals also required in Eq. (11b), I define the quantities

$$A^{kk'}_{ee'}(b,v_r,\Theta;\Delta)=(v_r/b)\int_{t_c^--t_c}^{t_c^+-t_c}A^{kk'}_{ee'}(\tau,b,v_r,\Theta) \times e^{-i\Delta(\tau+t_c)}\,d\tau \tag{16a}$$

and

$$\,^{kk'}A^K_Q(b,v_r,\Theta;\Delta)=(v_r/b)\int_{t_c^--t_c}^{t_c^+-t_c}\,^{kk'}A^K_Q(\tau,b,v_r,\Theta) \times e^{-i\Delta(\tau+t_c)}\,d\tau\,, \tag{16b}$$

which are also related via Eq. (14b). Equation (15) remains valid for $\,^{kk'}A^K_Q(b,v_r,0;\Delta)$.

It remains to specify the atom-field interaction $\vec{\mu}_T\cdot\vec{\mathcal{S}}_e$. The field amplitude may be written

$$\vec{\mathcal{S}}_e=\hat{\epsilon}\,\mathcal{S}_e\,,\quad |\hat{\epsilon}|=1 \tag{17}$$

where $\hat{\epsilon}$ is a complex polarization vector. One then finds

$$\vec{\mu}_T\cdot\vec{\mathcal{S}}_e=(\mu_T)^{(1)}_q\,\epsilon_{-q}\,\mathcal{S}_e\,, \tag{18}$$

where

$$\epsilon_1=-(\epsilon_x+i\epsilon_y)/\sqrt{2}\,,$$

$$\epsilon_{-1}=(\epsilon_x-i\epsilon_y)/\sqrt{2}\,,$$

$$\epsilon_0=\epsilon_z\,, \tag{19}$$

and

$$(\mu_T)^{(1)}_1=-[(\mu_T)_x+i(\mu_T)_y]/\sqrt{2}\,,$$

$$(\mu_T)^{(1)}_{-1}=[(\mu_T)_x-i(\mu_T)_y]/\sqrt{2}\,,\quad (\mu_T)^{(1)}_0=(\mu_T)_z\,. \tag{20}$$

The quantities $(\mu_T)^{(1)}_q$ are the components of an irreducible tensor operator of rank 1.

Since all the operators appearing in Eq. (6) have now been expressed in terms of the components of irreducible tensor operators, the matrix elements appearing in Eq. (6) are easily calculated using the Wigner-Eckart theorem[5] (see Appendix A). The resulting expressions for $\langle F|\,T(IF,t)\,|I\rangle$ and $\langle F_1|\,T(IF,t)\,|I_1\rangle^*$ are then inserted into Eq. (11b) and the integration over Θ is performed using the fact that[6]

$$(8\pi^2)^{-1}\int d\Theta\,\mathfrak{R}^K_{QQ'}(\Theta)\,(\mathfrak{R}^{\bar{K}}_{\bar{Q}\bar{Q}'}(\Theta))^* = (2K+1)^{-1}\,\delta_{K\bar{K}}\delta_{Q\bar{Q}}\delta_{Q'\bar{Q}'} \tag{21}$$

to arrive at a value for $R^{ff_1}_{ii_1}(b,v_r,\vec{R}_c,t_c)$ [Eq. (11b)] and $\rho_{FF_1}(t_c^+;b,v_r,\vec{R}_c,t_c)$ [Eq. (11a)]. The final expressions are rather lengthy and are given in Appendix A along with the details of the calculation.

Experimentally, one often observes the final-state properties of only one of the atoms. Imagine, for example, that one monitors the final-state coherence of atom A'. Mathematically, this coherence is described by the reduced density matrix obtained by tracing ρ_{FF_1} over the final-state variables of atom A. Explicitly, these reduced density-matrix elements $\rho^{f'}_{f'_1}$ are given by setting $F=ff'$, $F_1=ff'_1$ and summing over f, i.e.,

$$\rho^{f'}_{f'_1}(t_c^+;b,v_r,\vec{R}_c,t_c)=\rho_{ff';ff'_1}(t_c^+;b,v_r,\vec{R}_c,t_c)\,. \tag{22}$$

A calculation of these reduced matrix elements, those of atom A, and the connection between the two is also given in Appendix A.

The coherence properties of a system are conveniently expressed in terms of the irreducible tensor components of the density matrix. The transformation between matrix elements is given by

$$f'f'_1\rho'^K_Q = (-1)^{J_{f'}-m_{f'_1}}\begin{bmatrix} J_{f'} & J_{f'_1} & K \\ m_{f'} & -m_{f'_1} & Q \end{bmatrix} \times \langle f' J_{f'} m_{f'} | \rho' | f' J_{f'_1} m_{f'_1} \rangle \quad (23a)$$

along with the inverse transform

$$\langle f' J_{f'} m_{f'} | \rho' | f' J_{f'_1} m_{f'_1} \rangle = (-1)^{J_{f'_1}-m_{f'_1}}\begin{bmatrix} J_{f'} & J_{f'_1} & K \\ m_{f'} & -m_{f'_1} & Q \end{bmatrix} f'f'_1\rho'^K_Q , \quad (23b)$$

where it has been assumed that a state $|\alpha\rangle$ may be labeled by $|\alpha J_\alpha m_\alpha\rangle$ and that states within a given group of levels differ only in their J and m_J quantum numbers.[7] The ρ^K_Q are matrix elements of the density matrix expanded in irreducible tensor basis. When expressed in this fashion, one can see directly if there is any final-state coherence. The quantity ρ^0_0 is given by

$$f'f'_1\rho'^0_0 = (2J_{f'}+1)^{-1/2}\langle f' J_{f'} m_{f'} | \rho' | f' J_{f'} m_{f'} \rangle \delta_{J_{f'} J_{f'_1}} \quad (24)$$

and is proportional to the total final-state *population*. Any nonzero value of ρ'^K_Q for $K>0$ indicates that final-state coherence exists, since a totally unpolarized final state leads to $\rho'^K_Q = 0$ for $K \neq 0$.

In Appendix A, general expressions for $\rho'_{f'f'_1}$ and ρ'^K_Q are obtained, assuming an arbitrary initial state. These expressions are evaluated in detail in Appendix B for the case of an unpolarized initial state. In the following section, certain limiting cases of these calculations are discussed.

IV. RESULTS FOR A SPECIFIC MODEL

In order to illustrate the physical principles involved in the RAIC process, I consider a limiting case of the general results presented in Appendices A and B. The following model is adopted: (1) Each group of levels α can be represented by a single angular momentum quantum number J_α (valid for fine-structure splittings $> \tau_c^{-1}$). (2) The initial state is unpolarized. (3) Owing to a nearly satisfied resonance condition, only *one* group of levels enters in the summation over intermediate virtual states. In this limit, the reduced density matrix for atom A' is calculated. Since the final state of atom A' is characterized by a single J value $J_{f'} = J_{f'_1}$, the calculation of $f'f'\rho'^K_Q$ is essentially one in which the Zeeman coherences of level f' are determined.

In order for condition (3) to be satisfied *one* of the virtual levels shown in Fig. 3 must be nearly coincident with a real atomic level. This condition can be achieved with any of the level schemes shown in Fig. 4. For example, if the level scheme is as shown in Fig. 4(a), then the dominant contribution to the final-state amplitude comes from the diagram of Fig. 2(a) with the sum over intermediate states e restricted to the single group of states $e=r$; contributions from states $e \neq r$ as well as from the other diagrams of Figs. 2(b)–2(d) are relatively unimportant in this case in comparison with this nearly resonant contribution. Similarly, if the level scheme is as shown in Figs. 4(b)–4(d), the dominant contribution comes from the diagrams of Figs. 2(b)–2(d) with the summation over intermediate states restricted to $e=r$ or r'.

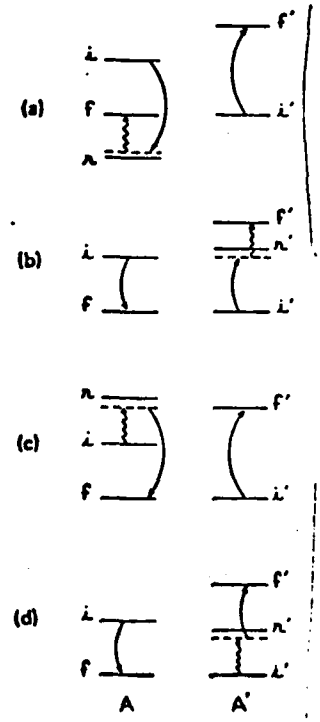

FIG. 4. Four different cases of energy-level schemes that lead to a single term dominating the sum over intermediate virtual states. Each level corresponds to a group of nearly degenerate levels.

$$\times |\langle r \| \mu^{(1)} \| i \rangle|^2 \langle f \| T^{(k)} \| r \rangle \langle f \| T^{(p)} \| r \rangle^* \langle f' \| T'^{(k')} \| i' \rangle \times \langle f' \| T'^{(p')} \| i' \rangle^* \begin{Bmatrix} 1 & 1 & K \\ J_r & J_r & J_i \end{Bmatrix} \begin{Bmatrix} k' & p' & K \\ J_{f'} & J_{f'} & J_{i'} \end{Bmatrix} \times \begin{Bmatrix} k & p & K \\ p' & k' & K' \end{Bmatrix} \begin{Bmatrix} k & p & K \\ J_r & J_r & J_f \end{Bmatrix}. \quad (30)$$

In terms of Fig. 4(c), one interprets this result as a field excitation from ii' to ri' followed by a collisional excitation to ff'.

Finally, for the level scheme of Fig. 4(d), one finds from Eqs. (B3), (B13), and (25d)

$$\times \delta_{kp} \delta_{k'p'} |\langle r' \| \mu'^{(1)} \| i' \rangle|^2 |\langle f \| T^{(k)} \| i \rangle|^2 |\langle f' \| T'^{(k')} \| r' \rangle|^2 \times \begin{Bmatrix} J_{f'} & J_{f'} & K \\ J_{r'} & J_{r'} & k' \end{Bmatrix} \begin{Bmatrix} 1 & 1 & K \\ J_{r'} & J_{r'} & J_{i'} \end{Bmatrix}. \quad (31)$$

In terms of Fig. 4(d), this result corresponds to a field excitation from ii' to ir' followed by a collisional excitation to state ff'.

Equations (26)–(31) characterize the final-state coherence of atom A' for the level schemes of Fig. 4. This coherence can be monitored by measuring the polarization of the fluorescence emitted by atom A' from state f' (see Sec. V).

A. Dipole-dipole interaction

As a somewhat more specific example, I now consider the case where the collisional interaction is of a dipole-dipole nature. For such an interaction, $k = k' = p = p' = 1$, $T = \mu$, and $T' = \mu'$. The corresponding ${}^{11}A_Q^K(b, v_r, 0; \Delta)$ are calculated in Appendix C, assuming straight-line collision trajectories.

The results for the dipole-dipole limit are conveniently expressed in terms of the Rabi frequencies

$$\chi_{\alpha\beta}^c = \tfrac{1}{2} \langle \alpha \| \mu^{(1)} \| \beta \rangle \mathcal{E}_c / \hbar, \quad (32a)$$

$$\chi_{\alpha'\beta'}'^c = \tfrac{1}{2} \langle \alpha' \| \mu'^{(1)} \| \beta' \rangle \mathcal{E}_c / \hbar, \quad (32b)$$

and a characteristic length $b_{\alpha\beta}^{\alpha'\beta'}$ defined by

$$b_{\alpha\beta}^{\alpha'\beta'} = \left| 2 \langle \alpha \| \mu^{(1)} \| \beta \rangle \langle \alpha' \| \mu'^{(1)} \| \beta' \rangle / \hbar v_r \right|^{1/2}. \quad (33)$$

The quantity $b_{\alpha\beta}^{\alpha'\beta'}$ is a radius that typically appears in theories of resonance broadening ("Weisskopf radius" for resonant broadening) and usually has a value in the 10 to 40 Å range. Moreover, it is useful to define the dimensionless quantity

$$D_K(\Delta b / v_r) = b^6 \sum_Q |{}^{11}A_Q^K(b, v_r, 0; \Delta)|^2. \quad (34)$$

For the level scheme of Fig. 4(a), the dipole-dipole limit of Eq. (26) is

$$\times (-1)^{K'} P_{KQ} \begin{Bmatrix} 1 & 1 & K \\ J_r & J_r & J_f \end{Bmatrix} \begin{Bmatrix} 1 & 1 & K \\ J_r & J_r & J_i \end{Bmatrix} \begin{Bmatrix} 1 & 1 & K \\ 1 & 1 & K' \end{Bmatrix} \begin{Bmatrix} 1 & 1 & K \\ J_{f'} & J_{f'} & J_{i'} \end{Bmatrix}, \quad (35a)$$

where

$$\varphi_a = J_f - J_{f'} - J_i - J_{i'}. \quad (35b)$$

For the level scheme of Fig. 4(b), the dipole-dipole limit of Eq. (28) is

$$\times D_{K'}(\Delta b / v_r) (-1)^K P_{KQ} \begin{Bmatrix} 1 & 1 & K \\ J_{f'} & J_{f'} & J_{r'} \end{Bmatrix}, \quad (36a)$$

one in which the lower limit of the b integral in Eq. (39) is replaced by b_0. This procedure underestimates σ'^{0}_{0} by 10 to 20% and provides a good approximation for σ'^{K}_{Q} ($K>0$). The perturbation theory results are valid if $v'_r \rho'^{0}_{0}(I'_c, b_0, v_r, \vec{R}_c, t) \ll 1$ (i.e., the final-state population is much less than unity). From Eqs. (32)–(38), and (C14), one can derive the validity condition

$$|\chi^c/\Delta_a|^2 (b_R/b_0)^4 \ll 1, \tag{41}$$

where χ^c is a Rabi frequency defined by Eq. (32), b_R is one of the characteristic *resonant* Weisskopf radii defined by Eq. (33), and Δ_a is a frequency mismatch defined by Eq. (25). Since $b_R/b_0 \simeq 4$ and $|\Delta_a| \gg 10^{12}$ sec^{-1}, Eq. (41) is easily satisfied for a large range of field strengths.

The RAIC excitation cross sections may now be easily obtained for the limiting cases of Fig. 4. For the case of *central tuning*, the RAIC cross section in the dipole-dipole limit for the level scheme corresponding to Fig. 4(a) may be obtained from Eqs. (39), (35a), and (C14) as

$$f'f'\sigma'^{K}_{Q}(v_r,0)_a = 8\pi N_I^{-1}(-1)^{\varphi_a}(\langle|\chi^c_{fr}|^2\rangle/\Delta_a^2)(b'^{f'i'}_{ri}/b_0)^2(-1)^{Q_s}\epsilon^{*}_{j}\epsilon^{*}_{s}\begin{bmatrix}1 & 1 & K\\ Q_j & -Q_s & Q\end{bmatrix}$$
$$\times\begin{Bmatrix}1 & 1 & K\\ J_r & J_r & J_i\end{Bmatrix}\begin{Bmatrix}1 & 1 & K\\ J_r & J_r & J_i\end{Bmatrix}\begin{Bmatrix}1 & 1 & K\\ 1 & 1 & 2\end{Bmatrix}\begin{Bmatrix}1 & 1 & K\\ J_{f'} & J_{f'} & J_{i'}\end{Bmatrix}(b'^{f'i'}_{ri})^2, \tag{42}$$

where

$$\langle|\chi^c_{\alpha\beta}|^2\rangle = |\chi^c_{\alpha\beta}|^2\langle\mathcal{S}_c^2\rangle/\mathcal{S}_c^2 \tag{43}$$

and

$$\langle\mathcal{S}_c^2\rangle = \frac{1}{T^+ - T^-}\int d\vec{R}_c \int_{T^-}^{T^+} dt_c |\mathcal{S}_c(\vec{R}_c, t_c)|^2 \Big/ \int d\vec{R}_c. \tag{44}$$

Similarly, for the level scheme of Fig. 4(b), from Eqs. (39), (36a), and (C14) one may obtain

$$f'f'\sigma'^{K}_{Q}(v_r,0)_b = 8\pi N_I^{-1}(-1)^{\varphi_b}[9(2J_{r'}+1)]^{-1}(\langle|\chi^c_{f'r'}|^2\rangle/\Delta_b^2)(b'^{f'i'}_{fi}/b_f)^2$$
$$\times(-1)^{Q_s}\epsilon^{*}_{j}\epsilon^{*}_{s}\begin{bmatrix}1 & 1 & K\\ Q_j & -Q_s & Q\end{bmatrix}(-1)^{K}\begin{Bmatrix}1 & 1 & K\\ J_{f'} & J_{f'} & J_{r'}\end{Bmatrix}(b'^{f'i'}_{fi})^2, \tag{45}$$

where

$$\langle|\chi^c_{\alpha'\beta'}|^2\rangle = |\chi^c_{\alpha'\beta'}|^2\langle\mathcal{S}_c^2\rangle/\mathcal{S}_c^2. \tag{46}$$

For the level scheme of Fig. 4(c), the RAIC cross section calculated from Eqs. (39), (37a), and (C14) is

$$f'f'\sigma'^{K}_{Q}(v_r,0)_c = 8\pi N_I^{-1}(-1)^{\varphi_c}(\langle|\chi^c_{ri}|^2\rangle/\Delta_c^2)(b'^{f'i'}_{fr}/b_0)^2(-1)^{Q_s}\epsilon^{*}_{j}\epsilon^{*}_{s}$$
$$\times\begin{Bmatrix}1 & 1 & K\\ Q_j & -Q_s & Q\end{Bmatrix}\begin{Bmatrix}1 & 1 & K\\ J_r & J_r & J_i\end{Bmatrix}\begin{Bmatrix}1 & 1 & K\\ J_{f'} & J_{f'} & J_{i'}\end{Bmatrix}\begin{Bmatrix}1 & 1 & K\\ 1 & 1 & 2\end{Bmatrix}\begin{Bmatrix}1 & 1 & K\\ J_r & J_r & J_f\end{Bmatrix}(b'^{f'i'}_{fr})^2. \tag{47}$$

Finally, for the level scheme of Fig. 4(d), one may use Eqs. (39), (38a), and (C14) to obtain

$$f'f'\sigma'^{K}_{Q}(v_r,0)_d = \tfrac{8}{9}\pi N_I^{-1}(-1)^{\varphi_d}(\langle|\chi^c_{r'i'}|^2\rangle/\Delta_d^2)(b'^{f'i'}_{fi}/b_0)^2(-1)^{Q_s}\epsilon^{*}_{j}\epsilon^{*}_{s}\begin{bmatrix}1 & 1 & K\\ Q_j & -Q_s & Q\end{bmatrix}\begin{Bmatrix}J_{f'} & J_{f'} & K\\ J_{r'} & J_{r'} & 1\end{Bmatrix}\begin{Bmatrix}1 & 1 & K\\ J_{r'} & J_{r'} & J_{i'}\end{Bmatrix}(b'^{f'i'}_{fi})^2. \tag{48}$$

Equations (42), (45), (47), and (48) give the RAIC excitation cross sections for level schemes corresponding to Fig. 4 in the limit of a dipole-dipole collisional interaction. It should be recalled that these are the RAIC cross sections for excitation from an *unpolarized initial state*; the quantities ϵ_j ($j=1,0,-1$) specify the polarization of the external field. As defined by Eqs. (33) and (40), the characteristic radii $b^{\alpha'\beta'}_{\alpha\beta}$ and b_0 are functions of v_r; $b^{\alpha'\beta'}_{\alpha\beta}$ is proportional to $v_r^{-1/2}$ and b_0 is proportional to $v_r^{1/(n-1)}$ for a level-shifting operator which varies as R^{-n} ($n>3$).

The physical significance of the various RAIC cross sections is discussed in Sec. VI. It may be noted at this point, however, that the RAIC cross sections vary as

$$\sigma' \simeq \Psi(\langle|\chi^c|^2\rangle/\Delta_a^2)(b_R/b_0)^2 b_R^2 , \tag{49}$$

where Ψ is a constant of order unity. Combining Eqs. (41) and (49), one finds that, if the perturbation theory is valid, then

$$\sigma' \ll b_0^2 . \tag{50}$$

Since $b_0 \approx 10$ Å, the maximum RAIC cross sections obtainable with fields satisfying the perturbation-theory requirement (41) are of the order of 100 Å^2. For larger field strengths, where Eq. (41) no longer holds, a strong-field (nonperturbative) theory is needed.

Corresponding results for noncentral tuning ($\Delta \neq 0$) may be obtained from Eqs. (39), (35)–(38), and (C13).

B. Fluorescence

The final-state coherence of atom A' is conveniently monitored by measuring the polarization or quantum beats in the fluorescence emitted from state f'. In this paper, the polarization of the fluorescence is calculated assuming that the external field participating in the RAIC excitation is linearly polarized in the z direction,

$$\epsilon_{s1} = 0, \quad \epsilon_0 = 1 , \tag{51}$$

and propagates in the y direction.

The fluorescence signal emitted from state f' to some lower state g' (characterized by an angular momentum quantum number $J_{g'}$) in atom A' is given by[9]

$$S \propto (-1)^{Q_n} \bar{\epsilon}_i \bar{\epsilon}_n^{*} (-1)^K \begin{bmatrix} 1 & 1 & K \\ Q_n & -Q_i & Q \end{bmatrix} \times \begin{Bmatrix} 1 & 1 & K \\ J_{f'} & J_{f'} & J_{g'} \end{Bmatrix} \langle f'f'|\rho'^K_Q(v_r)\rangle , \tag{52}$$

where the $\bar{\epsilon}_i$ ($i = -1, 0, 1$) specify the polarization of the fluorescence according to Eq. (19) (replacing the external-field polarization vector $\bar{\epsilon}$ by the vacuum-field polarization vector $\bar{\epsilon}$) and $\langle f'f'|\rho'^K_Q\rangle$ is the average value of the reduced density-matrix element $f'f'|\rho'^K$ of atom A'. Adopting a simple model, I assume that the lifetimes of the various $f'f'|\rho'^K_Q$, once created by RAIC, are determined only by the natural decay rate $\gamma_{f'}$ of level f' (i.e., the natural decay rate is much greater than the collision rate and the frequency separation of the final states). In that limit

$$\langle f'f'|\rho'^K_Q(v_r)\rangle = \mathfrak{N}_A(v_r) f'f'|\sigma'^K_Q(v_r) \times [N_p(T^+ - T^-)/\gamma_{f'}] , \tag{53}$$

where $\mathfrak{N}_A$ is the A-atom density and N_p is the number of pulses per second, each of duration $(T^+ - T^-)$. Thus, from Eqs. (52) and (53), one finds

$$S \propto (-1)^{Q_n} \bar{\epsilon}_i \bar{\epsilon}_n^{*} (-1)^K \begin{bmatrix} 1 & 1 & K \\ Q_n & -Q_i & Q \end{bmatrix} \times \begin{Bmatrix} 1 & 1 & K \\ J_{f'} & J_{f'} & J_{g'} \end{Bmatrix} f'f'|\sigma'^K_Q(v_r) . \tag{54}$$

For an external field polarized according to (51), it is convenient to measure the fluorescence also propagating in the y direction and polarized in either the x or z direction (Fig. 5). That is, one measures a signal S_x characterized by

$$\bar{\epsilon}_x = 1, \quad \bar{\epsilon}_y = \bar{\epsilon}_z = 0; \quad \bar{\epsilon}_1 = -\bar{\epsilon}_{-1} = \frac{-1}{\sqrt{2}} , \quad \bar{\epsilon}_0 = 0 , \tag{55a}$$

a signal S_z characterized by

$$\bar{\epsilon}_x = \bar{\epsilon}_y = 0, \quad \bar{\epsilon}_z = 1; \quad \bar{\epsilon}_{s1} = 0, \quad \bar{\epsilon}_0 = 1 , \tag{55b}$$

and forms the ratio

$$P = (S_z - S_x)/(S_z + S_x) . \tag{56}$$

Before explicitly calculating this ratio, it is useful to note that the general expression for $\rho'^{K^*}_{Q^*}$ and, consequently, for $\sigma'^{K^*}_{Q^*}$ is proportional to

$$P_{KQ} = \epsilon_j^{K} \epsilon_s^{*} (-1)^{Q_s} \begin{bmatrix} 1 & 1 & K \\ Q_j & -Q_s & Q \end{bmatrix}$$

so that, for the excitation scheme of Eq. (51) with the Q_i defined by Eq. (27b), one has

$$P_{KQ} = -(1/\sqrt{3})\,\delta_{K0}\delta_{Q0} + (2/\sqrt{6})\,\delta_{K2}\delta_{Q0} . \tag{57}$$

Thus only σ'^0_0 and σ'^2_0 enter the summation in Eq. (54). Using this fact that Eqs. (54)–(56), one can derive a polarization ratio

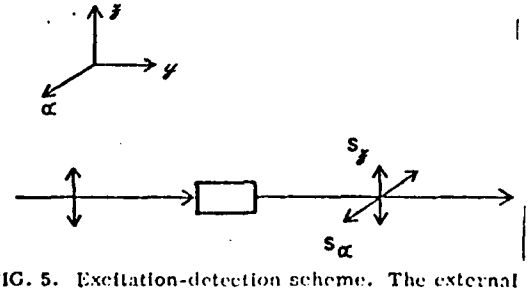

FIG. 5. Excitation-detection scheme. The external field is linearly polarized in the z direction and is incident in the y direction. The fluorescence from the $f' - g'$ transition of atom A', propagating in the y direction and polarized in either the x direction (S_x) or z direction (S_z), is monitored.

$$P(\Delta)=3\left(\frac{2\sqrt{6}(-1)^{J_{f'}+J_{g'}}}{3(2J_{f'}+1)^{1/2}}\begin{Bmatrix}1 & 1 & 2\\ J_{f'} & J_f & J_{g'}\end{Bmatrix}^{-1}\frac{f'f'\sigma'^0_0(r_r,\Delta)}{f'f'\sigma'^2_0(r_r,\Delta)}+1\right)^{-1}. \tag{58}$$

Within the confines of the adopted model, the ratio P depends only on *relative* RAIC cross sections and not on *absolute* cross sections. Consequently, it is a useful parameter in comparing theory with experiment.

The ratio P is now calculated for the level schemes of Fig. 4. For the level scheme of Fig. 4(a), it follows from Eqs. (58), (42), and (51) that, for central tuning, $\Delta=0$,

$$P_a(0)=3\left(\frac{20(-1)^{J_f+J_{g'}-J_i-J_{i'}}}{9(2J_{f'}+1)(2J_{r'}+1)\begin{Bmatrix}1 & 1 & 2\\ J_{f'} & J_f & J_{g'}\end{Bmatrix}\begin{Bmatrix}1 & 1 & 2\\ J_{r'} & J_r & J_f\end{Bmatrix}\begin{Bmatrix}1 & 1 & 2\\ J_r & J_{r'} & J_i\end{Bmatrix}\begin{Bmatrix}1 & 1 & 2\\ J_{f'} & J_f & J_{i'}\end{Bmatrix}}+1\right)^{-1}. \tag{59}$$

For the specific case,

$$J_{i'}=J_{g'}=J_i=J_f=0;\quad J_{f'}=J_{r'}=1;\quad P_a(0)=\tfrac{1}{7}, \tag{60}$$

while, for higher J values, $P_a(0)$ is smaller. For the level scheme of Fig. 4(b), one may derive from Eqs. (58), (45), and (51)

$$P_b(0)=3\left(\frac{2(-1)^{J_{r'}-J_{g'}}}{3(2J_{f'}+1)\begin{Bmatrix}1 & 1 & 2\\ J_{f'} & J_f & J_{g'}\end{Bmatrix}\begin{Bmatrix}1 & 1 & 2\\ J_{f'} & J_f & J_{r'}\end{Bmatrix}}+1\right)^{-1}. \tag{61}$$

Some specific cases are

$$J_{g'}=J_{r'}=1,\quad J_{f'}=2,\quad P_b(0)=\tfrac{21}{47}, \tag{62a}$$

$$J_{g'}=J_{r'}=0,\quad J_{f'}=1,\quad P_b(0)=1. \tag{62b}$$

For the level scheme of Fig. 4(c), it follows from Eqs. (58), (47), and (51) that

$$P_c=P_a. \tag{63}$$

This result is unique to the dipole-dipole interaction.

For the level scheme of Fig. 4(d), one may derive from Eqs. (58), (48), and (51) that

$$P_d(0)=3\left(\frac{2(-1)^{J_{g'}+J_{i'}}}{3(2J_{f'}+1)(2J_{r'}+1)\begin{Bmatrix}1 & 1 & 2\\ J_{f'} & J_f & J_{g'}\end{Bmatrix}\begin{Bmatrix}J_{f'} & J_{f'} & 2\\ J_{r'} & J_{r'} & 1\end{Bmatrix}\begin{Bmatrix}1 & 1 & 2\\ J_{r'} & J_{r'} & J_{i'}\end{Bmatrix}}+1\right)^{-1}. \tag{64}$$

Some specific cases are

$$J_{i'}=0,\quad J_{g'}=J_{r'}=1,\quad J_{f'}=2,\quad P_d(0)=\tfrac{21}{47}, \tag{65a}$$

$$J_{i'}=J_{f'}=1,\quad J_{g'}=J_{r'}=0,\quad P_d(0)=0. \tag{65b}$$

The physical significance of these results is discussed in the following section.

VI. DISCUSSION

A RAIC is one of the most basic forms of photochemistry. It is, therefore, of fundamental interest to understand the collisional interactions taking part in these reactions. The nature of the collisional interaction is reflected in (1) the total RAIC cross sections, (2) the dependence of RAIC cross sections on detuning Δ, and (3) the final-state coherences produced by RAIC. Total cross-section measurements are not very useful in distinguishing between various collisional interactions since accurate theoretical expressions are not available for comparison with experiment (i.e., there do not exist theoretical calculations in which matrix elements are accurately calculated along with a proper treatment of small-impact-parameter collisions). The dependence of RAIC total cross sections on Δ *does* provide a signature for the collisional interaction, provided one uses de-

tunings outside the impact core of the line $|\Delta|\tau_c > 1$. A limited number of experiments of this type have performed,[10] but no definite conclusion on the interaction potential was reached. It should be noted that, for $|\Delta|\tau_c > 1$, the RAIC excitation cross sections are relatively small. The study of final-state coherences produced by RAIC offers an additional method for probing the collisional interaction. In many cases (see below), measurements of RAIC-induced final-state coherences at central tuning $\Delta = 0$ (where signal is the largest) are sufficient to provide information concerning the collisional interaction.

Perhaps the most important aspect connected with the study of RAIC-induced coherences is the additional insight one can gain into the RAIC process. The calculation of final-state coherences introduces features into the problem that need not be considered when one calculates *total* RAIC cross sections. A particularly interesting feature can be already seen in the calculation presented in this paper, valid in the impact core of the RAIC profile and in the perturbation-theory limit. The collisional interaction can be viewed as the interaction of two unpolarized multipolar fields with atoms A and A'; the fields are incident from all directions and lead to the simultaneous (virtual) excitation of atoms A and A'. Although the fields are unpolarized, they are, in general, correlated to one another by the coupling coefficients of the collisional interaction [see the discussion of Fig. 4(a) below].

The unpolarized nature of the fields arises from the average over all possible collision orientations. This result may be seen mathematically in Eqs. (A20) and (B2). In Eq. (A20), starting from initial density matrix elements $\rho_Q^{K'}$, one excites final-state density-matrix elements ρ_Q^K with $|K - K'| \leq 2$. This type of selection rule is precisely that produced by the external field acting alone. In other words, the averaged collisional interaction does not modify the selection rule determined by the external field alone—an average collision acts as a scalar, i.e., as an unpolarized field. Similarly, in Eq. (B2), one sees that, starting from an unpolarized initial state, one excites reduced density-matrix elements ρ'^K_Q with $K \leq 2$; the selection rule is that associated with the external field only. In contrast to these results, one finds that, for a collision with a *specific* orientation, one could excite density-matrix elements ρ_Q^K from initial density-matrix elements $\rho_Q^{K'}$ such that $|K - K'| > 2$. It is only the *averaged* collisional interaction that acts as a scalar.

Thus the total RAIC reaction can be viewed as two unpolarized (but correlated) multipolar fields *plus* the external radiation field acting on atoms A and A' to produce the $ii' - ff'$ transition. To simulate the collisional interaction, the unpolarized fields are taken to act simultaneously on atoms A and A'; one field acts only on atom A while the other acts only on atom A' (in analogy with the fact that the collision operators act on either atom A or A', but not both). The external field acts on either atom A or A'. Using this model it is relatively easy to give a physical interpretation to the results obtained in Secs. IV and V for the level schemes of Fig. 4.

Figure 4(b). For the level scheme of Fig. 4(b), the collision first acts to produce the virtual state $|fr'\rangle$. If the collision is now replaced by two unpolarized multipolar fields incident from all directions, the coherence properties of this intermediate state are immediately determined. Since the initial state was unpolarized and the average collision operator now acts as a scalar, the intermediate state must also be unpolarized. Thus, when the external field completes the RAIC reaction by acting on atom A', the coherence properties of the final state f' of atom A' are the same as those produced by a radiation field exciting the $r' - f'$ transition in atom A' for an initially unpolarized state r'. The factor

$$\epsilon_f^{\kappa}\epsilon_s^{\kappa}(-1)^{Q_s}\begin{bmatrix} 1 & 1 & K \\ Q_f & -Q_s & Q \end{bmatrix}\begin{Bmatrix} 1 & 1 & K \\ J_{f'} & J_{f'} & J_{r'} \end{Bmatrix}$$

appearing in Eq. (45) for the excitation cross section is precisely that associated with the one-photon $r' - s'$ transition, assuming state r' to be unpolarized.

The collisional interaction affects the magnitude of the RAIC cross sections through a multiplicative factor. Consequently, the polarization ratio $P_\phi(0)$ discussed in Sec. V B is independent of the collisional interaction; it depends only on the values $J_{r'}, J_{f'}, J_{g'}$ reflecting the field excitation from $r' - f'$ followed by spontaneous emission from f' to g'. Thus, the level scheme [Fig. 4(b)] is not particularly well suited for probing the collisional interaction via polarization studies at line center; RAIC cross sections as a function of frequency are needed.

Figure 4(d). For the level scheme of Fig. 4(d), the field produces a polarized virtual state $|ir'\rangle$ and the two unpolarized fields (collision) complete the transition to state $|ff'\rangle$. The final-state coherence of atom A' can then be thought to be produced by the external field acting on the $i' - r'$ transition and an unpolarized multipolar field incident from all directions acting on the transition $r' - f'$. The transition amplitude for the $r' - f'$ transition depends on the multipolarity of the collision interaction; this dependence is given by the weighting factor

$$\begin{Bmatrix} J_f, & J_f, & K \\ J_r, & J_r, & k' \end{Bmatrix}$$

appearing in Eq. (48). Since this weighting factor couples K and k', the final-state coherence and the polarization ratio P_d can be used to distinguish different collisional interactions.

For the dipole-dipole interaction, $k'=1$, and the collision interaction on atom A' can be replaced by an unpolarized electric field incident from all directions producing the $r'-f'$ transition. Thus the coherence properties of state f' of atom A' are the same as those produced by *two-photon excitation* of atom A', the first photon provided by the external field producing the transition $i'-r'$ and the second by an unpolarized electric field incident from all directions producing the transition $r'-f'$. The polarization ratio $P_d(0)$ for the excitation-detection scheme of Fig. 5 is then easily calculated to be the simple function of $J_i, J_r, J_f, J_{r'}$ given by Eq. (64).

Figure 4(a). For the level scheme of Fig. 4(a), the two unpolarized multipolar fields incident from all directions first excite the virtual state $|rf'\rangle$ and the external field acts on atom A to complete the transition to state $|ff'\rangle$. One might think that the final state f' of atom A' would be unpolarized since it was produced by an unpolarized field incident from all directions. However, this conclusion need not be true owing to *correlation* effects between the unpolarized fields. This effect is best illustrated by the case of $J_i=J_f=0$, $J_r=1$, and an external field polarized linearly in the z direction. In order for the overall $\Delta m=0$ selection rule to be satisfied, only that part of the unpolarized field producing a $\Delta m=0$ transition is utilized. Thus, only a *part* of the unpolarized field acting on atom A is used. Owing to the coupling coefficients $A_{qq'}^{kk'}$ in the collisional interaction, this result implies that, correspondingly, only a *part* of the unpolarized multipolar field acting on atom A' contributes in the $i'-f'$ excitation. This result, in turn, implies that state f' can be polarized. For the conditions of Eq. (60), a polarization ratio $P_d(0)=\frac{1}{7}$ was found. Since the polarization ratio for case Fig. 4(a) is a function of the multipolarity of the collisional interaction, it can be used to provide an indication of the collisional processes participating in RAIC.

Figure 4(c). The analysis of the level scheme of Fig. 4(c) is similar to that for Fig. 4(a), except that the field acts on atom A' rather than on atom A. For the dipole-dipole interaction, in which the external field and the collisional operators have the same multipolarity ($k=k'=p=p'=1$), the RAIC cross sections for cases Figs. 4(a) and 4(d) are proportional to one another; for other collisional interactions, this proportionality is lost.

In order to have a more complete picture of the final-state coherences produced by RAIC, it is desirable to extend the theory to include the cases of large detuning ($|\Delta|\tau_c>1$) and large field strengths (nonperturbative solution). Such extensions may pose some interesting problems in the average over collision orientations, since the collision interaction no longer enters linearly in the final-state amplitude. Owing to this nonlinearity, the analog between an average collision and an unpolarized field may no longer be useful.

In summary, I have presented a calculation of the final-state coherences produced by RAIC in the weak-field limit that is valid in the impact core of the RAIC excitation profile. The resulting final-state coherences can be monitored by standard techniques (polarization of fluorescence, quantum beats) and may provide information on the collisional interactions occurring in the RAIC reaction.

ACKNOWLEDGMENT

This research was carried out while I was a guest at the Laboratoire Aimé Cotton, Orsay, France. The hospitality shown to me during my stay is deeply acknowledged as are conversations with C. Bréchignac, P. Cahuzac, J. L. Le Gouët, J. L. Picqué, and R. Vetter. I should also like to acknowledge financial support from the Fulbright Foundation. This research was also supported by the U. S. Office of Naval Research.

APPENDIX A

Appendix A is divided into three parts. In part A, some notation is introduced and the relationship between the direct product and irreducible-tensor subspaces is established. In part B, the relationship between the two-particle and single-particle (reduced) density-matrix elements is given. Finally, in part C, the final-state density-matrix for RAIC is calculated.

A. Relationship between bases

A state of the composite AA' system is represented by a capital letter, e.g.,

$$|F\rangle=|ff'\rangle=|f\rangle|f'\rangle'=|fJ_f m_f\rangle|f'J_{f'}m_{f'}\rangle', \tag{A1}$$

where it has been assumed that the angular momentum of a level can be represented by a J quantum number. The angular momenta appearing in the direct product basis (A1) can be coupled in the standard fashion,

$$|\bar{f}\rangle = |ff' J_f J_{f'} J_{\bar{f}} m_{\bar{f}}\rangle$$

$$= \begin{bmatrix} J_f & J_{f'} & J_{\bar{f}} \\ m_f & m_{f'} & m_{\bar{f}} \end{bmatrix} |fJ_f m_f\rangle |f' J_{f'} m_{f'}\rangle' , \quad \text{(A2)}$$

where the bar indicates this coupled basis. As in the main text, I use a summation convention in which all repeated indices (not including their appearance in phase factors or frequency denominators) are summed over.[2]

Matrix elements of the density-matrix operator in the barred basis are related to those in an irreducible tensor basis, ${}^{\bar{F}\bar{F}_1}\rho_Q^K$, via the transformations

$$\rho_{\bar{F}\bar{F}_1} = \langle \bar{F}|\rho|\bar{F}_1\rangle = (-1)^{J_{\bar{F}_1} - m_{\bar{F}_1}} \begin{bmatrix} J_{\bar{F}} & J_{\bar{F}_1} & K \\ m_{\bar{F}} & -m_{\bar{F}_1} & Q \end{bmatrix} {}^{\bar{F}\bar{F}_1}\rho_Q^K , \quad \text{(A3a)}$$

$${}^{\bar{F}\bar{F}_1}\rho_Q^K = (-1)^{J_{\bar{F}_1} - m_{\bar{F}_1}} \begin{bmatrix} J_{\bar{F}} & J_{\bar{F}_1} & K \\ m_{\bar{F}} & -m_{\bar{F}_1} & Q \end{bmatrix} \times \langle \bar{F} J_{\bar{F}} m_{\bar{F}} | \rho | \bar{F}_1 J_{\bar{F}_1} m_{\bar{F}_1}\rangle , \quad \text{(A3b)}$$

where the total J and m_J values of the barred basis are explicitly written in the right-hand side of Eq. (A3b).

The time rate of change of density-matrix elements produced by RAIC can be expressed as[4]

$$\dot{\rho}_{\bar{F}\bar{F}_1} = \Gamma^{\bar{I}\bar{I}_1}_{\bar{F}\bar{F}_1} \rho_{\bar{I}\bar{I}_1} \quad \text{(A4a)}$$

or

$${}^{\bar{F}\bar{F}_1}\dot{\rho}_Q^K = \Gamma^{K'Q'}_{KQ}(\bar{F}, \bar{F}_1, \bar{I}, \bar{I}_1)\, {}^{\bar{I}\bar{I}_1}\rho_{Q'}^{K'} . \quad \text{(A4b)}$$

The relationship between the Γ's may be obtained from Eqs. (A1)–(A4) as

$$\Gamma^{K'Q'}_{KQ}(\bar{F}, \bar{F}_1, \bar{I}, \bar{I}_1) = (-1)^{\bar{I}_1 - m_{\bar{I}_1}} (-1)^{\bar{F}_1 - m_{\bar{F}_1}} \begin{bmatrix} J_f & J_{f'} & J_{\bar{F}} \\ m_f & m_{f'} & m_{\bar{F}} \end{bmatrix} \begin{bmatrix} J_{f_1} & J_{f_1'} & J_{\bar{F}_1} \\ m_{f_1} & m_{f_1'} & m_{\bar{F}_1} \end{bmatrix}$$

$$\times \begin{bmatrix} J_{\bar{F}} & J_{\bar{F}_1} & K \\ m_{\bar{F}} & -m_{\bar{F}_1} & Q \end{bmatrix} \begin{bmatrix} J_i & J_{i'} & J_{\bar{I}} \\ m_i & m_{i'} & m_{\bar{I}} \end{bmatrix} \begin{bmatrix} J_{i_1} & J_{i_1'} & J_{\bar{I}_1} \\ m_{i_1} & m_{i_1'} & m_{\bar{I}_1} \end{bmatrix} \begin{bmatrix} J_{\bar{I}} & J_{\bar{I}_1} & K' \\ m_{\bar{I}} & -m_{\bar{I}_1} & Q' \end{bmatrix}$$

$$\times \Gamma^{\bar{I}\bar{I}_1}_{\bar{F}\bar{F}_1}(m_f, m_{f'}, m_{f_1}, m_{f_1'}, m_{i'}, m_i, m_{i_1}, m_{i_1'}) \quad \text{(A5)}$$

along with the corresponding inverse transformation.

B. Reduced density-matrix elements

The reduced density-matrix elements for atom A' are defined by

$$\rho'_{f'f_1'} = \langle ff'|\rho|ff_1'\rangle . \quad \text{(A6)}$$

In terms of the matrix elements of irreducible-tensor operators defined by Eq. (23a), one can use Eqs. (A1)–(A3) and some elementary properties of the Clebsch-Gordon coefficient to derive

$$\rho'^K_{f'f_1'Q} = (-1)^{J_{f_1'} + J_{\bar{F}} + J_f - K} [(2J_{\bar{F}} + 1)(2J_{\bar{F}_1} + 1)]^{1/2} \begin{Bmatrix} J_{\bar{F}} & J_{\bar{F}_1} & K \\ J_{f_1'} & J_{f_1} & J_f \end{Bmatrix} {}^{\bar{F}\bar{F}_1}\rho_Q^K(ff' J_f J_{f'}, J_{\bar{F}}; ff_1' J_f J_{f_1'} J_{\bar{F}_1}) . \quad \text{(A7)}$$

Equation (A7), in which the $\{\ \}$ represents a 6-J symbol, enables one to calculate the reduced density-matrix elements of atom A' from the two-particle density-matrix elements. Similarly, reduced matrix elements of atom A are given by

$$\rho_{ff_1} = \langle ff'|\rho|f_1 f'\rangle \quad \text{(A8)}$$

and

$${}^{ff_1}\rho_Q^K = (-1)^{J_f + J_{\bar{F}_1} + J_{f'} - K} [(2J_{\bar{F}} + 1)(2J_{\bar{F}_1} + 1)]^{1/2} \begin{Bmatrix} J_{\bar{F}} & J_{\bar{F}_1} & K \\ J_{f_1} & J_f & J_{f'} \end{Bmatrix} {}^{\bar{F}\bar{F}_1}\rho_Q^K(ff' J_f J_{f'}, J_{\bar{F}}; f_1 f' J_{f_1} J_{f'} J_{\bar{F}_1}) . \quad \text{(A9)}$$

$J_{\bar{F}_1}$

C. Calculation of $^{\bar{F}\bar{F}_1}\rho^K_Q$

Starting from Eq. (10), I now derive an expression for $^{\bar{F}\bar{F}_1}\rho^K_Q(t_c^+; b, v_r, \bar{R}_c, t_c)$. Equation (10) may be written

$$a_F(t_c^+) = \langle F|\bar{T}|I\rangle a_I(t_c^-) , \tag{A10a}$$

where

$$\langle F|\bar{T}|I\rangle = (i\hbar)^{-1}\int_{t_c^-}^{t_c^+}\langle F|\hat{T}(IF,t)|I\rangle e^{-i\Delta t}dt . \tag{A10b}$$

Equation (A10a) could equally well be given in the coupled (barred) basis as

$$a_{\bar{F}}(t_c^+) = \langle F|\bar{T}|\bar{I}\rangle a_{\bar{I}}(t_c^-) , \tag{A11}$$

so that the final-state density matrix is

$$\rho_{\bar{F}\bar{F}_1}(t_c^+; b, v_r, \Theta, \bar{R}_c, t_c) = \langle F|\bar{T}|\bar{I}\rangle\langle F_1|\bar{T}|\bar{I}_1\rangle^*\rho_{\bar{I}\bar{I}_1}(t_c^-) . \tag{A12}$$

The matrix elements of $\bar{T}$ are expanded as

$$\langle F|\bar{T}|\bar{I}\rangle = (-1)^{J_{\bar{I}}-m_{\bar{I}}}\begin{Bmatrix} J_{\bar{F}} & J_{\bar{I}} & G \\ m_{\bar{F}} & -m_{\bar{I}} & g\end{Bmatrix}\overline{FI}\bar{T}^G_g . \tag{A13}$$

Equation (A3a) is used, and some identities involving the angular momentum coupling coefficients are employed to transform equation (A12) into

$$\begin{aligned}\overline{FF}_1\rho^K_Q(t_c^+;\ b,\ v_r,\ \bar{R}_c, t_c) = (-1)^{2J_{\bar{F}}+G'+2J_{\bar{I}}+K'}(-1)^{g'+Q'}[(2G+1)(2G'+1)(2K+1)(2K'+1)]^{1/2}\\ \times\begin{bmatrix} K & K' & X\\ Q & -Q' & -m_x\end{bmatrix}\begin{bmatrix} G & G' & X\\ g & -g' & m_x\end{bmatrix}\begin{Bmatrix} F & F_1 & K\\ I & I_1 & K'\\ G & G' & X\end{Bmatrix}H(F,F_1,I,I_1,\ G,G',g,g')^{\overline{II}_1}\rho^{K'}_{Q'}(t_c^-) ,\end{aligned} \tag{A14}$$

where

$$H(F,F_1,I,I_1,G,G',g,g') \equiv (8\pi^2)^{-1}\int d\Theta\ ^{\overline{FI}}\bar{T}^G_g(\bar{F}_1\bar{I}_1\bar{T}^{G'}_{g'})^* \tag{A15}$$

and the quantity in large curly brackets is a 9-J symbol. The quantities $^{\overline{FI}}\bar{T}^G_g$ may be calculated by (i) using Eqs. (A13), (A10b), (6), (13), (18); (ii) expanding all intermediate states appearing in Eq. (6) in terms of the barred basis; and (iii) using the Wigner-Eckart theorem to evaluate matrix elements of $(\mu_T)^1_q$ and $^{bb'}V^K_Q$. One obtains

$$\begin{aligned}{}^{\overline{FI}}\bar{T}^G_g &= (-1)^{3J_{\bar{F}}+J_{\bar{I}}+2J_{\bar{E}}+K+1}\langle F\|(\mu_T)^{(1)}\|\bar{E}\rangle\langle\bar{E}\|{}^{bb'}V^{(K)}\|I\rangle(\omega_{EI})^{-1}\\ &\times(i\hbar)^{-1}\left(\frac{b}{v_r}\right)^{bb'}\Lambda^K_Q(b,v_r,\Theta;\Delta)\epsilon^*_j\begin{bmatrix} K & 1 & G\\ Q & Q_j & g\end{bmatrix}\begin{Bmatrix} K & 1 & G\\ J_{\bar{I}} & J_{\bar{F}} & J_{\bar{E}}\end{Bmatrix}\delta_c\\ &+(-1)^{J_{\bar{F}}+J_{\bar{I}}+G}\langle F\|{}^{bb'}V^{(K)}\|\bar{E}\rangle\langle\bar{E}\|(\mu_T)^{(1)}\|\bar{I}\rangle(\omega_{EF})^{-1}\\ &\times(i\hbar)^{-1}\left(\frac{b}{v_r}\right)^{bb'}\Lambda^K_Q(b,v_r,\Theta;\Delta)\epsilon^*_j\begin{bmatrix} K & 1 & G\\ Q & Q_j & g\end{bmatrix}\begin{Bmatrix} K & 1 & G\\ J_{\bar{I}} & J_{\bar{F}} & J_{\bar{E}}\end{Bmatrix}\delta_c\end{aligned} \tag{A16}$$

where $^{bb'}\Lambda^K_Q(b,v_r,\Theta;\Delta)$ is defined by Eq. (16b), $\langle\|\cdots\|\rangle$ is a reduced matrix element, ϵ_j is defined by Eqs. (17)–(19), and

The product of the C'_f can be calculated explicitly and the final expression simplified using identities involving the angular momenta coupling coefficients.[3]

One obtains 16 terms corresponding to the square of the four terms contributing to the amplitude in Fig. 2. The result may be written in the form

$$f'f_1\rho'^K_Q(\ell'_e;b,v_r,\vec{R}_e,t_e)=\left(\frac{h\delta_c}{hv_r}\right)^2 N_i^{1kk'}A^{K'}_{Q'}(b,v_r,0;\Delta)[^{pp'}A^{K'}_{Q'}(b,v_r,0;\Delta)]^*\epsilon^*_j\epsilon_s(-1)^{Q_s}\begin{bmatrix}1 & 1 & K\\ Q_j & -Q_s & Q\end{bmatrix}$$

$$\times\sum_{a,b=a}^{d}s_{ab}(k,k',p,p',K,K',f',f'_1)\,,\tag{B3}$$

where s_{ab} represents the contribution from diagram a and the complex conjugate of diagram b in Fig. 2. Explicitly,

$$s_{aa}=[(\omega_e+\omega_{f'}-\omega_I)(\omega_d+\omega_{f'}-\omega_I)]^{-1}(-1)^{J_e-J_d-J_f+J_f-J_i-J_i+K'+p'+k'}$$
$$\times\langle f\|\mu^{(1)}\|e\rangle\langle f\|\mu^{(1)}\|d\rangle^*\langle e\|T^{(k)}\|i\rangle\langle d\|T^{(p)}\|i\rangle^*\langle f'\|T'^{(k')}\|i'\rangle\langle f'_1\|T'^{(p')}\|i'\rangle^*$$
$$\times\begin{Bmatrix}1 & 1 & K\\ J_e & J_d & J_f\end{Bmatrix}\begin{Bmatrix}k & p & K\\ J_d & J_e & J_i\end{Bmatrix}\begin{Bmatrix}k' & p' & K\\ p & k & K'\end{Bmatrix}\begin{Bmatrix}k' & p' & K\\ J_{f'_1} & J_{f'} & J_{i'}\end{Bmatrix},\tag{B4}$$

$$s_{ab}=[(\omega_e+\omega_{f'}-\omega_I)(\omega_f+\omega_{d'}-\omega_I)]^{-1}(-1)^{K-2J_e+J_{d'}+J_f-J_i-J_{i'}+k'+p'}$$
$$\times\langle f\|\mu^{(1)}\|e\rangle\langle f'_1\|\mu'^{(1)}\|d'\rangle^*\langle e\|T^{(k)}\|i\rangle\langle f\|T^{(p)}\|i\rangle^*\langle f'\|T'^{(k')}\|i'\rangle\langle f'_1\|T'^{(p')}\|d'\rangle^*$$
$$\times\begin{Bmatrix}1 & 1 & K\\ J_{f'} & J_{f'_1} & J_{d'}\end{Bmatrix}\begin{Bmatrix}k & p & 1\\ k' & p' & K'\end{Bmatrix}\begin{Bmatrix}k & p & K\\ J_f & J_e & J_i\end{Bmatrix}\begin{Bmatrix}k' & p' & 1\\ J_{d'} & J_{f'} & J_{i'}\end{Bmatrix},\tag{B5}$$

$$s_{bb}=[(\omega_f+\omega_{e'}-\omega_I)(\omega_F+\omega_{d'}-\omega_I)]^{-1}(-1)^{K+J_{f'}+J_{e'}}[(2J_{e'}+1)(2k+1)(2k'+1)]^{-1}$$
$$\times\delta_{J_{e'},J_{d'}}\delta_{kp}\delta_{k'p'}\langle f'\|\mu'^{(1)}\|e'\rangle\langle f'_1\|\mu'^{(1)}\|d'\rangle^*|\langle F_i\|T^{(k)}\|i\rangle|^2\langle e'\|T'^{(k')}\|i'\rangle$$
$$\times\langle d'\|T'^{(k')}\|i'\rangle^*\begin{Bmatrix}1 & 1 & K\\ J_{f'} & J_{f'_1} & J_{e'}\end{Bmatrix},\tag{B6}$$

$$s_{ac}=[(\omega_e+\omega_{f'}-\omega_I)(\omega_d+\omega_{i'}-\omega_F)]^{-1}(-1)^{J_i+J_{i'}+J_d-J_e+K'+K+J_{f'}+k'+p+p'+J_{f'_1}}$$
$$\times\langle f\|\mu^{(1)}\|e\rangle\langle d\|\mu^{(1)}\|i\rangle^*\langle e\|T^{(k)}\|i\rangle\langle f\|T^{(p)}\|d\rangle^*\langle f'\|T'^{(k')}\|i'\rangle\langle f'_1\|T'^{(p')}\|i'\rangle^*$$
$$\times\begin{Bmatrix}k' & p' & K\\ p & k & K'\end{Bmatrix}\begin{Bmatrix}k' & p' & K\\ J_{f'_1} & J_{f'} & J_{i'}\end{Bmatrix}\begin{Bmatrix}1 & 1 & K\\ J_d & J_f & p\\ J_i & J_e & k\end{Bmatrix},\tag{B7}$$

$$s_{ad}=[(\omega_e+\omega_{f'}-\omega_I)(\omega_i+\omega_{d'}-\omega_F)]^{-1}(-1)^{J_i+J_{i'}+J_{d'}+J_{f'}+2J_f+k'+J_e+K}$$
$$\times\langle f\|\mu^{(1)}\|e\rangle\langle d'\|\mu'^{(1)}\|i\rangle^*\langle e\|T^{(k)}\|i\rangle\langle f\|T^{(p)}\|i\rangle^*\langle f'\|T'^{(k')}\|i'\rangle$$
$$\times\langle f'_1\|T'^{(p')}\|d'\rangle^*$$
$$\times\begin{Bmatrix}k & p & 1\\ p' & k' & K'\end{Bmatrix}\begin{Bmatrix}k & p & 1\\ J_f & J_e & J_i\end{Bmatrix}\begin{Bmatrix}1 & K & 1\\ J_{d'} & J_{f'_1} & p'\\ J_{i'} & J_{f'} & k'\end{Bmatrix},\tag{B8}$$

$$s_{bc}=[(\omega_f+\omega_{e'}-\omega_I)(\omega_d+\omega_{i'}-\omega_F)]^{-1}(-1)^{J_{i'}-J_i+1-J_{f'}+K+J_{f'_1}+K'-J_{e'}+k+k'+p+p'}$$
$$\times\langle f'\|\mu'^{(1)}\|e'\rangle\langle d\|\mu^{(1)}\|i\rangle^*\langle f\|T^{(k)}\|i\rangle\langle f\|T^{(p)}\|d\rangle^*\langle e'\|T'^{(k')}\|i'\rangle$$
$$\times\langle f'_1\|T'^{(p')}\|i'\rangle^*$$
$$\times\begin{Bmatrix}1 & 1 & K\\ J_{f'} & J_{f'_1} & J_{e'}\end{Bmatrix}\begin{Bmatrix}k & p & 1\\ J_d & J_i & J_f\end{Bmatrix}\begin{Bmatrix}k' & p' & 1\\ p & k & K'\end{Bmatrix}\begin{Bmatrix}k' & p' & 1\\ J_{f'_1} & J_{e'} & J_{i'}\end{Bmatrix},\tag{B9}$$

$$Q_1 = 1,\quad Q_{-1} = 1,\quad Q_0 = 0\,. \tag{A17}$$

Equation (A16) and its complex conjugate are now inserted into Eq. (A15), and Eqs. (15) and (21) are used to arrive at

$$\begin{aligned}\mathcal{U}(\bar{F},\bar{F}_1,\bar{I},\bar{I}_1,\ G,G',g,g') = \left(\frac{b\delta_c}{\hbar v_r}\right)^2 (2K+1)^{-1}\epsilon_j^2\epsilon_s^2\, {}^{kk'}A^K_Q(b,v_r,0;\Delta)[{}^{pp'}A^K_{Q'}(b,v_r,0;\Delta)]^* \\ \times\begin{bmatrix} K & 1 & G \\ Q & Q_j & g\end{bmatrix}\begin{bmatrix} K & 1 & G' \\ Q' & Q_s & g'\end{bmatrix} C(\bar{F},\bar{I},G,k,k',K)[C(\bar{F}_1,\bar{I}_1,G',p,p',K)]^*\,,\end{aligned} \tag{A18}$$

where

$$\begin{aligned}C(\bar{F},\bar{I},G,k,k',K) = (-1)^{2J_{\bar{F}}+J_{\bar{I}}+2J_{\bar{E}}+K+1}(\omega_{\bar{E}\bar{I}})^{-1}\langle\bar{F}||(\mu_T)^{(1)}||\bar{E}\rangle\langle\bar{E}||{}^{kk'}V^{(K)}||\bar{I}\rangle\begin{Bmatrix} K & 1 & G \\ J_{\bar{F}} & J_{\bar{I}} & J_{\bar{E}}\end{Bmatrix} \\ +(-1)^{J_{\bar{F}}+J_{\bar{I}}+G}(\omega_{\bar{E}\bar{F}})^{-1}\langle\bar{F}||{}^{kk'}V^{(K)}||\bar{E}\rangle\langle\bar{E}||(\mu_T)^{(1)}||\bar{I}\rangle\begin{Bmatrix} K & 1 & G \\ J_{\bar{I}} & J_{\bar{F}} & J_{\bar{E}}\end{Bmatrix}.\end{aligned} \tag{A19}$$

The quantity C is easily identified with the four diagrams of Figs. 2 and 3.

Combining Eqs. (A18) and (A19) and carrying out the summations over magnetic quantum numbers, one obtains

$$\begin{aligned}{}^{f'f}_{\bar{I}_1\bar{I}}\rho'^K_Q(t_c';b,v_r,\bar{R}_c,t_c) = (-1)^{2J_{\bar{I}}+2J_{\bar{F}}+G+K'+\bar{K}+X}(-1)^{Q'+Q_1+m_z}\left(\frac{b\delta_c}{\hbar v_r}\right)^2 \\ \times\epsilon_j^2\epsilon_s^2[(2G+1)(2G'+1)(2K+1)(2K'+1)]^{1/2}\begin{bmatrix} K & K' & X \\ Q & -Q' & m_z\end{bmatrix} \\ \times\begin{bmatrix} 1 & 1 & X \\ Q_j & -Q_s & m_z\end{bmatrix}{}^{kk'}A^{\bar{K}}_{\bar{Q}}(b,v_r,0;\Delta)[{}^{pp'}A^{\bar{K}}_{\bar{Q}}(b,v_r,0;\Delta)]^*\begin{Bmatrix} 1 & 1 & X \\ G & G' & \bar{K}\end{Bmatrix}\begin{Bmatrix} \bar{F} & \bar{F}_1 & K \\ \bar{I} & \bar{I}_1 & K' \\ G & G' & X\end{Bmatrix} \\ \times C(\bar{F},\bar{I},G,k,k',\bar{K})[C(\bar{F}_1,\bar{I}_1,G',p,p',\bar{K})]^*{}^{\bar{I}\bar{I}_1}_{\bar{F}\bar{F}_1}\rho'^{K'}_{Q'}(t_c^-)\,.\end{aligned} \tag{A20}$$

It is clear from this equation that $|K'-K|<2$, i.e., that the collision acts in some way as a scalar operator (see Sec. VI). Reduced density-matrix elements may be obtained from Eq. (A20) by use of Eqs. (A7) and (A9). Density-matrix elements in the magnetic sublevel basis are related to those in the irreducible tensor basis by Eqs. (A3) and (A2) or, for reduced density-matrix elements, by Eq. (23b).

APPENDIX B

Unpolarized initial state

In Appendix B, the reduced density-matrix elements for atom A' are calculated *for an unpolarized initial state.* An unpolarized initial state corresponds to

$${}^{\bar{I}_1}_{\bar{I}}\rho'^K_Q(t_c^-) = (2J_{\bar{I}}+1)N_I^{-1}\delta_{\bar{I}\bar{I}_1}\delta_{K0}\delta_{Q0}\,, \tag{B1}$$

where N_I is the total number of initial states. Using Eqs. (A7), (A20), and (B1), one may obtain after a little algebra[5] the reduced density-matrix elements for atom A',

$$\begin{aligned}{}^{f'f}_{\bar{F}_1\bar{F}}\rho'^K_Q(t_c';b,v_r,\bar{R}_c,t_c) = \sum_I (-1)^{J_{f_1}+J_f+K+K'+G+G'}\left(\frac{b\delta_c}{\hbar v_r}\right)^2(2G+1)(2G'+1) \\ \times[(2J_{\bar{F}}+1)(2J_{\bar{F}_1}+1)]^{1/2}[N_I(2K'+1)]^{-1}{}^{kk'}A^{K'}_{Q'}(b,v_r,0;\Delta) \\ \times{}^{pp'}A^{K'}_{Q'}(b,v_r,0;\Delta)]^*\epsilon_j^2\epsilon_s^2(-1)^{Q_2}\begin{bmatrix} 1 & 1 & K \\ Q_f & -Q_s & Q\end{bmatrix}\begin{Bmatrix} 1 & 1 & K \\ G & G' & K'\end{Bmatrix} \\ \times\begin{Bmatrix} G & G' & K \\ J_{\bar{F}_1} & J_{\bar{F}} & J_{\bar{I}}\end{Bmatrix}\begin{Bmatrix} J_{\bar{F}_1} & J_{\bar{F}} & K \\ J_{f'} & J_{f_1} & J_f\end{Bmatrix}C(\bar{F},\bar{I},G,k,k',K') \\ \times[C(\bar{F}_1,\bar{I},G',p,p',K')]^*\,.\end{aligned} \tag{B2}$$

$$\mathcal{S}_{bb}^{kk'} = [(\omega_f + \omega_{e'} - \omega_i)(\omega_i + \omega_{d'} - \omega_F)]^{-1}(-1)^{2J_i+J_{f'}-J_f+K'+J_d+J_{e'}+k'}$$
$$\times [(2k+1)(2k'+1)]^{-1}\delta_{pp'}\delta_{p'q'}\langle f'||\mu'^{(1)}||e'\rangle\langle d'||\mu'^{(1)}||i'\rangle^*$$
$$\times |\langle f||T^{(k)}||i\rangle|^2\langle e'||T'^{(k')}||i'\rangle\langle f_1'||T'^{(k')}||d'\rangle^* \begin{Bmatrix} 1 & 1 & K \\ J_f & J_{f_1'} & J_{e'} \end{Bmatrix}\begin{Bmatrix} J_{f_1'} & J_{e'} & k' \\ J_i & J_e & 1 \end{Bmatrix}, \tag{B10}$$

$$\mathcal{S}_{ee} = [(\omega_e + \omega_{i'} - \omega_F)(\omega_d + \omega_{i'} - \omega_F)]^{-1}(-1)^{-J_i-J_{i'}-J_{f'}+k+k'+p+p'-J_d-J_e-J_f+K'}$$
$$\times \langle e||\mu^{(1)}||i\rangle\langle d||\mu^{(1)}||i\rangle^*\langle f||T^{(k)}||e\rangle\langle f||T^{(p)}||d\rangle^*\langle f'||T'^{(k')}||i'\rangle\langle f_1'||T'^{(p')}||i'\rangle^*$$
$$\times \begin{Bmatrix} 1 & 1 & K \\ J_e & J_d & J_i \end{Bmatrix}\begin{Bmatrix} k' & p' & K \\ J_{f_1'} & J_{f'} & J_{i'} \end{Bmatrix}\begin{Bmatrix} k & p & K \\ p' & k' & K' \end{Bmatrix}\begin{Bmatrix} k & p & K \\ J_d & J_e & J_f \end{Bmatrix}, \tag{B11}$$

$$\mathcal{S}_{ed} = [(\omega_e + \omega_{i'} - \omega_F)(\omega_i + \omega_{d'} - \omega_F)]^{-1}(-1)^{J_i+J_{i'}+J_{d'}+K+K'+p+k+k'+J_f+2J_{f'}}$$
$$\times \langle e||\mu^{(1)}||i\rangle\langle d'||\mu'^{(1)}||i'\rangle^*\langle f||T^{(k)}||e\rangle\langle f||T^{(p)}||i\rangle^*\langle f'||T'^{(k')}||i'\rangle\langle f_1'||T'^{(p')}||d'\rangle^*$$
$$\times \begin{Bmatrix} k & p & 1 \\ p' & k' & K' \end{Bmatrix}\begin{Bmatrix} k & p & 1 \\ J_i & J_e & J_f \end{Bmatrix}\begin{Bmatrix} J_{f_1'} & K & J_{f'} \\ J_{d'} & 1 & J_{i'} \\ p' & 1 & k' \end{Bmatrix}, \tag{B12}$$

$$\mathcal{S}_{dd} = [(\omega_i + \omega_{e'} - \omega_F)(\omega_i + \omega_{d'} - \omega_F)]^{-1}(-1)^{J_i+2J_{e'}+J_{f_1'}+k'}[(2k+1)(2k'+1)]^{-1}$$
$$\times \delta_{kp}\delta_{k'p'}\langle e'||\mu'^{(1)}||i'\rangle\langle d'||\mu'^{(1)}||i'\rangle^*|\langle f||J^{(k)}||i\rangle|^2\langle f'||T'^{(k')}||e'\rangle$$
$$\times \langle f_1'||T'^{(k')}||d'\rangle^*\begin{Bmatrix} J_{f_1'} & J_{f'} & K \\ J_{e'} & J_{d'} & k' \end{Bmatrix}\begin{Bmatrix} 1 & 1 & K \\ J_e & J_{d'} & J_{i'} \end{Bmatrix}, \tag{B13}$$

and

$$\mathcal{S}_{\alpha\beta}(k,k',p,p',K,K',f',f_1') = (-1)^{J_{f_1'}-J_{f'}}[\mathcal{S}_{\beta\alpha}(p,p',k,k',K,K',f_1',f')]^* . \tag{B14}$$

Some of these terms may vanish owing to the selection rules appropriate to the level-coupling scheme and interatomic potential under consideration.

APPENDIX C

Dipole-dipole interaction

In Appendix C, the quantities $A_{qq'}^{kk'}$ and ${}^{kk'}A_Q^K$ are evaluated, assuming a dipole-dipole collisional interaction between atom A (dipole-moment operator $\vec{\mu}$) and atom A' (dipole-moment operator $\vec{\mu}'$) of the form

$$\mathcal{U} = (\vec{\mu}\cdot\vec{\mu}'R^2 - 3\vec{\mu}\cdot\vec{R}\,\vec{\mu}'\cdot\vec{R})/R^5 , \tag{C1}$$

where $\vec{R}$ is the separation between the atoms. For a given collision geometry, $\vec{R}$ is a function of $\tau = t - t_c$ (the collision is centered in time at $t = t_c$), b, v_r, and Θ.

Writing $\vec{\mu}$ and $\vec{\mu}'$ in the form of Eq. (20) and defining

$$R_1 = -\frac{(R_x - iR_y)}{\sqrt{2}}, \quad R_{-1} = \frac{R_x + iR_y}{\sqrt{2}}, \quad R_0 = R_z , \tag{C2}$$

one may rewrite Eq. (C1) as

$$\mathcal{U} = A_{qq'}^{11}(\tau, b, v_r, \Theta)\mu_q^1(\mu')_{q'}^1 , \tag{C3}$$

where

$$A^{11}_{qq'}(\tau, b, v_r, \Theta) = [R^2(\delta_{q0}\delta_{q'0} - \delta_{q1}\delta_{q',-1} - \delta_{q,-1}\delta_{q',1}) - 3R_qR_{q'}]/R^4 . \quad \text{(C4)}$$

Equation (C3) has exactly the same form as Eq. (12) since μ^1_q and $(\mu')^1_q$ are components of irreducible tensors of rank 1.

The quantities of interest in evaluating RAIC cross sections are the Fourier transform of the $A^{11}_{qq'}$ defined by Eq. (16a). Using Eqs. (C2), (C4), and (16a), one finds

$$A^{11}_{qq'}(b, v_r, \Theta; \Delta) = (v_r/b)e^{-i\Delta t_c}\int_{t_c^- - t_c}^{t_c^+ - t_c} A^{11}_{qq'}(\tau, b, v_r, \Theta)e^{-i\Delta\tau}d\tau , \quad \text{(C5)}$$

where

$$A^{11}_{11}(\tau, b, v_r, \Theta) = [A^{11}_{-1,-1}(\tau, b, v_r, \Theta)]^* = -3(R_x^2 - R_y^2 - 2iR_xR_y)/2R^5 , \quad \text{(C6a)}$$

$$A^{11}_{10}(\tau, b, v_r, \Theta) = A^{11}_{01}(\tau, b, v_r, \Theta) = -[A^{11}_{-10}(\tau, b, v_r, \Theta)]^* = -[A^{11}_{0-1}(\tau, b, v_r, \Theta)] = 3R_z(R_x - iR_y)/\sqrt{2}\,R^5 , \quad \text{(C6b)}$$

$$A^{11}_{00}(\tau, b, v_r, \Theta) = (R^2 - 3R_z^2)/R^5 , \quad \text{(C6c)}$$

$$A^{11}_{1-1}(\tau, b, v_r, \Theta) = A^{11}_{-11}(\tau, b, v_r, \Theta) = \tfrac{1}{2}A^{11}_{00}(\tau, b, v_r, \Theta) . \quad \text{(C6d)}$$

The corresponding equations for the ${}^{11}A^K_Q$ defined by Eq. (14b)

$${}^{11}A^K_Q(b, v_r, \Theta; \Delta) = (v_r/b)e^{-i\Delta t_c}\int_{t_c^- - t_c}^{t_c^+ - t_c} A^{K}_{qq'}(\tau, b, v_r, \Theta)e^{-i\Delta\tau}d\tau , \quad \text{(C7)}$$

$${}^{11}A^0_0(\tau, b, v_r, \Theta) = 0 , \quad \text{(C8a)}$$

$${}^{11}A^1_Q(\tau, b, v_r, \Theta) = 0 \quad (Q = 1, 0, -1) , \quad \text{(C8b)}$$

$${}^{11}A^2_2(\tau, b, v_r, \Theta) = [{}^{11}A^2_{-2}(\tau, b, v_r, \Theta)]^* = 3(R_x^2 - R_y^2 - 2iR_xR_y)/2R^5 , \quad \text{(C8c)}$$

$${}^{11}A^2_1(\tau, b, v_r, \Theta) = -[{}^{11}A^2_{-1}(\tau, b, v_r, \Theta)]^* = 6R_z(R_x - iR_y)/R^5 , \quad \text{(C8d)}$$

$${}^{11}A^2_0(\tau, b, v_r, \Theta) = 3(R^2 - 3R_z^2)/6^{1/2}R^5 . \quad \text{(C8e)}$$

It should be noted that the RAIC cross sections depend only on the quantity

$${}^{pp'}_{kk'}A_{K'}(b, v_r; \Delta) = {}^{kk'}A^{K'}_{Q'}(b, v_r, \Theta; \Delta)\overline{{}^{pp'}\Lambda^{K'}_{Q'}(b, v_r, \Theta; \Delta)}^* . \quad \text{(C9)}$$

The fact that $A_{K'}$ is independent of Θ follows directly from Eq. (15) and the orthogonality properties of the rotation matrices; from a physical viewpoint, this result is to be expected since the calculated cross sections cannot depend on the choice of the reference geometry $\Theta = 0$.

Straight-line trajectories

Under the assumption of straight-line collision trajectories, the various A's are easily calculated. Taking as a reference geometry $R_z = v\tau$, $R_y = 0$, $R_x = b$, and letting $(t_c^+ - t_c) \to \infty$ in Eqs. (C5) and (C7), one obtains

$$A^{11}_{11}(b, v_r, 0; \Delta) = -e^{-i\Delta t_c}b^{-3} \times [\alpha K_1(\alpha) - \alpha^2 K_0(\alpha)] , \quad \text{(C10a)}$$

$$A^{11}_{10}(b, v_r, 0; \Delta) = -\sqrt{2}\,e^{-i\Delta t_c}b^{-3}\alpha^2 K_1(\alpha) , \quad \text{(C10b)}$$

$$A^{11}_{00}(b;\, v_r, 0;\Delta) = -2e^{-i\Delta t_c} b^{-3}$$

$$\times[\,\alpha^2 K_2(\alpha) - \alpha K_1(\alpha)]\,, \qquad \text{(C10c)}$$

$$^{11}A^2_2(b,\, v_r, 0;\Delta) = A^{11}_{11}(b,\, v_r, 0;\Delta)\,, \qquad \text{(C11a)}$$

$$^{11}A^2_1(b,\, v_r, 0;\Delta) = \sqrt{2}\, A^{11}_{10}(b,\, v_r, 0;\Delta)\,, \qquad \text{(C11b)}$$

$$^{11}A^2_0(b,\, v_r, 0;\Delta) = 3A^{11}_{10}(b,\, v_r, 0;\Delta)/\sqrt{6}\,, \qquad \text{(C11c)}$$

where

$$\alpha = \Delta b/v_r \qquad \text{(C12)}$$

and $K_i(\alpha)$ is a modified Bessel function. The dimensionless quantity

$$\zeta_K(\alpha) = b^4 \sum_{q} |^{11}A^K_Q(b,\, v_r;\Delta)|^2$$

is given by

$$D_K(\alpha) = \{\,2[\alpha K_1(\alpha) - \alpha^2 K_0(\alpha)]^2 + 8\alpha^{-1}[K_1(\alpha)]^2$$

$$+ 6[\alpha^2 K_2(\alpha) - \alpha K_1(\alpha)]^2\}\,\delta_{K2}\,. \qquad \text{(C13)}$$

The central tuning being $\alpha = 0$, Eq. (C13) reduces to

$$D_K(0) = 8\delta_{K2}\,. \qquad \text{(C14)}$$

---

*Permanent address.

[1] P. R. Berman, Phys. Rev. A 22, xxx (1980).

[2] Labels appearing on *both* sides of an equation are not to be summed over.

[3] The final-state density-matrix elements are the same whether calculated in the "normal" or the interaction representation, owing to condition (2).

[4] In RAIC I, a quantity $\Gamma^{ii_1}_{ff_1}(v_r, t_c)$ was defined giving the (complex) rate at which RAIC procedure yields a final-state density-matrix element ρ_{ff_1} from an initial one ρ_{ii_1}. If Eq. (11) is multiplied by the number of collisions per unit time with the impact parameter between b and $b+db$ and relative speed v_r, and if an average over b and $\vec{R}_c$ is performed one finds

$$(\partial\rho_{ff_1}(v_r, t_c)/\partial t)_{\rm RAIC} = \Gamma^{ii_1}_{ff_1}(v_r, t_c)\rho_{ii_1}(v_r, t_c),$$

where

$$\Gamma^{ii_1}_{ff_1}(v_r, t_c) = \mathcal{N}_A \mathcal{N}_A v_r \int 2\pi b\, db \int d\vec{R}_c R^{ii_1}_{ff_1}(b, v_r, \vec{R}_c, t_c),$$

$\mathcal{N}_a$ is the a-atom density, and the $\vec{R}_c$ integral is over the atom-field interaction volume.

[5] A. R. Edmonds, *Angular Momentum Theory in Quantum Mechanics* (Princeton University Press, New Jersey, 1957).

[6] In averaging over Θ, it has been assumed that all Θ are equally likely, which is equivalent to assuming a uniform distribution of relative velocities. If one or both of the atoms is velocity selected, this assumption is no longer strictly true. One can incorporate the effects of a nonuniform relative velocity distribution into the average over Θ, but the results take on a much more complicated form.

[7] The symbol $f'(f_1)$ as a superscript on ρ'^K_Q is a shorthand notation for $f'J_{f'}(f'J_{f'})$; consequently, there is no summation on $J_{f'}$ or $J_{f'_1}$ in Eqs. (23).

[8] M. G. Payne, V. E. Anderson, and J. E. Turner, Phys. Rev. A 20, 1032 (1979); E. J. Robinson, J. Phys. B [illegible] (in press).

[9] S. Haroche, in *High Resolution Laser Spectroscopy*, edited by K. Shimoda (Springer, Berlin, 1976), pp. 275–279.

[10] S. E. Harris, J. F. Young, W. R. Green, R. W. Falcone, J. Lukasik, J. C. White, J. R. Willison, M. D. Wright, and G. A. Zdasiuk, in *Laser Spectroscopy IV*, edited by H. Walther and K. W. Rothe (Springer, Berlin, 1979), p. 349 and references therein; C. Bréchignac, Ph. Cahuzac, and P. E. Toschek, Phys. Rev. A 21, 1969 (1980).

PRA10003 PLRAA,s01000AQ1343.2

Theory of collisionally aided radiative excitation in three-level systems

S. Yeh† and P. R. Berman

Department of Physics, New York University, 4 Washington Place, New York, New York 10003

(Received 18 March 1980)

A theory of collisionally aided radiative excitation (CARE) for three-level systems in the weak-field limit is presented. Cross sections for the excitation of three-level atoms by two off-resonant pulsed radiation fields in the presence of collisions with structureless perturbers are calculated. Analytic expressions for the cross sections as functions of atom-field detunings are obtained under usual classical-trajectory and rotating-wave approximations using perturbation theory for various regions of detunings. Examples for the resulting excitation line shapes are given mostly for van der Waals potentials. A dressed-atom picture of the CARE processes is discussed, emphasis is put on an interesting effect arising from the interference between the "stepwise" and "direct" channel of excitation. Such an interference effect manifests itself as modulations in the total excitation cross section as a function of relative interatomic speed in some cases.

PACS numbers: 32.70. – n, 32.80. – t, 34.10. + x

I. INTRODUCTION

In this paper, we present a theory of collisionally aided radiative excitation (CARE) for three-level systems in the weak-field limit. CARE in two-level systems has been the subject of many recent studies.[1] Approximation schemes, valid in different regions of atom-field detunings, have been used and verified by numerical calculations.[2] In three-level systems, however, calculations have been limited to a narrow range of detunings.[3] It is thus desirable to have a theory which is free from such limitations.

In Sec. II, we state the problem to be investigated and define the conditions under which the treatment of this paper are applicable. The complexity of a three-level CARE problem over its two-level counterpart is due partly to the fact that there are two detunings which can be independently varied. In addition, the collision-induced energy shifts of these three levels can be of either a positive or a negative sign (relative to the detunings), leading to different physical situations. It becomes necessary, for the convenience of presentation, to classify the cases according to the sizes and signs (relative to those of the collision-induced energy-level shifts) of the detunings. This is done in Sec. III. A "dressed-atom" picture of the physical processes will be given in Sec. IV with discussions of interesting interference effects for some cases. In Sec. V, the basic equations involved are given. The solutions and results for cases as classified in Sec. III are obtained in Sec. VI. In Sec. VII, we discuss the advantages of using CARE over conventional atom-atom collision techniques to study the atom-atom interactions. The paper is concluded in Sec. VIII. Appendices A and B provide some calculational details.

Supported by the U.S. Office of Naval Research under Contract No. N00014-77-C-0553.

II. THE PROBLEM

Consider a three-level active atom, which may have one of the configurations shown in Fig. 1 with level separations $\hbar\omega_{21}$ and $\hbar\omega_{32}$, subjected to two off-resonant incident pulsed radiation fields of frequencies ω and ω' and amplitudes $E(t)$ and $E'(t)$. The atom simultaneously undergoes a collision with a structureless perturber. Under some conditions to be stated in this section, we calculate the $1-3$ excitation cross section as a function of detunings.

The fields $E(t)$ and $E'(t)$ are assumed to drive only 1-2 and 2-3 transitions, respectively, with interactions characterized by the coupling strengths $\chi(t) = \mu_{12}E/2\hbar$ and $\chi'(t) = \mu_{23}E'/2\hbar$, respectively, where μ_{12} and μ_{23} are the dipole matrix elements of the respective transitions. The collisions are assumed to shift only the energies of the active-atomic levels without coupling them (sometimes referred to as adiabatic approximation), a generally good assumption in the case of electronic transitions in the optical regime because of the lack of interatomic potential curve crossings (except perhaps at extremely small internuclear distance which cannot be reached with ordinary thermal energy).

If the atom-field detunings Δ and Δ', defined as $\Delta = \omega - \omega_{21}$ and $\Delta' = \omega' - \omega_{32}$, are larger than the Doppler width, and/or if the incident pulsed fields are adiabatic, the excitation cross sections are negligibly small in the absence of collisions. In both cases, the collision can greatly enhance the excitation by either broadening the adiabaticity or shifting the energy levels of the active atom into resonance (or near resonance) with the external fields. We shall confine the discussion of this paper to detunings larger than the Doppler width and assume that the pulses are slow enough such

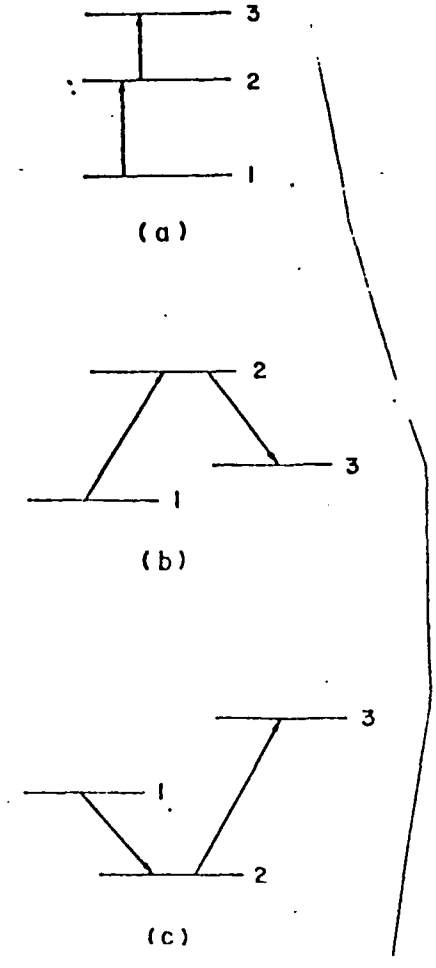

FIG. 1. Configurations of a three-level active atom for CARE. (a) Upward cascade, (b) inverse V, and (c) V.

that the pulse durations are much larger than the collision time, and that during a collision the field amplitudes are constants; that is,

$$|\Delta|, |\Delta'| \gg W_D, \tag{2.1}$$

where W_D is the Doppler width,

$$\lim_{t\to\infty} \chi(t), \chi'(t) = 0, \tag{2.2}$$

$$\frac{d\chi}{dt}, \frac{d\chi'}{dt} = 0, \tag{2.3}$$

and

$$\chi(t) = \chi_0, \chi'(t) = \chi_0' \tag{2.4}$$

during a collision.

In addition to conditions (2.1)-(2.4), the perturber density is assumed to be low enough that the time between collisions is much longer than the inverse of the detunings and the pulse durations. In such a pressure regime, one can take the CARE rate to be linear in the perturber density and calculate the CARE cross section for a single collision, from which the CARE rate is obtained by averaging over all possible collisions. This procedure is followed throughout this paper.

The conditions on the pulsed radiation [Eqs. (2.1)-(2.4)] can be met by ordinary laser pulses which have typical pulse lengths ($\gtrsim 10^{-9}$ sec) much longer than the collision time ($\sim 10^{-12}$ sec). The pressure range we are considering is typically of the order of 10 Torr or less in order to satisfy the conditions stated above.

III. CLASSIFICATION

For the convenience of presentation, the three-level atom is assumed to have a configuration shown in Fig. 1(a), unless otherwise stated. The theory to be presented is equally applicable to other configurations with suitable changes of the signs of detunings and of the relative energy-level shifts.

Consider such a three-level active atom [Fig. 1(a)] undergoing a collision with a structureless perturber. The energy levels are shifted during a collision, as shown schematically in Fig. 2, for some specific collision impact parameter b and relative velocity v in a manner depending on the assumed interatomic potential. The relative shifts of these levels can lead to an increase or decrease in the atomic transition frequencies over their unperturbed values. In the case shown in Fig. 2(a), both the 1-2 and 2-3 transition frequencies decrease (shift toward the red), and one speaks of (relative) attractive interatomic potentials. Conversely, the transition frequencies increase for repulsive potentials. Although different combinations of attractive and repulsive potentials for the 1-2, 2-3, and 1-3 (two-photon) transitions may occur in a three-level system, we shall be concerned only with attractive interatomic potentials. This restriction (to the attractive relative interatomic potentials) is for the convenience of the presentation; the theory to be presented is, nevertheless, applicable to all types of interatomic potentials.

What is essential in the theory is the existence (or lack thereof) of the collision-induced instantaneous resonances during a collision. When the detunings equal (both in signs and in magnitudes) the relative energy-level shifts, resonances occur. In Fig. 2(a), instantaneous resonances occur at $\pm\tau_0$ for 1-2 transitions, $\pm\tau_0'$ for 2-3 transition, and $\pm\tau_0''$ for 1-3 two-photon transition. Such instantaneous resonances enhance the absorption of radiation, especially in the case of large detunings.

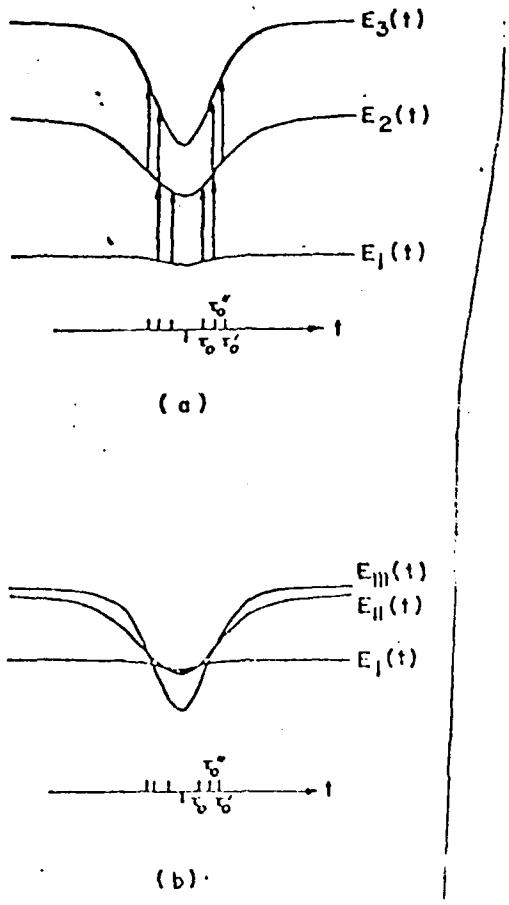

FIG. 2. Energy levels of a three-level active atom during a collision, schematically shown for a relatively attractive interatomic potential. (a) In a bare-state–classical-field picture, the energy levels, thus the detunings, are time dependent. As shown, resonances occur at $\pm\tau_0$ for 1-2 transition, $\pm\tau_0'$ for 2-3 transition, and $\pm\tau_0''$ for 1-3 two-photon transition. (b) In a dressed-state picture, the resonance points in (a) are transformed into level crossings of the dressed states.

The studies of two-level CARE (Ref. 2) have led to the understanding that the instantaneous resonances are important when the detunings are much larger than the inverse collision time τ_c^{-1}, i.e., $|\text{detuning}|\tau_c \gg 1$. For $|\text{detuning}|\tau_c \ll 1$ [impact region (I)], the existence or lack thereof of instantaneous resonances is unimportant, and the absorption cross section varies as $|\text{detuning}|^{-2}$, irrespective of the sign of the detuning. The case of $|\text{detuning}|\tau_c \sim 1$ can be divided into two regions according to the sign of the detuning relative to the interatomic potential: the quasistatic (Q) region where the instantaneous resonances can occur (e.g., red detunings for attractive potentials), and the antistatic (A) regions where *no* instantaneous resonance can occur (e.g., blue detunings for attractive potentials).[4] In the three-level problem, classification of the cases is complicated by the possible combinations of I, Q, and A regions for Δ, Δ', and $\Delta+\Delta'$. If there is no constraint, there would be a total of 27 cases to be discussed; the fact that $\Delta+\Delta'$ cannot be independently varied and that we restrict our discussion to attractive potentials reduces the number to 13 cases.

The cases to be considered are listed in Table I according to the region of each detuning. In the third column, the conditions, appropriate for attractive potentials only, are also listed to help clarify the cases considered. In subsequent sections, results are given mainly for attractive van der Waals potentials, although the treatments are generally applicable to other types of potentials. Table I exhausts all possible cases where attractive potentials only are considered. It does not, however, include all cases for a general interatomic potential. We choose not to include all possible cases because it is impractical to do so and may lead to confusion. At any rate, for the cases *not* included, one can find applicable treatments in one of the cases included.

It is natural to group together the cases in Table I for which the mathematical treatments are similar. In Sec. VI, we present the solutions and the results according to these groups. We group cases A, B, and C (Δ in the I region), cases D and E (Δ' in the I region), and cases F and G ($\Delta+\Delta'$ in the I region). Cases H and I, which have two of the three detunings in the Q region and the third detuning in the A region, will be grouped together. Case J, with all three detunings in the Q region, is the last and the most interesting case to be treated. Cases K and M will not be discussed since at least two of the detunings are in the A region, leading to exponentially small excitation cross sections. Although numerical calculations can be performed to obtain cross sections for these cases, reliable analytic approximation schemes have yet to be developed.

IV. THE DRESSED-ATOM PICTURE AND GENERAL CONSIDERATIONS

In this section we shall give a general description of the physical processes in terms of the "dressed-atom" picture[5] (sometimes referred to as the atom-field adiabatic representation)[6] in which the eigenstates of the Hamiltonian of free atom + free fields + atom-field interactions (i.e.,

TABLE I. Classification of cases.

Δ	Δ'	$\Delta+\Delta'$	Conditions appropriate for attractive potentials	Case
I	I	I	$\lvert\Delta\rvert\tau_c \ll 1$, $\lvert\Delta'\rvert\tau_c \ll 1$, $\lvert\Delta+\Delta'\rvert\tau_c \ll 1$	A
I	Q	Q	$\lvert\Delta\rvert\tau_c \ll 1$, $\lvert\Delta'\rvert\tau_c \gtrsim 1$, $\lvert\Delta+\Delta'\rvert\tau_c \gg 1$, $\Delta'<0, \Delta+\Delta'<0$	B
I	A	A	$\lvert\Delta\rvert\tau_c \ll 1$, $\lvert\Delta'\rvert\tau_c \gg 1$, $\lvert\Delta+\Delta'\rvert\tau_c \gg 1$, $\Delta'>0, \Delta+\Delta'>0$	C
Q	I	Q	$\lvert\Delta\rvert\tau_c \gg 1$, $\lvert\Delta'\rvert\tau_c \ll 1$, $\lvert\Delta+\Delta'\rvert\tau_c \gg 1$, $\Delta<0, \Delta+\Delta'<0$	D
A	I	A	$\lvert\Delta\rvert\tau_c \gg 1$, $\lvert\Delta'\rvert\tau_c \ll 1$, $\lvert\Delta+\Delta'\rvert\tau_c \gg 1$, $\Delta>0, \Delta+\Delta'>0$	E
Q	A	I	$\lvert\Delta\rvert\tau_c \gg 1$, $\lvert\Delta'\rvert\tau_c \gg 1$, $\lvert\Delta+\Delta'\rvert\tau_c \ll 1$, $\Delta<0, \Delta'>0$	F
A	Q	I	$\lvert\Delta\rvert\tau_c \gg 1$, $\lvert\Delta'\rvert\tau_c \gg 1$, $\lvert\Delta+\Delta'\rvert\tau_c \ll 1$, $\Delta>0, \Delta'<0$	G
Q	A	Q	$\lvert\Delta\rvert\tau_c \gg 1$, $\lvert\Delta'\rvert\tau_c \gg 1$, $\lvert\Delta+\Delta'\rvert\tau_c \gg 1$, $\Delta<0, \Delta'>0, \Delta+\Delta'<0$	H
A	Q	Q	$\lvert\Delta\rvert\tau_c \gg 1$, $\lvert\Delta'\rvert\tau_c \gg 1$, $\lvert\Delta+\Delta'\rvert\tau_c \gg 1$, $\Delta>0, \Delta'<0, \Delta+\Delta'<0$	I
Q	Q	Q	$\lvert\Delta\rvert\tau_c \gg 1$, $\lvert\Delta'\rvert\tau_c \gg 1$, $\lvert\Delta+\Delta'\rvert\tau_c \gg 1$, $\Delta<0, \Delta'<0, \Delta+\Delta'<0$	J
Q	A	A	$\lvert\Delta\rvert\tau_c \gg 1$, $\lvert\Delta'\rvert\tau_c \gg 1$, $\lvert\Delta+\Delta'\rvert\tau_c \gg 1$, $\Delta<0, \Delta'>0, \Delta+\Delta'>0$	K[a]
A	Q	A	$\lvert\Delta\rvert\tau_c \gg 1$, $\lvert\Delta'\rvert\tau_c \gg 1$, $\lvert\Delta+\Delta'\rvert\tau_c \gg 1$, $\Delta>0, \Delta'<0, \Delta+\Delta'>0$	L[a]
A	A	A	$\lvert\Delta\rvert\tau_c \gg 1$, $\lvert\Delta'\rvert\tau_c \gg 1$, $\lvert\Delta+\Delta'\rvert\tau_c \gg 1$, $\Delta>0, \Delta'>0, \Delta+\Delta'>0$	M[a]

[a] Not treated in this paper.

atomic dressed states) are taken as stationary states and the collision, which couples the dressed states as well as shifts their energies, is treated as a perturbation. The dressed states are generally linear combinations of the "bare states" (i.e., eigenstates of free atom + free-field Hamiltonian) and, in the weak-field limit, can be approximated as

$$
\begin{aligned}
|\mathrm{I}\rangle &= (1-\chi^2/2\Delta^2)|1,n,n'\rangle + (\chi/\Delta)|2,n-1,n'\rangle + [\chi\chi'/\Delta(\Delta+\Delta')]|3,n-1,n'-1\rangle,\\
|\mathrm{II}\rangle &= (-\chi/\Delta)|1,n,n'\rangle + (1-\chi^2/2\Delta^2-\chi'^2/2\Delta'^2)|2,n-1,n'\rangle + (\chi'/\Delta')|3,n-1,n'-1\rangle,\\
|\mathrm{III}\rangle &= [\chi\chi'/\Delta'(\Delta+\Delta')]|1,n,n'\rangle - (\chi'/\Delta')|2,n-1,n'\rangle + (1-\chi'^2/2\Delta'^2)|3,n-1,n'-1\rangle,
\end{aligned}
\tag{4.1}
$$

with eigenenergies

$$
\begin{aligned}
E_{\mathrm{I}} &= E_1 + n\hbar\omega + n'\hbar\omega' + \chi^2/\Delta,\\
E_{\mathrm{II}} &= E_2 + (n-1)\hbar\omega + n'\hbar\omega' - \chi^2/\Delta + \chi'^2/\Delta',\\
E_{\mathrm{III}} &= E_3 + (n-1)\hbar\omega + (n'-1)\hbar\omega' - \chi'^2/\Delta',
\end{aligned}
\tag{4.2}
$$

where E_1, E_2, and E_3 are energies of the atomic states 1, 2, and 3, respectively, with separations $E_2 - E_1 = \hbar\omega_{21}$ and $E_3 - E_2 = \hbar\omega_{32}$; the fields are represented by number states with photon numbers n and n' for fields E and E', respectively. For adiabatic pulses χ and χ', n and n' take on the instantaneous values.

In the weak-field limit, from Eqs. (4.1), the dressed states $|\mathrm{I}\rangle$, $|\mathrm{II}\rangle$, and $|\mathrm{III}\rangle$ are composed almost entirely of only states $|1,n,n'\rangle$, $|2,n-1,n'\rangle$, and $|3,n-1,n'-1\rangle$, respectively, with some small corrections; their energy separation are approximately $E_{\mathrm{II}} - E_{\mathrm{I}} \simeq -\Delta$, $E_{\mathrm{III}} - E_{\mathrm{II}} \simeq -\Delta'$, and $E_{\mathrm{III}} - E_{\mathrm{I}} \simeq -(\Delta+\Delta')$; during a collision, the time dependence of E_{I}, E_{II}, and E_{III} are almost the same as E_1, E_2, and E_3. Thus, the instantaneous resonance points in Fig. 2(a) (i.e., $\pm\tau_0$, $\pm\tau_0'$, and $\pm\tau_0''$) are transformed into crossing points as shown in Fig. 2(b), and a physical picture of CARE can be established similar to that of ordinary (radiationless) inelastic atomic collision, which has been under active research for several decades.

The coupling between the dressed states by the collision is characterized by the off-diagonal matrix elements

$$
\begin{aligned}
\langle \mathrm{I}|U(t)|\mathrm{II}\rangle &= \langle \mathrm{II}|U(t)|\mathrm{I}\rangle \simeq (\chi/\Delta)V(t),\\
\langle \mathrm{II}|U(t)|\mathrm{III}\rangle &= \langle \mathrm{III}|U(t)|\mathrm{II}\rangle \simeq (\chi'/\Delta')V'(t),\\
\langle \mathrm{I}|U(t)|\mathrm{III}\rangle &= \langle \mathrm{III}|U(t)|\mathrm{I}\rangle\\
&\simeq [\chi\chi'/\Delta(\Delta+\Delta')]V'(t) + [\chi\chi'/\Delta'(\Delta+\Delta')]V(t),
\end{aligned}
\tag{4.3}
$$

where $U(t)$ is the collision interaction which is diagonal in the atomic bare-state basis. $V(t) = \langle 2|U(t)|2\rangle - \langle 1|U(t)|1\rangle$ and $V'(t) \equiv \langle 3|U(t)|3\rangle - \langle 2|U(t)|2\rangle$ are the collision-induced relative energy-level shifts between states 1, 2 and states 2, 3, respectively. The off-diagonal matrix element $\langle \mathrm{I}|U(t)|\mathrm{III}\rangle$ is responsible for the "direct" (I $\leftrightarrow$ III) excitation corresponding to two photon absorption in the bare-state picture, while $\langle \mathrm{I}|U(t)|\mathrm{II}\rangle$ and $\langle \mathrm{II}|U(t)|\mathrm{III}\rangle$ form the chain for "stepwise" (I $\leftrightarrow$ II $\leftrightarrow$ III) excitation. By studying these matrix elements we can better understand dominant excitation processes in different regions of detunings. It is clear that when $|\Delta+\Delta'| \ll |\Delta|, |\Delta'|$, the direct process is the dominant one. When $|\Delta|$ (or $|\Delta'|$) is smaller than the other two detunings, Eq. (4.3) suggest that the "direct"

and the "stepwise" processes have comparable contributions. However, as we shall see later, cancellation between the two processes occurs, and the stepwise process remains dominant. This will be seen when the detailed calculations are given.

In the above discussion, the effects of the collision-induced curve crossings (i.e., of the collision-induced shifts of the dressed states) have not been included. As discussed earlier, the crossings are particularly important when the detunings are large, corresponding to large separations between the dressed states. When the detunings are small (corresponding to small-level separations between the dressed states), however, the crossings do not provide major contributions to the excitation, since Fourier frequencies are induced by the collision to cover the energy mismatch. To show the importance of curve crossings, we choose, in the remainder of this section, to discuss only the case where all the detunings are in the Q region, since an interesting interference effect occurs in this limit.

The interference effect is better described using a classical-trajectory approximation of the collision event. In this approximation, crossings, as shown in Fig. 2(b) in the time domain, occur at corresponding internuclear distances $R(\tau_0) = R_0$, $R(\tau_0') = R_0'$, and $R(\tau_0'') = R_0''$. For collision impact parameters such that the closest approach between the active atom and the perturber is smaller than R_0, R_0', and R_0'', all the crossings occur during the collision. For larger impact parameters, some or all of the crossings are not induced, and the excitation probability is reduced (as compared to the all-crossing case) by orders of magnitude. Hence, collisions with larger impact parameters do not contribute significantly to the excitation cross section and can be ignored. Consequently, we consider only the collisions with impact parameters small enough to induce all the crossings. Furthermore, since the radiation pulses are assumed to be adiabatic, the atom-field system is in its dressed state $|\mathrm{I}\rangle$ before the collision (which comes from adiabatic following of bare atomic state 1), and only the dressed state $|\mathrm{III}\rangle$ will adiabatically follow the pulses back to bare atomic state 3. Hence, calculating the $|\mathrm{I}\rangle \rightarrow |\mathrm{III}\rangle$ transition probability is equivalent to calculating the $1 \rightarrow 3$ transition probability.

When the detunings are large ($|\Delta|$, $|\Delta'|$, $|\Delta + \Delta'| \gg$ inverse collision time), all the transitions occur well localized near the crossings. It is not difficult to see that there are four channels for the $|\mathrm{I}\rangle \rightarrow |\mathrm{III}\rangle$ transition to occur, two from the stepwise process ($\mathrm{I} \rightarrow \mathrm{II} \rightarrow \mathrm{III}$) and two from the direct process ($\mathrm{I} \rightarrow \mathrm{III}$). With reference to Fig. 2(b), these four channels are

$$\left.\begin{matrix} |\mathrm{I}\rangle \xrightarrow[-\tau_0]{} |\mathrm{II}\rangle \xrightarrow[\tau_0]{} |\mathrm{III}\rangle \\ |\mathrm{I}\rangle \xrightarrow[\tau_0]{} |\mathrm{II}\rangle \xrightarrow[\tau_0']{} |\mathrm{III}\rangle \end{matrix}\right\} \text{stepwise}$$

$$\left.\begin{matrix} |\mathrm{I}\rangle \xrightarrow[-\tau_0'']{} |\mathrm{III}\rangle \\ |\mathrm{I}\rangle \xrightarrow[\tau_0'']{} |\mathrm{III}\rangle \end{matrix}\right\} \text{direct},$$

where the time below the arrows correspond to the crossing times shown in Fig. 2(b) and indicate when each transition takes place. Each of these four channels contributes to the $|\mathrm{I}\rangle \rightarrow |\mathrm{III}\rangle$ transition amplitude, and interference between them can exhibit interesting phenomena. In a recent article,[7] we have demonstrated that this interference effect gives rise to an oscillatory structure in the total excitation cross section as a function of the active-atom-perturber relative speed when the crossings are well separated and the interatomic potentials are such that the "stepwise" and "direct" processes have comparable contributions to the transition amplitude. This effect is similar to that discussed by Rosenthal and Foley[8,9] regarding He-He$^+$ charge-exchange inelastic collision in which the atom-ion interatomic potential curves are similar to those of CARE in the dressed-atom diabatic representation discussed here. In this paper, we provide a detailed calculation to supplement the discussion in Ref. 7. This interference phenomena is quite general and should be expected to occur in many systems where excitation is possible *via* several channels.

The interference effect discussed above requires a special crossing configuration, i.e., three well-separated crossings occurring at R_0, R_0', and R_0''. Since the existence of crossings and their positions and slopes depend on the interatomic potential as well as the detunings, other crossing configurations may occur leading to different manifestations of the interference effect in the total excitation cross section. In this paper, a treatment for the general case is given, and results for special cases follow.

We note that the interference between the stepwise and the direct processes occurs even in the case of small detunings. However, the interference does not give rise to interesting effects such as the oscillatory total excitation cross sections discussed above for the case of large detunings because, in the case of small detunings, the transitions do not occur at well-defined instants, which is required to obtain a definite phase relationship between amplitudes arising from the stepwise and the direct processes.

V. THE HAMILTONIAN AND THE EQUATIONS OF MOTION

The equations of motion to be derived in this section do not differ for quantized or classical fields. To be more in line with the discussion in the dressed-atom picture given earlier, we take the fields to be quantized and use the photon-number representation; however, the calculation is carried out in the bare-atom picture. Let us consider a system consisting of a three-level active atom interacting with two external fields and a perturber atom. The Hamiltonian of this system can be written as

$$H = H_A + H_R + H_{AR} + U(t), \tag{5.1}$$

where the following hold. (i) The free-atom Hamiltonian H_A has three eigenstates $|1\rangle, |2\rangle, |3\rangle$ with eigenenergies E_1, E_2, and E_3; $E_2 - E_1 = \hbar\omega_{21}$ and $E_3 - E_2 = \hbar\omega_{32}$. (ii) $H_R = \hbar\omega a_\omega^\dagger a_\omega + \hbar\omega' a_{\omega'}^\dagger a_{\omega'}$ is the quantized free-field Hamiltonian describing a two-mode external field with photon energies $\hbar\omega$ and $\hbar\omega'$, where $a_\omega^\dagger$, $a_{\omega'}^\dagger$, and $a_\omega, a_{\omega'}$ are the usual creation and annihilation operators of the photons for each mode. (iii) The active-atom-field interaction is given in the rotating-wave approximations by

$$H_{AR} = \hbar\xi_\omega (a_\omega R_{12}^\dagger + a_\omega^\dagger R_{12}) + \hbar\xi_{\omega'} (a_{\omega'} R_{23}^\dagger + a_{\omega'}^\dagger R_{23}), \tag{5.2}$$

where $R_{12}^\dagger$, $R_{23}^\dagger$ and R_{12}, R_{23} are the raising and lowering operators of the active-atomic states, the indices referring to the transition involved, and ξ_ω and $\xi_{\omega'}$ are the coupling constants related to the interaction strengths introduced in Sec. I by $\chi = n^{1/2}\xi_\omega$ and $\chi' = n'^{1/2}\xi_{\omega'}$ with n, n' the photon numbers. (iv) The effective interaction with the perturber $U(t)$ is taken to be time dependent, since the internuclear motion is not quantized, and is diagonal in the basis of $|1,n,n'\rangle$, $|2,n-1,n'\rangle$, and $|3,n-1,n'-1\rangle$ (eigenstates of $H_A + H_R$),

$$V_1(t) = \langle 1,n,n'|U(t)|1,n,n'\rangle,$$
$$V_2(t) = \langle 2,n-1,n'|U(t)|2,n-1,n'\rangle,$$
$$V_3(t) = \langle 3,n-1,n'-1|U(t)|3,n-1,n'-1\rangle \tag{5.3}$$

$$\langle 1,n,n'|U(t)|2,n-1,n'\rangle = \langle 2,n-1,n'|U(t)|3,n-1,n'-1\rangle = \langle 3,n-1,n'-1|U(t)|1,n,n'\rangle = 0,$$

owing to the absence of inelastic collisions.

The wave function of the system

$$|\Psi(t)\rangle = C_1(t)\, e^{-i(E_1 + n\hbar\omega + n'\hbar\omega')t/\hbar} + C_2(t)\, e^{-i(E_2 + (n-1)\hbar\omega + n'\hbar\omega')t/\hbar} + C_3(t)\, e^{-i(E_3 + (n-1)\hbar\omega + (n'-1)\hbar\omega')t/\hbar}$$

satisfies the time-dependent Schrödinger equation

$$i\hbar \frac{\partial}{\partial t}|\Psi(t)\rangle = H|\Psi(t)\rangle,$$

from which the equation of motion for the probability amplitudes $C_1(t)$, $C_2(t)$, and $C_3(t)$ are obtained,

$$\begin{aligned} i\dot{C}_1 &= C_1 V_1(t) + \chi C_2 e^{i\Delta t}, \\ i\dot{C}_2 &= \chi C_1 e^{-i\Delta t} + C_2 V_2(t) + \chi' C_3 e^{i\Delta' t}, \\ i\dot{C}_3 &= \chi' C_2 e^{-i\Delta' t} + C_3 V_3(t). \end{aligned} \tag{5.4}$$

With the substitution

$$C_1 = \tilde{C}_1 \exp\left(-i\int_{-\infty}^{t} V_1(t')dt'\right),$$

$$C_2 = \tilde{C}_2 \exp\left(-i\int_{-\infty}^{t} V_2(t')dt'\right),$$

and

$$C_3 = \tilde{C}_1 \exp\left(-i\int_{-\infty}^{t} V_3(t')dt'\right),$$

the equations become

$$\begin{aligned} i\dot{\tilde{C}}_1 &= \chi \tilde{C}_2 \exp\left[i\left(\Delta t - \int_{-\infty}^{t} V(t')dt'\right)\right], \\ i\dot{\tilde{C}}_2 &= \chi \tilde{C}_1 \exp\left[-i\left(\Delta t - \int_{-\infty}^{t} V(t')dt'\right)\right] + \chi' \tilde{C}_3 \left[i\left(\Delta' t - \int_{-\infty}^{t} V'(t')dt'\right)\right], \\ i\dot{\tilde{C}}_3 &= \chi' \tilde{C}_2 \exp\left[-i\left(\Delta' t - \int_{-\infty}^{t} V'(t')dt'\right)\right], \end{aligned} \tag{5.5}$$

where $V(t) = V_2(t) - V_1(t)$ and $V'(t) = V_3(t) - V_2(t)$ are the relative energy shifts of the active-atomic levels during a collision. All the relaxation rates are neglected in this equation owing to the condition of large detunings in Eqs. (2.1)–(2.4).

Equations (5.5) will be solved using the perturbation theory with the initial conditions $\tilde{C}_1(t=-\infty) = 1$, $\tilde{C}_2(t=-\infty) = 0$, and $\tilde{C}_3(t=-\infty) = 0$ corresponding to a three-level atom initially prepared in state 1. The probability of exciting the atom to state 3 is given by $|\tilde{C}_3(t=\infty)|^2$, and the corresponding total cross section is obtained by integrating over the impact parameter b,

$$\sigma = \int_0^\infty |\tilde{C}_3(t=\infty)|^2 2\pi b\, db. \tag{5.6}$$

VI. SOLUTIONS AND RESULTS

In the perturbation limit, Eqs. (5.5) are easily solved to obtain a formal expression for $\tilde{C}_3(t=\infty)$,

$$\tilde{C}_3(t=\infty) = -\int_{-\infty}^{\infty} \chi'(t) \exp\left[-i\left(\Delta' t - \int_0^t V'(t')dt'\right)\right] \int_{-\infty}^{t} \chi(t_1) \exp\left[i\left(\Delta t_1 - \int_0^{t_1} V(t')dt'\right)\right] dt_1 dt, \quad (6.1)$$

where an overall phase factor has been suppressed since it does not change the probability $|\tilde{C}_3(t=\infty)|^2$.

Equation (6.1) has to be evaluated using different techniques in different regions of detunings corresponding to different physical situations. We follow the classification of Table I.

A. Cases A, B, C

In this group, Δ is in the I region. We integrate by parts the t_1 integral in Eq. (6.1), neglecting the term containing $d\chi'/dt$ owing to the conditions (2.1)–(2.4), and obtain

$$\tilde{C}_3(t=\infty) = \frac{1}{i\Delta}\left\{\int_{-\infty}^{\infty} \chi(t)\chi'(t) \exp\left[-i\left((\Delta+\Delta')t - \int_0^t [V(t')+V'(t')]dt'\right)\right] dt \right.$$
$$\left. - i\int_{-\infty}^{\infty} \chi'(t) \exp\left[-i\left(\Delta' t - \int_0^t V'(t')dt'\right)\right] \int_{-\infty}^{t} \chi(t_1) V(t_1) \exp\left[-i\left(\Delta t_1 - \int_0^{t_1} V(t')dt'\right)\right] dt_1 dt\right\}. \quad (6.2)$$

Since $\chi(t)$ is a constant χ_0 over the range of $V(t)$, and $|\Delta|\tau_c \ll 1$, we can take $\chi(t_1)$ out of the t_1 integral in the second term of Eq. (6.2) and set $e^{-i\Delta t_1} \simeq 1$. One finds

$$\tilde{C}_3(t=\infty) = \frac{1}{i\Delta}\left\{\int_{-\infty}^{\infty} \chi(t)\chi'(t) \exp\left[-i\left((\Delta+\Delta')t - \int_0^t [V(t')+V'(t')]dt'\right)\right] dt \right.$$
$$- \chi_0 \int_{-\infty}^{\infty} \chi'(t) \exp\left[-i\left(\Delta' t - \int_0^t [V(t')+V'(t')]dt'\right)\right] dt$$
$$\left. + \chi_0 \int_{-\infty}^{\infty} \chi'(t) \exp\left[-i\left(\Delta' t - \int_0^t V'(t')dt'\right)\right] dt\right\}. \quad (6.3)$$

Up to this point, we have used the assumptions that the field, $E(t)$, is a slow pulse and that Δ is in the I region, which are common to all three cases A, B, and C. Further evaluation of Eq. (6.3) involves the other field, $E'(t)$, and the other detunings, Δ' and $\Delta+\Delta'$.

1. Case A

In this case, all the detunings are in the I region. We use the same technique used to obtain Eq. (6.3) from Eq. (6.2) to evaluate the integrals in Eq. (6.3). Namely, we integrate by parts once on each of these integrals, neglect the terms containing the derivatives of $\chi(t)$ and $\chi'(t)$, replace $e^{-i\Delta t}$, $e^{-\Delta' t}$, and $e^{-i(\Delta+\Delta')t}$ by 1, and set $\chi'(t) = \chi_0'$ to obtain the excitation amplitude

$$\tilde{C}_3(t=\infty) = -\chi_0\chi_0'\left(\frac{1-e^{i\theta'}}{\Delta\Delta'} - \frac{1-e^{i(\theta+\theta')}}{\Delta'(\Delta+\Delta')}\right), \quad (6.4)$$

where $\theta = \int_{-\infty}^{\infty} V(t')dt'$ and $\theta' = \int_{-\infty}^{\infty} V'(t')dt'$ are the usual impact phases associated with pressure broadening theories.[10] The amplitude depends on the collision impact parameter b, implicitly through $V(t)$ and $V'(t)$.

The excitation probability is obtained by squaring Eq. (6.4):

$$|\tilde{C}_3(t=\infty)|^2 = \chi_0^2\chi_0'^2\left(\frac{2(1-\cos\theta)}{\Delta\Delta'^2(\Delta+\Delta')} + \frac{2(1-\cos\theta')}{\Delta^2\Delta'(\Delta+\Delta')}\right.$$
$$\left. - \frac{2(1-\cos\theta'')}{\Delta\Delta'(\Delta+\Delta')^2}\right), \quad (6.5)$$

with $\theta'' = \theta + \theta'$. Equation (6.5) exhibits some interesting features. The first term dominates when $|\Delta'| \ll |\Delta|, |\Delta+\Delta'|$, and only the impact phase associated with the 1-2 transition θ appears. This suggests that the collisionally enhanced excitation to state 3 is determined by the collision rate associated with the 1-2 transition only. When $|\Delta| \ll |\Delta'|, |\Delta+\Delta'|$, the second term dominates, and the only relevant collision rate is that associated with the 2-3 transition. From the point of view of CARE, these two terms can be regarded as "stepwise," since no collision rate associated with 1-3 transition in involved. When $|\Delta+\Delta'| \ll |\Delta|, |\Delta'|$, however, the third term dominates, indicating that the "direct" process is responsible for the excitation. When $|\Delta|$, $|\Delta'|$ and $|\Delta+\Delta'|$ are comparable, contributions from both the "direct" and the "stepwise" processes interfere with each other.

The excitation cross section is obtained by integrating Eq. (6.5) over the impact parameter [i.e., Eq. (5.6)]:

$$\sigma = \frac{4\pi\chi_0^2\chi_0'^2}{\Delta\Delta'(\Delta+\Delta')}\left(\frac{A}{\Delta'} + \frac{B}{\Delta} + \frac{C}{\Delta+\Delta'}\right), \quad (6.6)$$

where

$$A=\int_0^\infty (1-\cos\theta)b\,db\,,$$

$$B=\int_0^\infty (1-\cos\theta')b\,db\,,$$

$$C=\int_0^\infty (\cos\theta''-1)b\,db\,.$$

This result does not specify the type of interatomic potential. For a given potential, A, B, and C can be calculated analytically or numerically. For van der Waals potentials with the straight-line-trajectory approximation

$$V(t)=C_{\rm VDW}/[R(t)]^6$$

and

$$V'(t)=C'_{\rm VDW}/[R(t)]^6$$

with $R(t)=(b^2+v^2t^2)^{1/2}$, analytic results can be obtained,

$$\sigma=\frac{4\pi\chi_0^2\chi_0'^2}{\Delta\Delta'(\Delta+\Delta')}\left(\frac{3\pi}{8v}\right)^{2/5}(-\Gamma(-\tfrac{2}{5})\cos\tfrac{1}{5}\pi)$$
$$\times\left(\frac{|C_{\rm VDW}|^{2/5}}{\Delta'}+\frac{|C'_{\rm VDW}|^{2/5}}{\Delta}-\frac{|C''_{\rm VDW}|^{2/5}}{\Delta+\Delta'}\right),\qquad(6.7)$$

with

$$-\Gamma(-\tfrac{2}{5})\cos(\tfrac{1}{5}\pi)\approx 3\,;$$

where v is the active-atom-perturber relative speed and $C''_{\rm VDW}=C_{\rm VDW}+C'_{\rm VDW}$.

2. Case B

Since Δ' and $\Delta+\Delta'$ are in the Q region, the integrals appearing in Eq. (6.3) can be evaluated by the stationary-phase method.[11] The first term and the second term in Eq. (6.3) cancel each other approximately because of the condition $|\Delta|\tau_c \ll 1$. The third term yields

$$\tilde C_3(t=\infty)=(-i\chi_0 b'_Q/\Delta)(\pi/\alpha')^{1/2}2\cos(\phi'+\tfrac{1}{4}\pi)\,,\qquad(6.8)$$

where

$$\alpha'=\frac{1}{2}\left|\left(\frac{dV'}{dt}\right)_{\tau_0'}\right|,\quad \phi'=-\Delta'\tau_0'+\int_0^{\tau_0'}V'(t')dt'$$

and τ_0' is the stationary-phase point defined to be the positive solution of $V'(t')=\Delta'$.

In obtaining Eq. (6.8), we have assumed that the impact parameter b is small enough such that the crossings are induced during a collision (i.e., we neglect collisions with large impact parameter which do not contribute significantly to the total cross section since no crossing is induced), and that $t=0$ is the time of closest approach between the active atom and the perturber.

Apart from the factor χ_0/Δ, Eq. (6.8) takes the form of the two-level result,[12] and a standard treatment for obtaining the total excitation cross section can be used. The excitation probability is obtained by taking the square of Eq. (6.8)

$$|\tilde C_3(t=\infty)|^2=(\chi_0^2\chi_0'^2/\Delta^2)(\pi/\alpha')4\cos^2(\phi'+\tfrac{1}{4}\pi)\,,\qquad(6.9)$$

from which the total excitation cross section is calculated using

$$\sigma=\int_0^{R_0'}|\tilde C_3(t=\infty)|^2 2\pi b\,db\,.\qquad(6.10)$$

The upper limit in this integral has been changed to R_0', the internuclear distance at which the instantaneous resonance for the 2-3 transition occurs, since for collision impact parameter larger than R_0', the excitation is negligibly small due to lack of crossings and Eq. (6.9) fails to be valid. Equation (6.9) diverges as the impact parameter approaches R_0'; however, Eq. (6.10) remains finite since α' varies as $(b^2-R_0'^2)^{1/2}$. The cutoff at R_0' may lead to an error of up to 15%, depending on the detuning. Better results can be achieved by numerical calculations for impact parameters near $b\simeq R_0'$, or by a uniform approximation[13] specially designed to overcome the difficulty of divergence.

For van der Waals potentials, $R_0'=(C'_{\rm VDW}/\Delta')^{1/6}$, and Eq. (6.10) leads to the total excitation cross section

$$\sigma=\frac{4\pi^2\chi_0^2\chi_0'^2}{3\Delta^2 v}|C'_{\rm VDW}|^{1/2}|\Delta'|^{-3/2},\qquad(6.11)$$

where $\cos^2(\phi'+\frac{1}{4}\pi)$ has been approximated by $\frac{1}{2}$, and v is the active-atom-perturber relative speed.

This result shows that the line shape varies as Δ^{-2} (since Δ is in the I region) and varies as $|\Delta'|^{-3/2}$, reflecting the fact that Δ' is in the Q region.[12]

3. Case C

In this case, Δ' and $\Delta+\Delta'$ are both in the A region. No crossing occurs for the 2-3 transition and the 1-3 two-photon transition at any collision impact parameter. Since Δ is in the I region ($|\Delta|\tau_c\ll 1$), the first two terms in Eq. (6.3) approximately cancel each other as in case B, leading to the excitation amplitude

$$\tilde C_3(t=\infty)=\frac{-i\chi_0}{\Delta}$$
$$\times\int_{-\infty}^{\infty}\chi'(t)\exp\left[-i\left(\Delta' t-\int_0^t V'(t')dt'\right)\right]dt\,.\qquad(6.12)$$

This equation is easily recognized as simply a two-level excitation amplitude (2-3 transition) multiplied by a factor χ_0'/Δ. Results for the two-level excitation probability are available from the numerical study of Yeh and Berman[2] for van der Waals potentials and Lennard-Jones–type potentials. Also available are approximate analytic results of Tvorogov and Fomin[11] and Szudy and Baylis[13] using saddle-point methods.[15] We now give only the essential features of the results. For details, the readers are referred to Ref. 2, 14, and 15.

The cross section, obtained by integrating $|\tilde{C}_3(t=\infty)|^2$ over the impact parameter b, shows a Δ^{-2} dependence as is clear from Eq. (6.12). The dependence on Δ' follows the antistatic wing behavior. For a van der Waals potential, Fig. 6 of Yeh and Berman[7] exhibits a line shape going as

$$|\Delta'|^{-7/3}\exp(-\beta|\Delta'|^{5/6})$$

with β a constant, which is in agreement with asymptotic results[14,15] to within a multiplicative factor of order 1.

B. Cases D, E

In these cases, Δ' is in the I region, while Δ and $\Delta+\Delta'$ are in the Q region (case D) or A region (case E). Since Δ' is in the I region, the integration-by-parts technique used in cases A, B, and C can be applied to the t integral in Eq. (6.1) for its evaluation.

We write Eq. (6.1) in the following form:

$$\tilde{C}_3(t=\infty) = -\int_{-\infty}^{\infty}\chi'(t)\exp\left[-i\left(\Delta' t - \int_0^t V'(t')dt'\right)\right]G(t)dt, \tag{6.13}$$

where

$$G(t) = \int_{-\infty}^{t}\chi(t_1)\exp\left[-i\left(\Delta t_1 - \int_0^{t_1}V(t')dt'\right)\right]dt_1. \tag{6.14}$$

An integration by parts is performed on Eq. (6.13), neglecting the term containing $d\chi'/dt$, setting $\chi'(t) = \chi_0'$ over the range of $V'(t)$, and setting $e^{-\Delta' t}\approx 1$ to obtain

$$\begin{aligned}\tilde{C}_3(t=\infty) = \frac{-i\chi_0'}{\Delta'}\Bigg\{&e^{i\theta'}\int_{-\infty}^{\infty}\chi(t)\exp\left[-i\left(\Delta t - \int_0^t V(t')dt'\right)\right]dt\\ &-\int_{-\infty}^{\infty}\chi(t)\exp\left[-i\left(\Delta t - \int_0^t [V(t')+V'(t')]dt'\right)\right]dt\\ &+\int_{-\infty}^{\infty}\chi(t)\exp\left[-i\left((\Delta+\Delta')t - \int_0^t [V(t')+V'(t')]dt'\right)\right]dt\Bigg\}.\end{aligned} \tag{6.15}$$

The second and the third terms approximately cancel each other because of the condition $|\Delta'|\tau_c \ll 1$, and we get

$$\tilde{C}_3(t=\infty) = \frac{-i\chi_0'}{\Delta'}e^{i\theta'} \times\int_{-\infty}^{\infty}\chi(t)\exp\left[-i\left(\Delta t - \int_0^t V(t')dt'\right)\right]dt, \tag{6.16}$$

where $\theta' = \int_{-\infty}^{\infty}V'(t')dt'$ is the impact phase[10] associated with the 2-3 transition.

Equation (6.16) is simply the 1-2 two-level transition amplitude multiplied by the factor $(\chi_0'/\Delta')e^{i\theta'}$. Its evaluation depends on the region of Δ. For case D (Δ in Q region) a stationary phase method[11] is used, and for case E (Δ in the A region) a method of steepest descent[16] or a numerical calculation[2] can be carried out.

1. Case D

The integral in Eq. (6.16) is evaluated using a stationary-phase method to yield

$$\tilde{C}_3(t=\infty) = (-i\chi_0\chi_0'/\Delta')e^{i\theta'}(\pi/\alpha)^{1/2}2\cos(\phi+\tfrac{1}{4}\pi), \tag{6.17}$$

where

$$\alpha = \frac{1}{2}\left|\left(\frac{dV}{dt}\right)_{t_0}\right|,$$

$$\phi = -\Delta\tau_0 + \int_0^{\tau_0}V(t')dt',$$

and τ_0 is the stationary-phase point of the integrand in Eq. (6.16), i.e., the solution of the equation $\Delta = V(t)$. τ_0 is taken to be positive, and we have taken $t=0$ to be the time of closest approach so that $\pm\tau_0$ are both stationary-phase points.

Equation (6.17) holds only for collision impact

tion cross section is given by

$$\sigma = \frac{4\pi\chi_0^2\chi_0'^2}{\Delta^2(\Delta+\Delta')^2}\left(\frac{3\pi C''_{VDW}}{8v}\right)^{2/5}\left(\frac{-\Gamma(-\frac{2}{5})\cos\frac{1}{5}\pi}{5}\right), \tag{6.24}$$

where $C''_{VDW} = C_{VDW} + C'_{VDW}$ is the van der Waals constant for the 1-3 relative potential, and $-\Gamma(-\frac{2}{5})\cos\frac{1}{5}\pi \approx \frac{3}{2}$.

The line shape varying as $\Delta^{-2}(\Delta+\Delta')^{-2}$ is typical of the impact region when the direct excitation process is dominant over the stepwise process. The line exhibits a Δ^{-2} rather than exponential Δ dependence, even though Δ is in the A region; in some sense, the direct excitation serves to break the adiabatic following of the field $\chi(t)$ on the 1-2 transition and changes the dependence from exponential to power law.

D. Cases II, I

In these two cases, Δ and Δ' are large ($|\Delta|\tau_c \gg 1$, $|\Delta'|\tau_c \gg 1$) and of opposite signs, and their sum $(\Delta+\Delta')$ is still in the Q region. We further focus our attention to the region of $|\Delta+\Delta'| \ll |\Delta|$, $|\Delta'|$. This region is of particular interest because the direct two-photon excitation process is dominant over the stepwise process and, by varying $|\Delta+\Delta'|$, the effects of stepwise process on the direct two-photon line shape can be determined. Moreover, this further restriction of detunings makes the mathematical treatment to be given below much simplified and equally applicable to both case II and case I.

If the condition $|\Delta+\Delta'| \ll |\Delta|, |\Delta'|$ holds, the instantaneous resonance for the direct (1 – 3) transition occurs at an internuclear distance (R_0'') much larger than that for the 1-2 transition (R_0) or the 2-3 transition (R_0') (i.e., $R_0'' \gg R_0, R_0'$). Thus, in the straight-line-path approximation, for collisions with impact parameter b such that $R_0'' > b > R_0, R_0'$, only the 1-3 instantaneous resonances occur during a collision. Collisions within this range of impact parameters give a major contribution to the total excitation cross section because of the condition $R_0'' \gg R_0, R_0'$, the weighting factor $b\,db$ in the definition of the total cross section [Eq. (5.6)], and the fact that collisions with impact parameters b larger than R_0'' do not contribute, due to lack of collision-induced resonance. Hence, we can do repeated integrations by parts on the t_1 integral in Eq. (6.1), each integration by parts producing a factor $|V(t)/\Delta| \ll 1$ for the range of impact parameters of importance determined by the $(\Delta+\Delta')$ crossing. The excitation amplitude is thus given, keeping only terms up to first order in $V(t)/\Delta$, by

$$\tilde{C}_3(t=\infty) = \frac{-i}{\Delta}\left\{\int_{-\infty}^{\infty}\chi(t)\chi'(t)\exp\left[-i\left((\Delta+\Delta')t - \int_0^t [V(t')+V'(t')]dt'\right)\right]dt + \int_{-\infty}^{\infty}\chi(t)\chi'(t)[V(t)/\Delta]\exp\left[-i\left((\Delta+\Delta')t - \int_0^t [V(t')+V'(t')]dt'\right)\right]dt\right\}. \tag{6.25}$$

Since $\Delta+\Delta'$ is in the Q region, Eq. (6.25) is evaluated using the stationary-phase method to obtain

$$\tilde{C}_3(t=\infty) = (-i\chi_0\chi_0'/\Delta)(\pi/\alpha'')^{1/2}2\cos(\phi'' + \tfrac{1}{4}\pi)[1 + V(\tau_0'')/\Delta], \tag{6.26}$$

where

$$\alpha'' = \frac{1}{2}\left|\left(\frac{d(V+V')}{dt}\right)_{\tau_0''}\right|,$$

$$\phi'' = -(\Delta+\Delta')\tau_0'' + \int_0^{\tau_0''}[V(t')+V'(t')]dt',$$

with $\tau_0'' > 0$ satisfying $\Delta+\Delta' = V(\tau_0'') + V'(\tau_0'')$. As before, we have taken $t = 0$ to be the time of closest approach between the active atom and the perturber.

The first term in Eq. (6.26) represents the direct two-photon process since it contains only quantities relevant to the 1-3 transition α'' and ϕ''. The second term represents the correction due to stepwise process, which affects the line shape somewhat, and may become important when $|\Delta+\Delta'|$ is increased, as will be shown below.

The excitation probability is given by

$$|\tilde{C}_3(t=\infty)|^2 = (4\pi\chi_0^2\chi_0'^2/\Delta^2\alpha'')\cos^2(\phi'' + \tfrac{1}{4}\pi) \times [1 + 2V(\tau_0'')/\Delta]. \tag{6.27}$$

The excitation cross section is obtained as usual by integrating over the impact parameter, cutting off the integral at $b = R_0''$, and approximating $\cos^2(\phi'' + \frac{1}{4}\pi)$ by its average value $\frac{1}{2}$. For van der Waals potentials, we obtain

$$\sigma = \frac{4\pi^2\chi_0^2\chi_0'^2}{3\Delta^2 v}\frac{|C''_{VDW}|^{1/2}}{|\Delta+\Delta'|^{7/2}} \times \left[1 + 2\left(\frac{C_{VDW}}{C''_{VDW}}\right)\left(\frac{\Delta+\Delta'}{\Delta}\right)\right], \tag{6.28}$$

where v is the active-atom perturber relative speed and C_{VDW} and C''_{VDW} are the van der Waals constants corresponding to the 1-2 and 1-3 relative interatomic potentials, respectively.

This equation has been obtained in a recent

paper by Nayfeh[3] using a Landau-Zener-type approximation and discussed in connection with the collision-induced three-photon ionization in which two photons are used to excite the atom, *via* CARE, to a bound excited state. A third photon then ionizes the atom. The present discussion makes clear the conditions under which Eq. (6.28) is valid.

The correction term in Eq. (6.28) shows the effect of the stepwise process on the direct two-photon process. It falls off as $|\Delta+\Delta'|^{-1/2}$ for fixed Δ, which is slower then the main part going as $|\Delta+\Delta'|^{-3/2}$. It is thus easier to observe such an effect at a larger $|\Delta+\Delta'|$; however, the correction term cannot become larger than the main part, since the treatment presented here ceases to be valid.

Digression. Before we go on to present the next case, it is advisable to show a spectrum so that we can have a better overall view of all the cases presented so far. In Fig. 3, the total excitation cross section is shown as a function of Δ' for a fixed $\Delta=-1.5\times10^{2}$ sec^{-1} and an attractive van der Waals potential with constants $C_{\rm VDW}=-1.2\times10^{18}$ Å^6 sec^{-1}, $C'_{\rm VDW}=-1.5\times10^{18}$ Å^6 sec^{-1}. In showing such a "complete" spectrum, we cannot avoid regions where *none* of the approximations employed in cases A and I is good (i.e., regions with |detunings| $\sim 1/\tau_c$). Hence, the line shape from numerical integrations of Eqs. (5.5) and Eq. (5.6) is also shown for comparison and to aid in gaining an appreciation of regions of each case. Since there are many curves on Fig. 3, and each curve only has a limited region of validity (for some cases the regions do not fall within this figure), the following points will help in reading this graph:

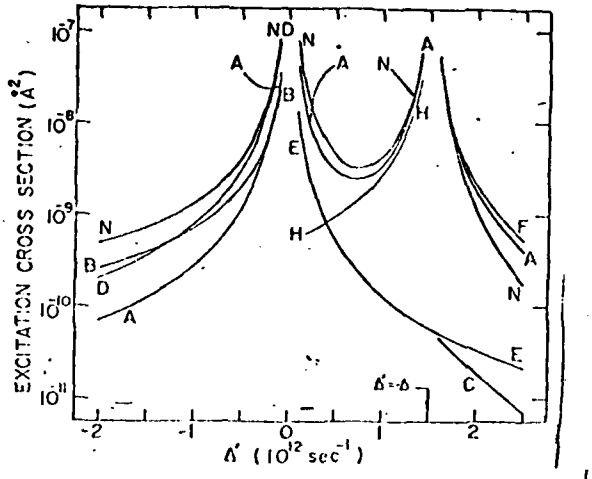

FIG. 3. Excitation cross sections versus Δ' for a fixed $\Delta=-1.5\times10^{12}$ sec^{-1} and an attractive van der Waals potential of constants $C_{\rm VDW}=-1.2\times10^{18}$ Å^6 sec^{-1}, $C'_{\rm VDW}=-1.5\times10^{18}$ Å^6 sec^{-1}, and $v=10^5$ cm sec^{-1}, $\chi_0=\chi'_0=10^9$ sec^{-1}. Curve *N* is the result of numerical integrations of Eqs. (5.5) and (5.6); others are plotted according to the equations in Table II. Only the regions, where at least the signs of the detunings are correct, are shown. See the text for discussion.

(1) Curves *A*, *B*, *C*, *D*, *E*, *F*, and *H*, representing cases covered so far, are plotted according to equations shown in Table II, and curve *N* is from numerical integrations of Eqs. (5.5) and Eq. (5.6). For curves *B*, *C*, *D*, *E*, and *F*, only the

TABLE II. Line shapes.

Case	Excitation cross section
A	$\frac{4\pi\chi_1^2\chi_0'^2}{\Delta\Delta'(\Delta+\Delta')}\left(\frac{3\pi}{8v}\right)^{2/5}\left(\frac{-\Gamma(-\frac{2}{5})\cos\frac{1}{5}\pi}{5}\right)\left(\frac{\lvert C_{\rm VDW}\rvert^{2/5}}{\Delta'}+\frac{\lvert C'_{\rm VDW}\rvert^{2/5}}{\Delta}-\frac{\lvert C''_{\rm VDW}\rvert^{2/5}}{\Delta+\Delta'}\right)$
B	$\frac{4\pi^2\chi_0^2\chi_0'^2}{3v\Delta'^2}\frac{\lvert C'_{\rm VDW}\rvert^{1/2}}{\lvert\Delta'\rvert^{3/2}}$
C[a]	$\frac{\chi_0^2\chi_0'^2\tau_c^{5/2}}{0.952\Delta'^2}\lvert C'_{\rm VDW}\rvert^{1/3}\lvert\Delta'\rvert^{-7/3}e^{-1.2(\lvert C_{\rm VDW}\rvert^{1/6}/v)\lvert\Delta'\rvert^{5/6}}$
D	$\frac{4\pi^2\chi_0^2\chi_0'^2}{3v\Delta'^2}\frac{\lvert C_{\rm VDW}\rvert^{1/2}}{\lvert\Delta\rvert^{3/2}}$
E[a]	$\frac{\chi_0^2\chi_0'^2\tau_c^{5/2}}{0.952\Delta'^2}\lvert C_{\rm VDW}\rvert^{1/3}\lvert\Delta\rvert^{-7/3}e^{-1.2(\lvert C_{\rm VDW}\rvert^{1/6}/v)\lvert\Delta\rvert^{5/6}}$
F, G	$\frac{4\pi\chi_1^2\chi_0'^2}{\Delta^2(\Delta+\Delta')^2}\left(\frac{3\pi\lvert C''_{\rm VDW}\rvert}{8v}\right)^{2/5}\left(\frac{-\Gamma(-\frac{2}{5})\cos\frac{1}{5}\pi}{5}\right)$
H, I	$\frac{4\pi^2\chi_0^2\chi_0'^2}{3v\Delta'^2}\frac{\lvert C''_{\rm VDW}\rvert^{1/2}}{\lvert\Delta+\Delta'\rvert^{3/2}}\left[1+2\left(\frac{C_{\rm VDW}}{C''_{\rm VDW}}\right)\left(\frac{\Delta+\Delta'}{\Delta}\right)\right]$

[a] The exponential line shape from the two-level asymptotic calculation of Tyorogov and Fomin (Ref. 14) is adopted.

portions, where at least the signs of detunings are correct, are shown.

(2) The conditions in the fourth column of Table I should be kept in mind in reading this figure.

(3) The detuning, $\Delta = -1.5\times10^{12}$ sec^{-1} ($|\Delta|\tau_c \sim 1$), is in neither the impact region nor the quasistatic region. Hence, only in the cases when Δ is unimportant, does the agreement with the numerical result become good, e.g., cases A, F, and G near $|\Delta + \Delta'|\tau_c \ll 1$.

(4) Curve B has the tendency of having the same Δ' dependence with the numerical result, if we extend the value of Δ' well into Q region. The numerical difference comes from the Δ^{-2} variation in case B, which is not a very good approximation for $\Delta = -1.5\times10^{12}$ sec^{-1}. The same statement holds for case C if we extend the value of Δ' well into the A region of $\Delta + \Delta'$.

(5) Curve E does not have any region of validity in this figure because of the sign and size of Δ. We show it for comparison.

E. Case J

We return now to case J, which is perhaps the most interesting case, since all the detunings are in the Q region and the curve crossings can interfere with each other, leading to a new type of interference effect. For the convenience of presentation, we give some of the details of the calculation in the Appendices and separate the discussions to calculations on (1) the amplitude and (2) the cross section. Since the detunings involved are large (typically of the order of 10^{13} sec^{-1}) in this case, a large amount of energy per collision ($\sim10^{-1}$ eV) is transferred from the atomic motion to the internal degrees of freedom. Some consideration of the energetics seems to be advisable to ensure the validity of the calculations below.

For such large kinetic energies, a temperature higher than the room temperature ($\gtrsim100$°C) is required, which in turn reduces the atomic collision time ($\tau_c \propto 1/v$). This, however, will not violate the condition for the Q region ($|\text{detunings}|\tau_c \gg 1$) in general, since one can keep this condition with a thermal energy ($\propto v^2$) $\gg \hbar|\text{detunings}|$. To be more specific, an estimate of the relevant quantities ($\hbar|\Delta|, E_{\text{thermal}}, v, |\Delta|\tau_c$) is given. For the largest detuning considered in case J ($\Delta = -8\times10^{13}$ sec^{-1}) and an atomic mass of forty times proton mass, $\hbar|\Delta| \simeq 5.31\times10^{-2}$ eV, $T = 410$ °K, $v \simeq 5.04\times10^{4}$ cm/sec, $\tau_c \simeq 9.85\times10^{-13}$ sec, and $|\Delta|\tau_c \simeq 79 \gg 1$. Hence, at a temperature higher than 137 °C, the kinetic energy will be large enough to overcome the energy mismatch ($\hbar|\Delta|$) while simultaneously maintaining the condition of the Q region ($|\Delta|\tau_c \gg 1$).

1. The amplitude

In this case, the instantaneous resonances for 1-2, 2-3, and 1-3 two-photon transitions occur at internuclear distances R_0, R_0', and R_0'', respectively, during a collision if the impact parameter is such that the distance of closest approach between the active atom and the perturber is smaller than the smallest of R_0, R_0', or R_0''. At such impact parameters, radiative excitation is enhanced owing to the collision-induced instantaneous resonances. At larger impact parameters, some of the instantaneous resonances cannot be induced, giving rise to a negligible contribution (compared with contributions from collisions with smaller b) to the total cross section. Therefore, in the straight-line-path approximation, it is sufficient to consider collisions with impact parameter $b < R_0$, R_0', or R_0''.

The instantaneous resonance points in the time domain correspond to the stationary-phase points of the integrals appearing in Eq. (6.1) and, owing to the conditions $|\Delta|\tau_c \gg 1$, $|\Delta'|\tau_c \gg 1$, and $|\Delta + \Delta'|\tau_c \gg 1$, major contributions to these integrals are from the neighborhood of these points. Hence, a stationary-phase method, of which the details are shown in Appendix A, is used to evaluate Eq. (6.1).

Assuming that the time of instantaneous resonances are all far from $t = 0$, where the collision is centered, the amplitude is given by

$$\bar{C}_3(t=\infty) = -\tfrac{1}{2}\chi_0\chi_0'(\pi/\alpha)^{1/2}[A_1 + A_2 + A_3], \quad (6.29)$$

where

$$A_1 = (\pi/\alpha')^{1/2} e^{-i(\phi_0+\phi'+\pi/4+s'^2/4)}[1 - s_1 - i\sqrt{2}\,s's_1(f_1^2+g_1^2)^{1/2}e^{is'\omega_1^2/4-is_1^2/2}] - i\sqrt{2}\,ss_2(\pi/\alpha'')^{1/2}(f_0^2+g_0^2)^{1/2}e^{i\phi_0-i(\phi_0''+s_2''^2/4)}[1 + i\sqrt{2}\,s''(f_2^2+g_2^2)^{1/2}e^{is''\omega_2^2/4-is_2''^2/2}], \quad (6.30)$$

$$A_2 = (\pi/\alpha')^{1/2} e^{i(\phi_0+\phi'+\pi/4+s'^2/4)}[1 + s_1 - i\sqrt{2}\,s's_1(f_1^2+g_1^2)^{1/2}e^{-is'\omega_1^2/4+is_1^2/2}] - i\sqrt{2}\,ss_2(\pi/\alpha'')^{1/2}(f_0^2+g_0^2)^{1/2}e^{-i\phi_0+i(\phi_0''+s_2''^2/4)}[1 - i\sqrt{2}s''(f_2^2+g_2^2)^{1/2}e^{-is''\omega_2^2/4+is_2''^2/2}], \quad (6.31)$$

$$A_3 = 2(\pi/\alpha')^{1/2} e^{-i(\phi_0+\phi'+\pi/4+s'^2/4)}, \quad (6.32)$$

$$\alpha = \frac{1}{2}\left|\left(\frac{dV}{dR}\right)_{R_0}\right|, \quad \alpha' = \frac{1}{2}\left|\left(\frac{dV'}{dR}\right)_{R_0'}\right|, \quad \alpha'' = \frac{1}{2}\left|\left(\frac{d(V+V')}{dR}\right)_{R_0''}\right|, \quad (6.33)$$

where

$$s=\mathrm{sgn}\left(\frac{dV}{dt}\right)_{\tau_0},\quad s'=\mathrm{sgn}\left(\frac{dV'}{dt}\right)_{\tau_0'},\quad s''=\mathrm{sgn}\left(\frac{d(V+V')}{dt}\right)_{\tau_0''}, \tag{6.34}$$

$$\phi=-\Delta\tau_0+\int_0^{\tau_0}V(t)dt,\quad \phi'=-\Delta'\tau_0'+\int_0^{\tau_0'}V'(t)dt,\quad \phi''=-(\Delta+\Delta')\tau_0''+\int_0^{\tau_0''}[V(t)+V'(t)]dt, \tag{6.35}$$

$$\theta_i=\tan^{-1}(g_i/f_i); \tag{6.36}$$

g_i, f_i are the auxiliary functions of Fresnel integrals evaluated at z_i,

$$z_0=\left|(2\alpha/\pi)^{1/2}(\tau_0''-\tau_0)\right|,\quad z_1=\left|(2\alpha'/\pi)^{1/2}(\tau_0'-\tau_0)\right|,\quad z_2=\left|(2\alpha''/\pi)^{1/2}(\tau_0''-\tau_0)\right|, \tag{6.37}$$

$$s_1=\mathrm{sgn}(\tau_0'-\tau_0),\quad s_2=\mathrm{sgn}(\tau_0''-\tau_0), \tag{6.38}$$

and $\tau_0, \tau_0', \tau_0''$ are the positive solutions of

$$\Delta=V(t),\quad \Delta'=V'(t),\quad \Delta+\Delta'=V(t)+V'(t), \tag{6.39}$$

respectively. If any of the times of instantaneous resonances is near $t=0$ (i.e., $\tau_0\simeq 0$, $\tau_0'\simeq 0$, or $\tau_0''\simeq 0$), the corresponding time derivative of the potential (α, α', or α'') approaches 0, and Eq. (6.29) becomes singular and is a poor approximation to the amplitude. Apart from this, Eqs. (6.29)–(6.39) provide good approximations for the amplitude, regardless of the type of potentials and the ordering of τ_0, τ_0', and τ_0'', as long as the conditions for this case (case J) hold. The essential difference between various types of potentials in determining the transition amplitude lies in the derivatives and their signs at the times of instantaneous resonance, which are given by α, α', and α'' and s, s', and s''. The ordering of τ_0, τ_0', and τ_0'' determines the values of s_1 and s_2. For given interatomic potentials and detunings, these parameters can be determined, and Eqs. (6.29)–(6.39) are greatly simplified.

In Eq. (6.29), it is natural to interpret the terms containing α' as the contribution coming from the stepwise process and the terms containing α'' as that from the direct process, since α' and α'' are associated with resonances of 2–3 transition and 1–3 transition, respectively.

Equations (6.29)–(6.39) represent the general form of the transition amplitude under the conditions of case J. They have been compared with the results of direct numerical integration of Eqs. (5.5) using attractive van der Waals potentials of constants $C_{VDW}=-1.2\times10^{16}$ Å^{6}sec^{-1}, $C'_{VDW}=-1.5\times10^{16}$ Å^{6}sec^{-1}, and several detunings of the order of 10^{13} sec^{-1}. For impact parameters smaller than the smallest of R_0, R_0', and R_0'', Eqs. (6.29)–(6.39) give very accurate results (see Fig. 4); for impact parameters outside this region, which contribute little to the total cross section, Eqs. (6.29)–(6.39) are not applicable as discussed above. There are two cases (a and b) of special interest in which Eqs. (6.29)–(6.39) can be very much simplified.

a. Exactly coinciding times of instantaneous resonance, $\tau_0=\tau_0'=\tau_0''$. All the times of instantaneous resonance coincide. In this case, $z_i=0$, $f_i=g_i=\frac{1}{2}$, and $\theta_i=\frac{1}{4}\pi$ so we obtain from Eqs. (6.29)–(6.39),

$$A_1=(\pi/\alpha')^{1/2}e^{-i(\omega_c\tau_0+\phi/4+s'\pi/4)}, \tag{6.40}$$

$$A_2=(\pi/\alpha')^{1/2}e^{i(\omega_c\tau_0+\phi'/4+s'\pi/4)}, \tag{6.41}$$

$$A_3=2(\pi/\alpha')^{1/2}e^{-i(\omega_c\tau_0+\phi'/4-s'\pi/4)}. \tag{6.42}$$

The amplitude is given by Eqs. (6.40), (6.41), (6.42), and (6.29). The contributions from the

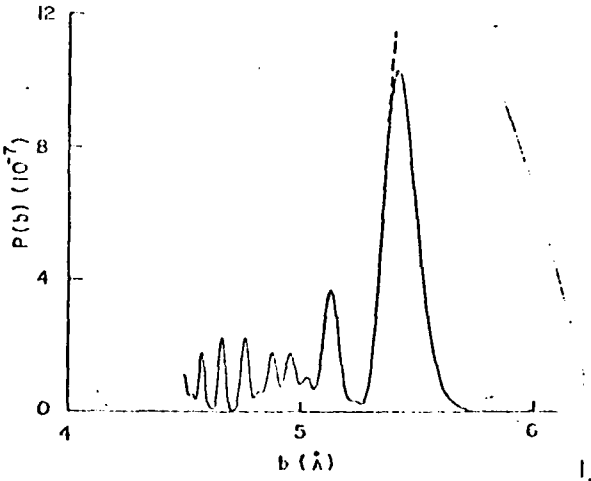

FIG. 4. Comparison of $P(b)$ vs b curves from the analytic expression [Eqs. (6.29)–(6.39)] and the numerical calculation [integration of Eqs. (5.5)] for an attractive van der Waals potential with $\chi_0=\chi_0'=10^{11}$ sec^{-1}, $\Delta=-4.0\times10^{13}$ sec^{-1}, and $\Delta'=-5.05\times10^{13}$ sec^{-1}. Other parameters are the same as those in Fig. 3. The analytic expression, which is singular at $b=5.57$ Å, was cut off at $b=5.40$ Å, where it begins to diverge. The agreement at smaller impact parameters is near perfect. ——— numerical integration of Eqs. (5.5); ----- analytic expression [Eqs. (6.29)–(6.39)].

direct process are *absent*, leaving a very simple form involving only the stepwise contributions.

For given interatomic potential and Δ, the condition $\tau_0 = \tau_0' = \tau_0''$ corresponds to a particular value of Δ' (e.g., $\Delta' = (C'_{VDW}/C_{VDW})\Delta$, for van der Waals potentials). Near this value of Δ', according to Eqs. (6.41)–(6.42), one would expect that the direct process would be less important than the stepwise process, which should be reflected in the line shape. We find this result when we numerically evaluate Eqs. (6.29)–(6.39) to obtain the total cross section, as will be shown later.

b. Well-separated times of instantaneous resonance. In this case, the arguments of f_i and g_i in Eq. (6.36) become large, and since f_i and g_i are rapidly decreasing functions with maximum values $f_1(0) = g_1(0) = \frac{1}{2}$, we can, to a good approximation, neglect terms containing factors $\sqrt{2}\,(f_i^2 + g_i^2)^{1/2}$, as compared with 1 in Eqs. (6.30) and (6.31). We obtain

$$A_1 = (\pi/\alpha')^{1/2} e^{-i(\epsilon_0 + \epsilon' - s\pi/4 + s'\pi/4)}(1 - s_1) - i\sqrt{2}\, s s_2 (\pi/\alpha'')^{1/2}(f_0^2 + g_0^2)^{1/2} e^{is\delta_0 - i(\epsilon_0 + \epsilon'' + s''\pi/4)}, \tag{6.43}$$

$$A_2 = (\pi/\alpha')^{1/2} e^{i(\epsilon_0 + \epsilon' - s\pi/4 + \pi + \pi/4)}(1 + s_1) - i\sqrt{2}\, s s_2 (\pi/\alpha'')^{1/2}(f_0^2 + g_0^2)^{1/2} e^{-is\delta_0 + i(\epsilon_0 + \epsilon'' + s''\pi/4)}. \tag{6.44}$$

The amplitude as given by Eqs. (6.43), (6.44), (6.27)–(6.39), and (6.29) contains contributions from the stepwise and the direct process that interfere with each other.

It is not difficult to understand the physical meaning of each term in Eqs. (6.32), (6.43), and (6.44) by tracing back the calculations leading to them in Appendix A. Term A_1 [Eq. (6.43)] contains the contributions from the instantaneous resonance points before $t = 0$; term A_2 [Eq. (6.44)] contains the contributions from the instantaneous resonance points after $t = 0$; and term A_3 [Eq. (6.32)] contains the contribution from the *stepwise process* in which 1-2 resonance occurs before $t = 0$ and 2-3 resonance occurs after $t = 0$. Terms A_1 and A_2 contain both stepwise contributions. For a given ordering of τ_0, τ_0', and τ_0'' some stepwise contributions will be absent. For example, when $\tau_0 < \tau_0'$, $s_1 = 1$ and the first term in Eq. (6.43) vanishes, indicating that no stepwise process is occuring before $t = 0$, since the 1-2 resonance happens at a later time than the 2-3 transition ($-\tau_0 > -\tau_0'$). The first term in Eq. (6.44) does not vanish because $\tau_0 < \tau_0'$ and the stepwise process can occur after $t = 0$. The situation is reversed when $\tau_0 > \tau_0'$ ($s_1 = -1$). However, A_1 always survives since the 1-2 transition occurs before $t = 0$ and the 2-3 transition occurs after $t = 0$. In any case, there are *four* terms in the amplitude corresponding to the *four* excitation channels discussed in Sec. IV.

2. *The total cross section*

It is straightforward to obtain the excitation probability by taking the modulus of Eq. (6.29). The resulting expressions are lengthy and are given in Appendix B. Only for the two special cases ($\tau_0 = \tau_0' = \tau_0''$ and $\tau_0, \tau_0', \tau_0''$ far apart) are the analytic expressions given in this subsection.

To demonstrate the success of the stationary-phase method used in Appendix A, we compare in Fig. 4 two $|\bar{C}_3(t = \infty)|^2$ vs b curves, one from numerically integrating Eqs. (5.5), the other from squaring Eq. (6.29) for an attractive van der Waals potential with $C_{VDW} = -1.2 \times 10^{18}$ Å^6 sec^{-1}, $C'_{VDW} = -1.5 \times 10^{18}$ Å^6 sec^{-1}, $\Delta = -4.0 \times 10^{13}$ sec^{-1}, and $\Delta' = -5.05 \times 10^{13}$ sec^{-1}. The agreement is near perfect except for $b \gtrsim 5.40$ Å, which is close to $R_0 = (C_{VDW}/\Delta)^{1/6} = 5.57$ Å, at which Eqs. (6.29)–(6.39) become singular. The values of detunings used are large ($|\Delta|\tau_c \gg 1$, $|\Delta'|\tau_c \gg 1$); however, for smaller values of detunings ($\sim 10^{12}$ sec^{-1}), good agreement (to within 10%) is still obtained.

To obtain accurate cross sections, we have to do numerical integrations of Eqs. (5.5) for impact parameters b near and larger than the smallest of R_0, R_0', and R_0'' and to use Eqs. (6.29)–(6.39) for smaller impact parameters. This procedure is used to obtain the total cross section as a function of Δ' in a range including the point $\Delta' = (C'_{VDW}/C_{VDW})\Delta$ at which all the times of instantaneous resonance coincide, for the attractive van der Waals potential used in Fig. 4, and for $\Delta = -2.0 \times 10^{13}$ sec^{-1}. The results are shown in Fig. 5 along with two curves, one with a $(\Delta + \Delta')^{1/2}$ dependence, the other which a $\Delta'^{-3/2}$ dependence. The calculated cross section lies between the two curves, which are normalized to the same value as the calculated one at $\Delta' = (C'_{VDW}/C_{VDW})\Delta$ ($= 2.5 \times 10^{13}$ sec^{-1} in this case).

From the discussion earlier, the contributions from the $(1 \to 3)$ direct process disappear at this point, since $\tau_0 = \tau_0' = \tau_0''$. The calculated line shape shows no marked structure due to this "interference" effect; the line profile is a smooth curve exhibiting the influence of both the stepwise and the direct processes. If the stepwise process is the only contributing one, the line shape would have followed the $\Delta'^{-3/2}$ curve; if, on the other hand, the direct process is the predominant one, the line shape should go as $(\Delta + \Delta')^{-3/2}$. Since the calculated curve on Fig. 5 tends to follow more closely the $\Delta'^{-3/2}$ curve, it suggests that at the

vicinity of $\Delta' = (C'_{VDW}/C_{VDW})\Delta$, the stepwise process is more important than the direct process, as previously discussed.

Simple analytic results can be obtained for the following two special cases (*i* and *ii*).

i. Exactly coinciding times of instantaneous resonance, $\tau_0 = \tau'_0 = \tau''_0$. Using Eqs. (6.29), (6.40), (6.41), and (6.42), we obtain

$$|\bar{C}_3(t=\infty)|^2 = (\pi^2\chi_0^2\chi_0'^2/\alpha\alpha')[\cos^2(\phi+\phi'+s\pi/4+s'\pi/4)+1 + 2\cos(\phi+\phi'+s\pi/4+s'\pi/4)\cos(\phi-\phi'+s\pi/4-s'\pi/4)]. \quad (6.45)$$

Although this is a simple expression, it cannot be used to obtain an accurate value for the total cross section for reasons to be discussed below. The time derivatives of the interatomic potentials α and α' can be expressed in terms of the internuclear distance and the impact parameter,

$$\alpha = (v/2R_0)(R_0^2-b^2)^{1/2}\left|\left(\frac{dV}{dR}\right)_{R_0}\right|, \quad (6.46)$$

$$\alpha' = (v/2R'_0)(R_0'^2-b^2)^{1/2}\left|\left(\frac{dV'}{dR}\right)_{R'_0}\right|. \quad (6.47)$$

When $R_0 = R'_0$ (as in this case), both α and α' approach 0 as b approaches $R_0(=R'_0)$, and Eq. (6.45) is singular, varying as $(R_0^2-b^2)^{-1}$. An approximate formula for obtaining the total cross section, such as Eq. (6.10), is not applicable since it leads to a logarithmic divergence. Therefore, for a certain range of impact parameter b near R_0, numerical integration of Eqs. (5.5) and of $\int|\bar{C}_3(t=\infty)|^2 2\pi b\,db$ are required to obtain an accurate value for the total cross section. The result for a specific van der Waals potential and a given Δ is represented by a point on the line-shape curve, such as the one in Fig. 5 [the point $\Delta' = \Delta(C'_{VDW}/C_{VDW})$].

ii. Well-separated times of instantaneous resonance. The probability can be obtained from Eqs. (6.43), (6.44), (6.27)–(6.39), and (6.29). Since the amplitude contains contributions from both the stepwise and the direct processes, there will be interference terms in the probability. The interference effect is best illustrated using a specific order of instantaneous resonances (e.g., $\tau'_0 > \tau''_0 > \tau_0$). For this order ($\tau'_0 > \tau''_0 > \tau_0$), the excitation probability is obtained as

$$|\bar{C}_3(t=\infty)|^2 = (\pi\chi_0\chi'_0)^2(P_S+P_D+P_{INT}), \quad (6.48)$$

with

$$P_S = 2(1-s\sin2\delta)/\alpha\alpha', \quad (6.49)$$

$$P_D = (f_0^2+g_0^2)[1-s''\sin2(\phi''-s\theta_0)]/\alpha\alpha'', \quad (6.50)$$

$$P_{INT} = -s\left(\frac{2(f_0^2+g_0^2)}{\alpha\alpha'\alpha''}\right)^{1/2}\{\sin[\phi+\phi'-\phi''+(s+s'-s'')\pi/4+s\theta_0] + \sin[\phi+\phi'+\phi''+(s+s'+s'')\pi/4-s\theta_0] + \sin[\phi'+\phi''-\phi+(s'+s''-s)\pi/4-s\theta_0] + \sin[\phi'-\phi''-\phi+(s'-s''-s)\pi/4+s\theta_0]\}, \quad (6.51)$$

where all the quantities have been defined in Eqs. (6.29)–(6.39). Equations (6.48)–(6.51) clearly show the contributions to the total cross section from the stepwise process, the direct process, and the interference between the two. This result has been obtained and discussed in a recent paper,[7] and we summarize only the essential features.

All the sine functions in Eqs. (6.48)–(6.51) oscillate rapidly as functions of impact parameter b, except the one varying as

$$\sin[\phi+\phi'-\phi''+(s+s'-s'')\pi/4+s\theta_0]$$

(the first term in P_{INT}), which is a slowly varying function of b. On integrating over b to obtain the total cross section, only this term survives to yield a term representing the interference of the stepwise and the direct processes which oscillates as a function of inverse active-atom-perturber relative speed $1/v$.

An approximation such as Eq. (6.10) is used to calculate the total cross section, yielding

$$\sigma = \frac{(\pi\lambda_0\lambda_0')^2 R_c}{v^2\left|\left(\frac{dV}{dR}\right)_{R_0}\right|}\left[\frac{4R_0'}{\left|\left(\frac{dV'}{dR}\right)_{R_0'}\right|}\ln\frac{R_0'+R_0}{R_0'-R_0}+\frac{2R_0''(f_0''^2+g_0''^2)}{\left|\left(\frac{d(V+V')}{dR}\right)_{R_0''}\right|}\ln\frac{R_0''+R_0}{R_0''-R_0}\right.$$

$$\left.-2\cos\left[\frac{2R_0'R_0''(f_0''^2+g_0''^2)}{\left|\left(\frac{dV}{dR}\right)_{R_0'}\left(\frac{d(V+V')}{dR}\right)_{R_0''}\right|}\right]^{1/2}\ln\frac{R_0'+R_0''+2R_0}{R_0'+R_0''-2R_0''}\sin\left(\frac{A}{v}+\phi_0\right)\right], \qquad (6.52)$$

where A is the area enclosed by the three crossings on the interatomic potential curves in a dressed-atom picture, and

$$\phi_0 = (s+s'-s'')\tfrac{\pi}{4}+s\theta_0$$

is a constant phase.

Equation (6.52) is not restricted to any specific type of potential, and the calculation of total excitation cross section using it is remarkably simple. For given interatomic potential curves and detunings, one can graphically obtain the slopes at the crossing points and the area A enclosed by them. Substitution of these values into Eq. (6.52) yields σ. A comparison of this cross section with the corresponding one obtained from computer solutions indicates that Eq. (6.52) is accurate to within 15%.

The third term in Eq. (6.52), which represents the interference between the stepwise and the direct processes, contains a sine function which will oscillate as the relative speed v is varied. It is clear from Eq. (6.52) that the area A determines the oscillation frequency, while the slopes at the crossing points determine the amplitudes of the oscillations. For given interatomic potential curves, these quantities (A and slopes) can be changed by varying the detunings, and hence the frequency and the amplitude of the oscillation in the total cross section.

The restriction to a specific ordering of the crossing times (i.e., $\tau_0' > \tau_0'' > \tau_0$) corresponds to confining the detunings in certain regions depending on the given interatomic potential. For detunings in different regions, the ordering will be different. However, it would be just as easy to obtain the excitation probability and the total cross section from Eqs. (6.43), (6.45), (6.32)–(6.39), and (6.29).

To illustrate this interference effect and to investigate the feasibility of its experimental observation, we use a specific potential, as shown in Figs. 6(a) and 6(b), instead of van-der-Waals-type potentials for detunings $\Delta = -8.0\times10^{13}$ sec^{-1} and $\Delta' = -3.0\times10^{13}$ sec^{-1}. The resulting total excitation cross section as a function of inverse relative speed $1/v$ is shown in Fig. 7, with $\chi_0 = \chi_0' = 10^{13}$ sec^{-1}. The curve rises as $(1/v)^2$ with equally spaced peaks when the speed is varied from 10^5 to 4×10^5 cm sec^{-1}. In terms of the laser power, the excitation cross sections are of the order of $(10^{-34} I_0 I_0')$ cm^2, with I_0, I_0' the peak power density in W/cm^2. Thus, the interference effect should be observable with moderate laser power. Although a specific potential [Figs. 6(a) and 6(b)] is used to demonstrate this effect, we emphasize that the oscillatory feature occurs regardless of the form of the potential as long as three conditions are satisfied. First, there must be three crossings, as shown in Fig. 6(b). Second, the area enclosed by the crossings must be large enough to produce a phase change of order π when the speed is varied in a convenient range. Third, the stepwise and the direct excitation contributions must be comparable. The first condition is required for there to be four excitation channels interfering with each other. This condition allows for a phase factor that is nearly independent of

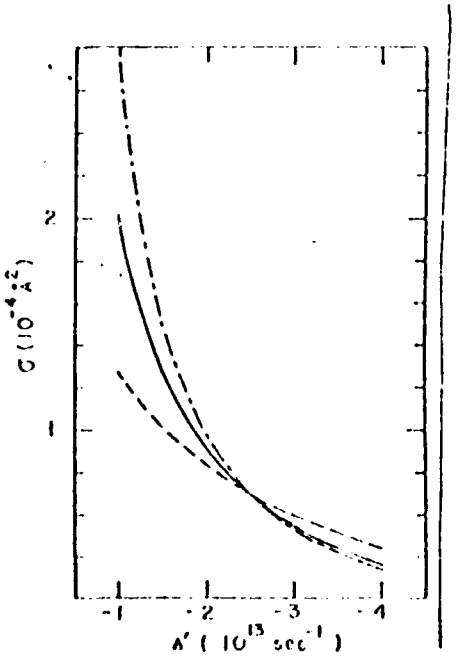

FIG. 5. The total excitation cross section as a function of Δ' or ω_0 Δ' $(C_{VLW}'/C_{VLW})\Delta'$ for a fixed $\Delta = -2.0\times10^{13}$ sec^{-1}. The interatomic potential and other parameters used are the same as those in Fig. 4. — — this calculation; ------ $\propto(\Delta+\Delta')^{-1/2}$; - - - - $\propto\Delta'^{-1/2}$. The three curves are normalized to the same value at Δ' $\Delta(C_{VLW}'/C_{VLW})$.

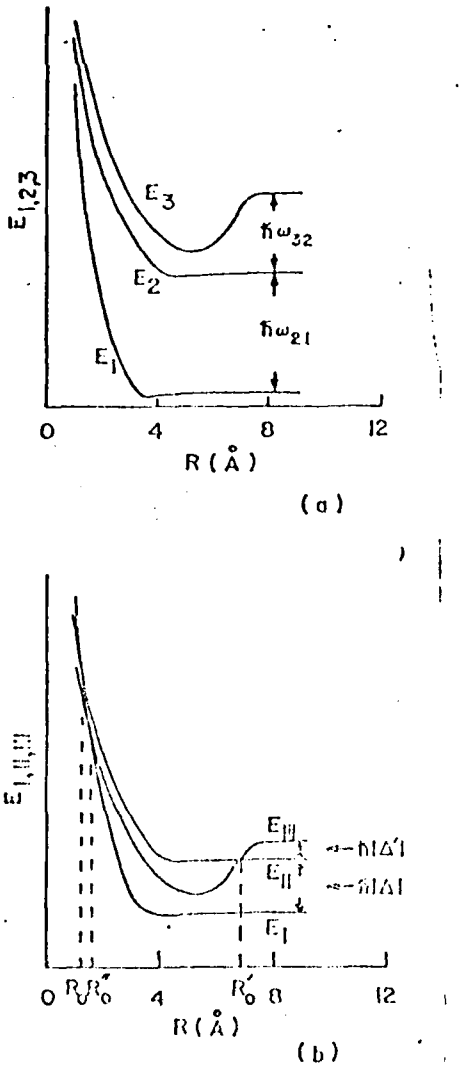

FIG. 6. Interatomic potential used to demonstrate the interference effect discussed in case J. (a) Bare-state-classical-field picture. (b) Dressed-atom picture. The dressed-state energies $E_{I,II,III}$ are related to the bare-state energies $E_{1,2,3}$ by Eqs. (6.2). In (a), the level separations are not drawn to scale; in (b), the energies $\hbar|\Delta|$ and $\hbar|\Delta'|$ set the energy scale. $\Delta = -8.0\times10^{13}$ sec^{-1}, $\Delta' = -3.0\times10^{13}$ sec^{-1}.

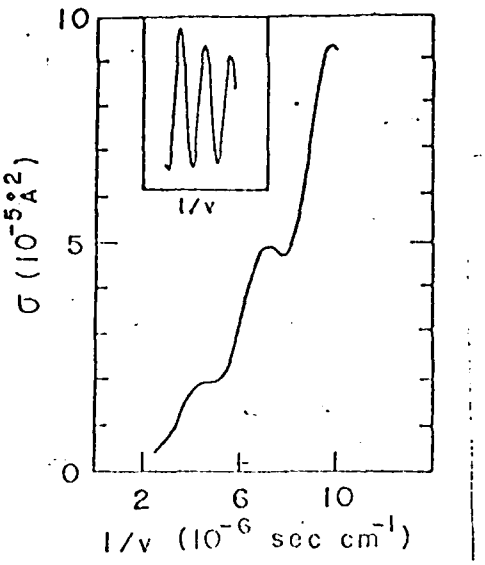

FIG. 7. Total excitation cross section as a function of inverse relative speed $1/v$ for a potential shown in Fig. 6, with $\chi_0 = \chi_0' = 10^{11}$ sec^{-1}, $\Delta = -8.0\times10^{13}$ sec^{-1}, and $\Delta' = -3.0\times10^{13}$ sec^{-1}. The curve rises as $(1/v)^2$. As the speed varies from 10^5 to 4×10^5 cm sec^{-1}, equally spaced peaks are clearly seen. In the inset, the product of the total cross section and v^2 as a function of $1/v$ is shown.

impact parameter b. The second and third conditions determine the frequency and amplitude of the oscillatory term.

VII. DISCUSSION

CARE, as presented in the dressed-atom picture, is similar to radiationless inelastic collisions. However, there is an important difference between the two. In the radiationless inelastic atomic collision, the process, and hence the cross section, is determined by the interatomic potential of the atom-atom system, which cannot be controlled once the system is chosen. In CARE, on the other hand, the corresponding interatomic potential (in the dressed-atom picture) depends not only on the atom-atom system, but also on the atom-field detunings as well as the field intensities. In the weak-field limit, one can vary the detunings to change the level spacings of the dressed states and the positions of, and the slopes at, the potential curve crossings (if any) which are the essential parameters determining the CARE cross section. Hence, the interaction between the two colliding atoms can be probed in a controlled fashion by using CARE, a great advantage over the ordinary radiationless atomic collisions. The three-level problem discussed in this paper provides a good example of the relationship between CARE and inelastic collisions. The oscillatory features obtained in case J of the previous section for the total CARE cross section as a function of active-atom-perturber relative speed are of similar nature to those obtained by Rosenthal and Foley[8] for He-He$^+$ charge-exchange inelastic collisions. The He-He$^+$ atom-ion interatomic potential curves are analogous to those of the three-level CARE in the dressed-atom picture [Fig. 6(b)]. The frequency and amplitude of oscillation in CARE can be varied by changing the detunings and thus the

potential-curve crossing properties (positions and slopes); such a variation is not possible in charge-exchange inelastic collisions. Although oscillation of this type continue to be discovered[18,19] for charge-exchange inelastic collisions in alkali-ion-noble-gas systems such as Na^+-Ne, K^+-Ar, Cs^+-Ar, they are confined in systems with atom-ion interatomic potentials bearing a resemblance to Fig. 6(b), and thus have limited value in investigating the atom-atom or atom-ion interactions. With CARE, the scope of such studies can be extended.

In case J of the previous section, we mentioned that the interference effect should be observable with moderate laser powers, without referring to any specific experimental setup. The experiment can be performed using crossed atomic beams or a beam interacting with a gas sample. The beam-gas sample method works only if the active-atom-perturber relative velocity is approximately equal to the beam velocity. In cases when better detection efficiency is required, one can use a third laser to ionize the active atom from the upper excited state (state 3) and thus detect the ions instead of the fluorescence.

Finally, let us mention another type of oscillation which can occur in a two-level system and should be distinguished from the present one. The modulation in the absorption coefficient as a function of *detuning* for atoms in a collisional environment was discussed by Mies,[20] Carrington *et al.*,[21] Shlyapnikov and Shmatov,[22] and observed by Schops *et al.*[23] and Bergeman and Lingo.[24] This has been attributed to the oscillatory structure of the vibrational wave function of the quasimolecule formed by the colliding atoms. Such an effect does not involve interference of different channels of excitation, and is due to oscillation in the transition matrix elements.

VIII. CONCLUSION

We have presented a theory of collisionally aided radiative excitation for three-level systems in the weak-fields limit. Attempts are made to cover as many cases as possible and to be as general as possible, although results are given for some specific potentials only. Because of the complexity of a three-level system and the distinct physical features and mathematical treatments in different limiting cases, we classified the problem into thirteen cases according to the sizes and the signs of the detunings. These cases were treated in detail, except the last three cases (K, L, M) which give rise to exponentially small excitation cross sections for which reliable analytic approximations are lacking at the present time.

A dressed-atom picture was also given which brought the CARE problem into complete parallel with the problem of radiationless inelastic atomic (or molecular) collisions. In this picture, the collision-induced instantaneous resonances between the atomic transitions and the external fields are transformed into interatomic potential curve crossings. Such curve crossings enhance the excitation, especially in the large detuning cases, and interfere with each other, leading to effects reflecting the crossing configurations. Some special crossing configurations yield particularly interesting interference effects (e.g., the modulation of the total excitation cross section discussed in case J). A quantitative examination indicates that experimental observations of such effects are feasible.

The theory does not include the cases of strong fields which are of increasing importance and interest with the advent of high-power lasers. The dressed-atom approach seems to be most suitable for attacking such cases, and numerical calculations may be inevitably needed. The established numerical method used in two-level CARE problems and the analytic methods presented in this paper can be combined to form useful tools in the investigation of these cases.

ACKNOWLEDGMENTS

This work was supported by the U. S. ONR through contract number N00014-77-C-0553. The authors thank Professor E. J. Robinson for many discussions during the course of the work.

APPENDIX A

In this appendix we give the details of calculations leading to Eqs. (6.29) (6.39) from Eq. (6.1). Assuming that the collision trajectories are symmetric about $t = 0$, the time of closest approach between the active atom and the perturber, we break the t integral of Eq. (6.1) into two parts, $t > 0$ and $t < 0$,

$$\dot{C}_3(t \to \infty) = -\int_{-\infty}^{0} \chi'(t) \exp\left[-i\left(\Delta' t - \int_0^t V'(t')dt'\right)\right] Q(t)\,dt - \int_0^{\infty} \chi'(t) \exp\left[-i\left(\Delta' t - \int_0^t V'(t')dt'\right)\right] Q(t)\,dt, \tag{A1}$$

where

$$Q(t)=\int_{-\infty}^{t}\chi(t_1)\exp\left[-i\left(\Delta t_1-\int_0^{t_1}V(t')dt'\right)\right]dt_1 .$$

Because of the condition $|\Delta|\tau_c \gg 1$, the contributions to Q are from the neighborhood of the crossing points $\pm\tau_0$, satisfying $\Delta = V(t)$ only. Thus, for the first term (restricted to $t<0$), we expand the exponent of the integrand in Q in Taylor series about $t_1=-\tau_0$, and for the second term (restricted to $t>0$), we break the Q integral into two parts, from $-\infty$ to 0 and from 0 to t, and expand the exponent about $t_1=-\tau_0$ and $t_1=\tau_0$ for each region, respectively. The factor $\chi(t_1)$ is evaluated at $\chi(\pm\tau_0)=\chi_0$. The Taylor series is terminated at terms $\propto(t_1\pm\tau_0)^2$, and the integrals obtained are evaluated exactly to yield

$$Q(t)=\chi_0 e^{-i(\phi+s\pi/4)}\tfrac{1}{2}(\pi/\alpha)^{1/2}\{1+\operatorname{erf}[\alpha^{1/2}(t+\tau_0)e^{is\pi/4}]\}\quad \text{for } t<0 \tag{A2}$$

and

$$\begin{aligned}Q(t)=\;&\chi_0 e^{-i(\phi+s\pi/4)}\tfrac{1}{2}(\pi/\alpha)^{1/2}[1+\operatorname{erf}(\alpha^{1/2}\tau_0 e^{is\pi/4})]\\&+\chi_0 e^{i(\phi+s\pi/4)}\tfrac{1}{2}(\pi/\alpha)^{1/2}\{\operatorname{erf}[\alpha^{1/2}(t-\tau_0)e^{-is\pi/4}]-\operatorname{erf}(-\alpha^{1/2}\tau_0 e^{-is\pi/4})\}\quad \text{for } t>0\end{aligned} \tag{A3}$$

where erf is the error function and ϕ, s, α are defined in Eqs. (6.29)–(6.39). Putting Eqs. (A2) and (A3) into Eq. (A1), using the relation $\operatorname{erf}(z)=1-\operatorname{erfc}(z)$, and combining terms, we can write $\bar{C}_3(t=\infty)$ as a sum of four terms. Under the assumption that the crossing points are far from $t=0$ ($\alpha^{1/2}\tau_0\gg 1$), one of the four terms, which contains a factor $\operatorname{erfc}[\alpha^{1/2}\tau_0 e^{is\pi/4}]$, can be neglected. Thus,

$$\begin{aligned}\bar{C}_3(t=\infty)=-\frac{\chi_0}{2}(\pi/\alpha)^{1/2}\Bigg\{&e^{-i(\phi+s\pi/4)}\int_{-\infty}^{0}\chi'(t)\exp\left[-i\left(\Delta' t-\int_0^t V'(t')dt'\right)\right]\operatorname{erfc}[-\alpha^{1/2}(t+\tau_0)e^{is\pi/4}]dt\\&+e^{i(\phi+s\pi/4)}\int_0^{\infty}\chi'(t)\exp\left[-i\left(\Delta' t-\int_0^t V'(t')dt'\right)\right]\operatorname{erfc}[-\alpha^{1/2}(t-\tau_0)e^{-is\pi/4}]dt\\&+e^{-i(\phi+s\pi/4)}\operatorname{erfc}[-\alpha^{1/2}\tau_0 e^{is\pi/4}]\int_0^{\infty}\chi'(t)\exp\left[-i\left(\Delta' t-\int_0^t V'(t')dt'\right)\right]dt\Bigg\}.\end{aligned} \tag{A4}$$

This, again, is to be evaluated using the stationary-phase method. Since the error functions with complex arguments are oscillatory functions, their presence in the integrands of the first two terms in Eq. (A4) will modify the stationary-phase positions of these integrals. To cope with this, we use Eqs. 7.1.2, 7.1.9, 7.1.10, 7.3.9, 7.3.10, and 7.3.22 of Abramowitz and Stegun[25] to express the error functions in terms of an exponential (oscillating) part and the auxiliary functions f, g of the Fresnel's integrals, which are slowly varying functions. By doing this, the integrals are written in a form suitable for the stationary-phase method. We shall now demonstrate the method by evaluating the first term in Eq. (A4), to be called W. The evaluation of the second term follows exactly the same procedure.

In terms of f, g and the exponential function, W can be written as a sum of three terms. In two of these terms a phase of the form $\phi+s\alpha(t+\tau_0)^2$ appears which is simply the Taylor-series expansion of $\Delta t-\int_0^t V(t')dt'$ at $t=-\tau_0$. We transform this term back to its original form and find

$$\begin{aligned}W=\;&2e^{-i(\phi+s\pi/4)}\int_{-\tau_0}^{0}\chi'(t)\exp\left[-i\left(\Delta' t-\int_0^t V'(t')dt'\right)\right]dt\\&+is\sqrt{2}\int_{-\tau_0}^{0}\chi'(t)(f^2+g^2)^{1/2}e^{i\theta}\exp\left[-i\left((\Delta+\Delta')t-\int_0^t[V(t')+V'(t')]dt'\right)\right]dt\\&-is\sqrt{2}\int_{-\infty}^{-\tau_0}\chi'(t)(f^2+g^2)^{1/2}e^{is\theta}\exp\left[-i\left((\Delta+\Delta')t-\int_0^t[V(t')+V'(t')]dt'\right)\right]dt,\end{aligned} \tag{A5}$$

where $\theta=\tan^{-1}g/f$ and the argument of f, g is

$$\left|(2\alpha/\pi)^{1/2}(t+\tau_0)\right| .$$

Other parameters are defined in Eqs. (6.29)–(6.39). The integrals in Eq. (A5) can be evaluated using the stationary-phase method. Since $\chi'=\chi_0'$, a constant during the collision, and f, g, θ are slowly varying functions compared with the rapidly oscillating exponential part, we can evaluate them at the stationary-phase points, $-\tau_0'$ for the first term, $-\tau_0''$ for the second and the third term, and take them out of the integrals. The remaining integrals are evaluated using the same method as that leading to Eqs. (A2) and (A3) for Q. Then, the error functions can again be written in terms of f, g functions, which leads to Eq. (6.30).

The same procedure applied to the second term in Eq. (A4) yields Eq. (6.31). The evaluation of the

third term in Eq. (A4) is particularly simple. For stationary-phase point τ_0 far from 0, the erfc function can be approximated by 2, and the integral is done by the stationary-phase method. This method yields Eq. (6.32).

APPENDIX B

The excitation probability can always be written as a sum of three terms, P_S, P_D, and P_{INT} representing the stepwise, the direct, and the interference contributions, respectively. In the most general case, they are

$$P_S = \frac{(\chi_0\chi_0'\pi)^2}{\alpha\alpha'}\{2 - (1+s_1)s\sin 2\phi - (1-s_1)s'\sin 2\phi'$$
$$+ (f_1^2+g_1^2)[1 - s\sin 2(\phi+\phi_{\tau_0}' - s'\theta_1)]$$
$$+ [2(f_1^2+g_1^2)]^{1/2}[s\sin(2\phi+\phi'+\phi_{\tau_0}' - s'\pi/4 - s'\theta_1) - \cos(\phi'-\phi_{\tau_0}' - s'\pi/4 + s'\theta_1)]$$
$$+ s_1[2(f_1^2+g_1^2)]^{1/2}[s\sin(2\phi-\phi'+\phi_{\tau_0}' + s'\pi/4 - s'\theta_1) - \cos(\phi'+\phi_{\tau_0}' - s'\pi/4 - s'\theta_1)]\}, \tag{B1}$$

$$P_D = [(\chi_0\chi_0'\pi)^2/\alpha\alpha'](f_0^2+g_0^2)\{1 - s''\sin 2(\phi'' - s\theta_0) + 2(f_2^2+g_2^2)[1 - \cos 2(\phi''_{\tau_0} - s\theta_0 - s''\theta_2)]$$
$$+ 2[2(f_2^2+g_2^2)]^{1/2}[\cos(\phi''+\phi''_{\tau_0} - 2s\theta_0 - s''\theta_2 - s''\pi/4) - \cos(\phi''_{\tau_0} - \phi'' - s''\theta_2 + s''\pi/4)]\},$$
$$P_{INT} = \frac{(\chi_0\chi_0'\pi)^2}{\alpha}\left(\frac{2(f_0^2+g_0^2)}{\alpha'\alpha''}\right)^{1/2} \tag{B2}$$
$$\times(-s_1s_2\{\cos[\phi+\phi'+\phi'' - (s-s'-s'')\pi/4 - s\theta_0] + \cos[\phi+\phi'-\phi'' - (s-s'+s'')\pi/4 + s\theta_0]\}$$
$$+ s_2\{\cos[\phi-\phi'+\phi'' - (s+s'-s'')\pi/4 - s\theta_0]$$
$$+ \cos[\phi-\phi'-\phi'' - (s+s'+s'')\pi/4 + s\theta_0]\}$$
$$+ s_1s_2s''[2(f_2^2+g_2^2)]^{1/2}\{\sin[\phi+\phi'-\phi''_{\tau_0} - (s-s')\pi/4 + s\theta_0 + s''\theta_2]$$
$$- \sin[\phi+\phi'+\phi''_{\tau_0} - (s-s')\pi/4 - s\theta_0 - s''\theta_2]\}$$
$$- s_2s''[2(f_2^2+g_2^2)]^{1/2}\{\sin[\phi-\phi'-\phi''_{\tau_0} - (s+s')\pi/4 + s\theta_0 + s''\theta_2]$$
$$+ \sin[\phi-\phi'+\phi''_{\tau_0} - (s+s')\pi/4 + s\theta_0 - s''\theta_2]\} - \sin[\phi-\phi'+\phi''_{\tau_0} - (s+s')\pi/4 - s\theta_0 - s''\theta_2]\}$$
$$- s_1s_2s'[2(f_1^2+g_1^2)]^{1/2}\{\sin[\phi+\phi''+\phi'_{\tau_0} - (s-s'')\pi/4 - s\theta_0 - s'\theta_1]$$
$$+ \sin[\phi-\phi''+\phi'_{\tau_0} - (s+s'')\pi/4) + s\theta_0 - s'\theta_1]\}$$
$$+ 2s_1s_2s's''[(f_1^2+g_1^2)(f_2^2+g_2^2)]^{1/2}[\cos(\phi+\phi'_{\tau_0}+\phi''_{\tau_0} - s\pi/4 - s\theta_0 - s'\theta_1 - s''\theta_2)$$
$$- \cos(\phi+\phi'_{\tau_0} - \phi''_{\tau_0} - s\pi/4 + s\theta_0 - s'\theta_1 + s''\theta_2)]), \tag{B3}$$

where

$$\phi'_{\tau_0} = -\Delta'\tau_0 + \int_0^{\tau_0} V'(t')dt', \quad \phi''_{\tau_0} = -(\Delta+\Delta')\tau_0 + \int_0^{\tau_0}[V(t')+V'(t')]dt',$$

and all the other quantities have been defined in Eqs. (6.29)–(6.39).

---

[1] An extensive list of papers, books, and reviews regarding radiative collisions and optical collisions (CARIC) in two-level systems for all limits, including impact and nonimpact regions, can be found in a recent review. See S. I. Yakovlenko, Sov. J. Quantum Electron. 8, 151 (1978).

[2] S. Yeh and P. R. Berman, Phys. Rev. A 19, 1106 (1979) and references therein.

[3] M. H. Nayfeh, Phys. Rev. A 20, 1927 (1979).

[4] We follow the terminology used in some pressure-broadening theories; for example, J. Szudy and W. E. Baylis, J. Quant. Spectrosc. Radiat. Transfer, 15, 641 (1975).

[5] C. Cohen-Tannoudji, *Cargèse Lecture in Physics* (Gordon and Breach, New York, 1968), Vol. 2, p. 347.

[6] See, for example, J. M. Yuan and T. F. George, J. Chem. Phys. 68, 3040 (1978).

[7] S. Yeh and P. R. Berman, Phys. Rev. Lett. 43, 848 (1979).

[8] H. Rosenthal and H. M. Foley, Phys. Rev. Lett. 23, 1480 (1969); H. Rosenthal, Phys. Rev. A 4, 1030 (1971).

[9] S. H. Dworetsky and R. Novick, Phys. Rev. Lett. 23, 1484 (1969).

[10] See, for example, S.-Y. Chen and M. Takeo, Rev. Mod.

Phys. 29, 20 (1957); R. G. Breene, Jr., *ibid.* 29, 94 (1957).
[11]See, for example, J. D. Murray, *Asymptotic Analysis* (Clarendon, Oxford, 1974).
[12]These are the standard results of pressure-broadened line shape for a van der Waals potential. See, for example, Ref. 10.
[13]The approximation has been used in connection with semiclassical atomic-collision theory, especially in two-level model calculation. See, for example, W. Fritsch and U. Wille, J. Phys. B 11, L13 (1978). For a detailed account, see M. S. Child, *Molecular Collision Theory* (Academic, London, 1974), pp. 191–194.
[14]S. D. Tvorogov and V. V. Fomin, Opt. Spectrosc. (USSR) 30, 228 (1971); V. V. Fomin and S. D. Tvorogov, Appl. Opt. 12, 581 (1973).
[15]J. Szudy and W. E. Baylis, J. Quant. Spectrosc. Radiat. Transfer 15, 641 (1975).
[16]See Ref. 11 or Ref. 14.
[17]This radius was originally defined by V. V. Weisskopf as the impact parameter at which $\int_{-\infty}^{\infty}[\omega_{31}(t)-\omega'_{31}]dt=1$.
[18]R. Odom, J. Caddick, and J. Weiner, Phys. Rev. A 15, 1414 (1977).
[19]J. Østgaard Olsen *et al.*, Phys. Rev. A 19, 1457 (1979).
[20]F. H. Mies, J. Chem. Phys. 48, 482 (1967).
[21]C. G. Carrington, D. Drummond, A. Gallagher, and A. V. Phelps, Chem. Phys. Lett. 22, 511 (1973).
[22]G. V. Shlyapnikov and I. P. Shmatov, Opt. Spectrosk. xx, xxx (19xx) Opt. Spectrosc. (USSR) 45, 117 (1978).
[23]R. Scheps, Ch. Ottinger, G. York, and A. Gallagher, J. Chem. Phys. 63, 2581 (1975); G. York, R. Scheps, and A. Gallagher, *ibid.* 63, 1052 (1975).
[24]T. Bergeman and P. F. Liao (unpublished).
[25]M. Abramowitz and I. A. Stegun, *Handbook of Mathematical Functions* (Dover, New York, 1972).

END

DATE
FILMED

11-80

DTIC